Multimodality based Tissue Classification Technique for Malignant Anomaly Detection

by

Parvind Kaur Grewal

M.Eng., Punjab Engineering College, 2004

Thesis Submitted in Partial Fulfillment of the
Requirements for the Degree of
Doctor of Philosophy

in the
School of Mechatronic Systems Engineering
Faculty of Applied Sciences

SIMON FRASER UNIVERSITY

Summer 2014

Approval

Name: **Parvind Kaur Grewal**

Degree: **Doctor of Philosophy**

Title: ***Multimodality based Tissue Classification Technique for Malignant Anomaly Detection***

Examining Committee: **Chair:** Woo Soo Kim
Assistant Professor

Farid Golnaraghi
Senior Supervisor
Professor

Ash M. Parameswaran
Supervisor
Professor

Carolyn Sparrey
Supervisor
Assistant Professor

Edward Jung Wook Park
Internal Examiner
Associate Professor
Mechatronic Systems Engineering
Faculty of Applied Science

Richard Leask
External Examiner
Associate Professor
Department of Chemical Engineering
McGill University

Date Defended: August 11, 2014

Partial Copyright License

Ethics Statement

The author, whose name appears on the title page of this work, has obtained, for the research described in this work, either:

a. human research ethics approval from the Simon Fraser University Office of Research Ethics,

or

b. advance approval of the animal care protocol from the University Animal Care Committee of Simon Fraser University;

or has conducted the research

c. as a co-investigator, collaborator or research assistant in a research project approved in advance,

or

d. as a member of a course approved in advance for minimal risk human research, by the Office of Research Ethics.

A copy of the approval letter has been filed at the Theses Office of the University Library at the time of submission of this thesis or project.

The original application for approval and letter of approval are filed with the relevant offices. Inquiries may be directed to those authorities.

Simon Fraser University Library
Burnaby, British Columbia, Canada

update Spring 2010

Abstract

A multi-sensor based tool has been developed to aid physicians performing clinical exams, focusing on cancer applications. Current research envisions improvement in sensor based measurement technologies to differentiate malignant and benign lesions in human subjects. The tool integrates (initially) three different modalities to detect malignant anomalies: electrical impedance spectroscopy, electronic palpation and skin surface thermometry. These methods each exploit different physical phenomena of tumors that aid in the early detection of cancers but individually are limited for accuracy and reliability. The multimodality tool has been tested over phantoms (tissue equivalent material), in vitro animal tissue (for establishing multi-modality tissue relationships; e.g. tissue mechanical, impedance properties etc.), in vivo healthy human tissue (for tissue characterization confirmation) and in vivo malignant human tissue (tested on skin cancer subjects). Additional decision making algorithms have further resulted in a more objective anomaly detection tool.

As a long-term goal, the development of a low cost, non-invasive, multimodality tool for clinical examination will be a valuable tool in physicians' office. This potentially will reduce health care costs by reducing unwanted diagnostic tests by providing more objective screening examination and will be very useful in improving rural health or in developing countries where screening/diagnostic resources are scarce.

Keywords: Clinical Exam; Palpation; Electrical Impedance Spectroscopy; Skin Surface Thermometry; Decision Making; Multiple Modality Integration

This thesis is dedicated to my husband and children who have always stood by me and dealt with all my absence with a smile

Acknowledgements

I would like to thank Dr. Golnaraghi for his encouragement, guidance and vision for interdisciplinary research. I would also like to thank Dr. Sparrey for her tissue research expertise, her thought provoking discussions throughout this process and for making me a better researcher. Dr. Ash Parameswaran, thank you for explaining me the intricacies of the sensor world. Thank you, Dr. Ramani, to introduce me to the clinical world of cancer diagnosis and treatment. Special thanks to Dr. Kirpal Kohli, Dr. Paris Ingeldew and Dr. Anand Karvat for helping me understand the challenges of clinical studies and helping me perform them.

Thank You Sukhpreet for believing in my goals and providing the support to help me realize them, you are the best husband ever! Thank You to my parents for their blessings and parents–in–law for taking up my responsibilities in all my absence. Thank you to my siblings and cousins for encouraging me and charging me up with all that positive energy.

To my group mates Amr, Hossein, Masih, Majid, Behzaad, Sepideh, Shima, Alex, Waris, Vishwananth, Abhishek who as part of the BCEDL research group have taken a part of this PhD journey with me.

Special thanks to SFU Office of Research Ethics and University Animal Care Committee of Simon Fraser University for providing the biosafety permit level 1 and giving the required approval to conduct the study.

I would also like to thank BCCA to support collaborative research.

Table of Contents

List of Tables

List of Figures

Chapter 1.

Introduction

The growing demand for cost-effective, reliable and easy-to-use screening devices capable of assisting healthcare professionals in decision-making belies the significant advances in computational finesse required to transform raw data into meaningful diagnostic parameters. Accurate on the spot interpretations need real-time signal processing of numerical data and images but they also need to define the stasis of the chosen indicators.

For example, an analysis of tissue can provide vital and significant information about the overall health of the tissue leading to the overall health of an individual. In response to an illness, human tissue reacts in several predictable variations: tissue surface thermal index, tissue precipitation, tissue elasticity, and tissue electrical or optical properties. Tissue parameters differential value comparison may help early detection, better prognosis, reduction in recovery time and resulting diminution in health cost. Can sensors help detect the differences between a lump and a tumor by measuring differential values of tissue parameters?

I propose to develop an intelligent, inexpensive and non-invasive screening tool aiding malignant anomaly detection objectively, to ensure early diagnosis, better prognosis and higher survival rate. Early detection is the best defence against cancer. Imaging techniques play a vital role in early diagnosis, mammography being one of the main techniques used. Ultrasound and Magnetic Resonance Imaging techniques are also popular. Though popular these techniques have limitations in terms of large equipment size and weight, sensitivity, specificity, external administration of energy into the human body- biological effects being harmful, discomfort and pain of patients and not to forget relatively high cost that adheres these techniques to be used widely.

1.1. Background & Overview

Half of the Canadian population (41% females and 46% male) are going to develop cancer during their lifetime; a quarter of them will die of it. Cancer is the leading cause of death in Canada. Cancer has also been the fourth-costliest disease in Canada in 2000, accounting $17.4 billion [1]. These are quite alarming figures and depict the urgent need to perform research in the early cost effective detection of cancer.

Cancer occurs as a result of mutations, or abnormal changes, in the genes responsible for regulating the growth of cells and keeping them healthy. The genes are in each cell's nucleus, which acts as the "control room" of each cell. Normally, the cells in our bodies replace themselves through an orderly process of cell growth: healthy new cells take over as old ones die out. But over time, mutations can "turn on" certain genes and "turn off" others in a cell. That changed cell gains the ability to keep dividing without control or order, producing more cells just like it and forming a tumor.

A tumor can be benign (not dangerous to health) or malignant (has the potential to be dangerous). Benign tumors are not considered cancerous because their cells are close to normal in appearance, they grow slowly, and they do not invade nearby tissues or spread to other parts of the body. Malignant tumors are cancerous. Left unchecked, malignant cells eventually can spread to other parts of the body.

1.1.1. Breast Cancer (BC)

Breast cancer is the most common malignant tumor in women. It is more prevalent than any other cancer in females and accounts for 30% of the new cancer cases in women. In 2008, 1.38 million women were diagnosed and a third died from the disease worldwide [2]. In 2013, 23,800 women and 400 men in Canada were estimated to be diagnosed with the disease [3]. It is estimated that the five year survival rate can be as high as 97% if the cancer is detected early, in a localized state, but drops to only 20% if distant metastases have occurred [4]; yet only 58% of cases are diagnosed at the early stage. Therefore early detection is essential to defend against cancer.

Breast cancer is an uncontrolled growth of breast cells and refers to a malignant tumor that has developed from cells in the breast. Usually breast cancer either begins in the cells of the lobules, which are the milk-producing glands, or the ducts, the passages that drain milk from the lobules to the nipple. Less commonly, breast cancer can begin in the stromal tissues(fatty and fibrous connective tissues) of the breast [5].

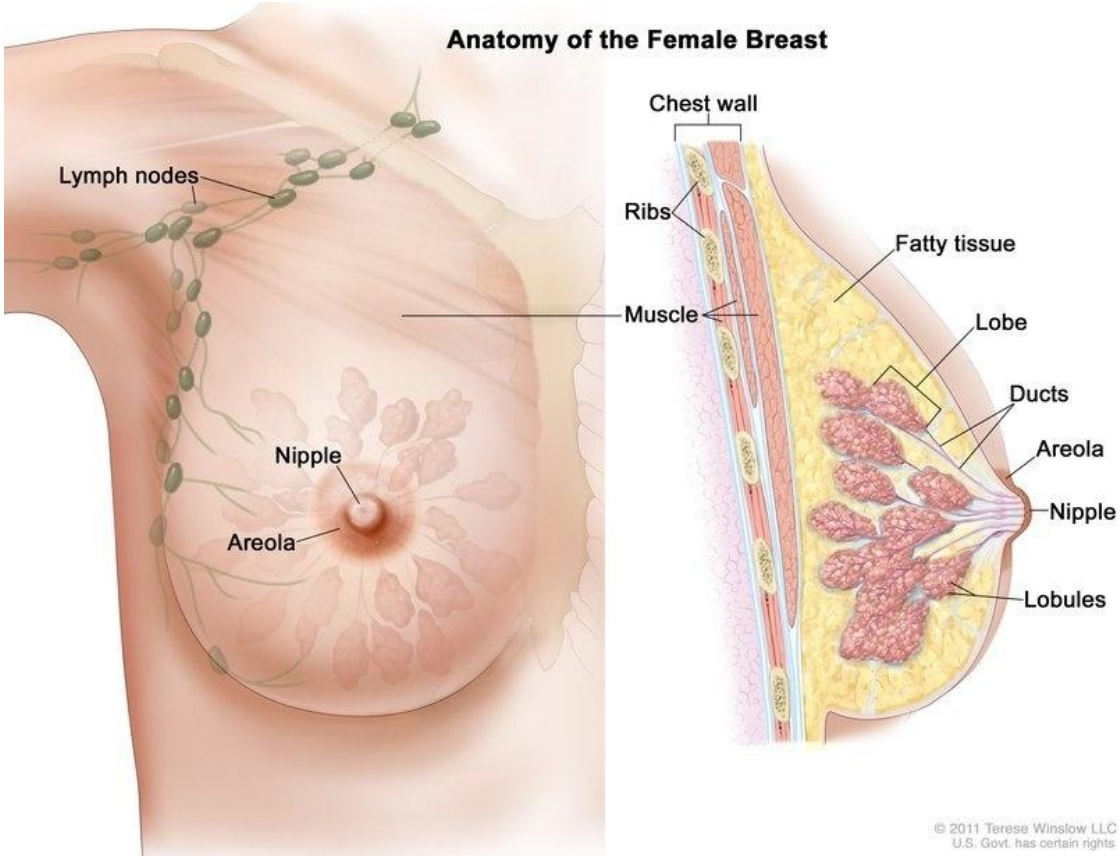

Figure 1-1 Anatomy of the Female Breast (Source: For the National Cancer Institute © 2011 Terese Winslow LLC, U.S. Govt. has certain rights)

The woman's breast sits over the pectoral muscle and extends from the level of 2nd rib to the 6th rib. The breast is an inhomogeneous structure consisting of different layers; however the two predominant types of tissue within the breast are the fat and glandular tissue. Under the skin adipose tissue consists of vesicular cells filled with fat and collected into lobules separated by Cooper ligament. Innermost tissue consists of mammary gland and connective tissue. There are 15-20 sections called lobes with smaller sections termed as lobules (glandular and fat).The tubes lactiferous ducts

connect these sections to nipple. There is abundant fatty tissue along with non-living intercellular matrix. The breast is separated from the great pectoral muscle by the retromammary fat (Figure 1.1). The dimensions and weight of breast can vary substantially between individuals. A small to moderate breast weighs about 500g or less [6], and large breast weighs around 750-1000g [7]. Some women have more glandular tissue; some have more fatty or connective tissue. The ratio of the fat to connective tissue determines the firmness of the breast. The size and shape also vary in the same woman over time due to menstrual cycle, pregnancy, after weaning, and during menopause.

A tumor, an abnormal growth of tissue, generally consists of a basic connective tissue framework, termed stroma, and cells (Figure 1.2 and Figure 1.3). In acellular tumors, stroma predominates and calcifications are common. Fibroadenoma is a common benign tumor of the breast. It shows up as a lump in the breast. A carcinoma is a disorderly growth of epithelial cells. Over time, cancer cells can invade nearby healthy breast tissue and make their way into the underarm lymph nodes. If cancer cells get into the lymph nodes, they then have a pathway into other parts of the body. Breast cancer is always caused by a genetic abnormality (a “mistake” in the genetic material). However, only 5-10% of cancers are due to an abnormality inherited from your mother or father. About 90% of breast cancers are due to genetic abnormalities that happen as a result of the aging process and the “wear and tear” of life in general.

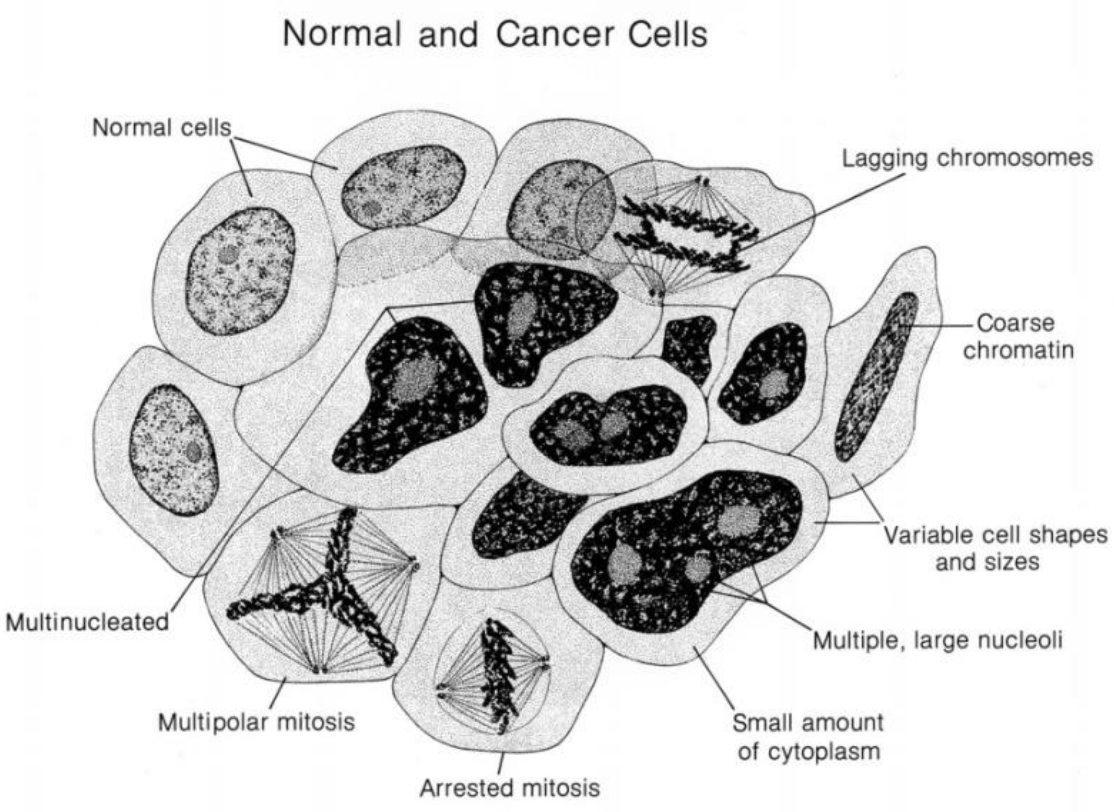

Figure 1-2 Normal and Cancer Cells Structure (Source: NCI, Pat Kenny (Illustrator))

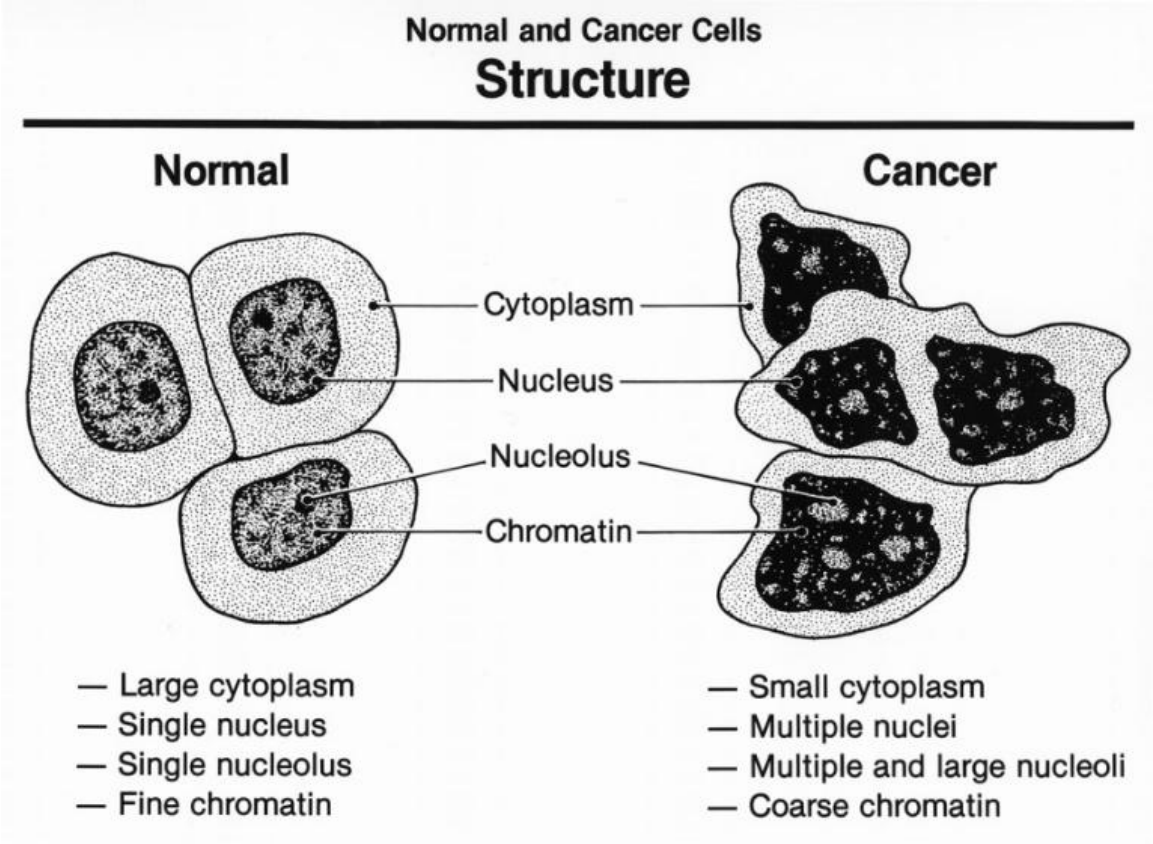

Figure 1-3 Normal and Cancer Cells Structure (Source: NCI, Pat Kenny (Illustrator))

1.1.2. Symptoms of Breast Cancer

Initially, breast cancer may not cause any symptoms. A lump may be too small to feel or to cause any unusual changes noticeable by a patient. Often, an abnormal area turns up on a screening mammogram (x-ray of the breast), which leads to further testing. In some cases, however, the first sign of breast cancer is a new lump or mass in the breast that the patient or doctor can feel. A lump that is painless, hard, and has uneven edges is more likely to be cancer. But sometimes cancers can be tender, soft, and rounded. So it's important to have anything unusual checked by your doctor. According to the American Cancer Society, any of the listed unusual changes in the breast can be a symptom of breast cancer: swelling of all or part of the breast, skin irritation or dimpling, breast pain, nipple pain or the nipple turning inward, redness, scaliness, or thickening of nipple, redness, scaliness, or thickening of breast skin, a nipple discharge

other than breast milk, a lump in the underarm area. These changes also can be signs of less serious conditions that are not cancerous, such as an infection or a cyst.

1.1.3. Breast Cancer Tests

Whether the patient never had cancer and want to increase his/her odds of early detection, has been recently diagnosed, or is in the midst of treatment and follow-up, cancer and medical tests go hand in hand. Most cancer related tests fall into one or more of the following categories:

Screening tests

Screening tests (such as yearly mammograms) are given routinely to people who appear to be healthy and are not suspected of having cancer. Their purpose is to find cancer early, before any symptoms can develop.

Diagnostic tests

Diagnostic tests (such as biopsy and MRI) are given to people who are suspected of having cancer, either because of symptoms they may be experiencing or a screening test result. These tests are used to determine whether or not cancer is present and, if so, whether or not it has traveled outside to other parts.

Monitoring tests

Once cancer is diagnosed, many tests are used during and after treatment to monitor how well therapies are working. Monitoring tests also may be used to check for any signs of recurrence.

1.2. Stages of Breast Cancer

Table 1.1 Stages of Breast Cancer (National Cancer Institute)

Stage	Definition
Stage 0	Cancer Cells remain inside the breast duct, without invasion into normal adjacent breast tissue.
Stage IA	The tumor measures up to 2 cm AND the cancer has not spread outside the breast; no lymph nodes are involved
Stage IB	There is no tumor in the breast; instead, small groups of cancer cells -- larger than 0.2 millimeter but not larger than 2 millimeters – are found in the lymph nodes OR there is a tumor in the breast that is no larger than 2 centimeters, and there are small groups of cancer cells – larger than 0.2 millimeter but not larger than 2 millimeters – in the lymph nodes.
Stage IIA	No tumor can be found in the breast, but cancer cells are found in the axillary lymph nodes (the lymph nodes under the arm) OR the tumor measures 2 centimeters or smaller and has spread to the axillary lymph nodes OR the tumor is larger than 2 but no larger than 5 centimeters and has not spread to the axillary lymph nodes
Stage IIB	The tumor is larger than 2 but no larger than 5 centimeters and has spread to the axillary lymph nodes OR the tumor is larger than 5 centimeters but has not spread to the axillary lymph nodes.
Stage IIIA	No tumor is found in the breast. Cancer is found in axillary lymph nodes that are sticking together or to other structures, or cancer may be found in lymph nodes near the breastbone OR the tumor is any size. Cancer has spread to the axillary lymph nodes, which are sticking together or to other structures, or cancer may be found in lymph nodes near the breastbone.
Stage IIIB	The tumor may be any size and has spread to the chest wall and/or skin of the breast AND may have spread to axillary lymph nodes that are clumped together or sticking to other structures or cancer may have spread to lymph nodes near the breastbone.
Stage IIIC	There may either be no sign of cancer in the breast or a tumor may be any size and may have spread to the chest wall and/or the skin of the breast AND the cancer has spread to lymph nodes either above or below the collarbone AND the cancer may have spread to axillary lymph nodes or to lymph nodes near the breastbone.
Stage IV	The cancer has spread — or metastasized — to other parts of the body.

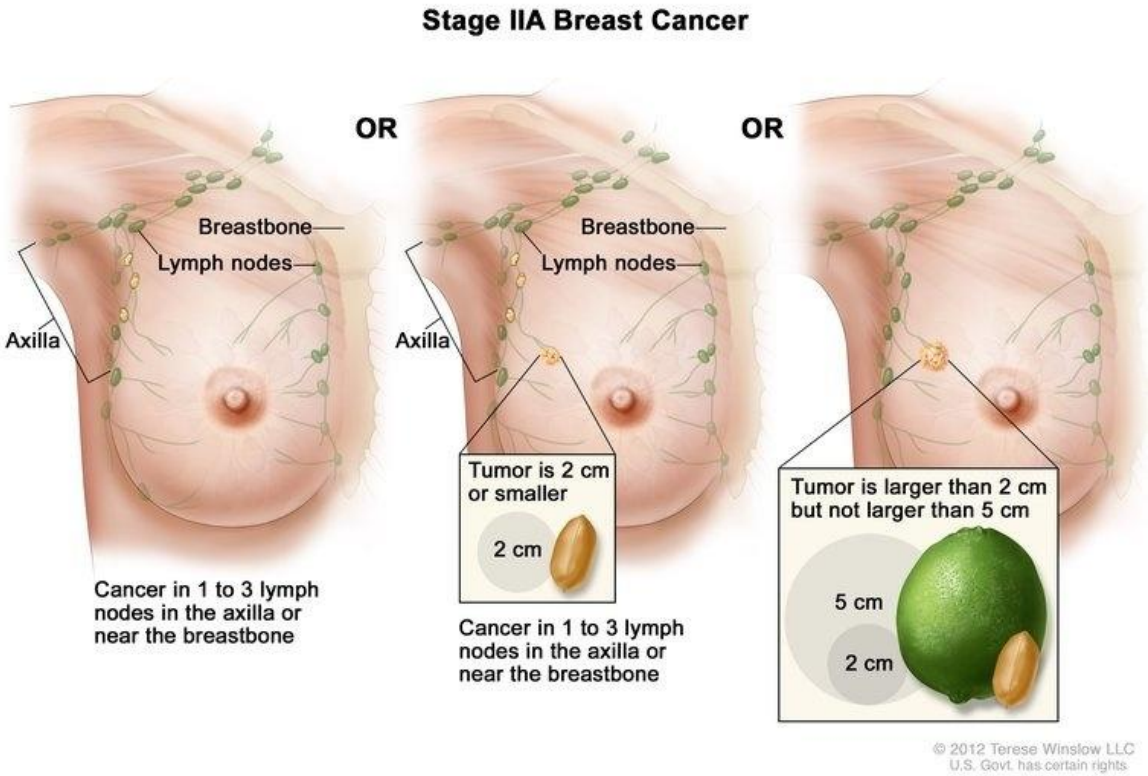

Figure 1-4 Stage IIA Breast Cancer (For the National Cancer Institute © 2012 Terese Winslow LLC, U.S. Govt. has certain rights)

1.3. Current Breast Cancer Detection Techniques

1.3.1. X-Ray mammography

The golden standard for screening breast cancer is X-Ray mammography[8] as; regular screening for breast cancer can reduce the mortality rate due to breast cancer[9][10]. X-ray imaging is a transmission-based technique in which X-rays from a source pass through the patient and are detected either by film or an ionization chamber on the opposite side of the body. Contrast in the image between different tissues arises from differential attenuation of X-rays in the body. Analysis of the mammogram includes an assessment of breast density, categorized as almost entirely fat, scattered fibro glandular densities, heterogeneously dense, and extremely dense. The density of the breast is significant, as the latter categories may obscure lesions and decreases the sensitivity of mammography. As demonstrated in randomized controlled trails, the

widespread use of screening mammography has significantly reduced breast cancer mortality.

Another form of X-ray screening is the X-ray computed tomography (CT).In CT, the X-ray source is tightly collimated to interrogate a thin slice through the patient. The source and detectors rotate together around the patient, producing a series of one-dimensional projections at a number of different angles. These data are reconstructed to give a two dimensional image and provide a reasonable contrast between soft tissues. The mathematical basis for reconstruction of an image from a series of projections is the Random transform. CT results in a very high radiation dose and is not advised for regular screening.

The Digital Breast Tomosynthesis also utilizes X-ray. Digital breast tomosynthesis uses a modified digital mammography platform in which the X-ray tube moves in an arc over the breast during the exposure. Patient positioning is similar to conventional mammography, although less compression is used. Radiation dose is comparable with standard digital mammography. This allows for a 3D examination of the entire breast volume. Recent research suggests that tomosynthesis is at least, if not more, accurate in assessing tumor size and stage compared with digital mammography. This technology is currently under FDA review. Digital mammography is more sensitive for detecting breast cancers in younger women. Research has demonstrated that for women younger than 50 or who have dense breast tissue, detection is higher with digital mammography. The Dedicated Breast CT uses cone beam geometry to scan the breast. The patient lies prone on a special CT scanner table and places one breast through an opening in the table. The CT scanner and detector rotate 360 degree around the pendant breast, gathering cross-sectional slices which are then reformatted into 3D image. The radiation dose is similar to standard digital mammography. This examination may be beneficial in women with dense breasts. Breast CT is not currently approved by the FDA.

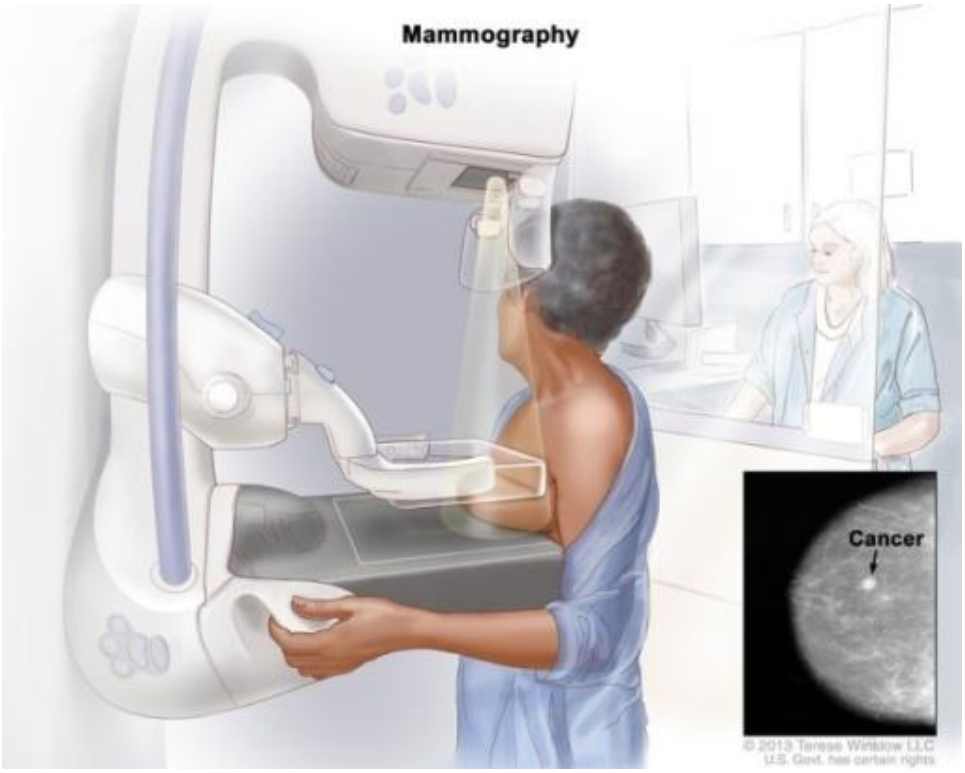

Figure 1-5 Mammography set Up (Source: For the National Cancer Institute © 2013 Terese Winslow LLC, U.S. Govt. has certain rights)

However, despite mammography screening programs across Canada, less than 75% of eligible women undergo regular screening and its efficacy is debatable for younger women with denser breasts. It also suffers from a high recall rate of 11% [11] and significant false negative detection rate from 4% to 34% [12][13]. Women living in rural areas may have decreased access to screening programs as well. Marginalized women (e.g. immigrants, low income) may also have barriers to screening mammography. Furthermore, mammography is: costly, requiring specialized X-ray equipment and skilled technicians; uncomfortable for the patient; and exposes the breast to a significant amount of radiation, a risk not deemed suitable for younger women where early repeated radiation exposure can lead to secondary malignancies later in life. In developing countries, where breast cancer rates are skyrocketing, the introduction of mammographic screening is cost prohibitive [14][15].There has also been debate regarding using mammography for screening [16]. The ionizing X-ray in mammography can result to cancer development [17][18].

The mammography screen test sensitivity is around 91% at 10mm size of tumor and highest for invasive ductal carcinoma(81%)[19] but screening mammography may miss tumors of lobular or mucinous histology and some rapidly proliferating, high-grade tumors [20].The limitations of mammography open doors to develop alternative breast cancer detection techniques.

1.3.2. Clinical Breast Examination

The common practice for women undergoing an annual physical examination is clinical palpation provided by their family physicians. The clinical breast examination (CBE), like any part of the physical examination, can be used either for screening (to detect breast cancer in asymptomatic women) or diagnosis (to evaluate breast complaints, primarily to rule out cancer). In primary care, screening CBEs are more commonly performed than diagnostic CBEs. CBE by health professionals is still the only way that more than 10% of breast cancers are detected. CBE is non-invasive and very cost effective technique of screening lumps in breast. Half of the breast cancers are still found by the patients themselves leading to the utmost importance of CBE [21][22]. Starting at age 40, women should have a CBE by a health professional every year, while American Cancer Society now recommends that women in their 20s and 30s should also have CBE by a health professional, at least every three years [23][24]. Also, some women are more willing to accept screening CBE than mammography [25], in which case screening CBE is particularly important. Therefore CBE is an effective, safe, and low-cost alternative, with diagnostic mammography available when so indicated[26].

CBE can find tumors that have only grown to a palpable size, the easiest to detect are those that are large, firm and near the surface [27]. Physician may detect lumps as small as 3.0 mm by CBE [28], which is well within the size range for survival advantage. However, the reported size when breast cancers become operationally detectable in absence of mammographic screening is 15 mm (symmetric around median), and with screening is 7.5 mm (asymmetric around median)[29].

1.3.3. Ultrasound / Elastography

An ultrasound image is created real-time from the reflections of the high-frequency sound waves that are produced and received by the ultrasound transducer. It is now frequently possible to distinguish malignant from benign solid lesions, and from complicated fluid collections. Ultrasound is convenient, is widely available, is relatively inexpensive, and does not require compression or intravenous contrast. Some patients believe it to be an attractive alternative to mammography. However, it must be stressed that ultrasound is not a substitute for mammography due to the considerable overlap benignancy and malignancy in ultrasound images and subjective interpretation. Breast ultrasound is a powerful adjunctive tool in the detection and treatment of breast abnormality. For patients younger than 30 years, only ultrasound may be performed. Ultrasound is typically useful to differentiate cysts from tumors [30]. Ultrasound in combination with mammography can increase cancer detection rate and is particularly useful in women with dense breasts; however, the false positive rate does increase [31]. Ultrasound also suffer from a false negative rate of 17% [32].

1.3.4. Magnetic Resonance Imaging (MRI)

Among all breast imaging modalities, MRI has the highest sensitivity for the detection of invasive breast carcinoma. Sensitivity of MRI is not decreased by the density of the fibro glandular tissue, presence of scar tissue, radiation therapy changes, implants or breast remonstration. Food and Drug Administration (FDA) approved computer-aided detection software systems are commonly used to analyze MR images. MRI is quite expensive and has low specificity therefore leads to over diagnosis [33][34].

1.3.5 Comparing the clinical utility and accuracy of each technique

Among the established diagnostic procedures for breast screening and the following treatment procedure, palpation, mammography, and ultrasound represent the standard of care. However, these classical techniques offer yet insufficient selectivity for biopsy. In one study[21], the false positive result was 49.1%, after 10 mammograms (9762 screening mammograms were used in the study), out of 5 patients biopsied only one tissue sample led to a malignant histological diagnosis. In another study,10-25% of

breast lesions were not even detected by the aforementioned methods in a 2 year follow up study [35]. This low sensitivity is attributed to dense breast tissue common in younger patients and post-menopausal women undergoing hormone replacement therapy[35].

In one study[32], 258 patients were tested using four cancer detection technologies: MRI, US, Clinical Examination and mammography. There were 177 patients with malignant tumors and 81 patients with benign tumors. The parameters used to test each detection technique were: sensitivity, specificity, positive predictive value, and accuracy. The parameters are defined as follows:

$$\text{Accuracy} = \frac{\text{No. of patients correctly diagnosed benign or malignant}}{\text{Total number of patients}} \quad (1)$$

$$\text{Sensitivity} = \frac{\text{No. of malignant tumors detected}}{\text{Total number of patients with malignant tumors}} \quad (2)$$

$$\text{Specificity} = \frac{\text{Patients correctly classified having benign tumors}}{\text{Total number of patients with benign tumors}} \quad (3)$$

$$\text{Positive Predictive Value} = \frac{\text{Patients correctly diagnosed with malignant tumor}}{\text{Total number of positive diagnoses}} \quad (4)$$

The total number of positive diagnoses consists of patients with malignant tumors correctly diagnosed as positive in addition to patients with benign tumors incorrectly diagnosed as positive. The study consisted of combining different stated technologies to detect the improvement in cancer detection. Table 1.2 summarises the results:

Table 1.2 Comparison of performance of Different Breast Cancer Detection Techniques

Modality	Sensitivity	Specificity	Positive Predictive Value	Accuracy
Mammography	67.8% (120/177)	75% (61/81)	85.7% (120/140)	70.2% (181/258)
Mammography and Clinical Examination	77.4% (137/177)	72% (58/81)	58.6% (137/160)	75.6% (195/258)
Clinical Examination	50.3% (89/177)	92% (75/81)	94% (89/95)	63.6% (164/258)
Ultrasound	83.0% (147/177)	34% (28/81)	73.5% (147/200)	67.8% (175/258)
Mammography and Ultrasound	91.5% (162/177)	23% (19/81)	72.3% (162/224)	70.2% (181/258)
Mammography, Clinical Examination and Ultrasound	93.2% (165/177)	22% (18/81)	72.4% (165/228)	70.9% (183/258)
MRI	94.4% (167/177)	26% (21/81)	73.6% (167/227)	72.9% (188/258)
Mammography, Clinical Examination, MRI	99.4% (176/177)	7 (6/81)	70.1% (176/251)	70.5% (182/258)

The highest sensitivity 99.4% corresponded to using Mammography, Clinical Examination, and MRI together, but the specificity decreased to 7%. The highest achieved accuracy was only 75.6%, for Mammography and Clinical examination combined together.

A review done on available electromagnetic techniques for breast cancer detection [36] discusses the available alternative technologies to mammography and their short comings. The paper reviews the modalities: microwave, electric impedance tomography, diffuse optical tomography, microwave radiometry, bio-potential and bio-magnetic and Magnetic Resonance Imaging (MRI). Other alternatives include Breast Specific Gamma Imaging (BSGI), Microwave Imaging, Electrical Impedance Tomography (EIT), Diffuse Optical Tomography, Microwave Radiometry, Thermography, Bio-potential Detection and Magnetic Resonance Imaging (Table 1.4).

Table 1.3 Advantages/Disadvantages of various breast cancer detection technologies

Technology	Advantages	Disadvantages
X-ray mammography	Approved by FDA, relatively high specificity, low cost, widely available	False negative detection is relatively high, Ionizing, low accuracy
Digital breast tomosynthesis	May decrease recall rates in screening mammography, as accurate as digital mammography in assessing tumor size	Ionizing radiation(comparable to digital mammography)
Dedicated breast CT	High resolution and sensitivity, better visualization of masses, no breast compression, 3D	Ionizing radiation, calcifications not as well visualized as with mammography
Ultrasound	**Non-invasive** imaging system, widely available, relatively inexpensive, high sensitivity, does not require compression	Low specificity and positive predictive value, for younger than 30 years old or dense breast , adjacent technique
Elastography	Non ionizing radiation, improved specificity compared to ultrasound, noninvasive imaging system	Operator dependent, may not improve diagnostic accuracy of ultrasound, adjacent technique
Breast-specific gamma imaging	High sensitivity, moderate to high resolution, functional imaging, not limited by breast density or implants, FDA approved adjunct	Requires radiotracer injection, long imaging time, higher radiation dose than mammography, systemic distribution of radiation dose, adjacent technique
Positron emission mammography	High sensitivity, high resolution, not influenced by breast density or hormone status, FDA approved adjunct	Requires radiotracer injection, higher radiation dose than mammography, requires fasting, 1 hour delay for imaging, adjacent technique
Electrical Impedance Tomography/EIS	**Non-invasive** ,2D AND 3D, imaging system, relatively high resolution, **FDA approved**	Difficulty in detecting tumors close to breast nipple, very dependent to breast tissue, operator dependent
MRI	High sensitivity, relatively high accuracy, for dense breast, **FDA approved**	High cost, low specificity
MR spectroscopy	**Non-ionizing radiation**, quantitative, can increase specificity of MRI, early tumor response to neo adjuvant chemotherapy, **FDA approved adjunct**	Voxal placement is operator dependent, technical challenges, more suitable for large tumor, adjacent technique
Diffuse Optical Tomography	High accuracy, relatively high specificity and sensitivity,	Typical imaging depth is in the range of 5 to 10cm,
Microwave	Relatively high accuracy(under study), **Non-ionizing**	Accuracy reduced in younger/dense breast patients, low contrast
Thermography	**Non-invasive**, Detects fast growing active tumors, for dense breasts, **FDA approved**	High false positive rate

1.4. Motivation for the Research

North America breast cancer statistics for the past years show an alarming number of breast cancer diagnosed cases [37] as compared to other cancers. In 2013, it was expected to diagnose about 256,140 women with breast cancer in North America. It was also anticipated that 44,620 women would die from breast cancer in 2013 in Canada and USA [1], [38]. As early detection is one of the best defences against breast cancer, the survival rate increases to 97% from 20% [4]; therefore, I wanted to work on a breast cancer detection method that is effective in finding the tumor in the early stages rather than distant metastases when survival rate decreases. In developing countries the breast cancer rates are skyrocketing and the introduction of mammographic screening cost prohibitive [14]. This further motivated me to work in this field. Currently, the incidence in the developed and developing world is similar but, whereas incidence rates are tending to plateau or decline in the west, they are increasing in the developing world, presumably related to changes in dietary and reproductive behaviours and ageing populations [2][15]. Whilst mortality is declining in most western countries, it is estimated that it will increase by over 100% in developing countries by 2020 [15]. As compared to developed countries the total mortality rate in developing countries is higher [2]. Whereas less than one-third of women diagnosed with breast cancer in developed countries die from the disease, this proportion reaches over two-thirds in developing countries and is directly related to income per capita [2][39]. Berry and colleagues [40] developed a series of independent statistical models of breast cancer incidence in order to determine the relative importance of the contribution of mammographic screening and adjuvant therapy to the marked decline in breast cancer mortality in the majority of developed countries. They estimated the mortality decline was related equally to screening and therapy and that mortality would increase in countries with limited facilities for screening and treatment.

Through new collaboration with BC Cancer Agency it was recognized that for screening breast tumors early there was limited non-invasive cost effective technology available. After a thorough literature review it was found that the palpatory self-examination of breast is a widely advised preclinical testing method. Half of the breast tumors are diagnosed by CBE (refer section 1.3.2), but lacks standardisation and is

highly dependent on the skill of the physician performing the exam. Another non-invasive method capable of early tumor detection is Electrical Impedance Spectroscopy (EIS); the method has been used for differentiating benign from malignant tissue. Further, a non-invasive tumor screening methodology with FDA approval is thermography imaging (refer table 1.4); the technique has been studied by researchers since decades however; high rate of false positive results has limited the technology from becoming a standard early detection method.

A multimodality approach was envisioned through miniaturization and modification of the aforementioned technologies, using multiple force sensors with normalisation algorithms, multi frequency Electrical Impedance Spectroscopy (EIS) system and Long Wavelength Infrared (LWIR) sensors with decision making algorithms.

1.5. Research Objectives

The primary objective of this research was to develop a multimodality based non-invasive and cost effective supplementary malignant tissue screening tool, based upon tissue classification, to aid physicians during clinical examination and provide more accurate and possibly earlier detection of malignant anomalies.

To accomplish the primary objective, a series of secondary objectives were established:

- To determine the modalities, develop the integrated hardware after identifying modality based off the shelf sensors and develop the associated software algorithms.
- To establish testing procedures and protocols to test each modality individually over tissue equivalent material ‘phantoms’.
- To establish decision making capability into the system by obtaining training and testing data over phantoms to identify the extent to which the tool is capable of classifying tissue based upon individual modalities.
- To test the multimodality system over *in vivo* healthy tissue to establish the usability of the tool
- To test the multimodality tool over *in vivo* malignant tissue to establish the usability of the system to detect tumors and verify acceptable working of the tool for the proposed application

- To create a foundation of common ground to facilitate collaboration between the Departments of Mechatronic Systems Engineering, Simon Fraser University, BC Cancer Agency Fraser Valley Cancer Centre and Fraser Health Authorities.

1.6. Research Scope

This research focused on the development of a multimodality tool for early detection of breast cancer. The research encompasses the validation of the tool with decision making capability over phantoms and *in vitro* animal tissue. Due to variation in tissue properties after death, especially electrical impedance, the testing of the tool was required to be done over *in vivo* tissue. The sample size for *in vivo* healthy tissue testing is limited to 20 subjects, based upon resource equation method [41] that states a requirement of minimum 11 subjects for complex biological experiments with quantitative outcomes.

The study was limited to testing the tool over malignant skin tumors with contralateral healthy tissue as control, allowing for the possibility of measuring multimodality tissue characteristics, verifying the advantage of multimodality concept over single modality approach. The sample size was limited to 6 subjects due to the unavailability of inclusion criteria based population. Further talks with the Oncologist have been initiated to include a dermatologist to have greater access to specific patient population.

Verification of breast tumor detection was beyond the scope of the work because building and testing the tool was already a significant contribution to the work. Verification can only be done once the tool is shown to be operational. The diagnostic capabilities of the tool in regard to the specificity and sensitivity of the tool need to be determined following standard clinical trial methodology. That is for future work

1.7. Thesis Outline

Chapter one is the introduction to the thesis discussing the background of breast cancer, its symptoms, and the tests involved in detecting breast cancer and the

prevalent system for grading breast cancer. Section 1.2 is about the various stages of breast cancer and section 1.3 elaborating on the commonly used breast cancer detection techniques. The chapter ends with the objective, scope and motivation for the present research.

Chapter two is based upon the multimodality concept. The hardware and software development of a multimodality device has been detailed, leading to the development of a multimodality glove. The built graphical user interface and real time data collection capabilities have been elaborated in section 2.3 followed by the discussion and conclusion.

Chapter three, four and five discuss each modality individually and the validity of the device to measure each modality. The validation is performed over phantoms. After validation decision making algorithms have been incorporated into the system. In vivo healthy human tissue data has been collected using the developed device and decision making algorithms have been integrated, followed by the discussion and conclusion of the results.

This research was not complete until the multimodality device was validated over malignant tissue. Chapter six discusses six cases of data collected over malignant tissue and comparison of the extracted parameters to contralateral healthy tissue.

Overall conclusions, discussion and future work of the research work have been elaborated in chapter seven.

Chapter 2.

Tissue Anomaly Screening Technology: Multimodality Concept

2.1. Introduction: Multimodality Concept

To develop an optimum tool it is first required to understand the growth of tumor cell and the histological and molecular types of breast cancer. Most normal cells undergo a programmed form of death. However, when normal cells get activated by oncogenes they change the designated path of apoptosis to survive and proliferate instead; leading to tumor. Breast tumors show distinctive histological patterns and different biological features and clinical behaviours. The WHO (World Health Organisation) classification of breast cancer shows 50-80% of breast carcinomas to be invasive ductal carcinomas (IDC) and 5-15 % invasive lobular carcinomas (ILC). 'Histological special types' account for 25% of all breast cancers [42]. Therefore, most of the breast tumors are either ductal carcinomas or lobular carcinomas. Results from a large data set study[43] concludes that ILC and IDC are different entities with different clinical courses and different biologic phenotypes.

Studies show that the false-negative rate for the diagnosis of invasive lobular carcinoma ILC is higher than that of other invasive cancers, due to low rate of suspicious calcification found with invasive lobular carcinoma and its tendency to be of low opacity[44].

The primary method and gold standard in breast cancer screening is mammography (refer to section 1.3.1). The utmost importance of regular screening is depicted in the fact that it has led to decreased frequency of palpable presentation as presented in a study in 2010 [45]. Mammography was able to pick up 57% of the tumors

and 43% of these were palpable. The detected palpable tumors were more prevalent in patients with no previous screening and in younger patients. Breast cancers were missed in screening in patients with higher breast density. Out of the 43% palpable tumors 86% of the cancers were found by patient incidentally or during breast self-examination and 14% were detected during Clinical Breast Examination (refer to section 1.2.2). The study shows that both BSE and CBE still play a role in detecting breast cancer. Radiation exposure and reduced sensitivity and specificity of mammography in dense breast tissue, commonly seen in young patients, also support the importance of CBE/BSE. Therefore CBE is an effective, safe, and low-cost complimentary modality, with diagnostic mammography available when so indicated.

The usefulness of the CBE is, however debated, due to the subjective nature of each clinician's diagnostic decision making. Studies show that physicians felt a need to improve their techniques in CBE [28]. In that study one third physicians judged that their training during and since medical school was inadequate and urged improved training and accuracy. The objective of CBE screening is earlier detection of cancer; failure to do so may even have legal implications [46]. The general limitations of CBE include the special skills to perform the examination, the subjectivity, and the low sensitivity involved in the technique. Results from community practice showed sensitivity ranging from 28% to 54% [47][48][49] [50]. In one study 40% of physicians (34 out of 80) who performed a breast examination on manufactured breast models used no discernible systematic search pattern at all [28]. The sensitivity of examinations improved by spending more time [47][51] and by using a thorough, systematic technique [28], [47][48][49],[50]. To overcome these limitations, devices have been developed using pressure sensor arrays such as the SureTouch™ by Medical Tactile Inc. [52], but such a device takes away the physicians personal sense of touch and is limited by diagnosis only based upon a single pressure modality. The drawbacks of CBE regarding subjective nature of each clinician's diagnostic decision making and the general limitations of CBE including the special skills to perform the examination and the subjectivity involved in the technique were the issues that needed to be addressed by developing a non-invasive and cost effective supplementary screening too.

Previous studies have demonstrated an increase in diagnostic sensitivity when several modalities are combined; however, the technologies used in those studies were each the size of a physician's office and were prohibitively expensive [30]. Another study involving the correlation of image information from EIS (Electrical Impedance Scanning), NIR(Near Infrared Imaging),and MIS(Microwave Imaging Spectroscopy) resulted in improving the overall reliability of tumor detection [53]. Due to the complexity of diagnosing breast disease and the wide variation in breast tissue composition, it is essential to utilize combined information from multiple modalities to provide a more complete screening tool.

This research aims to decrease the false positive results of CBE and improve sensitivity through development of a non-invasive and cost effective screening tool capable of providing supplementary information about anomalies leading to earlier detection. Currently considered non-invasive, early tumor detection modalities include CBE through electronic palpation, Electrical Impedance Spectroscopy (EIS), and Tissue Thermal Analysis (usually performed as thermography). The selection is based upon the criteria that these techniques are well known for early breast cancer detection with FDA approval (refer to table 4) and are non-invasive, cost effective and capable of detecting different kinds of tumors as each one of them provides supplementary information regarding the anomaly. The non-invasive technologies use different tissue characteristics to determine anomaly. The stiffness (Young's modulus of the cells) of the tissue changes due to increased cell packing density leading to development of lumps that are screened during CBE, while the electrical impedance of the tissue changes due to the change in the cellular water and sodium content and thermal characteristics change due to the high volume of blood required for the fast growing cancer cells. The hypothesis in this research is that the clinical examination for tumor detection will improve when information from multiple non-invasive sensor technologies is combined together and artificial intelligence is added for decision making.

BSE/CBE is useful in detecting palpable tumors of breast [45], that constitute 43% of the total breast tumors. Patients with palpable tumors usually have larger tumor sizes and more advanced stages[45] (Figure 2.2). By the time cancer is detected by CBE, it is at a more advanced stage. The sensitivity of detecting palpable masses is

increased using electronic palpation [52]. To improve CBE non-palpable cancerous masses need to be detected along with palpable masses. Electrical Impedance Spectroscopy has the ability to detect non palpable tumors in dense breast [54], where mammography is not recommended and CBE suffers from lower sensitivity. The study [54] states that EIS has higher sensitivity in detecting smaller (≤10mm) tumors than larger tumors (>10mm). EIS is capable of identifying women at high risk of breast cancer, in the absence of a specific lesion that can be localized. EIS is useful for identifying patients in need of additional diagnostic imaging and clinical follow-up. EIS also overcomes some challenges associated with mammography screening of young women: it is non-invasive, is free of radiation, and is associated with minimal risk. The device is also easy to use and breast tissue density does not alter algorithm performance. The high specificity of EIS reduces the need for unnecessary additional testing and potentially invasive diagnostic procedures. The study [54] hints and concludes that EIS may become an integral part of breast cancer screening, a process considered to be deficient when young women are examined with CBE alone. The study also states that this technology could be developed for use during routine periodic examination of women at the gynaecologist or general practitioners office. Additionally, invasive ductal carcinomas (IDC) that constitute 50-80% of breast cancer[42] can be detected early using Electrical Impedance Spectroscopy (Figure 2.1) as Ductal Epithelial Impedance Spectroscopy[55].This study concludes that electrical signature of ductal epithelium may be used to identify patients with benign, proliferative or malignant breast disease. During early stages of carcinogenesis, increase in electrical resistance dominates the ductal epithelial profile, whereas later as breast tumors become invasive and cell mass increases, resistance decreases and tumor capacitance increases. Besides the IDC and Lobular Ductal Carcinoma (LDC), 'Histological Special Types' carcinomas account for 25% of all breast cancers. The diffuse disease type is usually inflammatory type with no distinct margins. Thermography is capable of picking up such aggressively growing anomalies (Figure 2.3). Breast thermography is a non-invasive and non-contact imaging techniques used in the medical imaging area and it can be used as an adjacent imaging tool in the early detection of breast cancer (screening), diagnosis and monitoring [56]. It is based on the principle that chemical and blood vessel activity in both pre-cancerous tissue and the area surrounding a developing breast cancer is usually higher than in the normal breast. Since pre-cancerous and

cancerous masses are highly metabolic tissue, they need an abundant supply of nutrients to maintain their growth (metabolic activity) and this can increase the surface temperature of the breast 1 to 3ºCelsius[57-58]. Though, thermography has high sensitivity and negative predictive value[58], but is not accepted as an stand-alone screening technology for breast cancer [60-62]. Breast thermography has an average sensitivity and negative predictive value of 90% and does not require ionizing radiation, compression, contact or intravenous injection. When used with mammography, thermography has been found to increase the sensitivity of mammography from 83% to 93% and a combination of clinical examination, mammography and thermography increased the sensitivity to 98% [62], [63].

Conclusively, the three modalities: CBE through electronic palpation, EIS and thermal analysis together are capable of detecting nearly the full spectrum of the various types and stages of breast tumors much earlier than traditional CBE alone.

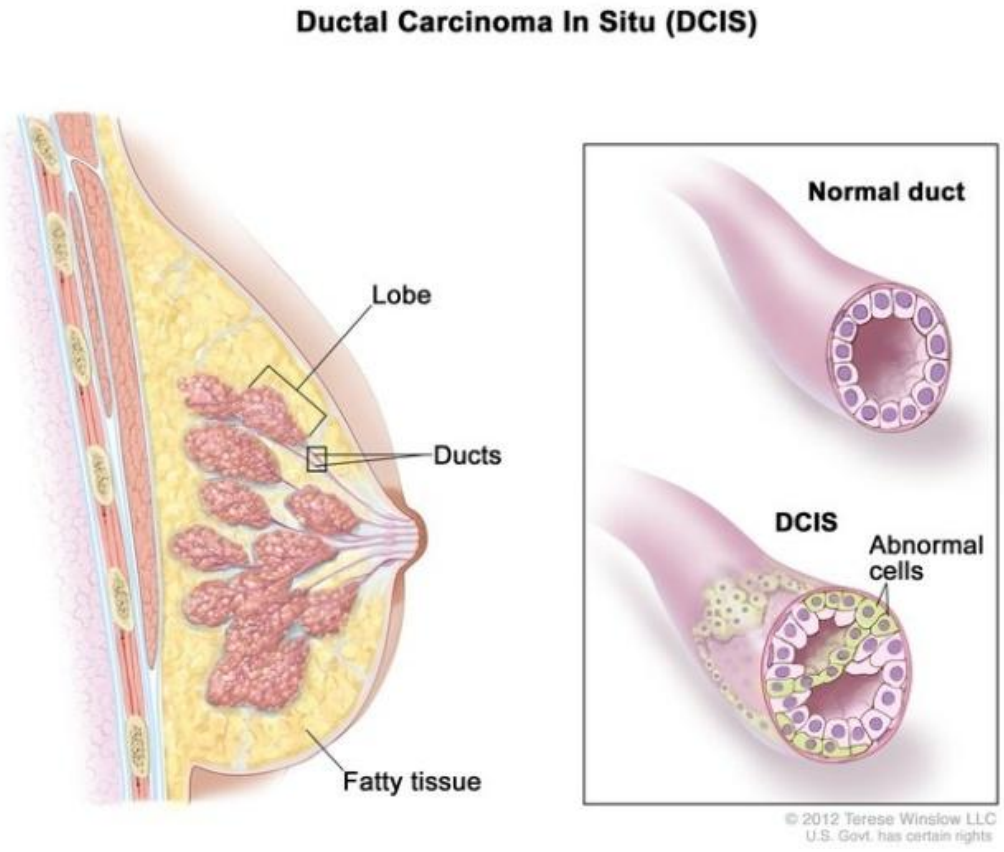

Figure 2-1 Electrical Impedance Spectroscopy is useful in detecting DCIS (Source: DCIS For the National Cancer Institute © 2012 Terese Winslow LLC, U.S. Govt. has certain rights)

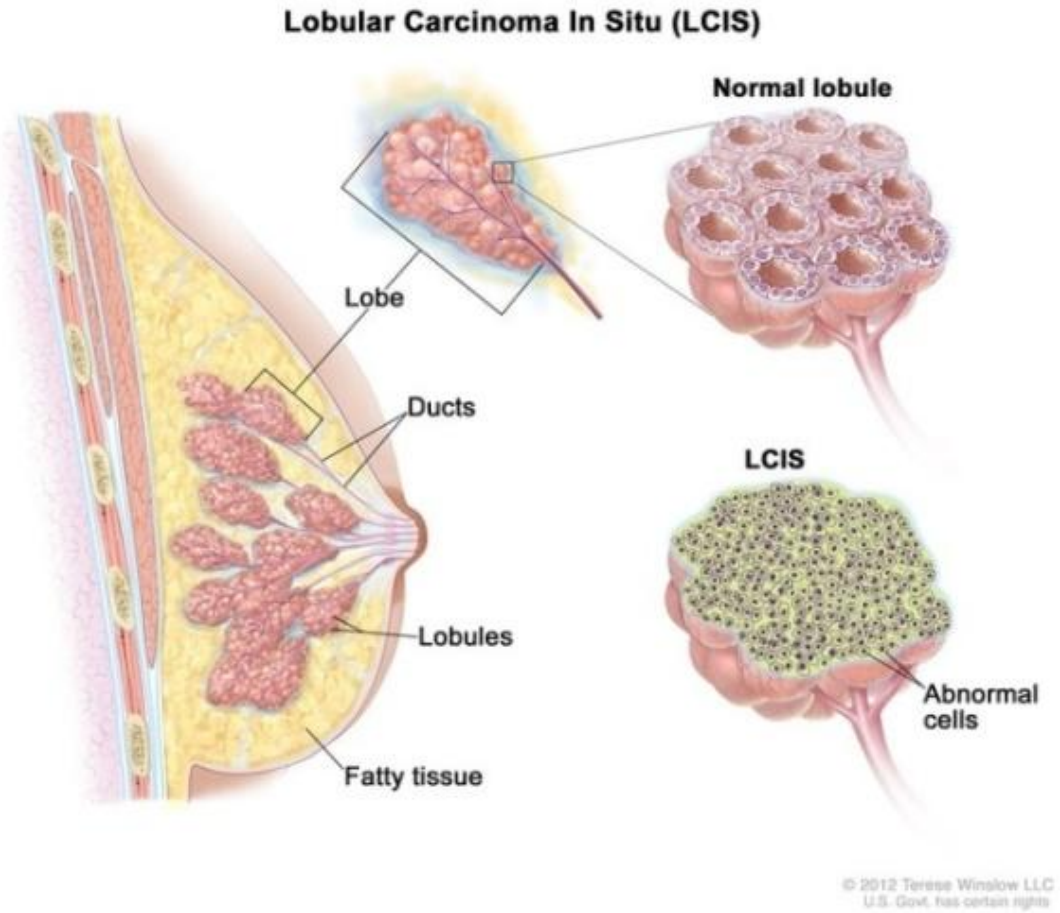

Figure 2-2 Clinical Breast examination is useful in detecting LCIS (Source: LCIS For the National Cancer Institute © 2012 Terese Winslow LLC, U.S. Govt. has certain rights)

Figure 2-3 Thermography is useful in detecting Inflammatory Breast Cancer (Source: For the National Cancer Institute © 2007 Terese Winslow, U.S. Govt. has certain rights)

A novel way to improve CBE and overcome its limitations was to develop a glove that has aforementioned non-invasive tumor detection technologies integrated in it along with the capability of decision making. The objective was to develop a "Cancer Screening (decisive) Glove" that incorporates multiple sensors integrated as smart sensory units embedded in the glove. The originality lies in enhancing the physician's diagnostic capabilities by providing supplementary screening information without taking away the physician's sense of touch in performing CBE. The developed non-invasive and cost effective screening glove prototype will be a supplementary tool to aid physicians during clinical breast examination and provide more accurate and possibly earlier detection of anomalies. The prototype "screening glove" will incorporate wearable multi force sensors for electronic palpation, Ag/AgCl electrodes with impedance spectroscope for EIS and Long Wavelength Infrared (LWIR) temperature sensors for tissue thermal analysis, all incorporated as a single entity, as shown in Figure 2.4. A trainable intelligent software support tool, capable of assisting healthcare professionals in diagnostic decision-making will help transform the sensor generated raw data into meaningful diagnostic parameters.

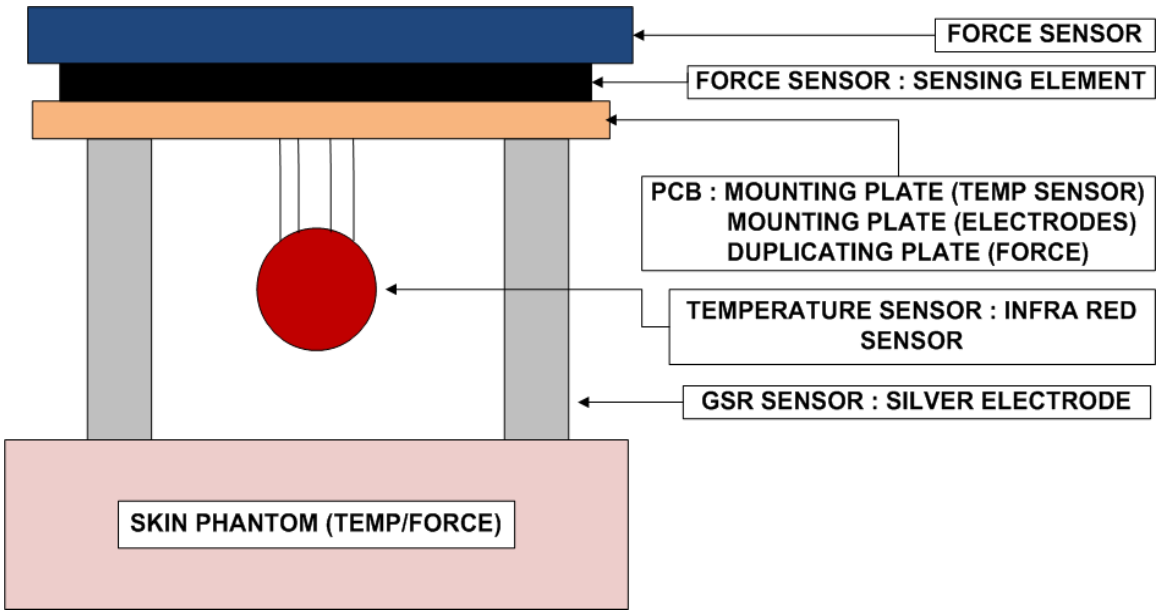

Figure 2-4 Multimodality concept based integrated Sensor Design

The innovation in present research is in the multimodality concept and integration of three different tumor detection modalities into an affordable and accessible screening glove. Thus making this advanced screening capacity available as a preliminary screening technology in a general practice setting. Miniaturization of these technologies should not take away the usefulness of the technology to provide tissue information. For example, smart thermometer technology for detection and monitoring of more than 100 diseases has been recently introduced [64] as a miniaturized form of the thermography concept.

The concept of developing an integrated wearable sensor (single package of three off the shelf sensors identifying stiffness, electrical impedance, and thermal analysis of tissue simultaneously) and, adding decision making to the device adds to the novelty of this work. Only when relevant data has been interpreted in the context of the diagnosis of each individual, will the physician feel that they have enough information to make a decision. And when the decision may impact survival and quality of life, it is the correct interpretation of relevant data that is the key to delivering optimum care. As accurate real time interpretations will require real-time signal processing of numerical data and images therefore, a decision making software support tool, capable of assisting healthcare professionals in decision-making, had to be developed to transform the

sensor generated raw data into meaningful screening information. The supplementary information obtained from these sensors with decision making algorithms is anticipated to enhance the clinical breast examination in providing better screening than CBE alone. The affordability, portability and improved screening capacity of the glove is expected to reduce health care costs by reducing the number of lab visits, improve patient outcomes through earlier diagnosis, and improve access to breast cancer screening for rural and developing countries' female population. The novelty and originality of the proposed research are summarized below.

Table 2.1 Novelty and Originality of Proposed work

Degree of Innovation, Novelty and Originality based on literature search and interactions with BCCA	
Multimodality Concept	The proposed non-invasive technologies already exist and have been studied as individual sensors, however never integrated into a single module with simultaneous data capture
Integrated Sensor Design	Development of an integrated sensory system encapsulating all the sensors
Glove Concept	Incorporating the sensors into a glove design for easy and more practical use
Decision making	Using built in intelligent diagnostic capability

2.2. Methodology: Integrated Multimodality Glove Module

Numerous prototype probes and measurement systems were developed before the multimodality glove concept was prototyped (refer to Appendix A: Probe Prototypes). These probes and systems though very useful are not relevant to the current research. The research done during these studies was instrumental for determining the requirements of a screening device for the early detection of breast cancer.

2.2.1. Hardware Development

Considering the advantages of multi-frequency mapping in EIS, multi-frequency mapping of electrical impedance spectroscopy was incorporated. The complex impedance data was collected using an Impedance Spectroscope HF2IS from Zurich instruments [65], along with trans-impedance amplifier HF2TA[66]. The impedance can be measured using two methodologies: Two point measurement or the four point

measurement. In the current study two point measurements have been considered due to its simple design approach. The HF2IS generates an output signal of amplitude V_Z (1 Volt). A reference electrode is attached to this output of the HF2IS. A measuring electrode, attached to the tissue, measures the output signal that has been modified due to the tissue properties based on the transfer function of the tissue. One volt input (generated by the Impedance Spectroscope) is applied to the tissue using the reference electrode. This voltage has been swept from 300 Hz to 1 MHz in order to have impedance spectrum of the tissue in this frequency range at 50 different frequencies. The current flow through the tissue is measured with the measuring electrode represented as I_z. The measuring electrode is virtually grounded thus the voltage that is applied to the tissue is V_z and the current passing through the tissue is I_z, hence the impedance spectrum of the tissue can be calculated as $Z=V_z/I_z$. ohms.

Figure 2-5 HF2IS Impedance Spectroscope from Zurich Instruments

Impedance Spectroscope HF2IS

HF2IS has a frequency range of 1µHz to 50MHz with 210MSamples/s (mega samples /sec) sampling rate that is 4 times the analog bandwidth, to ensure full capture of the signal and avoid aliasing, allows 14 bit AD conversion and simultaneous mapping of four frequencies. This device is capable of analyzing the frequency response of extremely noisy and low-voltage systems. It has two differential measurement units with a wide frequency range and 4 dual-phase demodulators, along with a high precision 128-bit DSP engine. These specifications permit multi-frequency measurements with very high sensitivity and precise static impedance characterization. The advantages over common analog instruments are higher dynamic reserve, zero drift, accurate phase

shifts, and orthogonality. An integrated oscilloscope with memory for 2048 samples provides direct signal-vs.-time and spectral views on the input signal. The user obtains an overview of the incoming and generated signals at any time to quickly find the right settings. A frequency-response sweeper provides accurate signal-vs-frequency plots.

HF2TA current amplifier

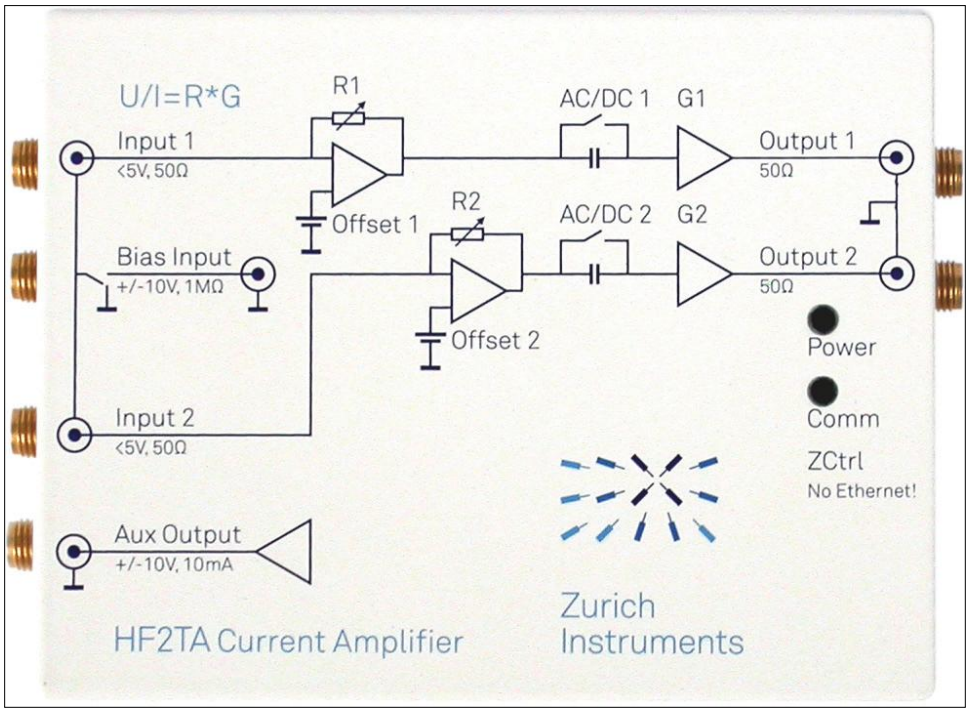

Figure 2-6 HF2IS Current Amplifier from Zurich Instruments

The HF2TA is a current amplifier that converts the output current from the tissue to voltage that is measured through the impedance spectroscope. This device is an active probe which can be conveniently placed close to the measurement setup. It supports most applications where a current must be converted to a voltage. The dedicated design of the HF2TA ensures stability and a smooth operation over the entire frequency range. It has a 50 MHz operating range, two independent amplification channels, a wide range of precision transimpedance gain settings (100 V/A to 100 MV/A), input offset voltage adjustment and extremely low noise and low input leakage. Providing two input and two output connectors, the HF2TA features transimpedance architecture with a variable precision resistor as the gain parameter (R). The transimpedance architecture matches the current through the feedback resistor and

keeps the input at the virtual ground. The second amplification stage provides decoupling from the first stage and an additional gain (G). The resulting output voltage corresponds to U = R * G * I. Configurable settings include the transimpedance (R1, R2), the output voltage gain (G1, G2), the switch to control signal shield bias, the AC/DC coupling switch to suppress DC current offsets, the offset voltage compensation adjustment, and the output bias voltage.

Frequency Sweeping

The objective of frequency sweeping an electrical system is to identify points of interest in the frequency spectrum. Such points of interest are poles and resonances – these are important to know as they characterize the system. Frequency sweeping consists of applying a stimulus signal and then measuring the system's response to many frequencies, one after another. The results plotted show the power or the amplitude of the measured signal over the defined frequency range. The output can either be relative to the stimulus signal (in dB) or absolute (VRMS/Hz). Frequency sweeping is also sometimes referred to as frequency response analysis. A sweeper will be sure that no energy is left undetected during a sweep. In order to achieve this, the step size and the measurement bandwidth must be adapted accordingly. Any frequency sweeper will follow a generic algorithm which is repeated for every measurement point within the defined range. A frequency sweeper requires a sinusoidal frequency generator and a demodulator to perform the amplitude and phase measurement. Various types of frequency sweeps are available: Linear Frequency Sweep, Logarithmic Frequency Sweep, Segmented Frequency Sweep and Harmonic frequency Sweep. The HF2IS has an integrated frequency response sweeper. The HF2IS Impedance Spectroscope with the HF2TA current amplifier is used to take EIS readings in terms of complex impedance over a selected frequency sweep range, in terms of magnitude and phase. The magnitude and phase are further used to perform the post-processing of the data.

Long Wavelength Infrared (LWIR) Sensor

The aim of this research was to provide a cost effective solution to screen breast tumors. A cost effective approach to the available thermographic imaging cameras is to use the multiple sensor devices such that they fulfill the required minimum design specifications to produce accurate, reproducible and clinically relevant data. A recently

introduced device based on a similar concept is the smart thermometer technology for detection and monitoring of more than 100 diseases [64].

Figure 2-7 Melexis MLX90615 LWIR Sensor (diameter=2mm)

After a thorough market research, the Melexis MLX90615ESG-DAA-ND (~$22 USD) Infrared Sensor was selected[67]. The sensor is a contactless infrared sensor. It consists of a thermopile detector chip and the signal conditioning chip (MLX90325) both integrated in the same TO-46 package. It has a high accuracy and resolution due to the low noise amplifier, 16-bit ADC and powerful DSP unit. It is factory calibrated in standard temperature ranges from: -40 to 85ºC for the ambient temperature and from -40 to 115ºC for the object temperature. The calculated object and ambient temperatures are stored in the RAM memory of the MLX90325 and its readout resolution is 0.02ºC. It has an accuracy of +/- 0.1ºC at body temperature. It has a 2 wire serial SMBus interface enabled and also has a 10-bit PWM (Pulse Width Modulated) signal from the device. A total of 127 sensors can be read via the two common wires through SMBus. Current source pull-ups may be preferred with higher capacitive loading on the bus; else simple resistive pull-ups provide the low cost advantage. In the present study, pull up resistances have been used.

It is delivered with a programmed object emissivity (ε) of 1, and can be programmed for other emissivity from 0.1 to 1 without the need to recalibrate with a black body. Emissivity is the ratio of power radiated by a surface to the power radiated by a blackbody at the same temperature. Melexis infrared is calibrated in front of a black body with the emissivity of 99.2%. The emissivity of human skin is .97, and that of a perfect radiator is 1. Human skin is a near- ideal radiator in the infrared spectrum [68]. Different Emissivity of surfaces does pose a problem to the accurate measurement of temperature as well as human skin, showing a temperature variation of 1ºC, when ε (λ) vary by 5% over the skin [69]. This would not be a concern in the present study as the skin surface being considered (human breast is homogeneous mass without any bones), therefore can be considered to have the same uniform emissivity. The hot spot will be inside the homogeneous mass, and therefore should have same emissivity. The sensor also has an emissivity compensation feature.

The temperature an infrared sensor measures is an average of the temperature of all surfaces in the field of view of the sensor. The field of view (FOV) of the sensor, determined at 50% of voltage signal is 100º, at a distance of 2mm this results to a spot size close to 2mm diameter. The thermopile die is sensitive to radiation coming from all angles, 180º front view as well as radiations from the back too. The reduction of the FOV is possible by reducing the opening of the TO-can, but the energy can become quite low using this technique and bring in instability. The minimum viewing angle should be 60º. Lenses can be used to reduce the FOV. The sensor works on a 3Volt supply, therefore can be battery powered. It has an optical filter (5.5µm to 14µm long-wave pass) that cuts off the visible and near infra-red radiant flux making the sensor insensitive to visible light. Its response time is .5s but a counterpart MLX90614ESF has response time of .15s in case speed needs to be increased [67]. This sensor has been made using the CMOS material for the manufacturing of its thermopile. It has been a trade-off comparing the sensitivity of the Bi/Sb solution but benefits from the reliability, stability over time and temperature operating range offered by CMOS technology. The high accuracy is obtained by making the ambient compensation and linearization in the digital domain. Thermopile and thermistor output are converted to digital. The ambient temperature is calculated based upon amplified thermistor voltage and thermistor calibration constants

stored in the EEPROM. The object temperature is calculated by solving the 4th order equation:

$$V_{TP} = \alpha(T_0^4 - T_a^4) \quad (5)$$

T_0 is the object temperature, T_a is the ambient temperature of the sensor, V_{TP} is the amplified thermopile voltage and α is the calibration constant determined during object calibration of the module using a precision black body. The calibration constants can be stored in the EEPROM for 10yrs. The error checking code (ECC) is run after each power up, it allows automatic correction of single bit errors and multiple bit errors lead to error message. The thermal gradient problem is also addressed by placing sensors in metal cans of highly thermally conductive material, to keep the thermal gradient small. The specifications of this sensor were compared to the IACT (International Academy of Clinical Thermology) guidelines for thermography standards and protocols and, the comparison is elaborated in table 2.2. The infrared sensor meets most of the requirements when appended with a novel design to maintain the sensor at specific distance from the skin, decision making expert system and imaging software.

Table 2.2 Comparative Table between Melexis sensor and IACT guidelines

International Academy of Clinical Thermology Thermography Guidelines. Standards and protocols	Melexis MLX90615
Spectral bandwidth encompassing the 8-10 micron region	5.5µm to 14µm long-wave pass
Accurate data repeatability in temperature value and location	Good repeatability using phantoms
Direct linear correspondence between the distance traveled, anatomic location and the displayed temperature values	Real time data representation of temperature
Controlled beam collimation to prevent sensor cross-talk	By controlling the FOV and specific distance from the skin, the cross talk between sensors can be eliminated
A reasonable range of distance from the skin, the recorded temperature, and the spot size being measured, should not vary.	Novel design proposed to keep the distance constant
Skin surface covered by the sensor must be controlled within a small enough area to yield data with a sufficiently detailed graph	Spot size 2mm circle at 1mm from detector, can be adjusted using FOV programming
Sufficient number of infrared samples	Real time data acquisition

Repeatability and precision of 0.1 degree C detection of temperature difference	.02ºC of resolution with SMBus communication
Accuracy of +/-2%	Accuracy of .2 ºC
Ability to perform accurate quantitative differential temperature analysis	Decision making algorithms incorporated to provide quantitative differential temperature analysis with Matlab GUI
High-resolution image display for interpretation	Data interpretation done using Matlab GUI
Ability to archive images for future reference and image comparison	Algorithms store all the captured data for future analysis, Matlab GUI images can be stored too
Software manipulation of the images should be maintained within strict parameters to insure that the diagnostic qualities of the images are not compromised	Advance Imaging will be included in the future, presently working on it

LWIR Array Hardware and Software

After the sensor has been finalized, the electronic circuitry is developed to acquire and present data in a useful form as shown in figure 2.8.

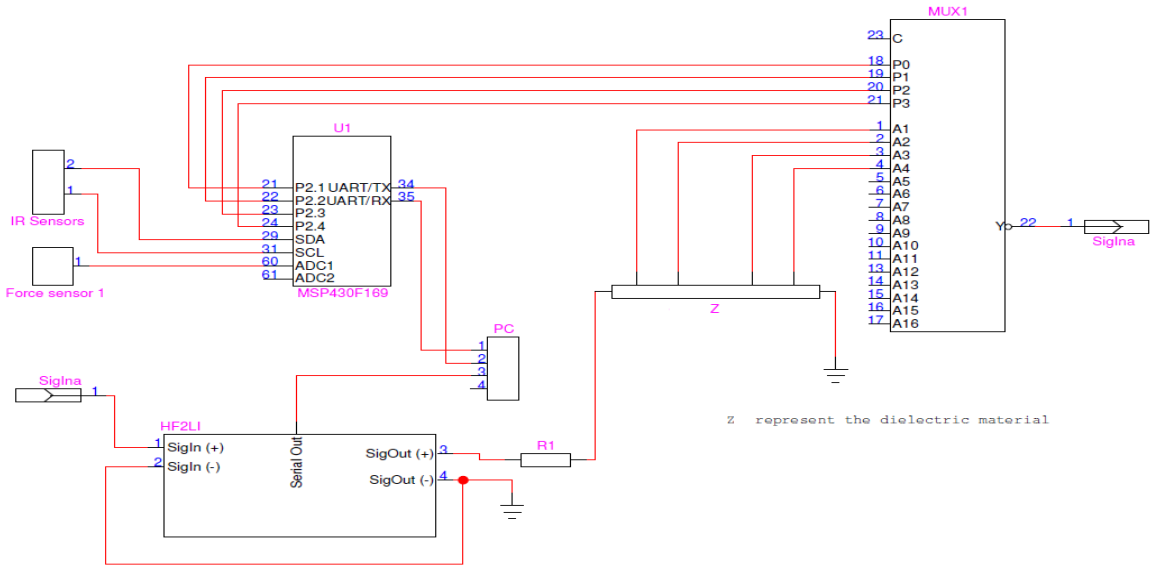

Figure 2-8 Schematics of the circuits

Advanced designing, filtering and platform techniques were used for the development of the electronic module. Circuit design involved designing and testing low power and single supply circuits (attenuators, integrators, amplifiers, etc.) and interfacing

with a communication module. Sensor data acquisition and processing is done through the Texas Instruments microcontroller MSP430F16. The MSP430 microcontroller has been chosen because of its low cost and low power consumption features. External high frequency oscillator 8 MHz has been used, basic clock module being XT2CLK and the XT2 equal to the Master Clock MCLK. The ADC sampling time is set to 1024. The sensors were used in the slave mode, with the microcontroller in the master mode. The sensors were each programmed with a specific address that was stored in the EEPROM. IAR Embedded Workbench Integrated Development Environment (IDE) was used to program and debug the controller. All the digitized signals were tested using the Intronix 34 channel logic analyzer.

The schematic shown in figure 2.9 is for using five LWIR sensors. Pull up resistors were used to overcome high capacitive loading on the bus. The 2 wire SMBus communication protocol was used. This could be further expanded to include 127 sensors.

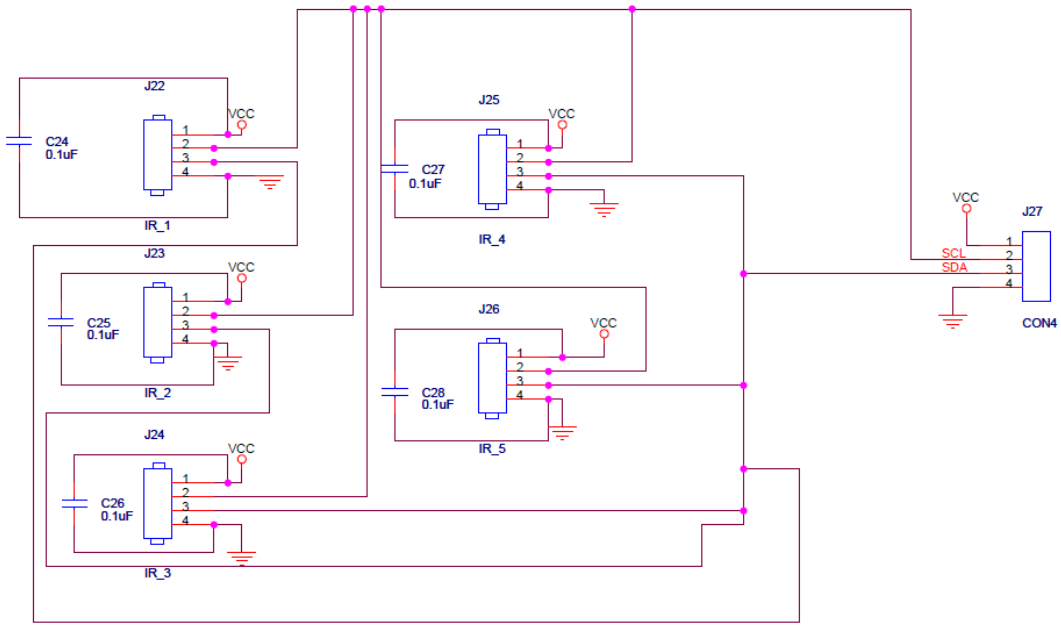

Figure 2-9 LWIR Sensor Hardware Schematic

As per application and usability, a multi-sensor embedded glove is closer to clinical breast examination; therefore a multimodality based wearable glove design was developed. The first stage was to develop finger cap wearable multiple sensors as shown in figure 2.10.

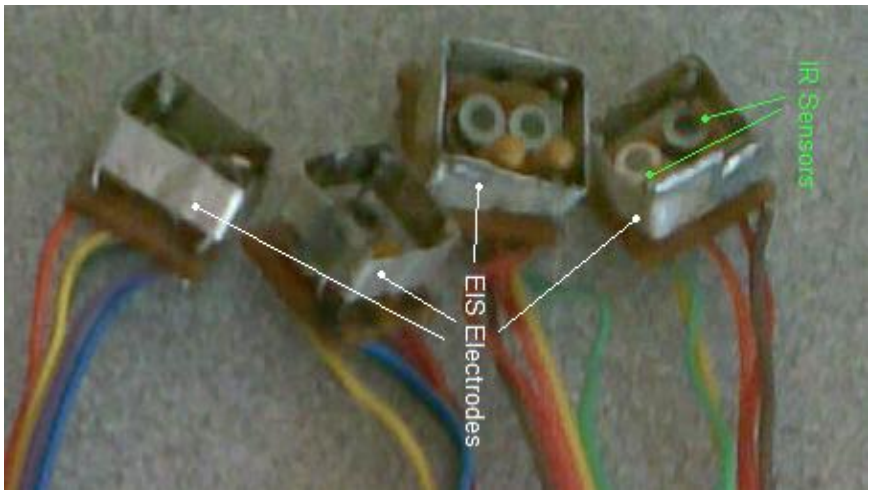

Figure 2-10 Finger Cap Wearable Integrated Sensor Design

The EIS electrodes were made with silver metal and had a height of around 1.5cm to maintain a constant distance from the skin. Two LWIR sensors were used in each finger cap to provide redundancy. The sensors were mounted over general purpose boards that were the size of the finger pad such that it could be fitted on the finger pad. Each unit was placed over a force sensor FS03 by Honeywell[70]. The size of the sensing unit of the force sensor and the general purpose board was kept the same, so that the board could sit on the force sensor. A total of four integrated sensors were developed for the four fingers of the hand. The thumb was not considered as thumb is not used during CBE.

2.2.2. Software Development and Testing

IAR Embedded Workbench Integrated Development Environment (IDE) was used to program and debug the controller. All the digitized signals were tested using the Intronix 34 channel Logic Analyzer. The baud rate used is 115200.Force data is received as a voltage level by the ADC module (analog-to-digital converter) of the microcontroller, which converts the voltage level to digital output. The digital value is then attached to an

identifier character ‘F1’ to show that it is force data and sent to PC via UART. This data is yet to be calibrated by the receiving software. Calibrated temperature data is read directly from the device using the I2C interface. Each sensor is polled by its 8-bit address, and then data can be read from that sensor. The data is attached to an identifier (‘I’, ‘J’, ‘K’… ‘P’) and sent to PC via UART. Contrary to the other two types of data, EIS data is never received or transmitted by the microcontroller. Instead, the PC reads EIS data from the HF2IS. The role of the microcontroller in the EIS measurement is to control the multiplexers select bits. An ISR (interrupt service routine) has been written so that the PC can ‘tell’ the microcontroller which electrode to read from. The multiplexing system is constructed solely to control which electrode the EIS data will be taken from. As described above, the select bits are controlled by the MSP430 microcontroller as shown in figure 2.11.

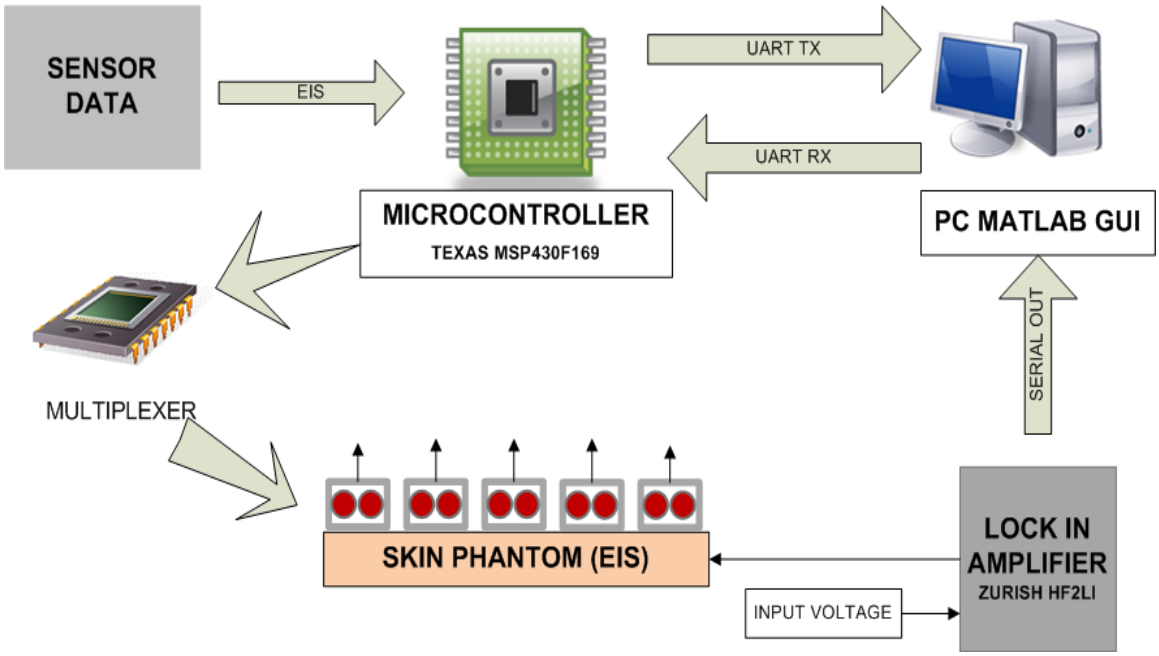

Figure 2-11 Block Diagram of the set up

The data is analyzed and filtering techniques incorporated to overcome any negative error value using high and low data limits. In case of error an error bit is also activated. To return calibrated data custom algorithm (developed in Matlab®) is used. Further, custom algorithms (developed in Matlab®) are used to test run for up to 300 samples in total for all incoming data, take the average for each sensor and output an

array with these values. This brings down the error further (refer section 5.2.1). The output is given in form of least mean square error as well as the mean temperature. The LWIR sensor provides two 16 bit outputs, temperature of the object being measured T_o and ambient temperature of the surrounding T_a. Both these temperatures are stored in the internal RAM and are accessible through the I2C of the microcontroller. The external microcontroller reads the data from the sensor internal RAM and based upon the calibration data stored in the EEPROM memory along with the address of the sensor, calculates the temperature for each sensor. This is done through external post processing of the thermal data for calculating the T_o and T_a using Matlab programming. To read the temperature in Celsius following equation is used according to the data sheet.

$$T_o\ ℃\ = \mathrm{RAM}\ \ 0\mathrm{x}0060\ \ \mathrm{x}0.02 - 273.15$$

2.2.3. Phantom (Tissue equivalent material) for System Testing

The dielectric properties of gelatine phantoms have been used in the past to simulate biological tissue [71]. The tissue equivalent material to be used in this research had to mimic three different properties of human tissue: electrical properties of healthy as well as malignant tissue, the dynamic thermal properties and the elastic properties of human tissue. The material that fulfilled the objectives of the present study to the closest was described by M. P. Robinson et al. [72]. This material consisted of two different materials developed to simulate the dielectric properties of human muscle and fat at 1000 MHz. The materials were easily made from ethanediol and gelatine (cheap and readily available ingredients) and showed good mechanical properties. The high permittivity material that simulated muscle had the composition: 48% ethanediol, 40% water, 2% salt and 10% gelatine. The ingredients get dissolved at around 55-60ºC. The low permittivity material simulating fat had composition: 55% ethanediol, 5% gelatine, 40% polythene powder and a drop of detergent. The materials are rigid enough to hold their shape but soft enough to be cut with a knife. The muscle equivalent material is rigid, transparent and mixing process gives a homogeneous material. The complex permittivity of each material measured using a network analyser at 1000 MHz and room temperature is (49.4-24.4j) for muscle-equivalent material and (8.2-3.6j) for fat equivalent material. These match the values for tissue at body temperature as per the

literature [73][74] that predicts the values as ((49-52) – (23-24)j) for muscle and ((5.3-7.5) – (1.5-2.7)j) for fat. The static thermal properties of the material had also been measured using scanning calorimetry and were close to the values predicted by theory of human fat [75][76][77]. Thermal properties were also similar to muscle tissue at body temperature (specific heat capacity c of phantom at room temperature is 3.07Jg-1K-1, density ρ is 1.10g cm-3) and similar to fat tissue at body temperature (specific heat capacity c of phantom at room temperature is 2.25Jg-1K-1, density ρ is .95g cm-3) . Though present research focused on the dynamic thermal simulation, in which not only the heating pattern but also the thermal transport processes of conductivity and perfusion are simulated, but these phantoms only satisfied the static thermal simulation. Interestingly, specific heat of tissue anomaly (fibrosis and adenocarcinoma) is closer to muscle than to fat [72]. In order to simulate an anomaly that has higher temperature than the normal surrounding tissue, a 100Ω resistor with 5V potential across is embedded inside the phantom constructed with 10.77% of Knox gelatine powder and 89.23% of distilled water.Lastly the densities were also calculated along with the thermal conductivities. At 20°C the phantoms simulate the dielectric properties of muscle or fat (adipose tissue) at 37 °C and tissue static thermal properties (Table 2.3):

Table 2.3 Phantom material properties

Material/tissue	c (J g-1K-1)	ρ (g cm-3)	Cρ (J cm-3K-1)
Simulated Muscle Tissue (20ºC)	3.07	1.10	3.37
Simulated Fat Tissue (20ºC)	2.25	.95	2.13
Muscle (37-43 ºC)	3.55	1.044	3.71
Fat (abdomen) (37-43 ºC)	2.43	.938	2.28
Fat (breast) (37-43 ºC)	2.22	.934	2.07

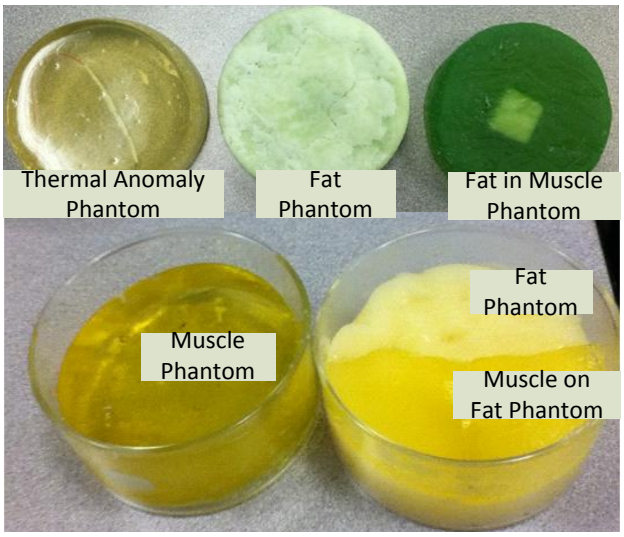

Figure 2-12 Muscle and Fat phantom

Test Bed

A test bed was developed using a vice. Through this set up the precise displacement moved by the vice could be measured. A phantom was created [72], and anomaly consisting of a liquid inclusion of calcium, vegetable oil, and salt is inserted at a defined position. Thermal anomaly was created by inserting a resistor attached to a current source, therefore had higher temperature than surrounding. The EIS data was captured at a frequency of 100 KHz.

a) 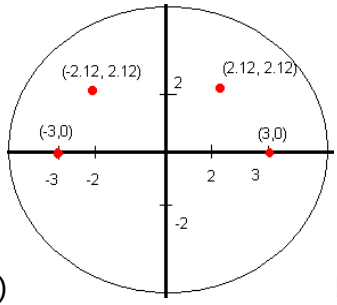

b) 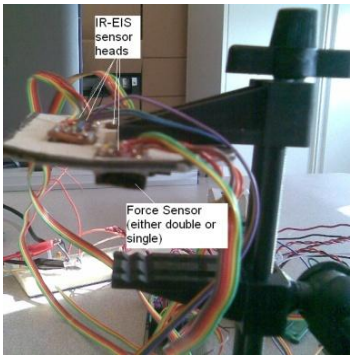

c) 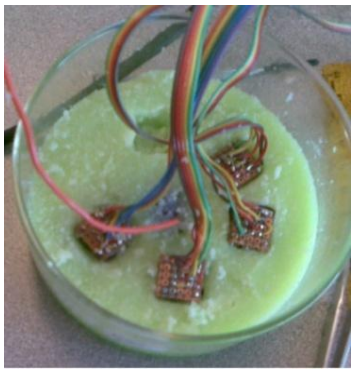

Figure 2-13 a) Position of Integrated sensors b) Final Set up c) Phantom

Figure 2.13(a) shows the position of the sensors (b) shows the final setup from which all 3 types of data can be collected simultaneously (c) shows the sensors over the phantom. Table 2.4 shows the data obtained after testing the integrated system on the integrated phantom.

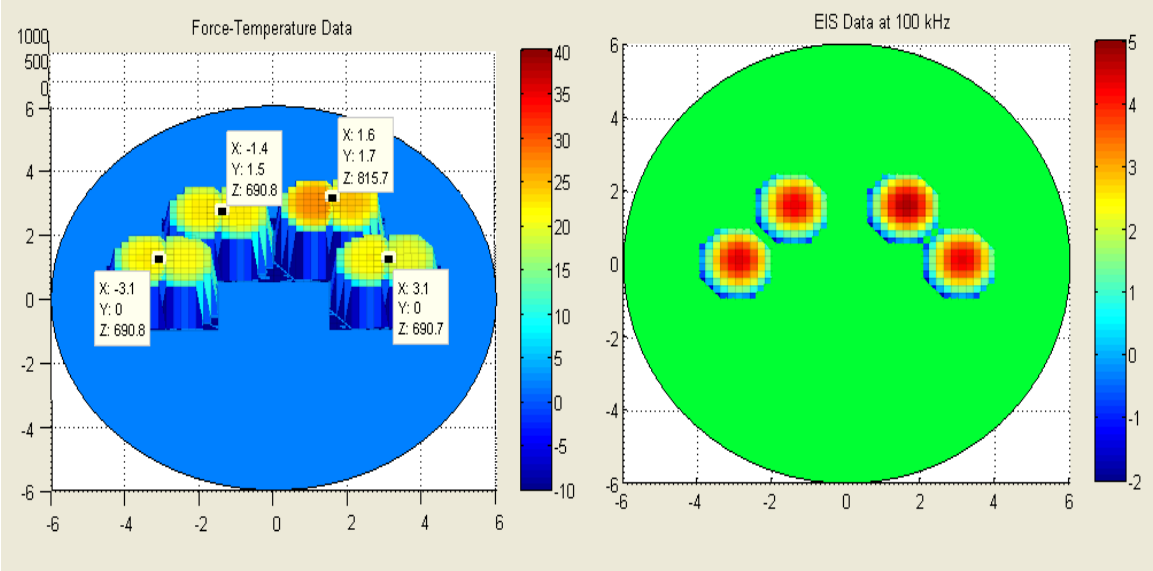

Figure 2-14 Result from data captured over phantom. The anomaly is located at X,Y location [1.5, 1.5].

Figure 2.14 shows the result of reading all three parameters simultaneously from the phantom. As shown, the force constant of the hard region is 815.7 N/m, and that of soft region is 690.8 N/m. The temperature of the anomaly is about 3-4 degrees higher than the normal region, while the conductivity of the anomaly is about 0.5 S/m greater.

Table 2.4 Raw data for the experiment on the integrated phantom. The anomaly is at (1.5, 1.5)

X Position (cm)	Y Position (cm)	Conductivity (S/m)	Absolute Permittivity (F/m)	Temperature (°C) (rounded to nearest 0.5 °C)	Force (N/N)
1.5	1.5	4.7441	0.079154	22	815.7
3	0	4.3058	0.022506	20.5	690.7
-1.5	1.5	4.3027	0.014864	20	690.8
-3	0	4.2825	0.042064	19	690.8

Printed circuit boards were designed and developed after verification of the circuits. Figure 2.15 shows a single integrated sensor being used along with the

developed hardware over muscle tissue equivalent phantom and over a fat tissue equivalent phantom.

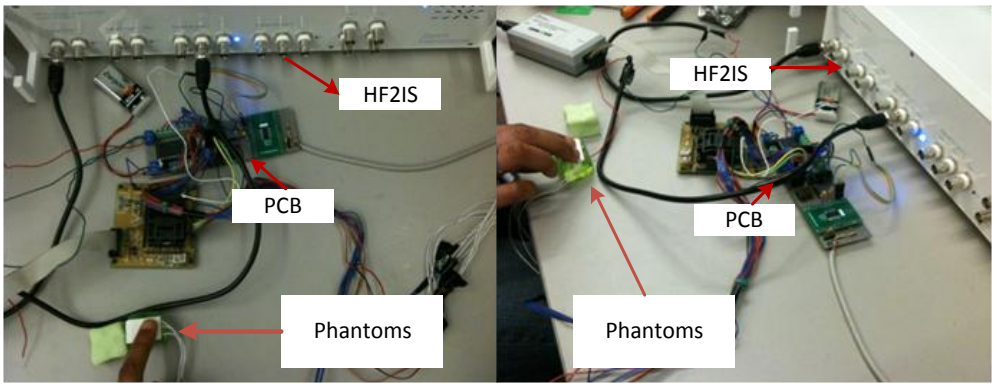

Figure 2-15 Hardware with Impedance Spectroscope from Zurich Instruments

2.3. Multimodality Sensor Glove

The first glove design was developed by attaching the finger wearable integrated sensor on one finger of a latex glove. The latex glove has been selected as the CBE is performed by the physicians using latex gloves. It was intended to minimally change the CBE procedure by the new introductory glove device. The integrated sensor design on single finger is shown below in Figure 2.16. The design was improved by replacing the silver electrodes with Ag/AgCl based electrodes that give higher stability over time. These electrodes were also smaller in size and were useful in developing a wearable integrated sensor design. In this design four Ag/AgCl palette electrodes, one LWIR sensor and one Honeywell FS03 sensor were used.

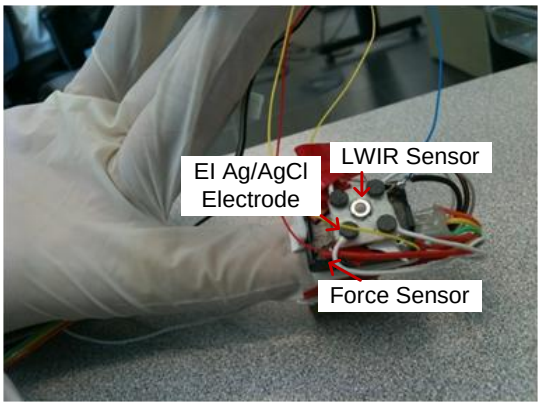

Figure 2-16 Finger Cap wearable integrated sensor on glove

For relative stiffness measurement multiple force sensors were required therefore a two finger glove design was developed. Figure 2.17 shows the two finger design. The second finger has force and LWIR sensor required for the relative temperature and stiffness values, EI electrodes are not put on the second finger as they measure absolute values and not relative values.

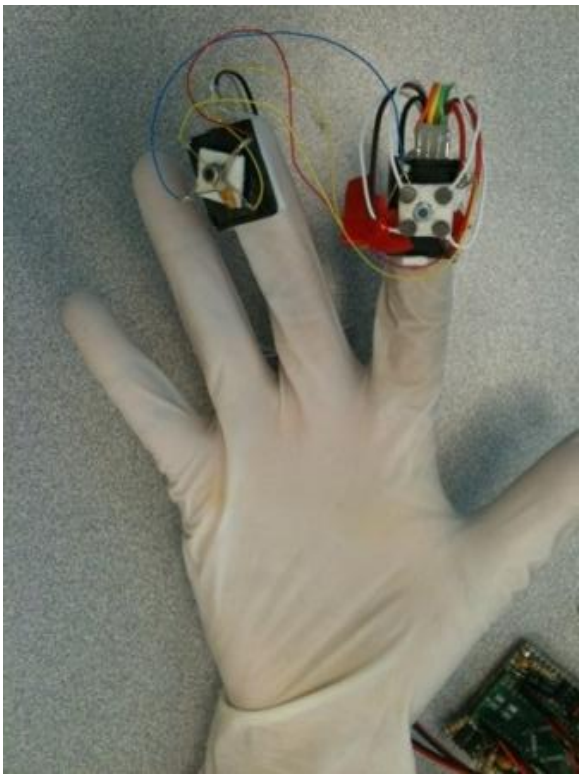

Figure 2-17 Two Finger Cap wearable integrated sensor module on glove for relative force measurement

To increase the resolution twelve electrical impedance Ag/AgCl electrodes and six temperature sensors are embedded onto a single probe as shown in Figure 2.18. With twelve electrodes, the resolution of electrical impedance scan increases making it capable to detect a small scale size of tumour. The number of temperature sensors do not only provide redundancy that enhances the reliability but also a greater area of scan.

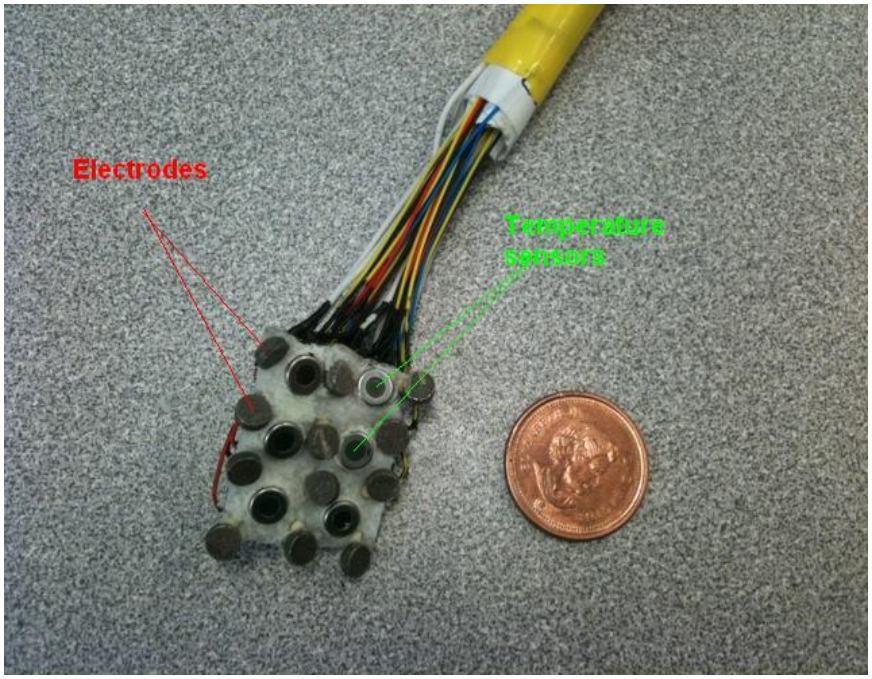

Figure 2-18 12 Ag/AgCl Integrated Sensor module

Wearable Force Sensor for Electronic Palpation

This glove prototype is a good start to modify the probe design into an integrated sensor glove design as a proof of concept but there were challenges associated with this design. The major challenge is that this design is not wearable due to the rigid structure of the FS03 sensor. A substitute for this sensor was required such that the sensor has comparable specifications to FS03 with respect to the sensitivity and range. The substitute sensor used is the Pressure Profile Finger wearable TPS sensors. Figure 2.19 is a picture acquired from Pressure Profile System's online website [78].

Figure 2-19 Pressure Profile System Finger sensors

This wearable tactile pressure sensor reliably quantifies forces applied by the human hand. The large size of this sensitive device has a surface area of 349 mm^2 and detects up to 10lbs. Since system is hard coded in C language, its software has already taken care of the calibration between analog and digital values. These sensors could be worn underneath the latex glove and still provide the output with good accuracy. Three TPS sensors were used for calculating the relative stiffness values. First the sensors are calibrated using the load cell and customised chameleon software available with the device. This particular set up gives great flexibility since it comes with a finger wearable shape. The fact having the sensing pad sewed on the finger shape cloth without any extra unnecessary room overcomes the issues that were encountered in the FS03 sensor setup. For data analysis, MATLAB program was chosen due to its flexibility in data representation. Some C++ was also required in bridging the connection between Pressure Profile System Fingertip sensors such as MEX files.

A new glove was created with integrated LWIR and EI Ag/AgCl electrodes. The integrated modules were embedded over three fingers of the latex glove. The PCB hardware was also assembled into cases to provide a more robust device. Figure 2.20 (a) shows the developed latex glove with LWIR and EI electrodes over three fingers. The PPS finger wearable tactile TPS sensors have been worn underneath the latex glove. Each module consists of two LWIR sensors (5mm apart) for redundancy and 4 Ag/AgCl electrodes, 4mm in radius, 1cm apart, in a square configuration. Each integrated module is embedded over the index, third and fourth fingers of the latex glove, as the standard method of clinical examination uses the pads of the index, third and fourth fingers. This latex glove is worn over the finger wearable pressure sensors (FingerTPS) to provide three multi-modality simultaneous sensing. The final developed prototype is shown in Figure.2.20(b) and the developed multimodality CBE glove with associated multimodality hardware set up is shown in Figure.2.20 (c).

Figure 2-20 (a) Three Integrated Sensor modules using finger wearable force sensors over latex glove, (b) Final Multimodality Sensor Glove prototype and (c) Hardware Set Up

Further modification of the design was done in the form of a hand held probe to be used for multimodality tissue classification of skin lesions as shown in Figure 2.21. The probe was 5cm X 4 cm in an oval shape. The probe consisted of one sensing and one reference Ag/AgCl electrode from Grass® for Electrical Impedance Spectroscopy.

The probe was placed over the tissue such that malignant tissue was placed between the EIS sensing electrodes. The EIS electrodes were around 1.5cm apart and 6 mm in diameter. For tissue thermal index measurement six LWIR Melexis sensors were used to provide redundancy. The centre sensors were placed at an angle to expose the malignant tissue to the field of view of the LWIR sensors and at the same time place the EIS electrodes at the closest distance possible. The pressure sensors used were the same as before, therefore the wearable finger TPS pressure sensors. A disposable glove is worn over them to avoid infection.

Figure 2-21 Final Multimodality Sensor Probe for Skin Lesion Analysis

Graphical User Interface (GUI)

A 3 dimension real time graph helps the user to notify the change in temperature with depth. A screen shot example is shown below in Figure 2.22, where the negative parabola indicates how much the user is pushing into the material.

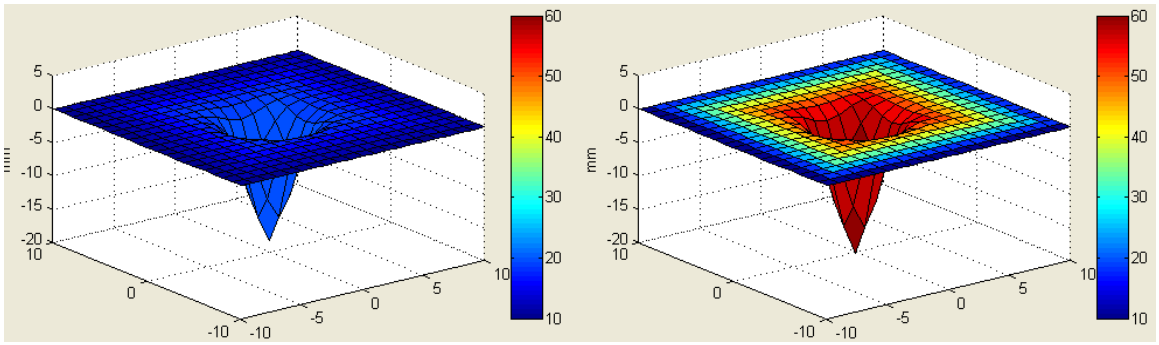

Figure 2-22 Graphical User Interface representing Temperature and Force level

Real Time Data Collection and Representation: Multimodality GUI

The main purpose of this research is to be able to detect possible malignant anomaly inside women breasts. Human tissue has countless variances including skin stiffness variability, electrical impedance variability and thermal variance. The variabilities make anomaly detection decision making challenging particularly when merging multiple modalities together. To depict a proof of concept decision making capability in the multimodality tool, algorithms based upon fuzzy logic are implemented in MATLAB® that provide instant feedback to the user. The proof of concept algorithms are trained and tested over phantoms. The system first requires the user to do a calibration for each phantom, calibrating the surface temperature. This step takes around ten seconds. The collected calibration data is the critical threshold used for anomaly detection. The fuzzy logic implementation is performed for thermal analysis. Each incoming data value is compared and analyzed based on the calibration that was obtained in the first step. A rating from 0 to 10 is established indicating the probability of hitting an anomaly. Lastly, a final decision can be made combining all the ratings from the previous step. This is for future work.

The screen shot below, Figure 2.23, is an example of the graphical user interface based upon the developed decision making algorithms. Depending on user's interests, these data graphs can easily be adjusted. At the moment, top left plot represents the force recorded from the pressure profile system sensor, top right plot shows the average temperature of all sensors, and bottom left is the combination of displacement sensor and temperature sensors in 3D. The panel located at the bottom right of the GUI allows

the user to calibrate, start, stop, and turn off the system. Real time values from the sensors and the status of the materials being tested are also shown to the user in this area.

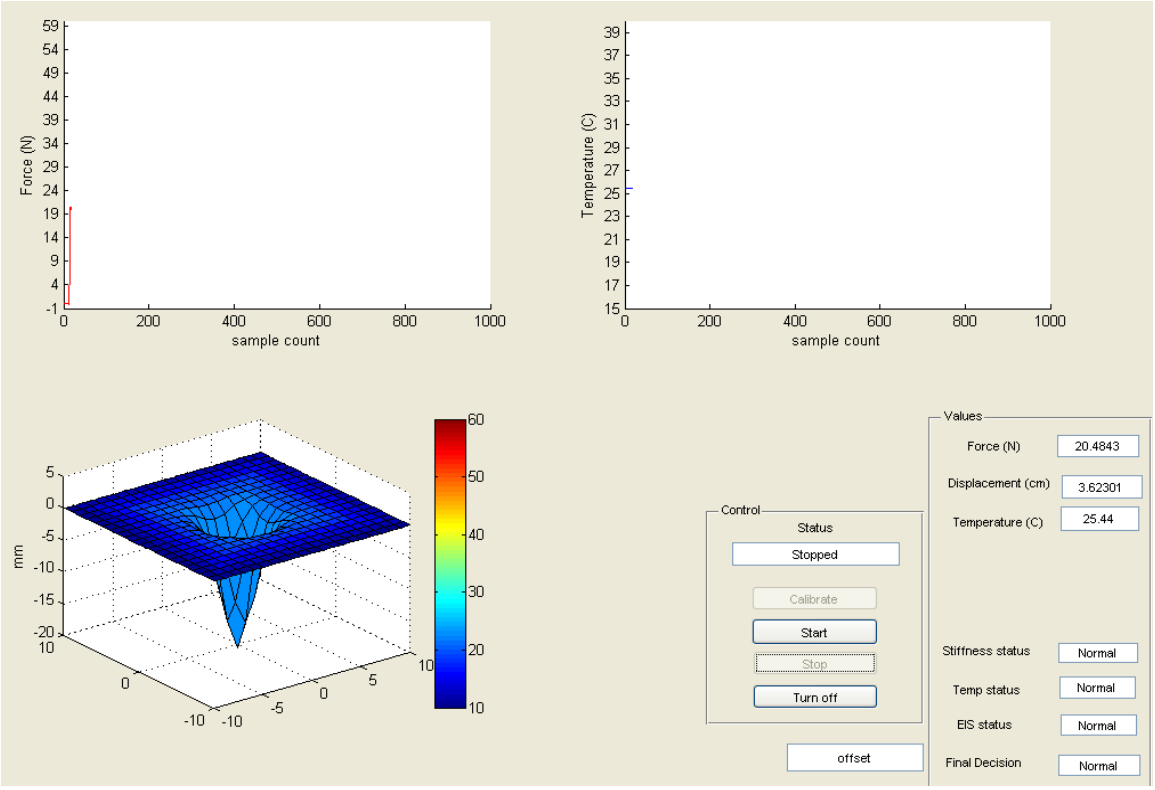

Figure 2-23 Graphical User Interface with Decision making

2.4. Discussion and Conclusion

I proposed to develop an intelligent, inexpensive and non-invasive screening tool aiding malignant anomaly detection objectively, to ensure early diagnosis, better prognosis and higher survival rate. The innovation in present research was in the integration of present available non-invasive breast screening modalities into an affordable and accessible screening glove.

A multimodality based tissue classification screening glove and probe has been developed based upon three identified non-invasive modalities: Electrical Impedance Spectroscopy, Electronic Tissue Palpation and Tissue Thermal Analysis. For miniaturization, off shelf sensors and measurement systems were identified with the

required resolution and repeatability to measure the specific tissue properties with good accuracy. For modality integration circuits were designed, developed and tested on the hardware level using microcontroller as well as on software level using MATLAB® and C programming.

The developed probe was disinfected using disinfectant cleaners to disinfect the body of the probe. The sensors were non-contact and never came in direct contact of the skin. A disposable glove was worn over the force sensors, eliminating the force sensors coming in direct contact with the skin. This was in accordance with the provided guidelines from the manufacturer. The prototype glove design is not disposable, that is for future work.

The developed system was tested using tissue equivalent phantoms and a test bed. Mimicked anomaly with thermal, electrical and stiffness properties embedded inside homogeneous phantom was detected using the developed multimodality system. A graphical user interface depicting real time data and with decision making capability was also developed and tested over the phantoms.

Extensive market search was required to fulfill the quest for off the shelf sensors with the required accuracy, repeatability and resolution with digital output for easy system integration. Limitation of market available application based sensors fitting the proposed application forced the development to be more focussed on integration of the individual modalities hardware and software rather than resolution of the tool.

The MATLAB® based GUI is capable of providing real time data representation of thermal and stiffness properties of tissue, but is not capable of providing real time representation or decision making based upon electrical impedance of tissue. Work needs to be done in introducing and applying electrical impedance tomography by increasing the resolution of the system through number of electrodes and incorporating more advanced decision based algorithms.

Further improvement of the design requires more in depth experiments or simulations to be performed over the effect of electrode size, distance between the electrodes, and distance from the skin surface to get optimum results. The developed

prototype is a first generation prototype and developed with the facilities available in the research lab. The prototype can definitely be improved in resolution and appearance using commercial available technologies for electrode deposition on the glove surface.

2.5. Ethics approvals

During this research three studies were conducted over human tissue *in vivo*. Ethics approval was taken to perform the studies from three different authorities: Office of Research Ethics Simon Fraser University, BC Cancer Agency Research and Ethics Board and, UBC Research and Ethics Board. The details of the approvals are as follows:

- Study Number. #2011s0523, Office of Research Ethics Simon Fraser University under Dr. Farid Golnaraghi as the Principal Investigator, "*in vivo* data collection of dielectric, thermal and elastic properties of human tissue"
- REB Number H13-02887, UBC BCCA Research Ethics Board under Dr. Paris Ann Ingledew as the Principal Investigator, "Electrical Impedance Analysis of Malignant and Benign Tissue: Effects of Temperature and Pressure". In April 2014 an amendment was approved to the protocol.
- Study Number. #2014s0134, Office of Research Ethics Simon Fraser University under Dr. Farid Golnaraghi as the Principal Investigator, "Electrical Impedance Analysis of Malignant and Benign Tissue: Effects of Temperature and Pressure"

Bio-safety permit was also obtained from Simon Fraser University to conduct research over human pathogens and animal pathogens, permit number 323-2013.

The protocols for the studies have been documented in Appendix C.

Chapter 3.

Tissue Classification: Tissue Stiffness (Phantom and *in vivo* Healthy Human Tissue Study)

3.1. Introduction

Tissue stiffness provides extensive information regarding the overall health of the tissue [79] [80]. Pathology detection is related to stiffness of the tissue and leads physicians to screen or diagnose an underlying problem in the tissue. Likewise, breast stiffness is an indicator of breast health [81]. Stiffness increases, hard lump formation, movable or immovable masses are important to diagnose breast health [82].

BSE/CBE is useful in detecting palpable tumors of breast[45], that constitute 43% of the total breast tumors. Patients with palpable tumors usually have larger tumor sizes and more advanced stages of cancer[45]. The sensitivity of detecting palpable masses is increased using electronic palpation [52].

3.1.1. Background and overview of present state of technology

Tissue classification based upon tissue stiffness is very useful in early diagnosis of disease. Specifically, breast tissue health is diagnosed through tissue stiffness. During breast clinical examination, the physician identifies abnormalities in the breast by detecting variation in the breast tissue stiffness. Many breast examination technologies have been proposed for screening[83][84][85][86]. Ultrasound has also been used extensively for soft tissue classification [87][88][89], but the associated cost of ultrasound makes it difficult for ultrasound to be practiced routinely in clinical practices. 2D networks of smart cells have been developed to implement acoustic impedance that foresees development of artificial skin for pathological findings' quantification [90].Other tissue

stiffness determination methodologies include resonance sensing [91], tissue hardness sensing [92], two sensor probe configuration[93] and determination of interstitial fluid pressure [94]. Force and position patterns have also been studied to get information regarding the state of manipulation of a biological tissue [95]. Pressure threshold for quantification of deep muscle tenderness [79] and pressure distribution measurements made at the surface of the tissue when it is loaded have also been proposed [85].[96][97].

Further, tactile sensors inspired by the human finger have been used for tissue stiffness detection[98]. Tactile mapping is becoming quite popular and uses an array of pressure sensors to non-invasively record the tissue stiffness variability [99][100]. Micro tactile sensor design and fabrication have also been recently introduced [101]. Artificial tactile sensing has been used to characterize a tumor in the soft tissue [102][103]. Artificial palpation with force and position profiles provides immense information regarding the underlying biological tissue [104]. Extraction of features from these tactile maps has demonstrated that tactile imaging has the potential to improve the accuracy of CBE, due to the difference in the stiffness of malignant and healthy breast tissue[105]. Models have been developed to predict tactile image pressure distributions from geometric and material properties. Further, inversion algorithms have been used in order to provide information in assessing the size and shape of the lump using analytical methods with the tactile sensing. The study results showed mean absolute error between *ex vivo* size measurement of the lump and ultrasound measurement to be 34%, for CBE 47% and for tactile mapping 17%. The average standard deviation for the size of the lump was 15%. [99]. Type of breast cancer has also been differentiated using tactile images [106].A study on registering mammography with tactile imaging have promising results with increased stiffness areas being indicated that were not earlier identified using mammogram alone [100].

3.1.2. Breast Tissue: Mechanical Properties

All soft tissue of breast can be assumed to be nearly incompressible, i.e. with poison's ratio of ~0.5 [107] [108]. Breast tissue is considered to be hyperelastic, isotropic and nearly incompressible [109][107][110]. For simplification, breast tissue may be

considered as elastic and the reported elastic modulus for different components of the breast are: Pectoralis fascia: 100-2000 kPa, suspensory ligaments 80,000-400,000 kPa, Glandular Tissue 7.5-66 kPa, Adipose .5-25 kPa, and skin 200-3000 kPa [108].

A study conducted to find correlations between histological diagnosis and breast tissue stiffness in compression [111], found a significant difference in stiffness and rate of increase in stiffness with strain between cancerous and benign breast tissues. Infiltrating ductal cancer was found to be 10 times as stiff as normal fat tissue at 1% strain, and more than 70 times as stiff at 15% strain. Normal glandular tissue was found to be 2.5 times as stiff as fat tissue at 1% strain and nearly 5 times as stiff at 15% strain, concluding that relative stiffness is a good indicator of histological diagnosis. Carcinomas are seen to be highly nonlinear and quite stiff, while fat is nearly linear and extremely soft.

3.1.3. Procedure used to perform CBE

In order to determine wearable cost effective sensors that could be used by physicians during clinical practice, the procedure that a physician uses to perform the tissue examination needed to be analysed. Therefore, a study was conducted that consisted of 5 participants that were physicians and nurses from BC Cancer Agency. These sets of participants were specifically chosen as they perform clinical palpation on human breasts routinely to locate lumps in breasts or examine the growth of tumors after surgeries. Therefore, the group consisted of experts in the field of tissue classification based upon tissue stiffness properties. The procedure consisted of providing the participants with a gelatine based phantom mimicking tissue. The hardness of the phantom was measured using a durometer (TECLOCK-GS-721G), that showed the hardness of the material as a numerical value on the scale of 0-100, 100 being non elastic rigid surface. The readings from the durometer are “relative amounts” with no units. The durometer showed a hardness value of 9-10 over the phantom. From the study it was concluded that the most predominant methodology used by a physician during tissue examination is using three fingers (centre finger, ring finger, and index finger) and the 180-degree distal pad press: The forearm and wrist are in a position such that the palm is down and the index finger is in line with the wrist. Force is exerted at the

pad of and perpendicular to the finger as shown in the Figure 3.1. The range of force the physicians' used was from 2N to not more than 5N.

Figure 3-1 Breast Self-Exam (Source: National Cancer Institute)

From the experiments and the above study it was concluded that using PPS Finger TPS sensors over the index, centre and ring finger is the best methodology to perform and quantify the results of clinical breast examination, based upon palpation. Therefore, in the further study Finger TPS sensors in the distal pad position have been used.

3.2. Phantom Study: Test Set Up and Methodology

A number of Phantom Based Studies were performed to determine the most appropriate technique and correct stiffness of the breast tissue phantom and tumor mimicking anomaly. These experiments and associated results have been attached in Appendix D. Several set up that were tested included indentation method and tactile mapping method. Indentation method was tested with different set ups: single force sensor (Honeywell FS03) with displacement measurement, two force sensors (Honeywell FS03) with displacement measurement, wearable force sensors (PPS Finger Wearable TPS system) with displacement measurement. Tactile mapping method was tested using wearable force sensors (PPS Finger Wearable TPS system) without displacement measurement providing relative stiffness information. The sensors were calibrated and various stiffness phantoms, with known compositions, were tested. Varying the gelatine concentration by mixing it with distilled water was used to create

phantoms. Percentage of gelatine in water by weight can represent human tissue such as muscle and fatty tissue, as well as abnormal fibroglandular and cancerous tissues [72]. In this study, the experiment emphasized the fatty and cancerous tissues which were simulated at 10.77% (durometer reading 10) and 20.75% (durometer reading 30) of gelatine respectively. Therefore simulated cancerous tissue is three times stiffer than the surrounding fat simulated tissue.

Figure 3-2 Phantom

An integrated phantom with embedded tumor mimicking anomaly (20.75% gelatine) was developed. The mimicked anomaly material is inserted into mimicked tissue material at different depths (1cm/2cm) from the surface using various anomaly sizes ($1cm^3$ and $8cm^3$). The stiffness difference measured using a durometer is 50%. The test results show the size of the anomaly is an important factor that affects the measurements, and the displacement difsference is higher in bigger size anomaly (8 cm^3).

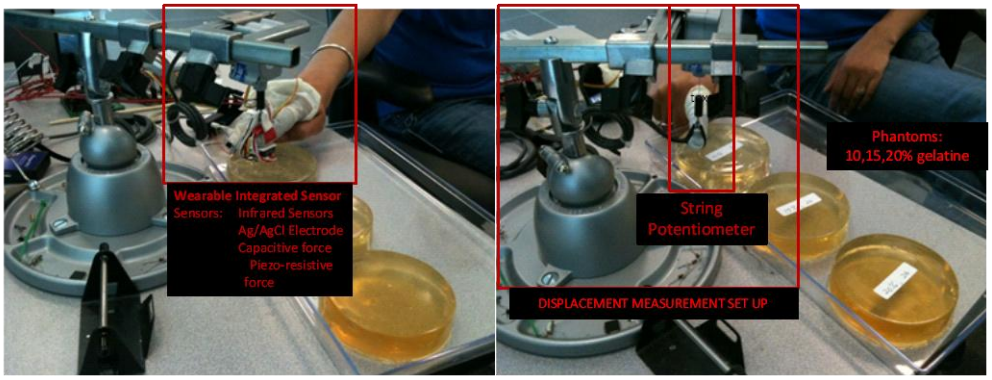

Figure 3-3 Experimental Set Up

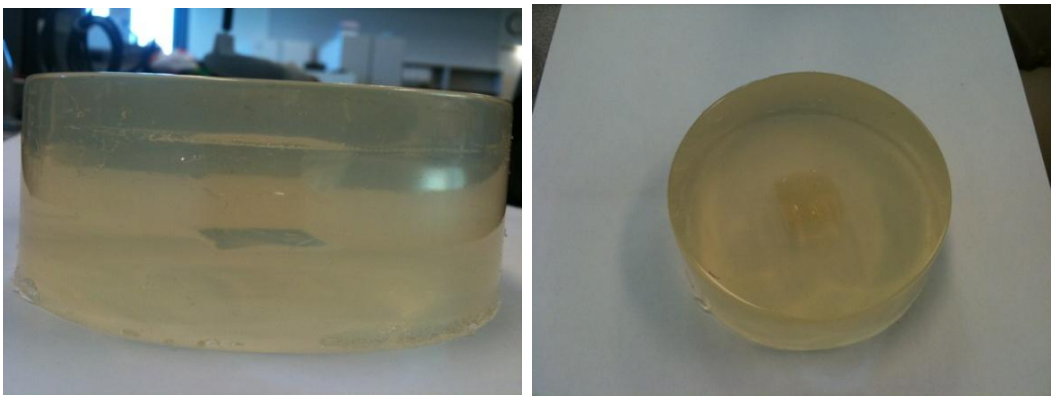

Figure 3-4 Phantom with tumor mimicking anomaly

The initial results using the fat/tumor elastic property phantoms are promising but due to the inherent size of the sensory unit, it was possible only to detect tumor size around 2x2x2cm^3 at a depth of 2cm, Similarly the size of the force sensors is 349mm^2, it is anticipated that smaller size custom force and displacement sensors will increase the sensitivity and specificity of the system.

A graphical user interface in MATLAB® was developed to depict the results more clearly. The height of the parabola corresponds to the amount of displacement caused due to application of force experienced by the material under observation.

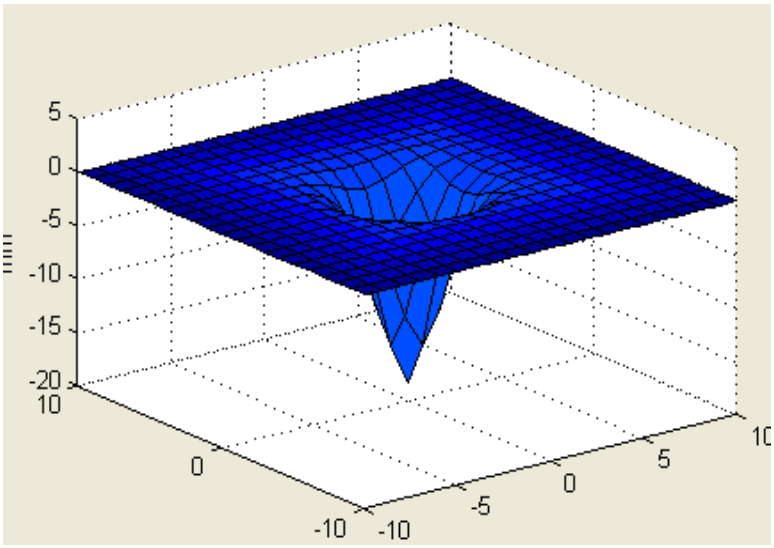

Figure 3-5 Graphical User Interface, height of parabola depicts the displacement due to amount of force experienced by the material under observation

Phantom Study: Discussion and Conclusion

Several set ups (Appendix D) indeed verify or provide significant clues to determine the differences between various materials stiffness. Although many constraints and conditions were applied to minimize the factors that could affect the outcome, the displacement achieved between developed fatty and cancerous phantom differed by up to 40%. For tissue stiffness measurement set up it is concluded that though indentation method involving measurement of displacement along with force is more accurate approach compared to tactile mapping using multi force sensors; but the indentation set up is very hefty and large. Therefore, tactile mapping using wearable PPS finger tactile system is a promising tissue stiffness characterization methodology. It is easy to wear and can be easily interfaced with a computer to map the sensor outputs.

Though market available wearable sensors have been identified based upon theoretical and experimental results using gelatine based tissue equivalent material phantoms or realistic test bed; but further study on improving the wearable design and multiple sensor usage methodology needs to be further incorporated for reliable, repeatable, and clinically relevant data; quantifying physicians' decision.

3.2.1. Decision based algorithm implementation

The main purpose of this research is to determine the presence of an anomaly that has greater stiffness compared to an otherwise homogeneous surrounding tissue. A decision based algorithm using fuzzy logic has been implemented in MATLAB® to identify the stiffness difference and provide instant feedback to the user regarding the presence or absence of an anomaly. The system is first calibrated in such way that it recognizes the stiffness of a normal healthy material/ tissue during system calibration; Intelligence algorithms based on fuzzy logic are further merged into the system to make it a decision based feedback system.

Fuzzy Inference Systems

Fuzzy inference is the process of formulating the mapping from a given input to an output using fuzzy logic. The mapping then provides a basis from which decisions

can be made, or patterns discerned. The process of fuzzy inference involves using membership functions, logical operations and If-Then rules.

Data Collection and Analysis

To implement the fuzzy inference system for detecting anomalies with higher tissue stiffness inside a lower stiffness breast tissue, a phantom acquired from CIRS[112] has been used. This phantom model 013 has been developed for biopsy training. Its required features among other available features are as follows:

- Compressible
- Contains various sizes of dense masses
- Contains calcification clusters
- Anthropomorphic shape for accurate simulation of breast compression
- Palpable lesions
- Physical consistency similar to human tissue
- Works on digital systems

The phantom is made from a proprietary gel, and the gel is surrounded by an elastic skin-like membrane, which enables palpation of the embedded masses making this phantom appropriate for the required study. The phantom shape is like a partially compressed breast. It can further be compressed to 4.5 cm thickness. Inside the phantom numerous solid black masses in numerous sizes have been embedded to mimic lumps.

Figure 3-6 Breast Phantom with embedded anomaly of various sizes

Setup and Calibration Procedure

The Figure 46 below depicts the components and the setup of PPS sensors. There are three finger wearable capacitive pressure sensors that are supposed to be worn on the index, middle and ring finger of the right hand (refer section 3.1.1). The load sensor is used for system calibration.

Figure 3-7 PPS Finger TPS system

‘‘Chameleon TVR”, customized software available with PPS sensors is used for calibration and measurement. For calibration, the Calibrate option is selected from the data acquisition drop down on the main toolbar. All three sensors are calibrated separately. For each sensor, the load on the load cell is increased and decreased gradually to a certain limit (3/5 lb). On completing calibration for the sensors, the Fuzzy Inference System is trained.

Fuzzy Inference System (FIS) Training

For the FIS training a tumor less patch of tissue is needed. Once such a patch is recognised in the phantom, the inference system is trained. The software records real time force data from the sensors. After recording the data, it is necessary to export the

data to a txt file. MATLAB® programming is used to do all the post processing. The first segment of the MATLAB® code, extracts the training data from the text file and converts it into MATLAB® recognisable data. The second segment of the code, takes this MATLAB® training data and trains the FIS. The FIS had three inputs, representing data from each sensor. As three sensors were used in the proposed design therefore the FIS had three inputs. The FIS had six membership functions each: very low, low, below normal, above normal, high and very high. The exact range of the membership functions was determined through repetitive trials. The FIS had one output with 3 membership functions. The data obtained during the calibration run provided the base input data (BID) for comparison. The range of the membership function of each input is defined as '[BID -1, BID+2]'. These values were obtained through repeated trials and were phantom dependent. The output had 3 membership functions: Absent, Not Sure and Present. All the output membership functions are singleton sets with values 0, 0.5 and 1 respectively.

Measurement and Evaluation

After training the FIS, the sensors are used to collect real time data using the Chameleon TVR software. Once the data recording is over, this data is exported to a txt file. The first segment of the code again converts this txt file data to MATLAB usable data. The third segment of the code, namely FIS Evaluation, uses this data to give a result. The system identifies whether a lump is present or not and if it is present, under which sensor. The segments of the above code are explained in detail below:

FIS Testing: Discussion and Conclusion

To test the limits of the Fuzzy Inference System, the CIRS Model 013 phantom with embedded artificial lumps is used. The PPS Finger TPS wearable finger sensors are used to sense 4 different lumps of varying size and depths in the phantom as shown below. FIS Algorithms along with Data Acquisition and evaluation codes are used to obtain the test results. The results obtained from these tests are elaborated in table 3.1.

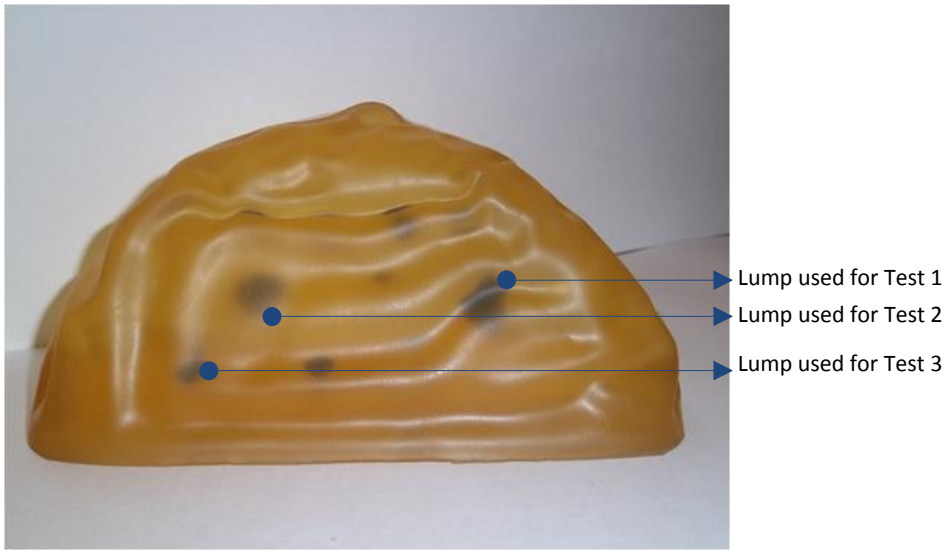

Figure 3-8 Position of various embedded lumps used for FIS Results

Table 3.1 Fuzzy Inference System Testing Results

Force Ratio	Index Finger (lbs.)	Middle Finger (lbs.)	Ring Finger (lbs.)
Test 1	Lump Diameter (approx): 1.3cm	Lump Depth (approx): 4 cm	
No lump Position	0.7	0.7	1.5
Lump under index Finger	1.1	0.7	1.6
Lump under middle finger	0.9	1.2	1.2
Lump under ring finger	0.7	0.9	2.5
FIS Results	Correctly identified the lump in all cases		
Test 2	Lump Diameter (approx): 1.1cm	Lump Depth (approx): 4 cm	
No lump Position	0.7	0.7	1.5
Lump under index Finger	1.7	0.8	.6
Lump under middle finger	1.0	1.3	1.3
Lump under ring finger	0.8	0.8	2.7
FIS Results	Correctly identified the lump in all cases		
Test 3	Lump Diameter (approx): .8 cm	Lump Depth (approx): 6 cm	
No lump Position	0.7	0.7	1.5
Lump under index Finger	1.8	0.9	.7
Lump under middle finger	0.8	1.9	.8
Lump under ring finger	0.8	0.7	2.8
FIS Results	Correctly identified the lump in all cases		
Test 4	Lump Diameter (approx): .5 cm	Lump Depth (approx): 3 cm	
No lump Position	0.7	0.7	1.5
FIS Results	Can not identify lump in any cases		

The results from the above tests conclude that the FIS algorithms cannot detect lumps of diameter less than 0.8 cm. The code was able to detect lumps having diameter more than 0.8 cm up to a depth of 6 cm. The limitation of the system was that only one standard phantom was used to train the algorithm and has provided proof of concept results. Generalisation of the algorithm to encompass broad range of tissue requires FIS training over large population, this is for future work.

3.3. In vivo healthy human tissue study

Similar to the phantom based study, the characterization of *in vivo* tissue was evaluated by capturing responses of three soft tissues of healthy subjects to a compressive loading[113].The spring potentiometers used for displacement measurement were calibrated by quantifying the output voltages at different positions using a voltmeter. The calibration formulas related to both spring pots were extracted from those measurements as follow:

$$X_{output} = 0.0648 \times V_{output} - 6.3058,$$

$$X_{output} = 0.1361 \times V_{output} - 5.5211,$$

where X_{output} is in millimeter and V_{output} is in millivolt. These equations show that there is a linear relationship between spring potentiometer voltage outputs and displacement outputs.

3.3.1. Methodology

The spring potentiometer was fixed over a piece of wood, and the string end was fixed over the fingertip force sensor worn by the tester. As the index finger was moving towards the tissue, force and displacement data were measured simultaneously in real time. The operator performed several loading and unloading trials to make sure that the strain rate was constant and the position sensor was in vertical direction. The index finger pressed the phantom by more than 10% thickness of the testing section.

In-vivo indentation testing involves using a fingertip force sensor and Celesco position sensor to capture force-displacement data on soft tissue of healthy human subjects. Palm, forearm, and bicep of ten healthy human subjects were tested over a rigid surface and compared – because those tissues contain soft tissue with specific thickness. The raw data of *in-vivo* testing were converted to relative indentation and load

distribution obeying Boussinesq theory. The subjects were three females and seven males age 24 to 45. Figure 3.9 shows the experimental configuration for *in-vivo* testing.

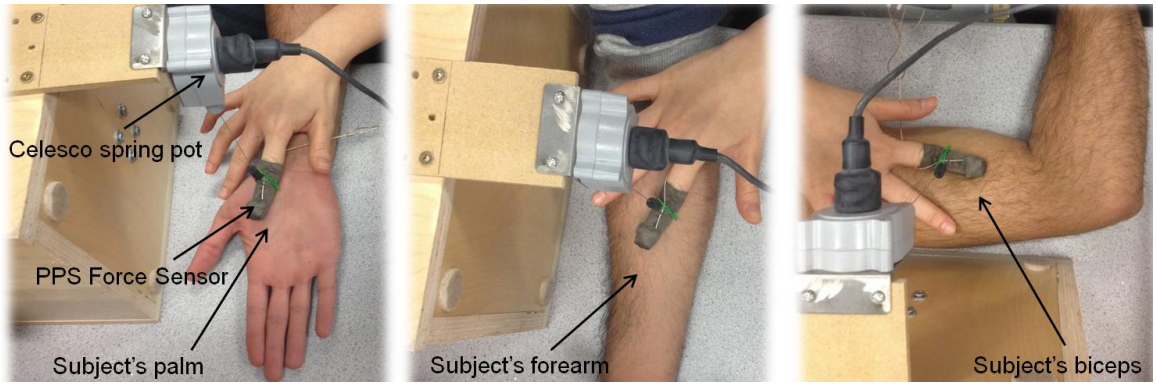

Figure 3-9 Experimental set up for in-vivo compression testing—as the finger wearing force sensor attached to the spring of spring pot went down, force-displacement data was acquired

3.3.2. Results

The results from 10 subjects are presented below. The tissue showed hysteresis as depicted in Figure 3.10.

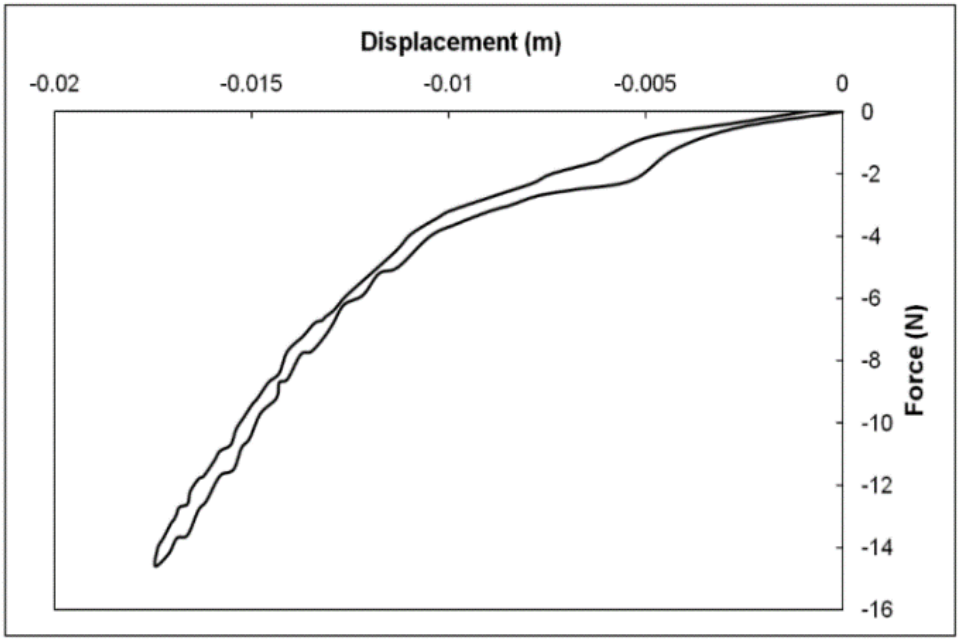

Figure 3-10 Hysteresis behavior of in-vivo palm.

Indentation results are shown in Figure3.11. The palm, forearm and biceps showed hyperelastic behaviour.

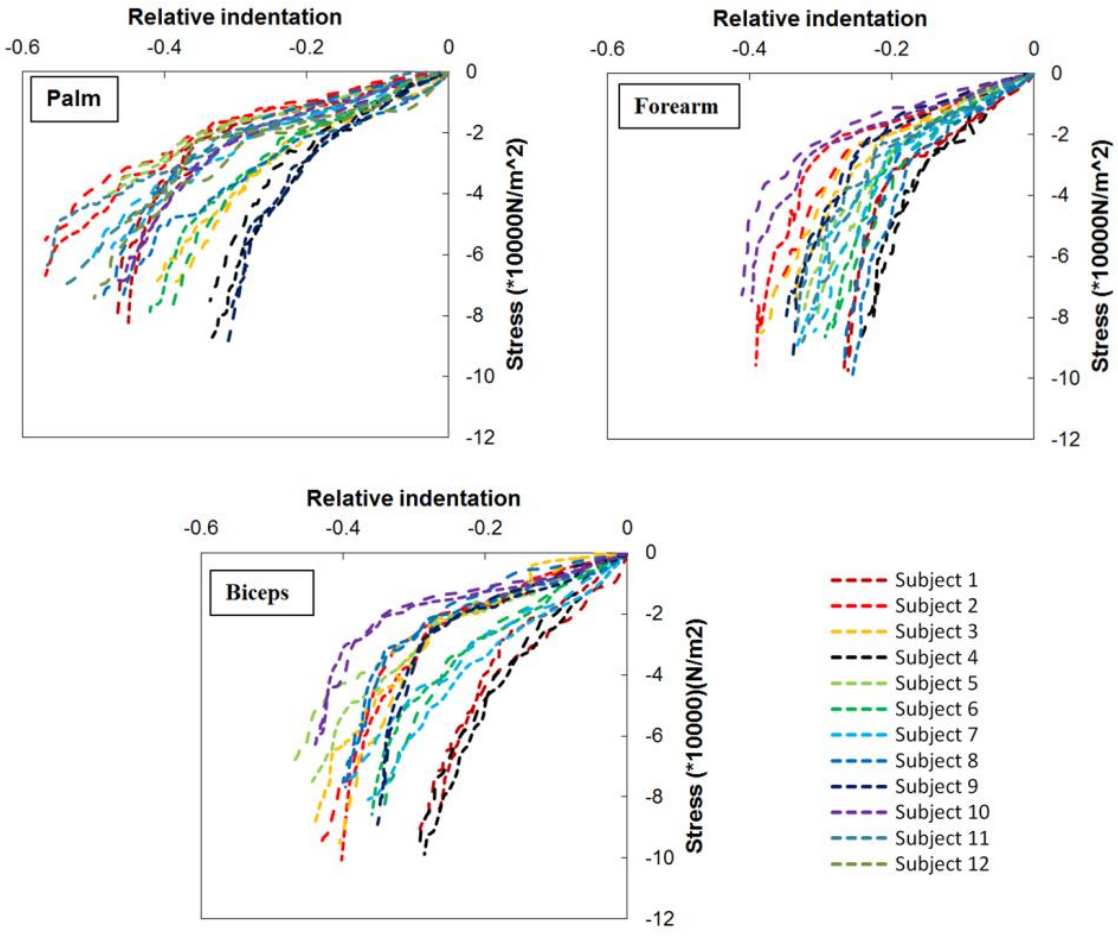

Figure 3-11 Stress-relative indentation raw data of loading stage-in-vivo tissues

Inter-subject data has been represented in Figure 3.12 and 3.13.

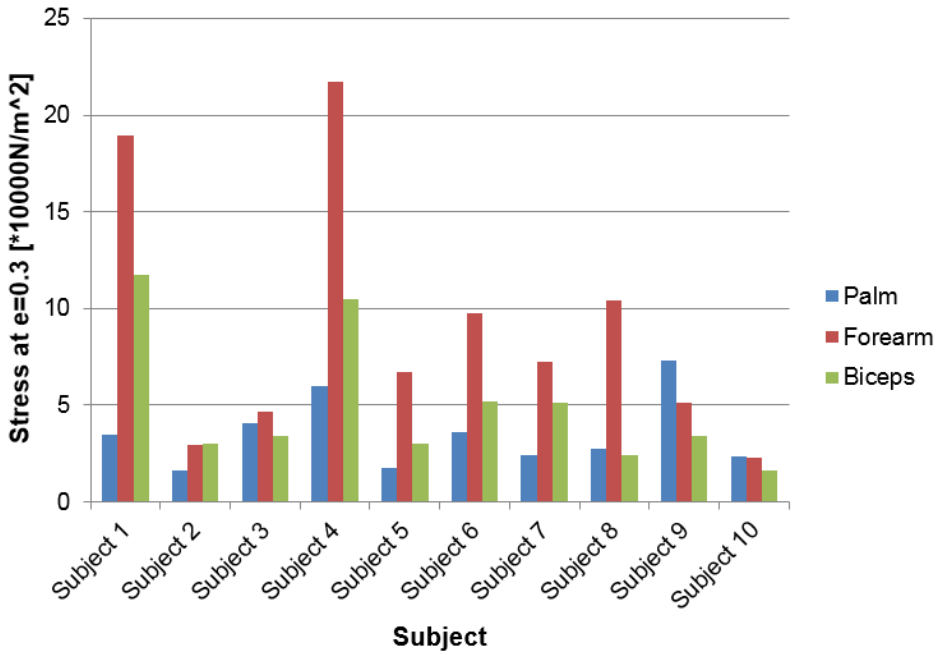

Figure 3-12 The trend between palm, forearm and biceps of each subject

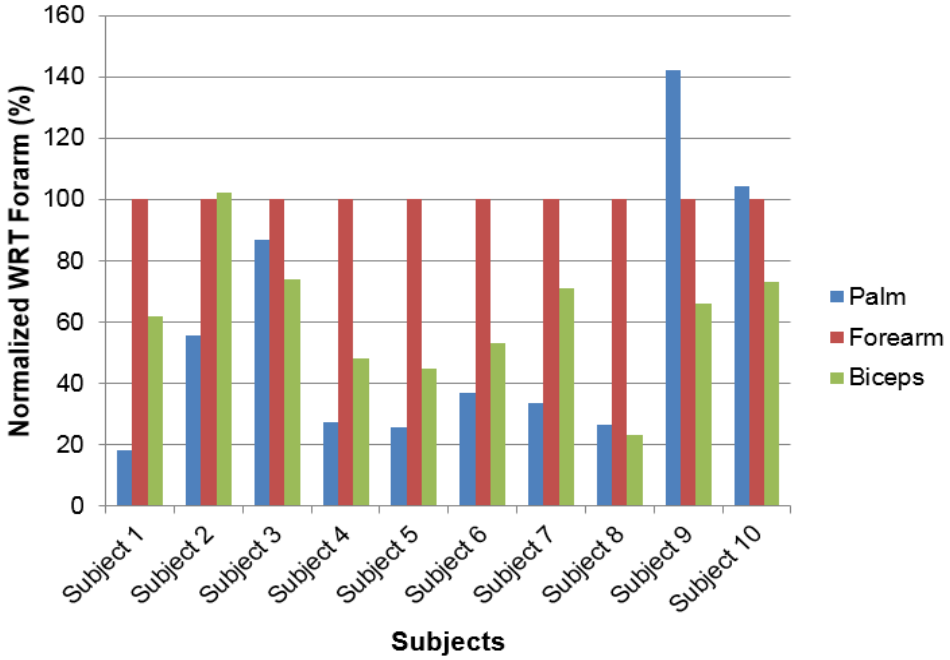

Figure 3-13 The relationship of palm and biceps with respect to forearm

3.4. Discussion and Conclusion

The goal in this research section was to validate the usability of identified off the shelf sensors to detect an anomaly inside otherwise homogeneous breast phantom, based upon relative stiffness of the anomaly to the surrounding material. In this respect various test set ups and sensors were analysed. The stiffness of the simulated tumorous tissue is three times the stiffness of the simulated healthy fat tissue. This is in line with the literature [105] that states infiltrating ductal cancer to be 10 times stiffer than normal fat tissue at 1% strain and 2.5 times stiffer than glandular tissue at 1% strain.

Through the phantom based study it is concluded that though indentation method involving measurement of displacement along with force is more accurate approach compared to tactile mapping using force sensors; but the indentation set up is very hefty and large. Therefore, tactile mapping using PPS finger tactile system is a promising tissue stiffness characterization methodology. It is easy to wear and can be easily interfaced with a computer to map the sensor outputs.

Though market available wearable sensors have been identified based upon theoretical and experimental results using gelatine based tissue equivalent material phantoms or realistic test bed; but further study on improving the wearable design and multiple sensor usage methodology need to be incorporated for reliable, repeatable, and clinically relevant data; quantifying physicians' decision. The initial results using the fat/tumor elastic property phantoms are promising but due to the inherent size of the sensory unit, it was possible only to detect tumor mimicking phantom around 2x2x2cm^3 at a depth of 2cm, Similarly the surface area of the force sensors is 349mm^2, it is anticipated that smaller size custom force sensors will increase the sensitivity and specificity of the system. Once the sensors were identified, decision based algorithms were tested over a commercially available phantom system. Training as well as testing data was acquired using the breast phantom from CIRS Model 013. The decision making algorithm were based upon Fuzzy Inference System (FIS). The results from the above tests conclude that the FIS algorithms cannot detect lumps of diameter less than 0.8 cm. The code was able to detect lumps having diameter more than 0.8 cm up to a depth of 6 cm. Therefore, addition of FIS to the developed relative stiffness

measurement hardware increased the capability of the overall system to find three times deeper (up to 6 cm deep) and half the size smaller (up to .8cm diameter) anomalies with stiffness comparable to tumors. Market available tactile sensing systems[52] show the capability of detecting as small as 5 mm lesions under the skin surface, but as no information regarding the depth is available therefore a direct comparison is not possible.

The limitation of the test set up and analysis includes the assumption made in this study that breast muscle consists of homogeneous stiffness tissue. Human breast is composed of a number of tissue types (refer section 1.1.1) and in reality is a non-homogeneous mass. This limitation can be overcome only when the system is tested over in vivo human breast. Ethics application is under review in front of the FHREB to move forward with this study. Another limitation is the use of the commercial phantom Model 013 obtained from CIRS. The application of this phantom is in biopsy training. Though the phantom is made from a proprietary gel with a physical consistency similar to human tissue, surrounded by an elastic skin-like membrane but is not specifically made for CBE training therefore the relative stiffness of the anomalies with respect to surrounding tissue is not available.

Chapter 4.

Tissue Classification: Electrical Impedance Spectroscopy (Phantom and *in vivo* Healthy Human Tissue Study)

4.1. Introduction

Electrical Impedance Spectroscopy (EIS) are measurements of electrical properties at multiple frequencies, made over the surface. It is a quick and comfortable method and, a non-invasive cost effective approach to tumour detection. The equipment is a fraction of cost of other screening systems. Electrical Impedance Scanning has especially been useful in detecting anomaly in human breast (promising adjunct to mammography [114]) and, differentiating benign and malignant skin lesions [115]. Additionally, Invasive Ductal Carcinomas IDC that constitute 50-80% of breast cancer[42] can be detected early using Electrical Impedance Spectroscopy as Ductal epithelial impedance Spectroscopy[55].The study concludes that Electrical signature of ductal epithelium may be used to identify patients with benign, proliferative or malignant breast disease. During early stages of carcinogenesis, increase in electrical resistance dominates the ductal epithelial profile, whereas later as breast tumors become invasive and cell mass increases, resistance decreases and tumor capacitance increases. The advantages of the EIS modality are attractive to be used as an integration modality to improve the clinical breast examination. The limitations of EIS that need to be addressed are: the difference in the electrical properties of various breast pathologies is not well documented, more data is required to better categorize the information contained in the EIS maps. The frequency response of both normal and pathological breast tissue need to be better understood as key features to identify cancer may be located at frequencies not typically used. Further, post processing of EIS breast information is still limited and

needs to looked more into. For clinical application three-dimensional reconstruction algorithms also need to be improved.

4.1.1. Background and Overview of present state of Technology

Electrical properties of tissue have been studied since late 1800s, though active research in this field began around 1920s [116]. *In-vitro* testing of normal healthy breast consisting of different types of tissue showed moderate variations in impedance values, but malignant tumours showed increased capacitance and conductivity values [117],[118],[119],[120],[121]. *In-vivo* impedance measurements support these findings [122][123][124]. EIS measurements are based upon tissue specific electric field distribution and the measurability of currents or potentials on the surface of the body at the region of interest. Simulation results show that conductivity disturbance inside the breast can be measured by planar electrode array set on the surface, in such simulations the healthy breast was approximated as a uniform distribution in electrical conductivity and the malignant tissue was approximated as a higher conductivity disturbance within the uniform distribution [125]. The basic principle of EIS is based upon the classic trans-impedance measurement method [126]. The dipole method was used to calculate the distribution of the current density on the surface with a higher conductivity object placed below the surface. The three element model was used and the solution was found at one frequency that leads to the maximum imaginary part. Through better post-processing algorithms the sensitivity was further stabilised [127]. Two main predictors were used: frequency and phase at which imaginary part reaches maximum and, phase at 5 kHz on the lesion and the nipple respectively. Further space-frequency multiple signal classification (MUSIC) was done to get the three-dimensional position information too. Moreover, attempt has been made to find the depth and radius estimation of a single lesion at one driving frequency [128]. EIS data has also been examined using empirical algorithms that take into account data across seven frequencies [129].

Based upon these findings Electrical Impedance Scanning was developed for identifying the malignant from the benign or normal tissue during breast examination. It helped decrease the number of biopsies performed. EIS is inexpensive and the maps

take about 15 minutes but its current form has clinical limitations i.e. detection of lesions directly behind the nipple, artifacts from superficial lesions and poor contact. An imaging device based upon this modality is TranScan TS2000 [126], it was granted FDA approval for adjunctive use with X-ray Mammography [130], it uses a model that describes the electrical field surrounding a lesion in otherwise homogeneous surroundings. Other Electrical Impedance Scanning systems developed include electrical transimpedance scanning (ETS) system [131], this system provided 8x8 and 16x16 electrodes in the probe, with each electrode the area of 1x1 mm^2 and the space between adjacent electrodes 2.5 mm. The driving frequency is from 100Hz to 10 kHz. Rensselaer group is developing the ACT4 system [132], [133]. It is confirmed to support 60 electrodes in two 5x6 radiolucent arrays. The frequency range is from 5 to 1000 kHz.

The current mapping methods are based upon parameters of trans-admittance at single frequency; multiple frequency data of EIS is very important and needs to be explored more. Further, Electrical Impedance Tomography is the imaging modality introduced in UK in 1982[134], and produces images from the internal conductivity distribution of an object. It is based on the measurements collected from the surface of the object [135][136][137].

4.1.2. Electrical Properties of Biological Tissue

Human tissue is electrically conductive, and the tissue conductivity varies significantly between different tissues. The changed electrical properties of malignant tissue with respect to healthy tissue are attributed to increased cellular water and sodium content, altered membrane permeability, and changed packing density and orientation of cells [138],[139],[140]. Tissue can be considered as a collection of conducting intracellular fluids (electrolytes) bound by insulating membranes, these membranes themselves existing in a conductive suspension, extracellular fluid [141]. The first model showed the cells as a number of resistances representing the extracellular and intracellular media, and capacitances representing every minute section of the membrane [142]. Apart from the change in actual component values, single cell in suspension and tissue can be represented by the same electrical model.

At the macroscopic level, a tissue's impedance depends upon the tissue composition, structure, fat and water contents and varies with the pathological state of the tissue (e.g. oedema, ischaemia, cell proliferation). The variability of impedance has been studied in normal and pathological breast tissue [143]. The study calculated the mean m, the standard deviation s, and the 'reduced standard error' ($\varepsilon = s/(m/N)$) (N being the number of samples) of the magnitude and phase angle of impedance at each frequency. 12 frequency points were used from .488 kHz to 1 MHz. The reduced standard error was found to be about .01 or less for frequency greater than 10 kHz. "Smaller variabilities were observed in the adipose tissue, the carcinoma and the fibroadenoma, indicating that these tissues can be readily characterised by impeditivity". The study also suggested that frequencies greater than 1 MHz were needed for bio-electrical characterisation of breast tissue.

The study regarding the analysis of impedivity of freshly excised normal and pathological human breast tissue[118] indicates that impedance spectroscopy is appropriate for the detection of breast cancer. This study classified tissue samples in six groups of tissue; three tissue were normal tissue: mammary gland (group MG), connective tissue (group CT), and adipose tissue (group AT). The other three groups were pathological tissue: mastopathy (group MA), it is a general term for various benign breast diseases, fibroadenoma (group FA), and carcinoma (group CA). The results from the study showed that there was an absence of correlation between impedivity (or admittivity) and patient's age therefore; the responses of different type of tissue depend only on the nature and structure of the tissue. The measured modulus and phase angle of impedance were considered optimal set of parameters for the statistical analysis of bioelectric spectra collected in freshly excised breast tissue. Impedance, low-frequency limit resistivity or fractional power did not show any significant difference between the group of normal and benign tissue. Similar results were observed in another study [144] that concluded no significant difference between fibroadenoma and normal breast tissue. The data from the study has further been utilized in other studies [125] to calculate the frequency dependence of the real parts of conductivities and permitivities, and the imaginary parts of the conductivities for different tissues.

Yet another study [145] showed high significant differences in carcinomas and mastopathy forms. These differences are not detectable in comparison to normal tissue and fibroadenomae. The cancerous tissue group (CA) differed significantly from group FA and MG (non-cancerous) by the modulus of impedance up to 31.25kHz and from all groups of tissues by the low frequency limit resistivity and phase angle from 125kHz to 1MHz. The low-frequency-limit resistance of carcinoma was larger than other fatty groups (excluding CT and AT). The value was 389+/- 108 Ω cm for carcinoma (CA) and 1263 +/- 387 Ω cm for connective tissue (CT). These are in agreement to other calculated values of [146] 250-500 Ω cm in central part of tumor and > 1000 Ω cm in surrounding tissue. The larger values were attributed to the change in biophysical properties of tissue, tumour stroma being denser than normal interlobular connective tissue along with calcification [147]. The results were similar to another result [148] that were for *in vivo* impedance measurements that reported values of low-frequency-limit resistance, R_e, of 1445 Ω in breast cancer, 954 Ω in fibroadenoma and 780 Ω in normal breast tissue. This was done by a three electrode method by inserting a fine needle electrode into the tumor. The extracellular resistance, the intracellular resistance, and the membrane capacitance were calculated based upon the complex impedance and model circuit. The frequency range was 0-200 kHz. Another contradictory study reported the relative conductivity of breast tissue ranges from 2 to 34 mS cm-1, from 7 to 49 mS cm-1 for benign breast tumors, from 3.7 to 34 mS cm-1 in normal breast and from .5 to 2.9 mS cm-1 in fatty tissue [149]. The study concluded “the properties of benign and malignant tumours may not be distinguishable dielectrically”. This study was done over samples that were kept refrigerated and measurements made between 24h of excision, therefore the difference in the conclusion of the study. The metabolism of tissue starts to decrease immediately after excision, resulting in changes in tissues’ passive electric properties. It was reported [150] that “... the beta-dispersion began to decline noticeable only after metabolism had almost entirely ceased...”. It has also been stated [151] that “ the passive electrical properties remain stable for 30 min after the tissue removal” further the mobility of ions in electrolytes is affected by temperature [150].

Therefore, the bioelectric parameters and the profile spectra in different groups of tissue can be used for tissue classification. The possible future studies recommended

are to extend the measurement frequency range for better tissue classification, a comparison between normal and pathological tissue in same patient, measurements *in vivo* and, development of data processing techniques for classification of multifrequency impedivity spectra.

4.1.3. Determination of Tissue Impedance

The bulk tissue model most prevalent and used today, 'Debye model' [152] is the resistor R_1 (extracellular resistance) in parallel with a combination of a capacitor C (membrane capacitance) and a resistor R_2 (intracellular resistance) as shown:

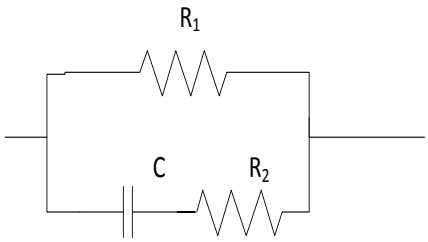

Figure 4-1 The Debye model of tissue impedance

In a simplified model R_2 has been shown in series with both R_1 and C being in parallel [153].

Tissue properties are due to the associated cell and extra cellular medium properties that consist of ionic solutions. The cell further consists of cellular membrane and the intra-cellular medium. The cellular membrane consists of lipid bi-layer and proteins. The cell membrane is capacitive in nature but with selective permeability as ions can become charged and move from one field to another on application of electric field. Therefore the frequency dependent behaviour of tissue is beyond simple RC circuits. It is due to the fact that at different frequencies different components contribute to impedance differently. Therefore, tissue impedance is frequency dependent and has complex value. The electrical properties of the tissue can be described by the

conductivity σ and dielectric permittivity ε. The permittivity depends on the frequency of the electric field and the conductivity is static.

The electrical conductivity is tissue specific as it depends on the mobility of ions in the extracellular fluid in presence of the electric field. The tissue composition affects the current. Permittivity on the other hand is related to the polarization of the media. Time-varying polarizations due to time-dependent electric fields cause polarization currents. The polarization processes involved are displacement and orientation polarization. In the bio-impedance measurements frequency range (up to MHz range), displacement of electron clouds with respect to their nuclei and of positive ions with respect to negative ions in large molecules are instantaneous. The orientation and polarization of existing dipoles of different sizes, formed by cells or molecules, are time-delayed due to relaxation processes. They introduce phase shifts with respect to the applied time-varying electric field. For the ease of simpler calculations, polarization processes including relaxation are commonly described by a complex permittivity, relating the polarization and electric field vectors, also considered to be complex [125].

As tissue incorporates a reactive component, therefore rather than conductivity or resistivity of tissue, impedance or admittance of tissue need to be referred. EIS requires the calculation of the complex impedance (Z) of the tissue. Complex Impedance (Z) of an RC circuit is given as $Z = R + jX_c$, where $X_c = 1/\omega C$ ($\omega = 2\pi f$, where f is the frequency). It can also be represented in polar form $Z = Z/\theta$, where Z is the magnitude and θ is the phase angle of the impedance. Z is the square root of $R^2 + X_c^2$ and $\theta = \arctan(X_c / R)$.

The frequency response of biological tissue depends on its physical and physiological parameters, i.e. on its nature and structure [154]. The impedance frequency response of living tissue in the frequency range used for electrical impedance scanning is described as follows[155]:

$$Z = R_\infty + \frac{R_0 - R_\infty}{1 + (j\omega T)^\alpha} \quad (6)$$

Where R_0 is the low-frequency limit resistance, R_∞ is the high frequency limit resistance, α is the "fractional power" (α<1), T is the time constant of the tissue ($1/T = F_c$ the characteristic frequency), ω the pulsation (ω = 2πf, with f the frequency) and j is the base of imaginary numbers ($j^2 = -1$).

Three relaxation regions were identified for tissue [125]: α, β, and γ, at frequencies approximately 100Hz, 500kHz, and 25 GHz. The α region is related to the extracellular surface polarizations of large cell, β region is the result of increasing capacitive charging and discharging of cell membranes and γ region is the relaxation of the water molecules. At low frequencies the current is extracellular but intra cellular frequencies become more significant with increasing frequencies.

4.1.4. Calculation of Parameters for Characterization of Breast Tissue

To study the frequency dependant behaviour of tissue, the most prevalent method is the Cole-Cole plot [156] used to observe the relationships between pathology and locus of Z versus frequency. A variety of cell types were examined by Cole and he observed that the variation of impedance with frequency approximates a semicircle on the resistance-reactance plane. The centre of the semicircle is displaced positively on the resistance axis, at the characteristic frequency (F_T). The semicircle has a radius of $r = (\rho_0 - \rho_\infty)/2$ where ρ_0 represents the DC frequency and ρ_∞ represents the value that the resistance approaches as frequency approaches infinity. Semi-circle locus works well in theory but most of the collected data shows a depressed centre. Therefore, Cole further modified the derived equation. Cole found that when the impedance representing the membrane was modified such that the phase angle was constant over all frequencies, the locus represented a depressed circle and was closer to experimental data. The bioelectric parameters ρ_o, ρ_∞, α and F_T can be calculated by fitting circular arcs to experimental data. But the experimental data collected in the study [118] showed the few loci did not have a maxima therefore calculation of ρ_∞ and F_T was impossible. In certain cases, the loci formed quasilinear arcs, with a very small curvature (essentially in group MG and FA). Further, the frequency responses of certain samples were more complex than circular arcs, and formed "composite loci", comprising two relaxation

domains, presumably due to the compound structure of the tissue. In such loci, principally in CT and CA groups, a minimum in the imaginary part was observed at a certain “notch frequency”. Most of the loci differed from the “classical semicircular arcs, which rendered impossible the calculation of the usual set of bioelectrical parameters. This was attributed to the several factors including the presence of different tissues within the examined sample, the complex tissue structure involved, and the presence of several dielectric relaxation mechanisms within the measurement frequency range. Further, deconvolution [157] and CNLS (Complex Nonlinear Least Squares) data –fitting method [158] enables the calculation of the elements of equivalent circuit models, but as stated [159]”..the main difficulty is in finding a realistic electrical model to biological processes” Therefore alternative parameters were suggested [160], that did not require arc fitting or equivalent circuit model.

The basic four parameters used were: Low- frequency- limit resistivity, ρ_o, High-frequency-limit resistivity $\rho_\infty = 1/\sigma_\infty$, fractional power, α, and the top frequency F_T. ρ_o and α were calculated by extrapolation using second order polynomials fitting the low frequency points of each spectrum. For groups where second order polynomial did not fit, linear regression equation was used. The values of top frequency were interpolated (using four or five points) using a second order polynomial. Similar procedure was used for notch frequencies. The ρo of groups CT and AT were quite different from other groups and even for α, the comparisons were valid. Further, the measured impeditivity spectra were transformed into admittivity spectra, to relate directly to conductivity and permittivity of tissue.

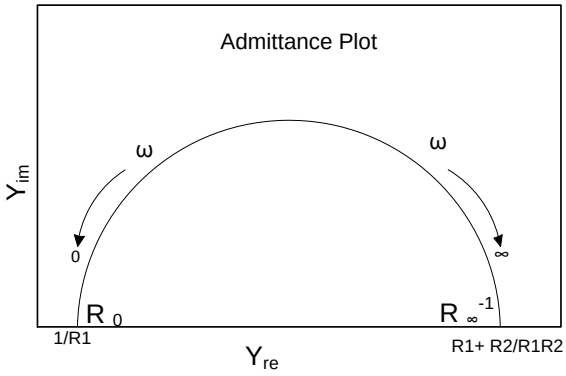

Figure 4-2 The Cole-Cole plots of tissue admittance

To improve classification, attempts were made to increase the number of parameters [160]. This study used absolute parameters but relative parameters can also be used. A total of eight parameters were defined, but for less complex loci only four parameters can also be used.

- σ_0 :Low Frequency Limit Admittivity, Five low frequency points to calculate the real part value for low frequency
- α: Fractional Power, Calculated at low frequency end of spectrum, it is the slope of the extrapolation polynomial at the intersection point with the horizontal axis
- Q_{LF}: Ratio σ_0/ σ_∞ (ratio low limit admitivity/ high limit admitivity, ratio of admitivity at 10 KHz and 1 MHz.)
- D_A: Distance to the Low-Frequency Intercept, It is the distance between the spectral ends
- Φ_{500}: Magnitude of the Phase Angle at 500kHz
- S_{HF}: High-Frequency Slope in Phase Angle (250, 500 and 1000KHz point): Slope of the phase angle against frequency in the high frequency region of spectrum
- K_Φ: Integrated Phase Angle Ratio, The ratio between the area below the curve in two adjacent frequency domains, 10 kHz- 100 kHz and 100 kHz- 1 MHz. Phase angels were used instead of reactance. The surface area was calculated according to the following equation:

$$K_\Phi = \frac{\frac{\Phi_6 + \Phi_9}{2} + \Phi_7 + \Phi_8}{\frac{\Phi_9 + \Phi_{12}}{2} + \Phi_{10} + \Phi_{11}} \quad (7)$$

Later on more parameters were added [161]:

- BREAK: Spectral Break Point
- NOTCH: Spectral notch Point
- AREA: Area under Spectrum
- AREA_D_A: Area normalised by D_A
- IP_{MAX}: Maximum of the spectrum
- D_R: Distance between I_0 and real part of the maximum frequency point

- PERIM : Length of Spectral Curve
- SLOPE: Slope of the spectral curve obtained by linear regression

Due to the reduced number of cases representing each class in the data set, linear discriminant analysis approach was used to classify the spectra. The classification was performed in two hierarchical stages. The straightforward one-step six class discrimination (based on the design of six linear discriminant functions) performed poorly therefore the hierarchical approach was used [162] for difficult multiple class separation problems to characterise biomedical data. The results state that firstly calculating the features for tissue classification did not require any particular model for the tissue. The features that proved to be most discriminative for the classification were low frequency limit admittivity, IPMAX: Maximum of the spectrum and AREA_DA: Area normalised by DA. It was impossible to discriminate with reasonable accuracy between mastopathy, fibro-adenoma and glandular tissues. But carcinoma discrimination was good, showing EIS to be a potential candidate for screening applications in breast cancer detection. This classification was better than previous classification as the overall efficiency in discriminating carcinoma increased from 78% to 82%. A recent paper [163] uses multiple frequency approach compared to the classical single frequency approach. It states that multiple frequency approach is a novel vision to study EIS. From the plots, it has been able to find abnormal tissue, by just using multi-frequency measured data from the same subject. The results are also more stable compared to single frequency data. Lastly they have been able to pick out the bad contact and air bubbles occurring in commonly EIS examination. Results showed that compared to classical EIS mapping, the multi-frequency parameter mapping EIS shows four advantages:

- Parameter mapping can obtain four mappings by the selected model, helps identifying different types of disease
- From the plots of the real and imaginary parts of admittance, it can easily be deduced whether abnormal tissue exists or not from the multi-frequency measured data from the same subject. Thirdly, the results are more stable than just using single frequency.
- The artificial positive results can be picked out.

Some other studies also show other methods to determine if the electrodes are making contact with the breast of the patient. Similar study using five frequency sweeps was done to compare Cole-Cole plots and distinguish benign and malignant lesions [164]. Further, simulated data along with data from Jossinet [165] has been used for classification based upon learning vector quantization algorithms [166]. One of the classification methods: Support Vector Machine (SVM) [167], has been used in classification for prostate cancer biopsies [168] as well to distinguish the simulations of malignant and benign tissues in breast [169]. Moreover, resonance-frequency based electronic impedance spectroscopy has been used with genetic algorithms and SVM to classify as: biopsy recommended or non-biopsy recommended [170]. Further, feature extraction using machine learning along with Support Vector Machine has been used to classify breast tissue [171].These studies, simulation based and feature extraction based, illustrate the ability of the SVM classifier for tissue characterization.

4.2. Phantom Study: Test Set Up and Methodology

In the present study, an Electrical Impedance set up has been designed for measuring tissue electrical impedance. It consists of 16 sensing electrodes; these are pre-gelled electrodes from Vermed [31]. The data is collected by interfacing the electrodes with an Impedance Spectroscope HF2IS along with transimpedance amplifier HF2TA. The complex conductivity and permittivity measurement is done using frequency sweep to get multi-frequency mapping. The developed software is such that when run, a trigger is given to the Impedance Spectroscope that starts the device, and all the settings of the device are programmed using the Software code. These settings can be changed through the code, no manual settings needs to be done.

The impedance can be measured using two methodologies: Two Point Measurement or the Four Point Measurement. In the current study two point measurements have been considered as represented in Figure 3. The HF2IS generates an output signal of amplitude V_Z (1 Volt). A reference electrode is attached to this output of the HF2IS. A measuring electrode, attached to the tissue, measures the output signal that has been modified due to the tissue properties based upon the transfer function of the three element model. One volt input (generated by Impedance Spectroscope) is

applied to the tissue using the reference electrode. This voltage has been swept from 300 Hz to 1 MHz in order to have impedance spectrum of the tissue in this frequency range at 50 different frequencies. The current flow through the tissue is measured with the measuring electrode represented as I_z. Measuring electrode is virtually grounded thus the voltage that is applied to the tissue is V_z and the current passing through the tissue is I_z, hence impedance spectrum of the tissue can be calculated by $Z=V_z/I_z$. While taking the measurement from the breast, the reference electrode is attached to the centre of subjects' palm. The current travels from the subjects' hand to arm and reaches the highly conducting pectoralis muscle that can be considered iso-potential plane [8]. The measuring electrode is placed over the breast that senses the incoming current I_z, that is altered according to the transfer function of the underlying tissue; malignant tissue have a different transfer function compared to healthy tissue.

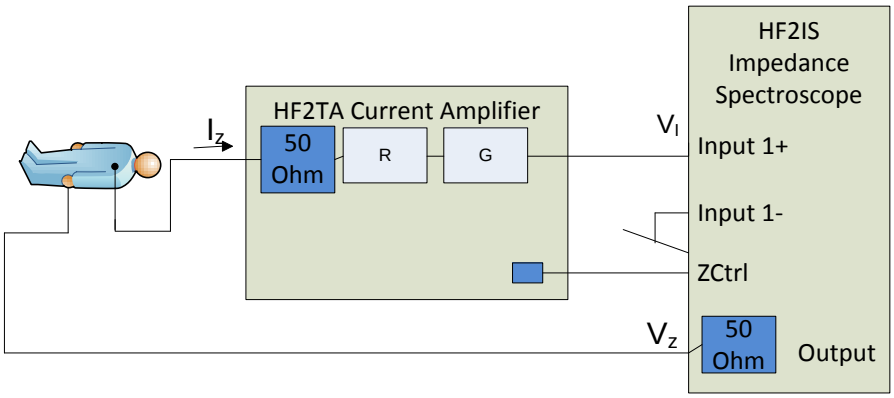

Figure 4-3 Set up Block Diagram

Complex impedance is therefore calculated as:

$$Z = \frac{\mathrm{conj}(v_z)}{\mathrm{conj}(I_z)} \tag{8}$$

The conjugate is used as there are different ways to extract R and C values one method uses conjugated values. As transimpedance amplifier is inverting the voltage, so a minus in put in front of the formula where current is calculated from demodulator data (x, y) of the impedance spectrometer.

The config.i.preamp.totalGain is transimpedance settings and has been set to

$$I_z = \frac{-(x + 1i * y)}{\text{config.i.preamp.totalGain}\ \ (\text{config.i.gain50})} \tag{9}$$

1K, and the config.i.gain50 is set as .5 because of voltage divider that exists due to 50 Ohm input impedance of HF2IS and 50 Ohm output impedance of TA. The complex impedance data is displayed as Nyquist plots (Real Impedance verses Imaginary Impedance) or Cole-Cole plots (Reactance verses Resistance).

To calibrate the system, a parallel RC circuit (1MΩ, 2.2 nF) is used. The value of Z is calculated by the following formula:

$$Z\_theoretical = \frac{R}{1 + j * 2 * \pi * f * R * C} \tag{10}$$

The impedance plots are preferred to be shown in the form of admittance (A) plots; therefore the conversions were performed as follows.

$$A = \frac{conj(I_z)}{conj(V_z)} \tag{11}$$

The data was collected over three phantoms fat equivalent phantom, muscle equivalent phantom and muscle embedded in fat phantom depicting anomaly in homogeneous tissue as shown in Figure 4.4(refer section 2.2.3).

Figure 4-4 Phantom Test set up for measuring Electrical Impedance at multiple frequencies

Further, an integrated phantom is made as shown in Figure 4.4; the mimicked tumor embedded inside the fat phantom is made by adjoining a fat equivalent phantom over an fat phantom that has a layer of muscle phantom. The size of the muscle phantom is cut to 2 cm x 2 cm x 2 cm cube. Two set of measurements are taken, at 5N and at 25N (Figure 4.7). The results show no major effect of force on phantom impedance. The impedance nyquist plots of all the three different types of phantoms are variable enough to be classified into different groups.

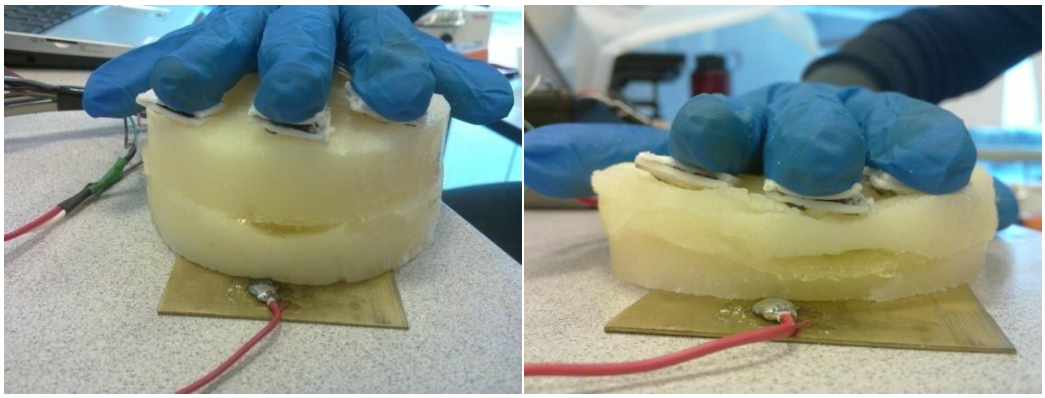

Figure 4-5 Integrated Muscle (2cm cube block) in Fat Phantom, Right: 5N force applied, Left: 25N force applied

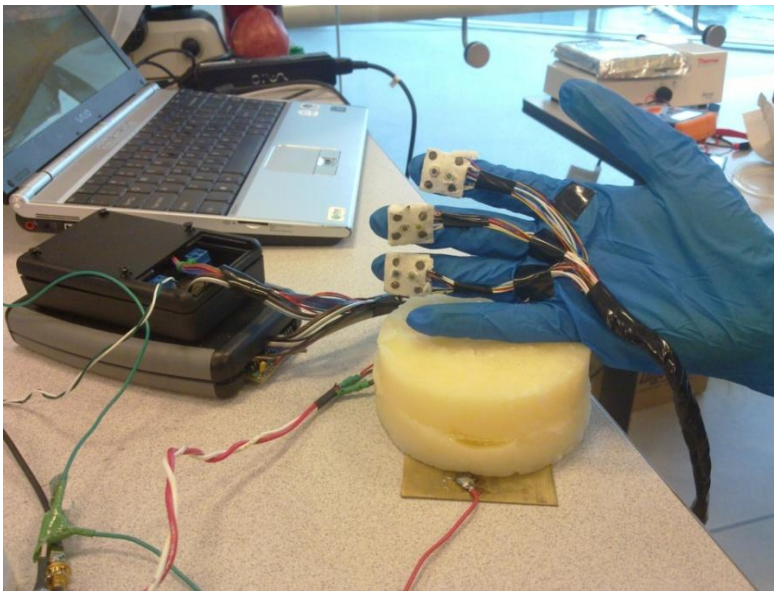

Figure 4-6 Electrical Impedance Spectroscopy Phantom Test Set Up

4.2.1. Decision based algorithm implementation: Adaptive Neuro Fuzzy Inference System (ANFIS)

The data collected is quite repeatable and reliable, Figure 4.7, except few glitches that can be attributed to the electrode contact loss. This data was further used to develop a decision making algorithm that categorised the data into fat or muscle phantom group. The decision making algorithms were built by training the system using Adaptive Neuro Fuzzy Inference System (ANFIS). The number of membership functions used was 5, the membership function type was ‘gbellmf’ and the number of epochs was 20. These parameters were adopted after repeated trials and experiments using different values and adopting the best fit values.

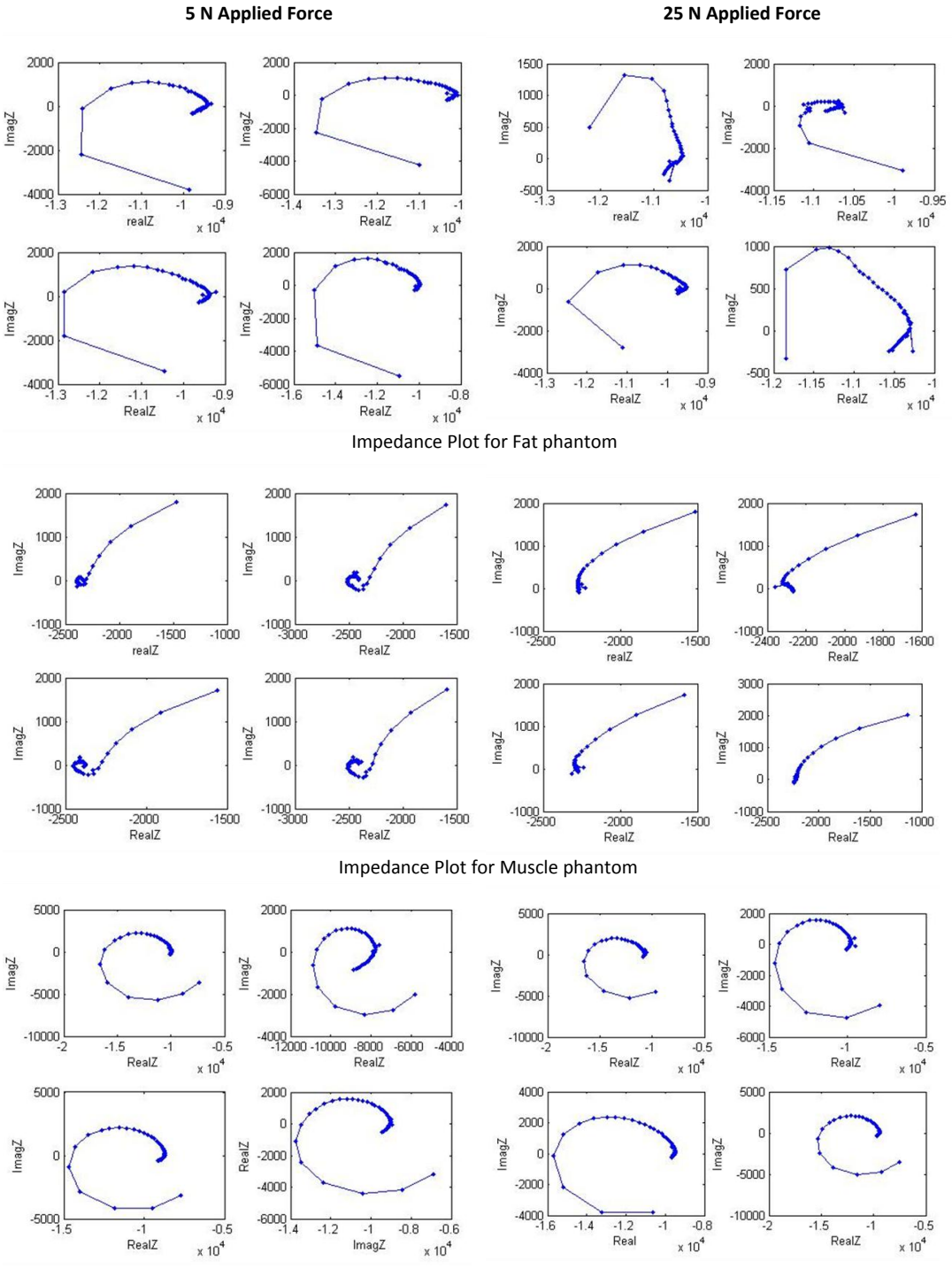

Figure 4-7 Impedance plots for different kinds of phantoms (4 trials) at two force levels: 5N and 25N

Result

ANFIS results, Figure 4.8, show that the system can be trained to distinguish the fat phantom from the muscle, but the system was incapable of differentiating the muscle embedded in fat phantom group from other groups due to the close association of this group data to the fat phantom data. Four trials for each frequency sweep were taken; the resultant training data is represented by the blue line. The resultant figure shows the decisive graph. The same methodology was further applied over muscle embedded fat phantom but the system was is incapable of detecting an anomaly (muscle phantom) embedded inside the fat phantom. This can also be attributed to the availability of small set of training data along with small number of electrodes.

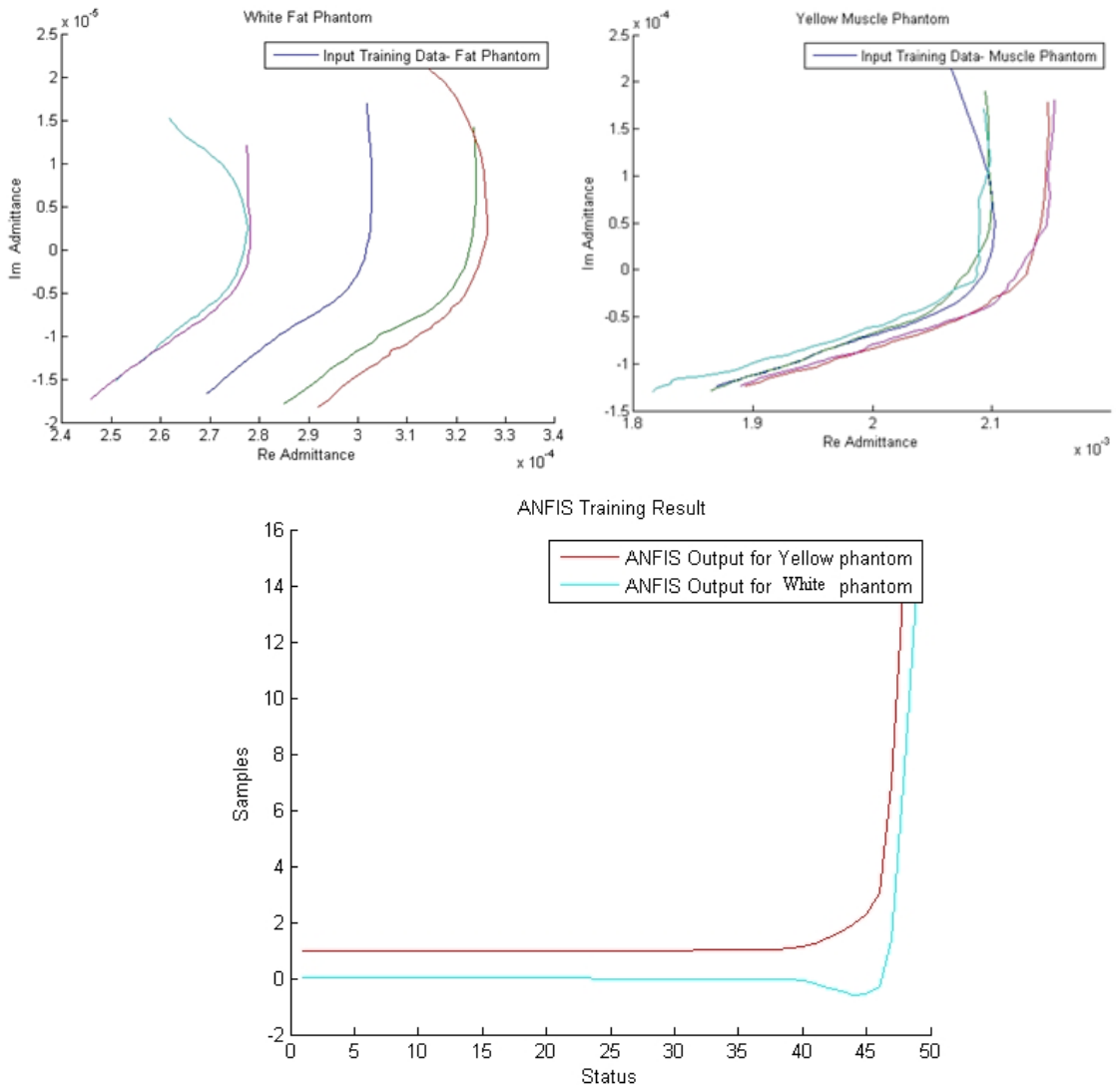

Figure 4-8 ANFIS training data (Upper two graphs). Four trials for each sample type, resultant training data is represented by blue line. The decisive plot (lower graph) for classifying muscle and fat phantom, any value greater than 1 is classified as belonging to muscle phantom

4.3. Tissue study

After verification of the developed screening glove hardware using phantoms the next step was to test it over *in vivo* tissue. Ethics approval for two different studies was taken. The first study involved the collection of *in vivo* data over healthy subjects. Tissue complex impedance data, thermal data and elastic properties data was taken at various

levels of pressure. This study adhered to all human testing standards and was reviewed and approved by the Office of Research Ethics, Simon Fraser University in the study named "*In Vivo* Data collection of dielectric, thermal and elastic properties of human tissue"; APPL. #2011s0523. The study originally did not consider collecting data from breast tissue but after recommendation from supervisory committee the application was revised and approved to include data from the four quadrants of healthy human breasts. For this 20 subjects were recruited.

Promising results of the study over classification of healthy human tissue using complex impedance parameters lead to extending the multimodality data collection over malignant tissue to observe the variation of electrical impedance with pressure or temperature. This study was carried over malignant skin tumors with the control as a contralateral healthy body tissue. This was collaborative research with the BC Cancer Agency. The research had to be carried over skin tumors as after repetitive meeting with oncologists it was suggested that due to the sensitivity involved in breast cancer patient population it will be best to test the device over skin tumors first. This study 'Electrical Impedance Analysis of Malignant and Benign Tissue: Effects of Temperature and Pressure' was done under the UBC BCCA Research Ethics Board under Dr. Paris Ann Ingledew as the Principal Investigator and REB Number H13-02887.Approval was also taken from SFU REB 'Electrical Impedance Analysis of Malignant and Benign Skin Tissue: Effects of Temperature and Pressure, Study Number: 2014s0134' to conduct this study.

4.3.1. Methodology

The study aimed to characterize the specificity and sensitivity of the developed multisensory detection system on live human tissue. The following tasks were performed during the study:

- Determine the temperature of tissue using a non-contact infrared temperature detection sensor.
- Determine the elastic properties of tissue using a contact type force sensor
- Determine the electrical properties of tissue using a contact type Ag/AgCl electrodes and low current/voltage signals from a Lock in Amplifier.

The subject was asked to lie in the supine position so that data collection location is kept nearly same for all the data collection points. In order to overcome the skin resistance, data was collected using pregelled self-adhesive SilveRest® pregelled EKG electrodes from Vermed A10009-100F[172]. Five body locations were considered to get a comparative study done. The reference electrode was placed in the centre of the hand on the palm. The body locations considered for data collection were; tissue in between the thumb and the forefinger, the wrist bone, the nail of the centre finger, the tissue over the arm, tissue over the bicep and the four quadrants of the breast. The breast was divided into four quadrants: Upper Outer, Upper Inner, Lower Outer and Lower Inner. The centre of the breast was not considered for the data collection. To get the repetitive same position on different individual breast a specific position marking procedure was followed. According to the Breast Cancer Research [173] tumors in breast are more prevalent in the left breast and in the upper quadrant. Therefore in the present study the left breast was divided into four quadrants and data from each quadrant was taken. As each individual has different size of breast therefore to keep consistency in the location of data collection point we considered the centre of the breast to be the reference point and all four data collection points were around this centre placed at same distance in the four quadrants (Figure 4.9).

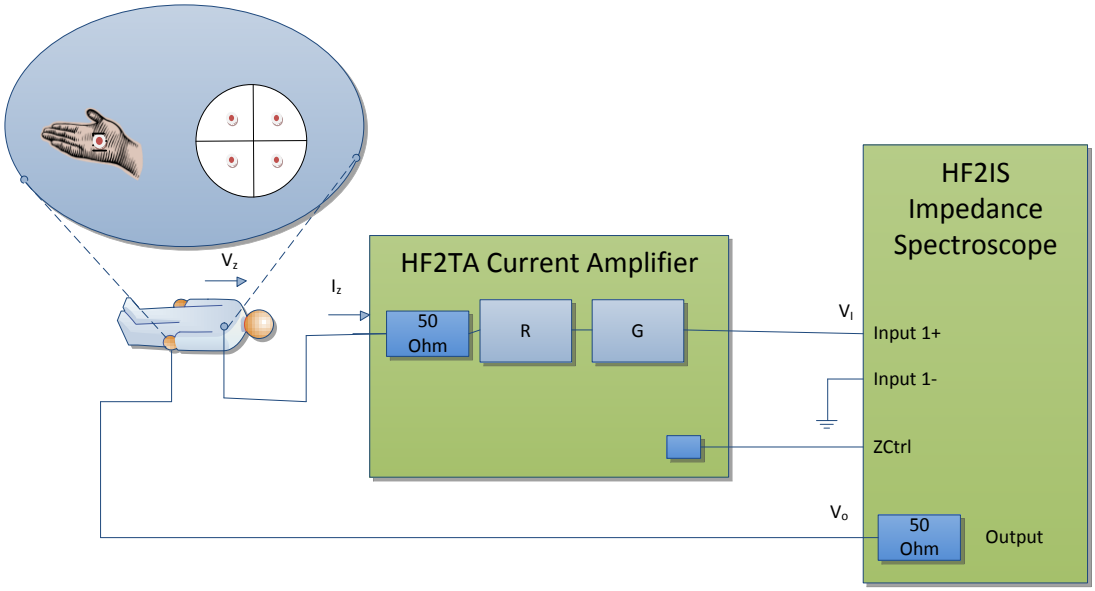

Figure 4-9 EIS measurement set up with magnified view of electrode placement

The setup is elaborated in the form of a human breast model (Figure 4.10).

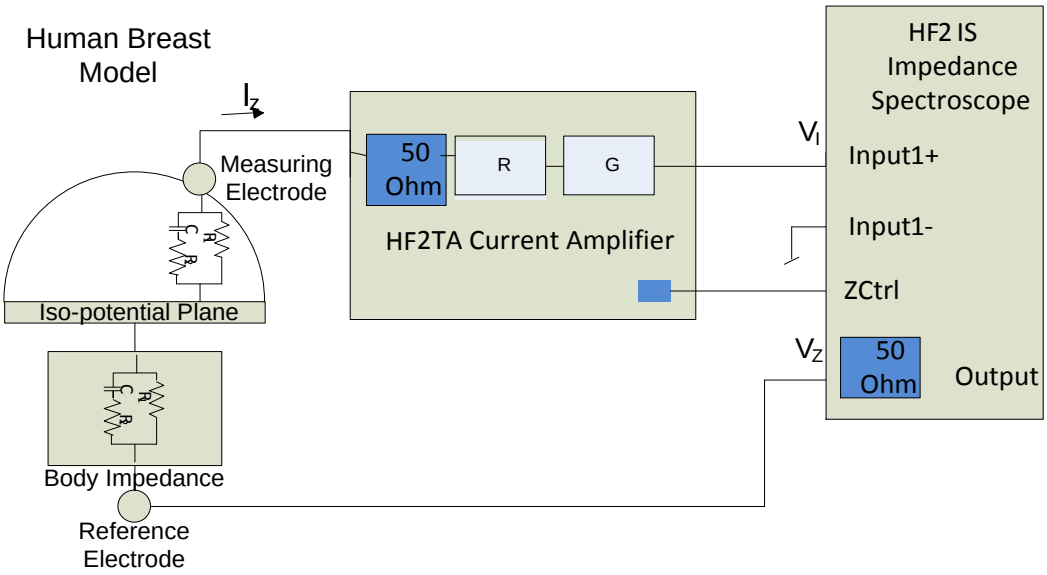

Figure 4-10 Measurement Set Up and Human Breast Model

The frequency response of living tissue, in frequency range, used for electrical impedance scanning is described as follows [174]:

$$Z = R_\infty + \frac{R_0 - R_\infty}{1 + (j\omega T)^\alpha} \qquad (12)$$

Where R_0 is the low-frequency limit resistance, R_∞ is the high frequency limit resistance, α is the "fractional power" (α<1), T is the time constant of the tissue (1/T = Fc, the characteristic frequency), ω the pulsation (ω = 2πf, with f the frequency) and j is the base of imaginary numbers ($j^2 = -1$).Cole also presented a similar relationship [152].

Cole-Cole plots, being most popular for impedance representation, have been used in the present study, plotting real and imaginary admittance over a sweep of frequency from 300Hz to 1 MHz. The frequency increases from left to right in the

admittance. Considering the tissue 'three element RC model' (Fig.1) transfer function is calculated as follows:

$$Y = \frac{1 + C^2 {R_2}^2 \omega^2 + C^2 R_1 R_2 \omega^2 + jC\omega R_1}{R_1 + C^2 {R_2}^2 R_1 \omega^2} \qquad (13)$$

where, Y is the admittance.

The admittance sweep data collected using the developed system, from a single subject is shown below. The admittance plots for various tissues have been shown using different colors' and identifiers. The average of the five trials for each location has been depicted in Figure 4.11. The four closely spaced spectral loci represent the data obtained from the four quadrants of the breast. The objective was to distinguish breast tissue from other tissue data.

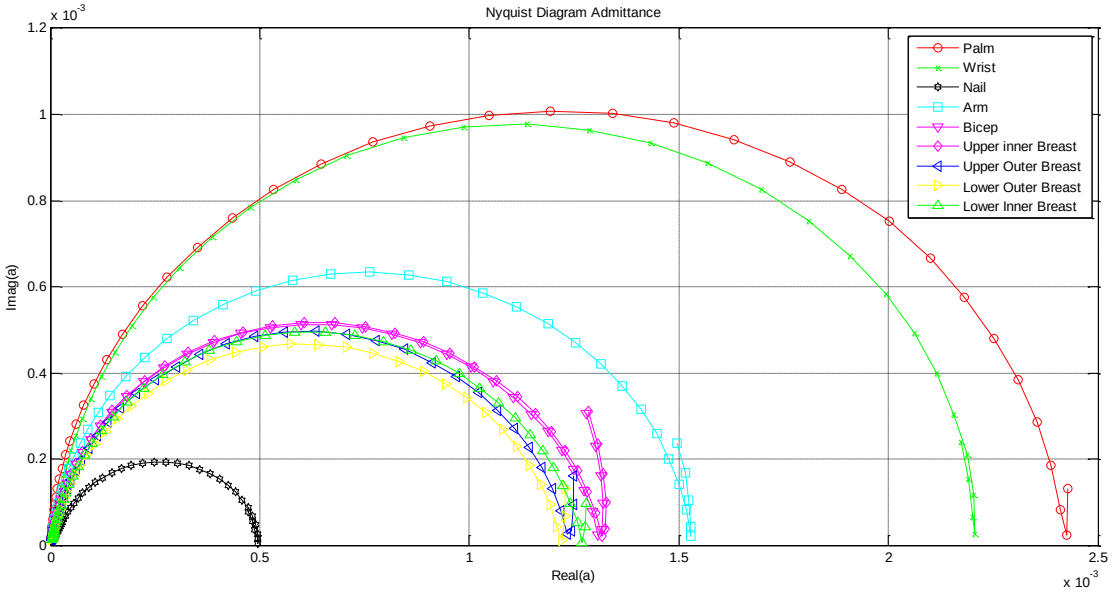

Figure 4-11 Admittance plot for various tissues represented as Cole-Cole plots

From each tissue five repetitive plots were collected to overcome statistical errors. The profiles in magenta, blue, yellow, green represents the data obtained over 5 trials from the four quadrants of the breast. The objective was to distinguish this data

from other tissue data. The weight and height of the subjects was recorded for comparison purpose and the body mass index (BMI) is calculated as shown below.

Table 4.1 Body Mass Index

SUBJECT NO.(SEX)	BMI (Kg/m2)	SUBJECT NO.(SEX)	BMI (Kg/m2)	SUBJECT NO.(SEX)	BMI (Kg/m2)	SUBJECT NO.(SEX)	BMI (Kg/m2)
1(F)	23.5	6(F)	21	11(F)	22	16(M)	25.9
2(F)	16.8	7(F)	22	12(F)	15.9	17(M)	23.5
3(F)	24.4	8(F)	20.7	13(F)	24.8	18(F)	19.4
4(F)	31.4	9(F)	24.6	14(M)	28.6	19(F)	23.8
5(F)	25.2	10(F)	40.3	15(M)	22.1	20(F)	20.8

4.3.2. Decision based algorithm implementation: Support Vector Machine (SVM) Classification

Further, SVM classifier has been used to classify tissue based upon the tissue impedivity as ‘belonging to breast data’ or ‘not belonging to breast data’ using multi-frequency approach over in-vivo collected data. As, impedance values of living tissue (in-vivo) differ significantly from dead tissue, phantoms or simulations, therefore impedance measurements used for classification must occur in-vivo [175][176]. In-vivo complex admittance data has been collected from various body tissues from 30Hz to 1 MHz, at 50 different frequencies. The real and imaginary parts of admittance are used as the data input for the classifier. This approach is a step towards incorporating computer aided decision making, for tissue classification into an EIS system using in-vivo data and multiple frequency approach. Hence, after verifying the electrical impedance measurement set up using tissue equivalent material called phantoms, the data used for tissue classification is collected over different in-vivo human tissues and further post processing of the data is done by SVM machine learning algorithms.

Background and Theory

Classification of breast tissue, based upon spectral features of impedance loci, was first introduced by Jossinet et.al. [161]. It was suggested to use more complex classification methodologies to improve the characterization. One of the classification methods introduced in 1995 and gaining interest for tissue classification is support vector

machines (SVM) [166]. Recently, SVM has been gaining popularity in tissue classification [168][169][170][171]. The SVM based classifications have utilized training data from prior work done by Jossinet [120] or through simulations. SVM classifier has prior also been used for classification of malignant and benign microcalcification showing superior performance compared to other classification approaches[177]. In present study, in-vivo collected training and testing data has been used with support vector machine learning model for tissue classification, as SVM has been very popular and effective in classifying high dimensional feature space.

In machine learning, SVM are supervised learning models with associated learning algorithms that analyze data and recognize patterns, used for classification and regression analysis. SVM is a constructive learning procedure with roots in statistical learning theory [167]. SVM uses structural risk minimization rather than least mean square error, minimizing the generalization error, the error that occurs on unseen data by machine learning. This provides a good generalization with good performance when applied to the testing data. The simplest form of SVM classifier has been used in this study to classify the data in two classes (binary classification) using a hyperplane, rather than the multi-class classification [178] that is usually used for complex classification problems. The aim is to use SVM to segregate breast data from the entire data set, classifying it as belonging to breast data or not belonging to breast data. Similar approach can be used to segregate anomaly data from healthy human breast data.

The basic SVM takes a set of input data and predicts, for each given input, which of two possible classes forms the input, making it a non-probabilistic binary classifier. Given a set of training examples, each marked as belonging to one of two categories, an SVM training algorithm builds a model that assigns new examples into one category or the other. An SVM model is a representation of the examples as points in space, mapped so that the examples of the separate categories are divided by a clear gap that is as wide as possible. New examples are then mapped into that same space and predicted to belong to a category based on which side of the gap they fall on.

The classification involves separating the data into training and testing data. The training data set contains the target value (class label) and several attributes (features or observed variables). The goal of SVM is to create a model using the training data such that the target values of the test data are determined knowing only the test data attributes. For a training set (xi, yi) i = 1….l, where xi ∈ Rn and y ∈ {+1,-1}, the SVM requires the solution to the following optimization problem [179]:

$$\min_{w,b,\varepsilon} \quad \frac{1}{2} w^T w + C \sum_{i=1}^{l} \varepsilon_i \tag{14}$$

Subject to

$$y_i \; W^T \emptyset \; X_i \; + \; b \; \geq 1 - \varepsilon_i; \quad \varepsilon_i \geq 0 \tag{15}$$

The training vector X_i is mapped to higher dimensional space by the function ∅. SVM finds the linear separating hyperplane with maximum margin in this higher dimensional space. C> 0 is the penalty parameter of the error term. The cross products in the larger space are defined in terms of a kernel function K(x,y) $K(x_i,y_j) \equiv \emptyset(Xi)^T \emptyset(Y j)$ that is selected according to the suitability for the application. Two common kernel functions for nonlinear feature mapping are: Gaussian function and Polynomial function [180]. Many classification problems are usually separable in feature space and obtain better accuracy by using Gaussian radial basis function than the linear and polynomial kernel function [180][181]. The Gaussian radial basis function (RBF) kernel used has the form,

$$K(x, y) = \exp \; -\frac{x - y \; ^2}{2\sigma^2} \tag{16}$$

Where σ > 0, is a constant used for defining the kernel width.

An SVM classifies data by finding the best hyperplane that separates all data points of one class from those of the other class. The best hyperplane for an SVM means the one with the largest margin between the two classes. Margin means the maximal width of the slab parallel to the hyperplane that has no interior data points. The support vectors are the data points that are closest to the separating hyperplane; these points are on the boundary of the slab. The following Figure 4.12 illustrates these definitions, with + 1 indicating data points of one class , –1 indicating data points of second class and circle ○indicating support vector.

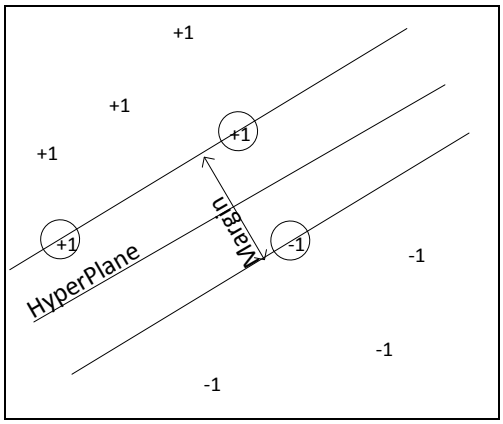

Figure 4-12 Support Vector Machine based classification, + 1 indicating data points of one class , –1 indicating data points of second class and circle ○indicating support vector

Methodology

The SVM is used to classify the tissue based upon the electrical impedance value of tissue. The SVM training algorithm creates a supervised model that categorizes the data as belonging to or not belonging to the breast impedance class. As SVM requires each data set to be represented as vectors of real numbers, therefore the measured complex impedance is used as the input data set consisting of vectors with columns representing the real and imaginary part of the impedance, at 50 discrete frequencies from 300Hz to 1 MHz, each row representing one observation. The training data contains the impedance values along the frequency spectrum (all tissues) from any one randomly selected subject.

To classify the new data, svm classifier function in MATLAB® is used. To train an SVM classifier, the svm train function is used. The tuning of the SVM classifier is done by applying various parameters while training, as kernel function RBF has been used, which is the Gaussian radial basis function kernel with a sigma value of 0.85. This is a reasonable choice as it maps data into higher dimensional space and can be used when the relation between class labels and attributes is nonlinear. The RBF kernel also has fewer numerical difficulties [179]. Each data point after classification is classified as belonging to the group value of +1 or -1 (groups are classified as logical entries). If majority of the data points fall in the group value of +1 then the whole data set is considered as a positive example (belonging to breast tissue) else it is considered as a negative example falling in group -1(not belonging to breast tissue). Thus, the sum of the group vectors of the classified points is taken to add a decision making, whether the data belongs to breast tissue impedance class or not.

Two SVMs were trained with different methodologies and training examples to compare the results. In the first methodology SVM-1(Without data binning & data pruning), no data pre-processing or data filtering was done. The electrical impedance data in form of real and absolute value of imaginary impedance are used as input data vectors. Data from subject 2 was used as training data. Through the training data the supervised learning model is created using svmtrain function, which is further used for testing the data as belonging to or not belonging to breast tissue data set using the svmclassify function of MATLAB®.

Figure 4.13 represents the flow chart of the methodology used for classification and Figure 4.14 represents the groups as logical entries of being a positive or negative example (1 or -1). The support vectors have been depicted as the black circles and the hyperplane is represented as the solid black line.

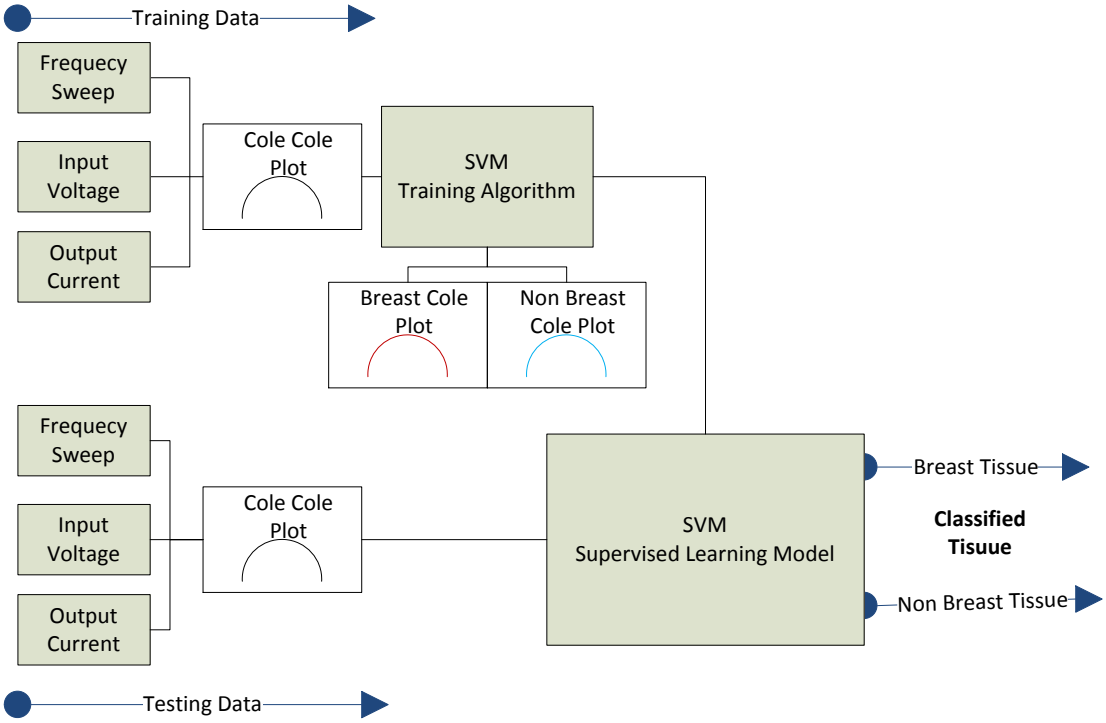

Figure 4-13 Tissue classification without data binning and pruning

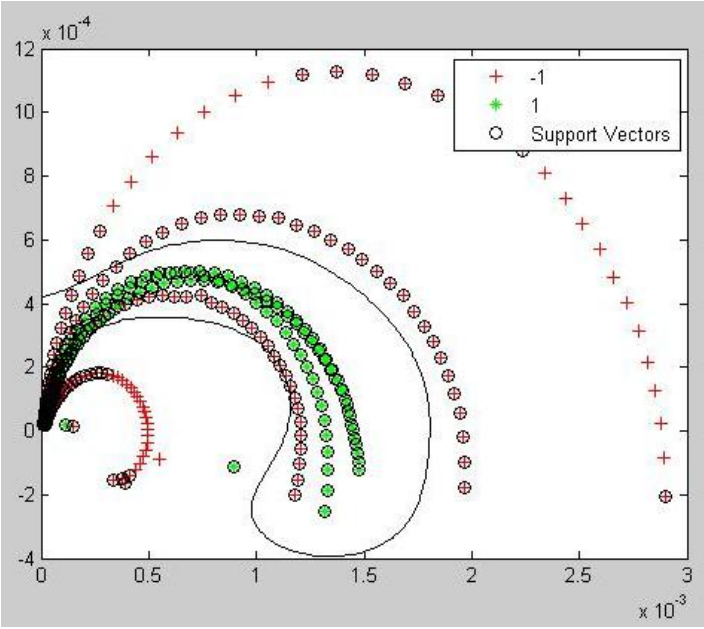

Figure 4-14 SVM-1 Results (Without data binning & data pruning) [Note: The green points are the +ve examples (breast tissue) and the red ones are the –ve examples (other tissues)]

Total of 340 breast tissue and 425 non breast tissue impedance data were tested using the developed model. As depicted in Table XV, the SVM classifier showed a sensitivity of 76.76% and a specificity of 76.23%.

Table 4.2 SVM-1 Results (Without data binning & data pruning)

No. of breast tissue examples used for testing	340
No. of breast tissue examples correctly classified	261
No. of breast tissue examples wrongly classified	79
No. of non-breast tissue examples used for testing	425
No. of non-breast tissue examples correctly classified	324
No. of non-breast tissue examples wrongly classified	101
% of correct positive results (sensitivity)	76.76%
% of correct negative results (specificity)	76.23%

The second methodology SVM-2, used data pre-processing techniques: data binning and data pruning as shown in Figure 4.15 as a flow diagram.

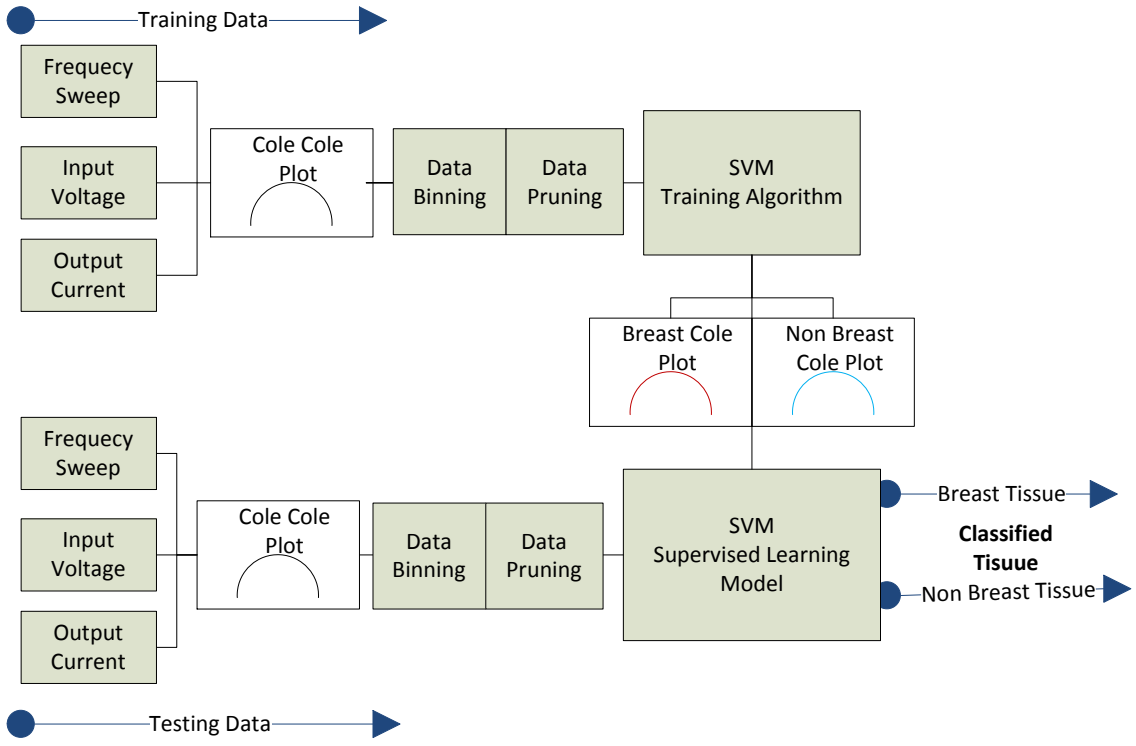

Figure 4-15 Tissue classification with data binning and pruning

Data Binning: For every set of data collected from all the subjects, 5 trials were conducted to reduce random error. For training the SVM, an average of these 5 trials was taken. Over-training is always a danger in machine learning. Hence to reduce this possibility and to neglect random error training, the average of the 5 trials was taken. This process is known as data binning. At the end of this process every subject had one set of readings (curve) for a single tissue (Figure9).

Data Pruning: The collected impedance data for a single tissue site consist of 50 observations at 50 frequencies, therefore 50 data readings at multi-frequencies. Since the first few observations overlap for majority of the overall data set, therefore they are not useful in classification. Similarly, the last few observations are also not helpful in classification. Hence, for the purpose of training, selective frequency range is considered. This is termed data pruning.

SVM Training: Data from 4 subjects out of 18 is taken for training. These were subjects 2, 3, 4 and 5. These subjects were selected randomly. The data from different tissues of these subjects was compiled into one big dataset in MATLAB®. All the data values obtained from the breast tissue were given a group value of +1 and the other values were given a group value of -1. Then this dataset with the corresponding group values was used to train a SVM using the ‘svmtrain’ function. The RBF was used as the Kernel Function with a sigma of 0.85.

SVM Testing: Once the SVM was trained, the second segment of the code is used for testing the remaining data. The impedance input data vector has 50 observations, if majority of the observations fall in the positive group value the data set is considered as a positive example. Figure 14.16 represents the results after classification.

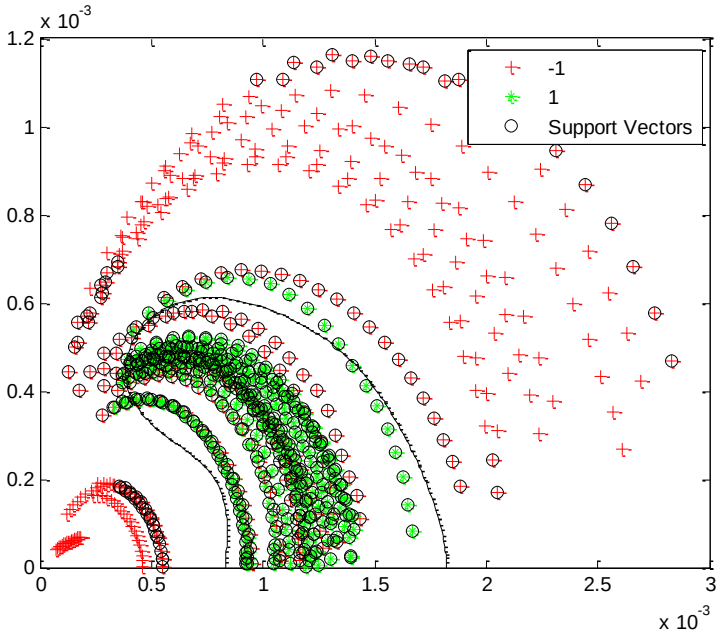

Figure 4-16 SVM-2 Results (With data binning & data pruning) [Note: The green points are the +ve examples (breast tissue) and the red ones are the –ve examples (other tissues)]

Table 4.3 SVM-2 Results (With data binning & data pruning)

No. of breast tissue examples used for testing	260
No. of breast tissue examples correctly classified	232
No. of breast tissue examples wrongly classified	28
No. of non-breast tissue examples used for testing	325
No. of non-breast tissue examples correctly classified	241
No. of non-breast tissue examples wrongly classified	84
% of correct positive results (sensitivity)	89.23%
% of correct negative results (specificity)	74.15%

Total of 260 breast tissue and 325 non breast tissue impedance data observations at 50 frequencies were tested using the developed model. The SVM classifier showed a sensitivity of 89.23% and a specificity of 74.15%, elaborated in Table 2. Data binning and data pruning were able to improve the sensitivity but decreased the specificity. The detailed results are presented in Appendix D.

Discussion and Conclusion

SVM is a promising classifier that can be used for computer aided analysis of electrical impedance to classify tissue. This technique can further be utilized for classification of malignant and benign tissue that may help in early detection of tumors through reliable objective decision making, based upon tissue classification through computer aided analysis. In the present study, data binning and data pruning have improved the sensitivity of the SVM from 76.76% to 89.23% but the specificity has decreased from 76.23% to 74.15%. This implies that the new SVM is better at classifying positive results but more error prone at classifying negative results. Future work is anticipated in characterizing malignant and benign tissue using SVM classifier for multi-class classification. Further improvement in classification is possible through feature extraction over malignant as well as healthy tissue, to improve the classification, using both conventional and non-conventional parameters.

4.4. Effect of compression over healthy in vivo tissue and in vitro tissue

The proposed multimodality based design in this research was in the form of a wearable glove. In this integrated multimodality design the correlation and effect of each modality over the needs to be studied and quantified.

In this study, the effect of compression on electrical impedance was observed *in vitro* over chicken breast tissue and rat breast tissue. The multimodality tool was used at various incremental pressures. Twenty samples from the same parts of ten chicken breasts were chosen for the measurements. The samples were cut in a cubic form with length, width and depth being 0.04 m, 0.035 m and 0.02 m respectively. One of the bio impedance electrodes was placed under the sample and the other one was located on top of the cubic sample. One finger wearable capacitive pressure sensors was worn on the index finger of the right hand. Force sensor was recalibrated. This pressure sensor was placed on top of the upper electrode for applying pressure. Seven pressure levels were applied to each tissue sample constantly and meanwhile the bio impedance data were collected by EIS electrodes. At each pressure level, the frequency was changing

from 1 Hz to 1 MHz, thus multi-frequency measurement dataset at 50 data points was obtained. One of the closest models to the bio impedance data is the Cole-Cole model in the form of admittance.

$$Y = G + jB = G_\infty + \frac{G_0 - G_\infty}{1 + (\frac{jf}{f_{yc}})^\alpha} \quad (17)$$

where Y is the whole admittance, G is the whole conductance and B is the whole susceptance. Also G_0 is the admittance at zero driving frequency, G_∞ is the admittance when the driving frequency is infinity, f is the driving frequency, f_{yc} is the frequency at which the imaginary part of the admittance reaches its maximum and α is the dispersion parameter.

The admittance was fit to Cole-Cole model using the least square method. This optimization method minimizes the summation of the squared error which can be found by subtracting each data point from the fitted data.

$$\text{Fitness Func.} = \min \sum_{i=1}^{n} e_i^2 = \sum_{i=1}^{n} (Y_{raw} - Y_{fitted})^2 \quad (18)$$

The Least Square Method has been earlier used [163] to fit Cole-Cole model to admittance data four parameters were extracted by the following formulas:

$$G_0 = m - \sqrt{r^2 - n^2} \quad (19)$$

$$G_\infty = m + \sqrt{r^2 - n^2} \quad (20)$$

$$\alpha = \frac{2}{\pi}\arccos\ -\frac{n}{r} \tag{21}$$

$$f_{yc} = \frac{1}{N}\sum_{k=0}^{N-1} f_k^{\ \alpha}\ \overline{\frac{2\,b_k\,r}{(g_k - G_0)^2 + b_k^2}} \tag{22}$$

where (m, n) is the center of the semicircle and r is the radius of the semicircle fitted to the admittance data. The Cole-Cole model considers the tissue as a circuit containing one resistance and one capacitance in series called intracellular resistance (R_{int}) and membrane capacitance (C_m) respectively both in parallel to another resistance called the extracellular resistance (R_{ext}), Figure1. All these three Cole-Cole circuit parameters can be calculated from the following equations:

$$R_{ext} = R_0 \tag{23}$$

$$R_{int} = \frac{R_0\,R_\infty}{R_0 - R_\infty} \tag{24}$$

$$C_m = \frac{1}{2\,\pi\,f_c\,(R_{int} + R_{ext})} \tag{25}$$

where $\mathrm{R}_0 = \frac{1}{\mathrm{G}_0}$, $\mathrm{R}_\infty = \frac{1}{\mathrm{G}_\infty}$ and $\mathrm{f_c} = \mathrm{f_{yc}}^{\ \alpha}\ \overline{\frac{\mathrm{G}_0}{\mathrm{G}_\infty}}$.

For each sample, the real and the imaginary parts of admittance were plotted in a complex plane which formed semicircles. By using the least square method, Cole-Cole equation was fitted to the data and according to the fitted plots and above equations, four electrical parameters of twenty samples, i.e. G_0, G_∞, α and $\mathrm{f_{yc}}$ were extracted. Cole-Cole circuit equivalent elements (R_{ext}, R_{int} and C_m) were calculated from those extracted parameters and were normalized to their uncompressed values. The mean values and

the standard error at each pressure level are illustrated in figure 2. The average Rext, R_{int} and C_m and their margins of error are$455.57 \mp 3.93\ (\Omega)$, $622.27 \mp 7.46\ (\Omega)$ and $6 \mp 0.098\ \times 10^{-9}(\mathrm{F})$ respectively. As shown in Figure 4.17(a), the extracellular resistance increases 42% when 3lb force was applied to the tissue. Figure 4.17(b) illustrates an increase of 70% at the membrane capacitance, while figure 4.17(c) shows a 28% decrease in the intracellular resistance.

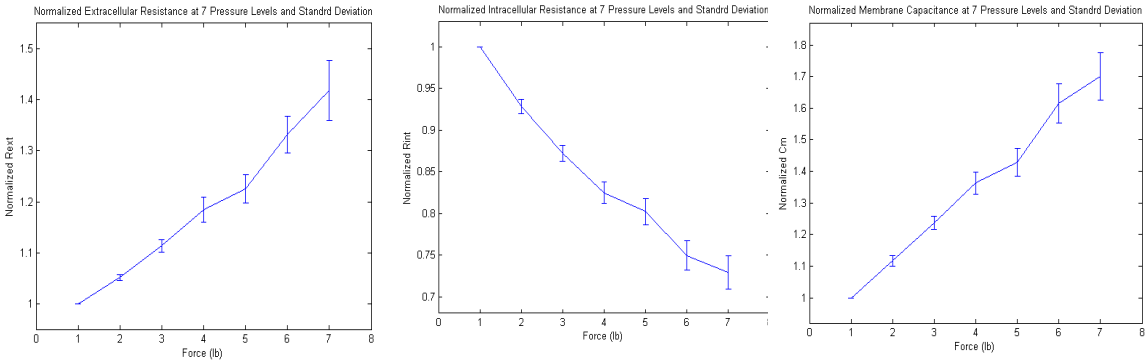

(a) (b) (c)

Figure 4-17 (a) Normalized extracellular resistance at 7 pressure levels (b) Normalized intracellular resistance at 7 pressure levels (c) Normalized membrane capacitance at 7 pressure levels

4.5. Discussion and Conclusion

The goal in this research section was to validate the usability of developed test set up to detect an anomaly inside otherwise homogeneous breast phantom, based upon electrical impedance of the anomaly to the surrounding material. The phantom material used in this study had dielectric properties close to human fat and tumorous tissue[72].

Through the phantom based study it was concluded that the electrical impedance spectroscopy set up when used with ANFIS based algorithms can distinguish the fat phantom from the muscle phantom, but the system was incapable of differentiating the muscle embedded in fat phantom group due to the close association of this group data to the fat phantom data. This can be attributed to the availability of small set of training data along with the low resolution of the system. Further, this classification was based

upon only the real part of impedance as gelatine based phantoms does not show complex impedance characteristics as shown by biological tissue. Therefore, these results were insufficient and *in vivo* complex impedance data definitely needed to be collected for tissue classification.

SVM based classification techniques, used over data collected from healthy *in vivo* human tissue, was successful in classifying breast tissue data. Data binning and data pruning improved the sensitivity of the SVM from 76.76% to 89.23% but the specificity decreased from 76.23% to 74.15% implying that the SVM with data binning and data pruning is better at classifying positive results but more error prone at classifying negative results. Further improvement in classification is possible and required through feature extraction in *in vivo* data collected over malignant and contralateral healthy tissue, using both conventional and non-conventional parameters.

As in a glove module the tissue electrical impedance will be varied by the amount of applied force, study involving *in vitro* animal tissue was performed to understand the relationship between the amount of applied pressure and the associated variability in tissue electrical impedance. In this context parameter extraction from the Cole-Cole plots was done and was found that the extracellular resistance increases by 42% when 3 (lb) force was applied to the tissue and an increase of 70% was observed at the membrane capacitance, and a 28% decrease was observed in the intracellular resistance.

The limitations in this study were firstly the low resolution of the system, more work needs to be done to increase the number of electrodes and decrease the distance between the electrodes. Systems in direct competition to this technology, like ACT4[182], support up to 60 electrodes in two 5X6 radiolucent arrays. In other EIS systems the electrode area are as small as 1X1 mm^2 and a space of 2.5mm between adjacent electrodes. The proposed system has a much lower resolution with finger module composed of 4 Ag/AgCl electrodes, 4mm in radius, 1cm apart, in a square configuration. This limitation exists because this is a first generation prototype and the electrodes have been manually placed over the glove. Use of commercially available techniques (sputtering techniques) will be useful to further improve the resolution of the system as the impedance spectroscope is capable of multiplexing 32 signals. Electrical

Impedance Tomography (EIT) can only be looked into once the required resolution of the system is obtained.

Chapter 5.

Tissue Classification: Surface Thermometry (Phantom and *in vivo* Healthy Human Tissue Study)

5.1. Introduction

Thermography in clinical environment is a diagnostic imaging procedure that detects records and produces an image of the subjects' skin surface temperatures and / or thermal patterns. It consists of high-resolution technology used to detect breast cancers and soft tissue injuries [183]. The equipment can provide both qualitative and quantitative representation of the skin surface temperature pattern. It is not an invasive procedure and does not pose any harm to the subject. It has been used for a differential diagnostic purposes, especially for breast tumor detection [184]. It measures the thermal properties of tissue, the more rapidly growing lesions with shorter doubling times usually show thermographic abnormalities consistent with the increased metabolic heat production associated with such cancers [185]. The differences in the energy dissipated between the normal and the cancerous tissue may be expressed as higher local temperature (up to 2-3ºC) on the skin surface of the tumour [186]. This test is designed to improve the probability of detecting of fast-growing, active tumors in the intervals between mammographic screenings or when mammography is not indicated by screening guidelines for women under 50 years of age [187]; however, the high rate of false positive results has limited the technology from becoming a standard early detection method [62]. Though, thermography has high sensitivity and negative predictive value[58], but is not accepted as an stand-alone screening technology for breast cancer[59]–[61]. Breast thermography has an average sensitivity and negative predictive value of 90% and does not require ionizing radiation, compression, contact or intravenous injection .When used with mammography, thermography has been found to increase the sensitivity of mammography from 83% to 93% and a combination of clinical

examination, mammography and thermography increased the sensitivity to 98% [62], [63].

5.1.1. Background and Overview of present state of Technology

Thermography for diagnosis of breast cancer was first introduced in 1956 [188], followed by a study in 1961 [189], concluding that cancerous tissue had an increase of 1-2°C from surrounding tissue, and long wavelength infra-red (LWIR) imaging was able to classify benign and malignant processes. Further, prognosis based on thermography was suggested [190][191][192] and vascular convention was also attributed to increase in temperature [193]. Number of studies showing high true positive rates [194], increased sensitivity in mammography combination studies [195][196][197][198] pointed towards significance of thermography in detecting tumors. Angiogenesis proposed in 1971 by Judah Folkman, described tumors as "hot and bloody" as illustrated by Penn [199]. But, few reports in 1970's [200][201], the BCDDP (Breast Cancer Detection Demonstration Projects) group [202] report and, mix sensitivity ranging from 88% to 68% [203][204][205][206], suggested that more objective means of interpretation facilitated by computerized evaluation were definitely required.

Most of the research has now been focused on improving the thermography to decrease the false negative predictions. Addition of Computer Simulations, Artificial Intelligence, Neural Network, Fuzzy Logic and evolutionary algorithms has been the trend in achieving this and improving the sensitivity as well as specificity of thermography[207],[208][209][210][211][212]. Also, to achieve consistency in thermal interpretations and maximize inter-examiner reliability interpretation, guidelines for breast thermography were introduced [213]. Dynamic area telethermometry [214][215], Dynamic Thermography [216] and high resolution cameras, with computerized LWIR imaging station helped improve LWIR imaging [186]. Quantification of the data with temperature profile depiction, size/location of tumor [59], numerical thermal modeling of the breast considering the bio-heat equation [217], four quadrant approach [218], Localized temperature increase (LTI) concept implemented to overcome the subjective decision making [45] are few of the techniques being applied to further improve LWIR.

Most recently, smart thermometer technology has been introduced as a local tissue detection and monitoring tool [64].

5.1.2. Determination of Surface Temperature of Tissue

Radiation is electromagnetic radiation emitted by all objects with a temperature greater than absolute zero. Radiation can be used to remotely determine the temperature of objects (if the emissivity is known). Infrared radiation extends from the red edge of the visible spectrum at 0.74 μm to 0.3mm. Further, the infrared spectrum is divided into near infrared (0.75- 1.4 μm), short-wavelength infrared (1.4-3 μm), mid-wavelength infrared (3–8 μm), long-wavelength infrared (8–15 μm), and far infrared (15 – 1,000 μm). According to the Wien's displacement law:

$$\lambda_{\max} T = b \qquad (26)$$

where λ_{max} is the wavelength of the peak of the emission from a black body, T is the temperature and b is the Wien's displacement constant given by 2.8977685(26) $x10^{-3}$ m·K. For normal human temperature of 37ºC, the corresponding wavelength using Wien's displacement law is around 9.3 μm. It falls in the long-wavelength infrared range. Therefore, long-wavelength infrared is the "thermal imaging region" in which sensors obtain a passive picture of the surface without the requirement of any external light or thermal source. Forward-looking infrared (FLIR) systems use this area of the spectrum called the "thermal infrared". When these infrared emissions are captured within the wavelength given off by human tissue, quantitative analysis of the thermal properties can be performed, determining whether a thermogram is abnormal. Various technologies are used to develop infrared sensors like micro-bolometer, pyrometry or thermopile (most popular for human application).

According to the thermography guidelines given by iact-org (International Academy of Clinical Thermology) [184], there are two recognized methods of clinical thermographic imaging: electronic infrared telethermography (IRT) and liquid-crystal

thermography (LCT). The guidelines further talk about other thermal detection devices that are available but are not suitable for full body or breast examination. These devices include microwave thermography that has concerns regarding the errors from surface contact, depth of analysis, area coverage, and low spatial and thermal resolution. Another device is the single sensor device; this consists of a single spot temperature reading using a contact type sensor (thermocouple or thermistor) or a contactless type (infrared sensor). Contact type sensors show inherent data acquisition problems and lack of absolute and spatial resolution. A modification of this method is the use of multiple contactless sensor devices that consist of three or more spot radiometers. When these sensors output is interfaced with a computer, the system is defined as surface thermometry or computer aided surface thermometry (CAST). If a device can plot enough data for analysis, the system can be called thermography and will have diagnostic value if it meets all quality standards (i.e. accuracy, repeatability, and thermal stability).

The present research is a step towards providing a cost effective tool that can be used in adjunct with computer aided analysis to support clinicians by improving the diagnosis for treatment. The approach is to use the multiple sensor device such that it fulfill the required minimum design specifications provided by iact-org [184] to produce accurate, reproducible and clinically relevant thermal data with good accuracy and sensitivity.

5.2. Phantom Study: Test Set Up and Methodology

5.2.1. Simulated Phantom Model and Results

As present study focused on the dynamic thermal behaviour, in which not only the heating pattern but also the thermal transport processes of conductivity and perfusion are simulated, the gelatine based phantoms only satisfied the static thermal simulation (refer section 2.2.3). In order to study the dynamic behaviour, the set-up is simulated in COMSOL1 and the results are compared. This simulation provides a comparative study to verify the experimental set up for the phantom. For simulation,

thermal conductivity k=0.48 (W/(m·K)), density ρ=1050 Kg/m3 and specific heat capacity c=3070 (J/(kg.K)) have been chosen that mimic thermal properties of biological tissue.

The experiment model created in COMSOL is illustrated in figure 6. In this simulation, the center red object (hot spot) defines the anomaly in otherwise homogeneous surrounding. The color bar defines the equivalent temperature. According to this simulation results, when the resistor heats to 24ºC the surface temperature vertically above the hot spot is around 16ºC and the surrounding body surface temperature is around 13ºC. These temperatures are measured after 600 seconds.

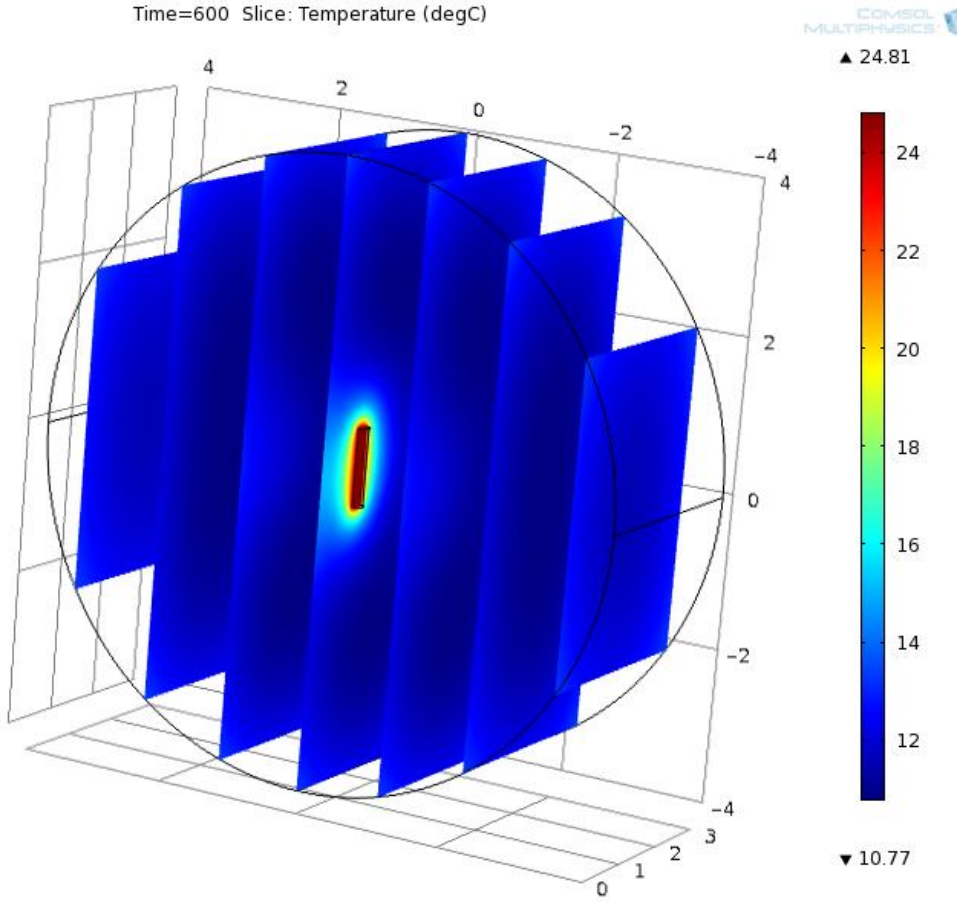

Figure 5-1 COMSOL model for simulation of phantom

Methodology

The phantom was tested through experiment as to how close can it mimic human tissue thermal properties. The temperature of the anomaly itself was not considered for

thermography, instead the temperature difference on the surface needed to be considered. First it was verified that the phantom absorbs 75% of the IR radiation similar to tissue that is has high percentage of water, as shown in the graph.

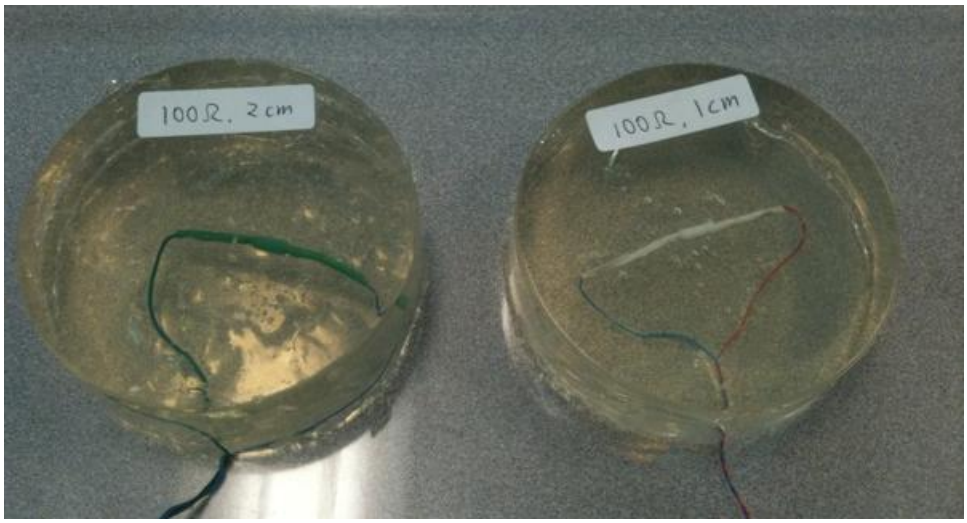

Figure 5-2 100Ω Resistors inserted at 1cm & 2cm

Two experiments were performed to validate the phantom. First paper dipped in water was placed between tissue and IR sensor and, the sensor response was documented. The sensor was unable to detect the tissue temperature verifying the absorption of the IR radiations by the water molecules present in the paper. The second experiment consisted of placing the phantom in between a heat source and the IR sensor without touching such that conduction of heat was not possible from the heat source to the phantom. The IR sensor did not show any response. Therefore it was verified that the phantom has properties very close to that of the tissue that consists of 75% water.

As shown in Figure 5.2, to observe the effect of distance of anomaly from the surface of the two phantoms are created with the resistors inserted at 1cm depth and 2cm depth to represent the anomaly at different depths. These resistors are covered with heat shrink tubing to prevent any short circuit since the water based phantom itself conducts. The lengths of copper wires coming out from both ends of the resistors are also carefully measured to maintain the same amount of heat dissipation. One of the main reasons why 100Ω resistor at 5V is chosen is because the phantoms are kept at

10ºC.With these specifications; it provides approximately 2-3°C difference at surface which represents the presence of an anomaly in the breast [193].

Two types of temperature sensors are used for the comparative study. Fluke 179 temperature meter with Fluke 80BK-A integrated DMM temperature Probe [219] consisting of a contact type thermocouple sensor with .1ºC resolution and accuracy of 1%, and non-contact type infrared MLX90615 with a resolution of .02°C and accuracy of .1ºC at body temperature .

Test Set Up

It is anticipated that different amount of force application on the sensor should affect the temperature measurement as greater force will result in a shorter distance between the anomaly and the sensor. Infrared temperature sensor is first placed at the surface of the phantom above the resistors and then at locations without the resistor. A set of force from 0 to 15N is then applied steadily in the vertical direction upon the phantom. The result shows no change in temperature in this range of force.

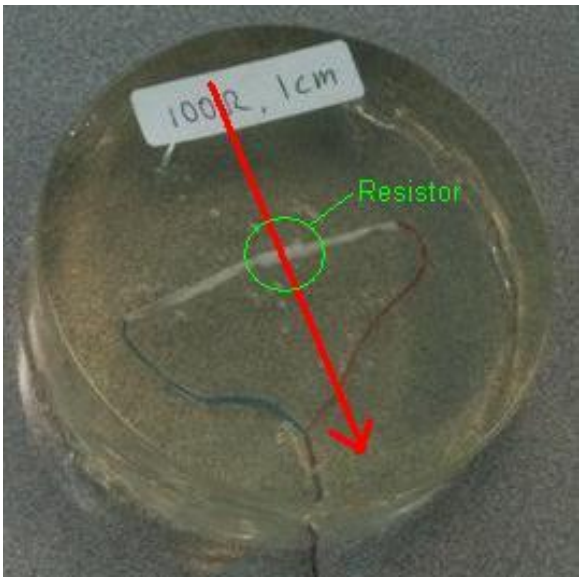

Figure 5-3 Experiment Illustration

Shown in Figure 5.4 is an illustration of the set up for calibration. Fluke 179 temperature meter is the top one applied on the resistor as it measures the temperature very precisely through contact, though it does have a slow response time. The other

sensor just beneath the resistor is the infrared non-contact sensor by Melexis. As shown in the figure, the temperature of the resistor in lab environment is at around 21.5 °C. In order to raise the surface temperature of the phantom above the resistor, 5 volts is applied through two ends of the resistor. The measurements on both sensor and meter first increased rapidly and eventually reached a steady state reading after approximately 2.5 minutes. The switch of the power supply is then turned off after 6 minutes and 22 seconds to allow cooling. The result with Melexis infrared sensor is shown in Figure 5.5.

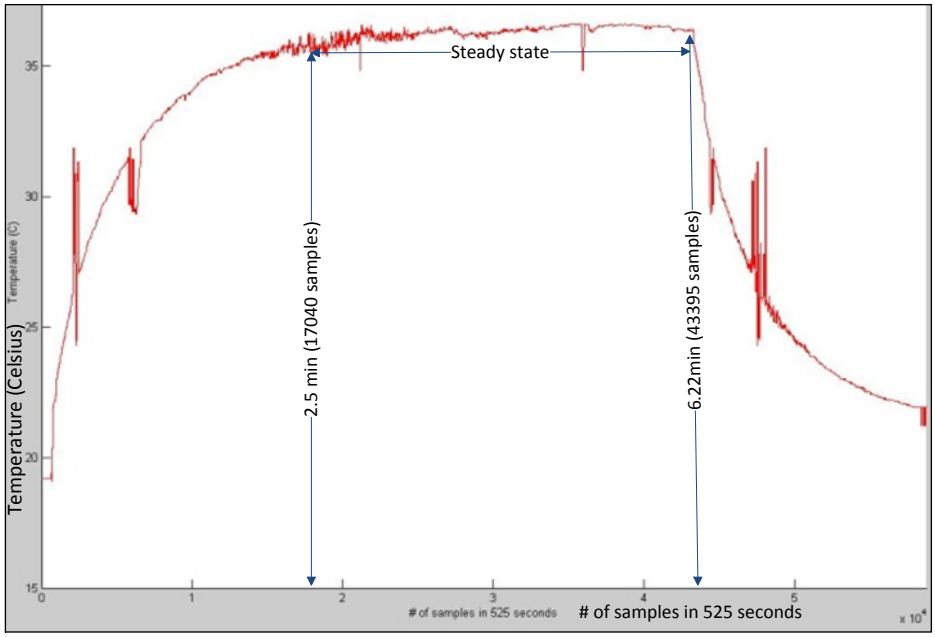

Figure 5-4 Steady State detection set up and thermal behavior

The x-axis is the number of samples and y-axis is the temperature reading in Celsius. In 525 seconds a total of around 60,000 samples were collected from the Melexis sensor. It is concluded that after around 2.5 minutes the temperature over the resistor becomes steady and can be used for further analysis. With the force and resistor thermal behaviour clarification, two sets of experiments are set up for detecting the change in temperature within the phantom. First one is performed with the sensor closely placed just above the phantom but with no contact while the second set up is performed with 5N applied between the phantom and sensor. As shown in figure 15, the resistor is placed in the middle of the phantom. Thus the experiment is performed in the

direction of the red arrow moving from phantom location without resistor into a resistor contained location and back to no resistor phantom location. This strategy can clearly indicate when any change in temperature is detected.

The sensor was tested for the sensitivity and the response time by calibrating the sensor over the human palm, and moving it over the fingers and the arm veins. When the sensor moved over the veins a hot spot was observed, the measured temperature of the palm using Fluke temperature sensor was 31.5 ºC and that above the vein was 32.7 ºC. Therefore the system proved to be sensitive enough for the application. The fingers showed a lower temperature due to low blood volume. Few experiments were performed over phantoms to test the sensor further.

Results

In the results of the experiment (Figure 5.5) each plot contains three repeated tests for stronger validity. The results are quite considerable when the parabola shape readings are taken into account. Each peak represents the moment when the sensor has pass through directly above the resistor where the distance between two is at shortest. Without any contacts between the phantom and infrared sensor, at a distance of around 1 cm from the surface, the greatest difference in temperature was determined to be 1.5°C when resistor is embedded at 1cm deep. On the other hand, the result with 5N applied was as high as 4°C. This fact further suggests that the magnitude of the temperature difference is heavily depended on the distance between object and sensor. The sensor provides better results when used contacting the skin. It is also important to note that the results for any of the 2cm depth experiments are not very significant although some difference can be detected. This is in accordance to the observation made by Sudharshan et al. [59]. That stated that surface temperature is dependent position of the carcinoma. The base line is different for the three trials as the phantom temperature keeps increasing with time as phantoms have been kept at 10°C and they tend to adapt to normal room temperature with time.

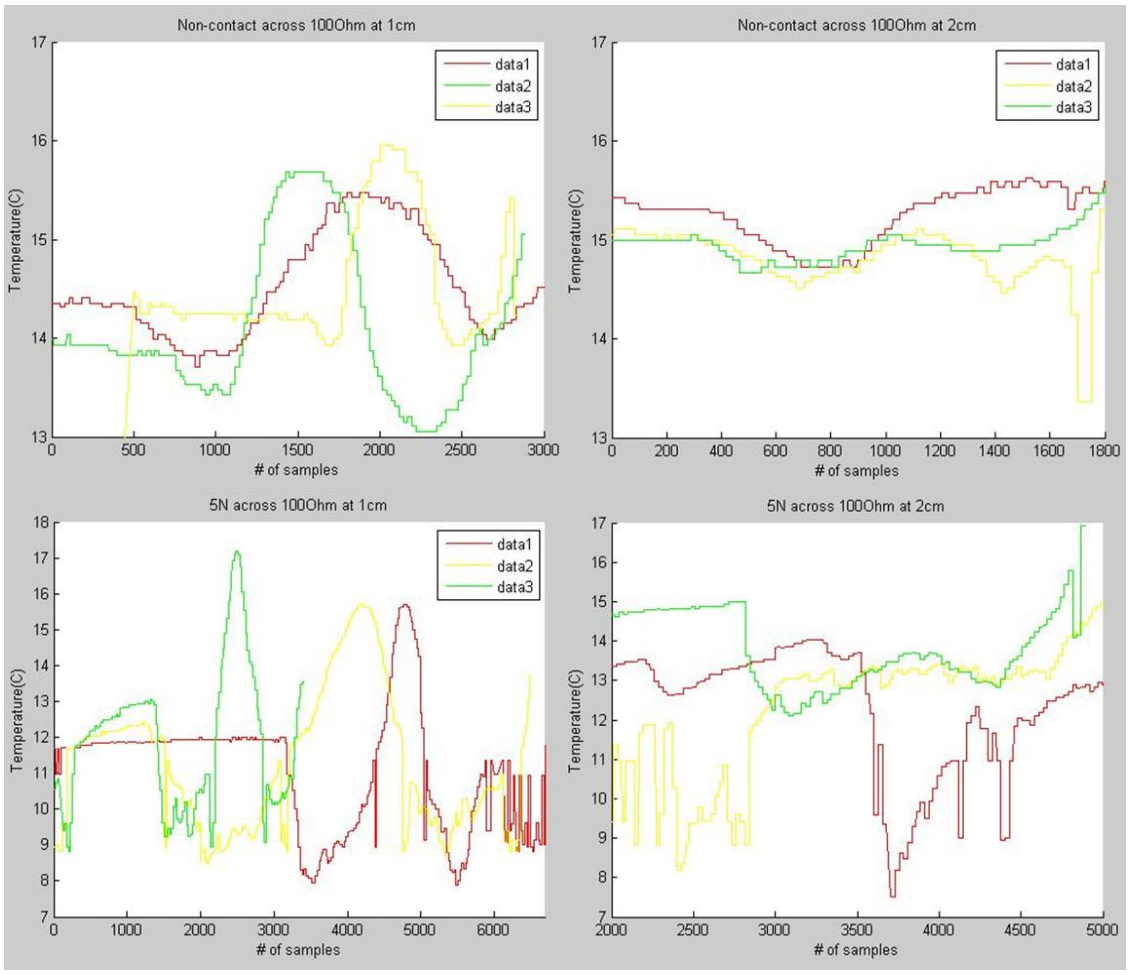

Figure 5-5 Infrared Sensor Response for non-contact type and contact type movement

The designed probe was tested over two phantoms which mimic the tumorous tissue. As mentioned earlier, the four surrounding sensors measured the temperature of the healthy part of tissue which encompasses the hotspot (tumor) and the center sensor measured the temperature of the hotspot. The temperature data were collected at three force levels; 2.5 N, 5 N and 7.5 N to see if applying pressure on the sensors has any effect on the temperature results. The mean temperature and margin of error of the four surrounding sensors at three pressure levels are $20.57 \mp 0.09℃$, $21.22 \mp 0.70℃$ and $21.21 \mp 0.65\ ℃$ respectively. Accordingly, the mean temperature and margin of error of the central sensor, which mimics the tumor are $22.95 \mp 3.30℃$, $22.6 \mp 1.94℃$ and $22.67 \mp 2.06\ ℃$ respectively. It can be seen that the effect of pressure

on the data reading of the temperature sensors was negligible and pressure does not affect the results in a noticeable way.

The experimental results over two phantoms are depicted in Figure 5.6. As observed, the temperature difference between the surrounding sensors and the central sensor at the first pressure level is 2.38 °C. Thus if central sensor is placed over the suspected area while the other sensors are sensing the healthy area around it, the difference between these two sets of temperature data will show the existence of a tumor below the central sensor.

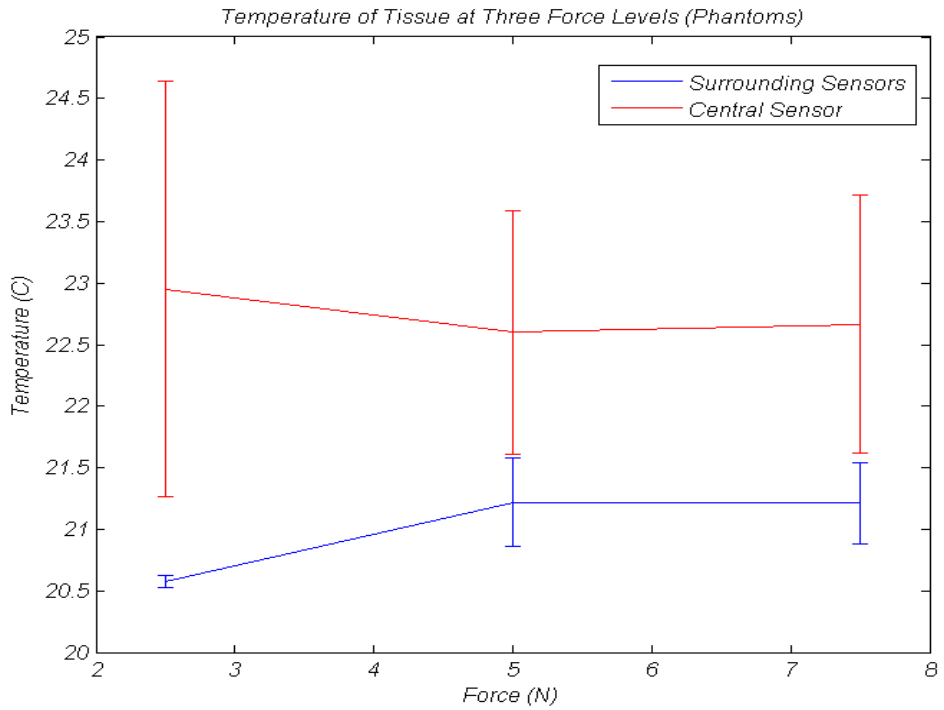

Figure 5-6 Phantom Temperature (Mean and Standard Deviation)

The LWIR sensor response will become clinically relevant when imaging and decision making algorithms are interfaced to it, resulting in computer aided surface thermometry. Through MATLAB® programming, a graphical user interface for surface thermometry has been designed and results are shown in Fig.5.7 as shown in figure 19; temperature output from 8 multiple sensors are depicted as 8 colour circles in blue background. The color to temperature mapping has been shown through the color bar.

The top graph depicts the output when the phantom has no resistor, therefore no anomaly; all the sensors show a uniform temperature of around 21°C (Room temperature). The bottom graph depicts the output when a resistor is present in the phantom; the color variation shows that around 3°C higher temperature object is present underneath one pair of sensors. It also shows the change in Z co-ordinate with the application of 5N force. The representation makes the system capable to display thermal data for interpretation, perform accurate quantitative differential temperature analysis and archive images for future reference and image comparison. But a lot of work in image analysis needs to be done to bring the system to the required standard of thermography and for software manipulation of the images within strict parameters to insure the diagnostic quality of the images.

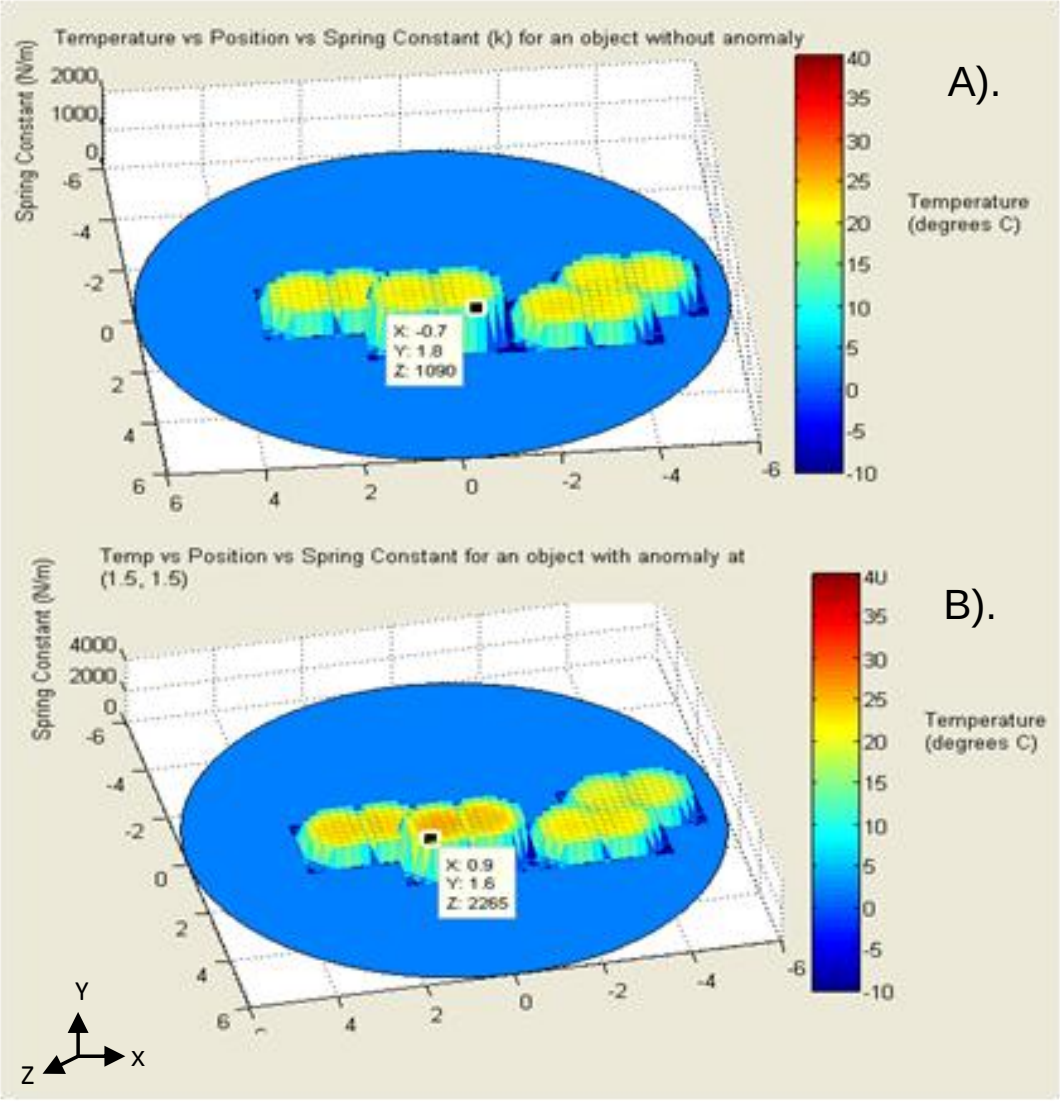

Figure 5-7 Surface Thermometry using multiple Infrared sensors

5.2.2. Real-Time Surface Thermometry

To improve the display for interpretation, perform accurate quantitative differential temperature analysis and archive images for future reference and image comparison, the graphical representation was improved through improved algorithms capable of real time temperature data representation. This not only provided the accurate temperature of the surface but also provided information regarding the location of the sensor. The algorithms have been attached in the index.

The improved algorithm were based upon the Localized Temperature Increase (LTI) concept [58]. Initially the localised temperature value of the breast was determined using a temperature calibration algorithm. This consisted of placing the sensors on a healthy part of the breast to determine the base temperature. Around 300 samples of the data are collected from each sensor and the average temperature as well as least square mean error (lsme) temperature is recorded. Thereafter an average of all the sensor temperature is taken to find the base temperature of the surface. Further, the algorithms were improved by incorporating filtering techniques by removing error bits from the captured data.

A 3D representation of the surface is done using 60 samples of temperature data/frame. Color mapping has been done using the colormaprange [10 60]. This range represents a blue-green-red range color scale. This gave a real time representation of the surface temperature at three locations on the surface. 6 IR sensors have been used in this set up. Each location has 2 IR sensors for redundancy to improve the reliability of the system. When no anomaly is present all the locations show the same colour (blue) representing the base temperature. When an anomaly is present, a higher temperature occurs on the surface just above the anomaly. When the IR sensor passes over this region the color changes from base blue to yellow followed by red depending upon the amount of temperature increase. Figure 5.8 shows an anomaly at the centre location. This was taken over a phantom with the anomaly at 1 cm in the centre of the phantom. The temperature measured with Fluke Thermometer showed a value of 24ºC over the phantom normal surface and 26ºC over the anomaly surface.

To improve the display for interpretation, perform accurate quantitative differential temperature analysis and archive images for future reference, the graphical representation was improved using algorithms capable of real-time thermal profile representation. The system provides instantaneous thermal images of surface in the FOV of the LWIR sensor. Figure 5.10 shows the surface thermometry MATLAB® GUI (Graphical User Interface) being used in real-time; without the force input. Here three positions were used to capture thermal data in three close vicinity locations in time domain. The color denotes the temperature in degree centigrade according to the color bar. Two images were captured over time while a resistor was heating up inside the

phantom depicting the real time application of the system. Figure 6(a) represents an image when the resistor (placed in the center location) is heating up, and Figure 6(b) is the image with the resistor temperature stabilized and defining a hot spot.

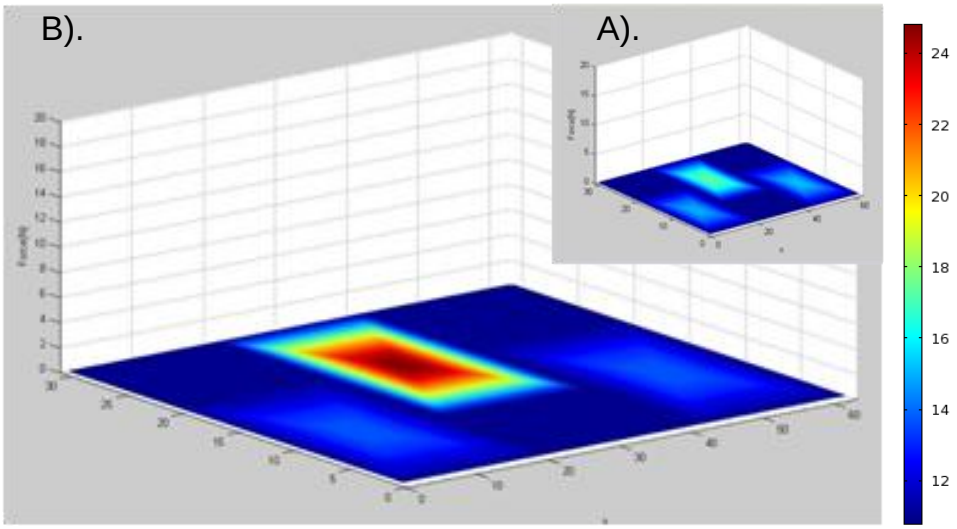

Figure 5-8 Surface Thermometry Graphical User interface

5.2.3. Decision Based Algorithm Implementation: Fuzzy Inference System (FIS)

To append decision making into the system; Fuzzy Logic based algorithm were used. Fuzzy Inference System editor (FIS) with a graphical user interface and real time temperature mapping were applied. The improved algorithms were based upon the Localized Temperature Increase (LTI) concept [58]. Initially the localized temperature value of the tissue is determined using a temperature calibration algorithm. In order to reduce noise; filtering and signal processing of the data is done. A Mamdani [220] style inference system is used as it is intuitive and is well suited for human based inputs, with centroid defuzzification and linear classifier. Two inputs (temp) High Temperature (s shaped membership function; smf) and Low Temperature (z shaped membership function; zmf) with range 0-50 and; two outputs (temp_decision) Hit (type smf), and No Hit (type zmf) with range 0-10, are identified. The weight of both rules is kept 1.

$$x_o = f(x_i) = \quad 1 \qquad x_o \geq x_n \tag{27}$$

$$f\ x_o \ = \ \begin{matrix} 0, & x_i < x_n \\ 1, & x_i \geq x_n \end{matrix} \tag{28}$$

The flow chart Figure5.9 elaborates the applied concept. The system was first calibrated using sample 1, which consists of normal body temperature tissue (healthy tissue) called the normalized base temperature. The Data stream from the LWIR was associated with the sensor identifier (added through microcontroller programming for identifying location), this was segregated to get the localized thermal data at the location of the LWIR, followed by calculating the mean temperature using LSE (Least Square Error) methodology. After calibration, the real-time thermal data was collected over the sample with a hot spot. Same procedure, as in calibration, was followed. Both; the calibrated data and the real-time data are analyzed using fuzzy logic algorithms. The FIS provides output in the form of the position; presence or absence of a hot spot; all in real-time.

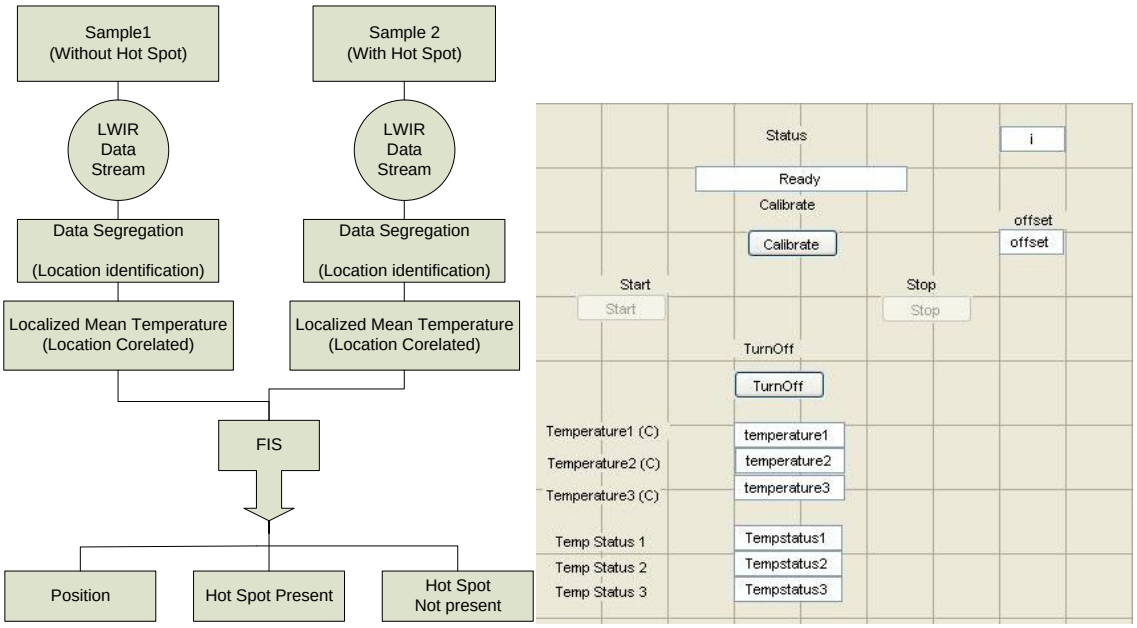

Figure 5-9 FIS Application to Surface Thermometry with associated GUI

The screen shot below is an example of the graphical user interface created combining sensor head and the FIS based decision making. The panel in the GUI allows the user to calibrate, start, stop, and turn off the system. Real time values from the sensors and the status: *hot spot present or hot spot not present* define the established decision using the algorithms.

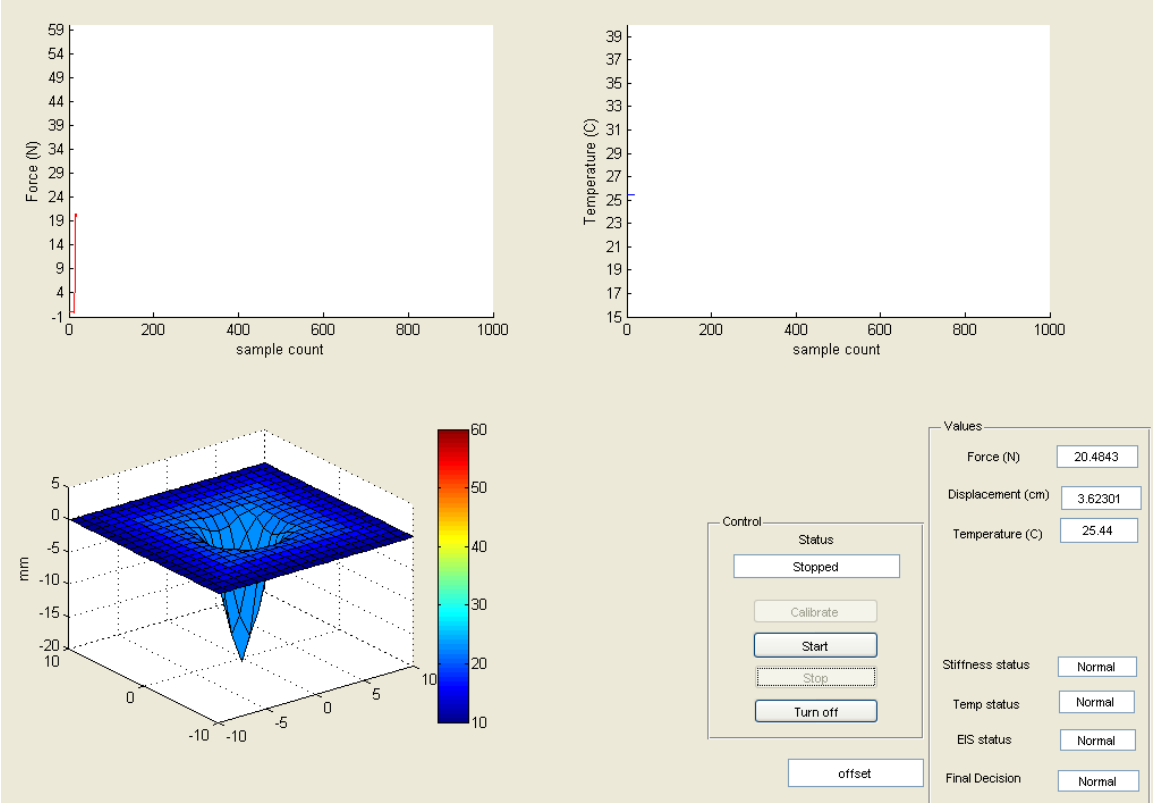

Figure 5-10 GUI for the FIS based decision system

In this GUI the user first checks the status of the system, no hardware and communication issue results to a READY status in the GUI. Thereafter, the base temperature of the surface is found using the Calibrate tab. Once calibrated the offset tab represents the base temperature. The parameters of the FIS are adjusted according to the base temperature of the surface. This is followed by the Start Tab to start capturing data from the surface. The three location temperatures are shown in the Temperature1, Temperature2 and Tempearture3 tab, followed by the Temp Status 1 as 'index normal obj' or 'index hot object', Temp Status 2 as 'centre normal obj' or 'centre hot object' and Temp Status3 as 'ring normal obj' or 'ring hot object'.

The GUI is able to provide a decision as to whether an anomaly is present depending upon the temperature gradient along with at what location is it present.

Results

The Melexis infrared sensor has proved to be capable of thermal anomaly detection in a uniform temperature phantom. But as the thermal properties of living tissue cannot be mimicked fully by the phantom therefore In Vivo testing of the computer enhanced surface thermometry system was required.

5.3. In vivo healthy human tissue study

Ethics approval for conducting the study named “In Vivo Data collection of dielectric, thermal and elastic properties of human tissue”; APPL. #2011s0523 had been taken from the Office of Research Ethics, Simon Fraser University. *In vivo* study using healthy human subjects was done to determine the thermal index of the palmar arm and bicep of 20 subjects. The aim of the study was to determine the usability of Melexis infrared sensor for computer enhanced surface thermometry of breast.

Methodology

The procedure consisted of data collection from the palmar arm and bicep of 20 subjects using 6 infrared sensors’ collecting data from three close vicinity sites (two sensors collecting data from same site for redundancy and reliability increase of the system). Statistical Analysis for 1440 data samples is represented in the table below, the two columns show data collected from 20 subjects Arm and Bicep. First Columns shows results without filtering and the second columns shows the improvement after applying error bit filtering techniques. The standard deviation (SD) for the improved algorithms is .83. The results show that the overall SD in the data collected from the subject bicep (.83) is less than from the arm (1.08). This can be attributed to the presence of veins (at higher temperature) close to the surface in arm compared to bicep due to lack of muscle and fat in the arm. As can be seen the mean temperature is not very variant especially in the bicep data. The mean arm temperature is lower than bicep due to less tissue depth

leading to less blood supply and lower temperature. The temperature over the bicep seems to be uniformly distributed.

Table 5.1 Temperature Data for Arm and Bicep tissue

Subject	Arm Temperature Data Using MELEXIS Sensor				Bicep Temperature Data Using MELEXIS Sensor			
	RAW DATA		**FILTERED DATA**		**RAW DATA**		**FILTERED DATA**	
	Standard Deviation	Mean	Standard Deviation	Mean	Standard Deviation	Mean	Standard Deviation	Mean
1	1.5155	33.4717	.1353	33.4742	4.7604	34.2147	.1665	34.2097
2	1.1842	30.1257	.2884	30.5503	2.8762	34.2644	.3866	34.2746
3	5.4729	34.1994	.1004	34.1356	2.5763	34.4833	.1650	34.4717
4	2.9128	33.0068	.2166	33.4547	1.4263	33.4322	.5413	33.4347
5	4.0385	34.0144	.0934	33.9969	1.9495	34.9103	1.1622	35.3854
6	1.9244	33.0335	.1465	33.4844	3.4557	33.6194	.5912	33.6492
7	1.1043	32.1011	.2106	33.0008	0.1994	34.9425	.1994	34.9425
8	1.0624	32.4129	.1478	32.8553	1.8984	33.9694	1.0105	34.4218
9	.9384	31.993	.1744	32.4103	2.8821	32.8538	.3669	33.2806
10	2.8356	33.7594	.1074	33.7503	3.1568	34.8358	.2983	34.8281
11	5.6525	33.6619	.6084	33.7943	2.8419	34.6492	.3849	34.6253
12	2.4076	29.6197	.8344	31.2756	6.4861	34.5183	.6012	34.5200
13	2.0778	30.1419	.7041	31.8400	.1890	33.3986	.1890	33.3986
14	2.7476	33.8472	.1993	33.8422	.0777	34.9447	.0777	34.9447
15	2.3439	30.1653	.5839	31.8475	6.4968	33.8758	.2124	33.8106
16	.1699	33.5489	.9491	34.0163	3.6117	35.3781	.2022	34.4350
17	1.3806	31.7164	.2544	32.6053	1.7523	33.4089	1.3552	33.8801
18	4.2249	34.3897	.3696	34.3936	.2407	33.2417	.2407	33.2417
19	.2510	33.2931	.2510	33.2931	.2893	33.7071	.2893	33.2342
20	2.0102	33.0751	.2681	33.5439	2.6285	32.3400	.3373	33.4580
TOTAL	3.1250	32.5792	1.0894	33.0782	2.9299	33.8302	.8343	34.1279

Results

The data shows promising results to be used for anomaly detection in breasts. The specifications of the sensor fulfill the desired Infrared criteria set by the *iact*. The improved algorithms with error bit filtering technique showed an improvement by lowering the standard deviation of the system from 8% relative standard deviation to

2.4% for the 20 Subject Arm data and 9.57% to 3.2% for the bicep data. But to be considered as equivalent to thermography extensive work in image processing needs to be done. Efforts are being made to improve image quality through Melexis 16x4 sensor array MLX90620 [221],that is capable of a 64 pixel image in 2D in real time, avoiding the need to scan the area with a single point sensor.

The sensitivity of the sensor is high enough to detect the veins in the arm and this makes the future work challenging as the overall sensitivity of the system needs to be programmed such that veins in the breast tissue are not detected as anomaly. The FIS seems to be a very valuable tool in overcoming this challenge, but its success depends upon training data that I am presently working on getting from BCCA.

Another parameter that if added to the fuzzy system, will highly increase the reliability of the system is adding information regarding the thermal profile of the breast. Work done by Sudharshan [210] when added to the existing FIS will result to a very promising anomaly detection modality. But as the false negative of thermography is really high therefore it will act only as an adjunct modality to be integrated with other anomaly detection methodologies.

5.3.1. In Vivo Tissue Thermal Analysis over contralateral body parts

Methodology

Data was collected over four contralateral parts of body, i.e. it was tested on bicep and forearm of both left and right hands at three pressure levels. 1320 data samples were collected from 11 healthy subjects (2 trials for each site). The mean temperature, standard error and margin of error of these four surrounding sensors and the central sensor on the left and right bicep and forearm of 11 subjects are illustrated in table 5.2 and figure 5.12. According to the results, the mean temperature of the surrounding parts of tissue is approximately equal to the temperature of the central sensor. It shows the fact that in healthy tissue, the temperature of all parts of tissue is approximately uniform. The maximum amount of temperature difference in surrounding tissue and the central tissue is 0.82 degree of centigrade, while the maximum

temperature difference in the tumorous mimicking phantom was 2.38 degree of centigrade.

Results

It is also observed that the mean forearm temperature is lower than the mean bicep temperature which is attributed to less tissue depth. The mean temperature over the tissue is observed to be not very variant, especially in the bicep data. The overall standard deviation of the bicep is less than standard deviation of the forearm. This can be attributed to the presence of veins (at higher temperature) close to the surface in arm compared to bicep and, due to lack of muscle and fat in the arm. The finding that various types of tissue have different mean temperature does not decrease the reliability of the proposed method. As for detecting thermal anomaly in any part of body, the temperature of the suspected area is compared relative to its surrounding tissue.

The most striking result to emerge from the data is that as the applied pressure increases, the mean temperature in all sensors increases. This can be as a result of more concentration of blood below the compressed tissue when pressure is applied to it. As the sensors used in this study are contactless, this effect of pressure on the temperature of tissue will be eliminated and thus the results will be more reliable.

These results proved the reliability, accuracy and repeatability of the sensor head to be reasonably fitting the requirements for computer aided surface thermometry. The next phase of this study will be to test the sensors on benign and malignant in vivo tissue.

Table 5.2 Mean Temperature and Standard Deviation at Different Pressure levels for Different Body Parts

	Sensors	Pressure Level 1 (2.5 lb)	Pressure Level 2 (5 lb)	Pressure Level 3 (7.5 lb)
Left Bicep	4 Surrounding	31.54 ∓ 0.74	32.01 ∓ 0.41	32.32 ∓ 0.44
	Center Sensor	31.43 ∓ 0.79	31.45 ∓ 0.69	31.76 ∓ 0.63
Right Bicep	4 Surrounding Sensors	31.17 ∓ 0.90	31.87 ∓ 0.43	32.71 ∓ 0.26
	Center Sensor	31.45 ∓ 0.88	31.51 ∓ 0.63	31.99 ∓ 0.74
Left Forearm	4 Surrounding Sensors	28.00 ∓ 1.47	31.10 ∓ 0.52	31.93 ∓ 0.57
	Center Sensor	28.36 ∓ 1.93	30.18 ∓ 0.94	31.11 ∓ 0.88
Right Forearm	4 Surrounding Sensors	28.83 ∓ 1.33	31.60 ∓ 0.56	32.00 ∓ 0.91
	Center Sensor	29.26 ∓ 1.97	31.02 ∓ 0.89	31.89 ∓ 0.65

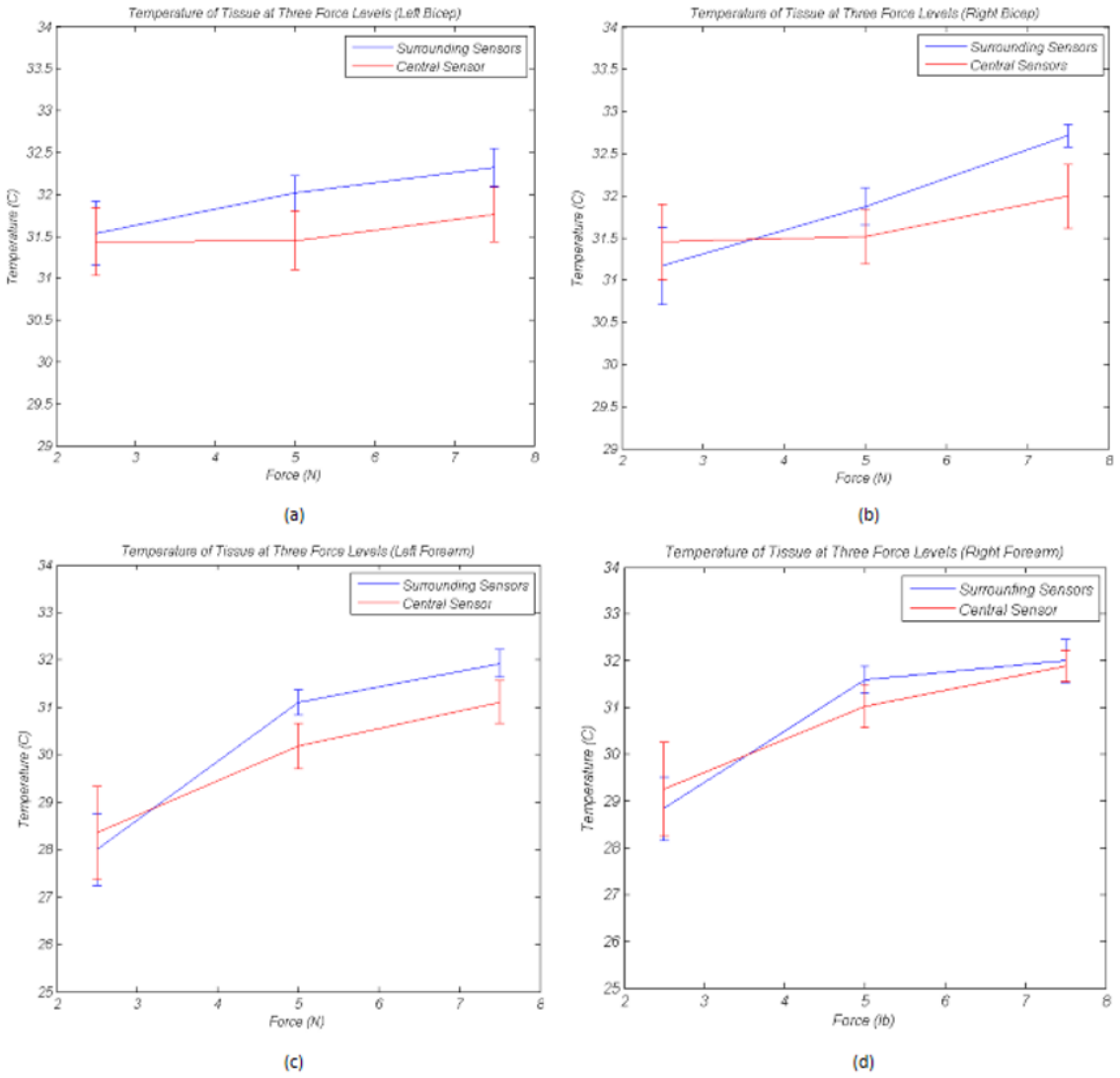

Figure 5-11 Tissue Temperature (Mean and Standard Deviation)

5.4. Discussion and Conclusion

This section was based upon the identified LWIR sensors' usability for the thermal analysis of tissue *in vivo*. In this section the focus has been on the verification of the developed surface thermometry system to identify anomaly having higher thermal gradient compared to the adjoining environment. A test bed set up was developed for this. The same tissue equivalent material [72] was used as described in section 2.2.3, as the material shows thermal properties similar to the fat and muscle tissue. The static thermal properties of the material measured using scanning calorimetry were close to

the values predicted by theory of human fat [75][76] [77].The specific heat capacity can be calculated from the values of the ingredients. Thermal Conductivity of fat is given as 0.200-0.246 W m-1K-1 and that of human muscle 0.449-0.546 W m-1K-1 [222]. Though present research focused on the dynamic thermal simulation, in which not only the heating pattern but also the thermal transport processes of conductivity and perfusion are simulated, but these phantoms only satisfied the static thermal simulation (heating pattern of the phantom corresponds the tissue).As these developed materials had properties closest to the required phantoms for present study therefore these phantoms were used. Interestingly, specific heat of tissue anomaly (fibrosis and adenocarcinoma) is closer to muscle than to fat [72]. Therefore fat phantom was used to mimic the breast tissue.

Presently, the infrared cameras available in the market and being commonly used for thermography have a spectral range of 7.5-13 µm, with standard temperature ranges and +/- 2.0ºC accuracy going to +/- 1.0ºC in limited range [223]. The specifications of the developed sensor head were compared to the *iact* guidelines for thermography standards and protocols [184] and, market available thermography camera FLIR SC600 Series [224]. The spectral bandwidth of FLIR SC600 is 7.5-13.0 µm and the spectral bandwidth of Melexis is 5.5µm to 14µm. Melexis sensor with computer analysis is capable of providing repeatable real time data with minimum cross talk by controlling the field of view (FOV), the FLIRSC600 also shows good repeatability. The sensor head design maintains a constant distance of the module from the skin resulting to a constant spot size of 2mm at 1mm from detector, as required per the guidelines. The FLIRSC600 is fixed at a position to maintain the distance. Melexis sensor head has an accuracy of 0.1ºC at body temperature and readout resolution of 0.02ºC compared to FLIRSC600 that has accuracy and resolution of 1ºC. Further as required by the guidelines, the quantitative differential analysis is being performed by the fuzzy inference system based decision algorithms and the image is represented using graphical user interface in Matlab® whereas FLIRSC600 does not have any analysis feature. The Matlab® software used with Melexis sensor head also has ability to store the data for future analysis. Therefore, when appended with a novel sensor head design to maintain the sensor at specific distance from the skin; decision making expert system and imaging software, the Melexis sensor head will reasonably meet the *iact* standards and

protocols for thermography. It has the required spectral bandwidth, repeatability, real-time data representation, spot size, accuracy and data analysis software but has limitations regarding the sensor sensitivity and spatial resolution.

The results using phantoms have been quite promising but there are further challenges to apply this system to biological tissue. The sensitivity of the sensor is high enough to detect the thermal variation due to surface veins in the arm and this makes the future work challenging as the overall sensitivity of the system needs to be programmed such that surface veins in the breast tissue are not detected as anomaly. The FIS seems to be a valuable tool in overcoming this challenge, but its success depends upon large amount of training data. The authors are in the process of obtaining the required training data on breast cancer patients. Adding information regarding the thermal profile of the breast will also highly increase the reliability of the system. But due to the inherent short comings of thermography, it will act only as an adjunct modality to be integrated with other anomaly detection methodologies.

Overall, the system shows good potential, but does lack high spatial resolution, resulting in low quality images. However, the sensor industry is growing considerably, providing improved and more accurate sensors. Melexis itself is providing array based sensors that would be capable of providing better improved surface thermal data. An improvement of the design will be to consider the MLX90620 array sensor from Melexis. To be considered as equivalent to thermography; further work in image processing and sensor integration is required.

Chapter 6.

Tissue Classification: Multimodality (*In vivo* Malignant Human Tissue)

The promising results from classification of healthy human tissue using complex impedance parameters motivated me to extend the multimodality data collection over malignant tissue and observe the variation of electrical impedance with pressure or temperature. This study was carried over malignant skin tumors with the control as a contralateral healthy body tissue. This was collaborative research with the BC Cancer Agency. Due to the sensitivity involved in breast cancer patient population it was best in the interest of the research to test the device over skin tumors first. The study 'Electrical Impedance Analysis of Malignant and Benign Tissue: Effects of Temperature and Pressure' was done under the UBC BCCA Research Ethics Board and SFU Ethics Board under Dr. Paris Ann Ingledew as the Principal Investigator and ethics application numbers REB Number H13-02887 and 2014s0134.

6.1. Establishing validity for use of contralateral *in vivo* healthy human tissue as control

The control used in this study was the contralateral healthy body tissue. The requirement for using this as a control was to first verify the suitability of the control for the defined study. To accomplish this healthy data collected from the prior ethical study '*In vivo* Data collection of dielectric, thermal and elastic properties of human tissue, APPL. #2011s0523' was analysed.

Contralateral data from left and right arm and bicep was compared. For comparison first parameter extraction was performed similar to the parameters extracted for the *in vitro* animal study. Along with parameters R_{ext}, R_{int} and C_m three more

parameters were extracted after consulting literature [54]. The extracted parameters were ω_c (critical frequency at maximum phase value), Φ_{max} (maximum phase value that is acquired in the given frequency range) and Φ_{5KHz} (phase value at 5 KHz). At a frequency above few kilohertz, the effect of high resistance of skin decreases due to large parallel capacitance, and the admittance of tissue beneath can be measured. The crossover frequency is defined as the characteristic frequency for the relaxation of the skin capacitance through the resistance of the breast tissue. This is usually 5 KHz. Phase based tissue classification is preferred as phase value is insensitive to the geometrical parameters (e.g. Depth of the breast).Algorithms were developed using Matlab programming for feature extraction. The extracted parameters were grouped into healthy left, right, arm, and bicep data respectively. ANOVA (Analysis of Variance) Matlab function was used for further analysis. One way ANOVA was used. The function performed a one-way ANOVA for comparing the means of two or more coloumbs of data in a matrix, where each coulomb represents an independent sample containing mutually independent observations. The function returns the *p*-value under the null hypothesis that all samples in x are drawn from populations with the same mean. The ANOVA test is performed under the assumption that the data in all populations are normally distributed, has equal variance, and all observations are mutually independent.

6.1.1. Results: Contralateral Healthy Tissue (Extracted Feature Comparison)

The representation of the ANOVA results has been done in the form of notch box plots. There is one box per column. On each box, the central mark is the median, the edges of the box are the 25^{th} and the 75^{th} percentiles, the whiskers extend to the most extreme data points not considered outliers, and the outliers are plotted individually. Data at three pressure levels (1, 2, and 3) has been considered, and each pressure level has three repeated trials. Data from 11 healthy subjects has been compared. In results LA1 represents left arm pressure level 1, RA1 is right arm pressure level1, LB1 is left bicep pressure level 1 and RB1 is right Bicep arm respectively. Units of R_{ext} and R_{int} are in ohms, Cm is in Farads, ω_c is in Hertz and Φ_{max} and Φ_{5KHz} are in degrees. The p-value is represented in the right bottom corner of each result.

1. Tissue Extracellular Resistance

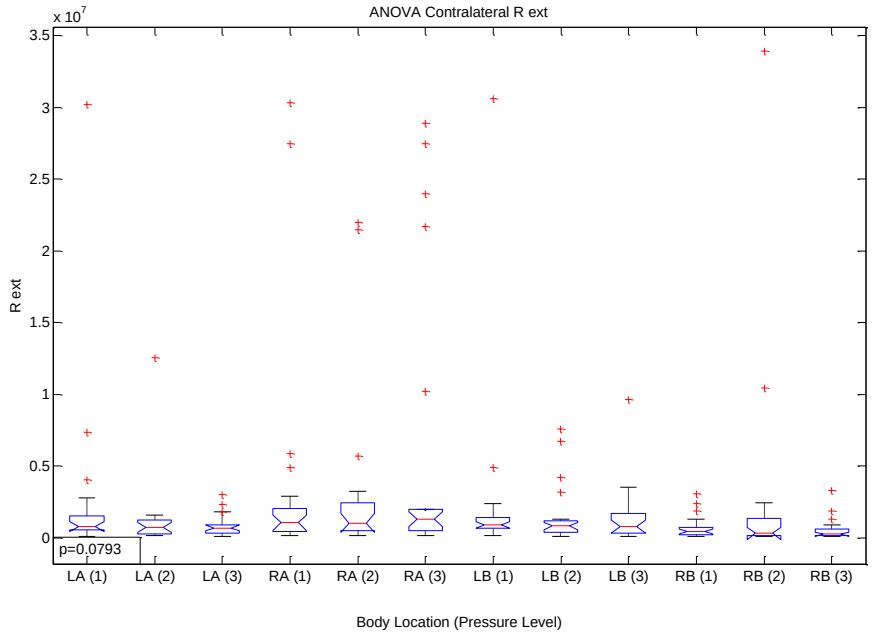

Figure 6-1 ANOVA1 for Extracellular Resistance of 11 healthy subjects' arm and bicep contralateral data

2. Tissue Intracellular Resistance

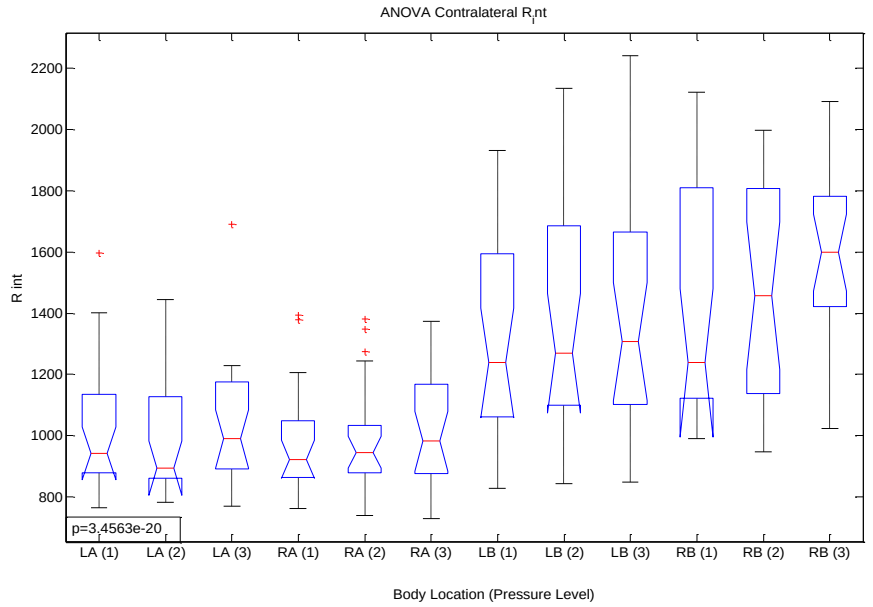

Figure 6-2 ANOVA1 for Intracellular Resistance of 11 healthy subjects' arm and bicep contralateral data

3. Tissue Membrane Capacitance

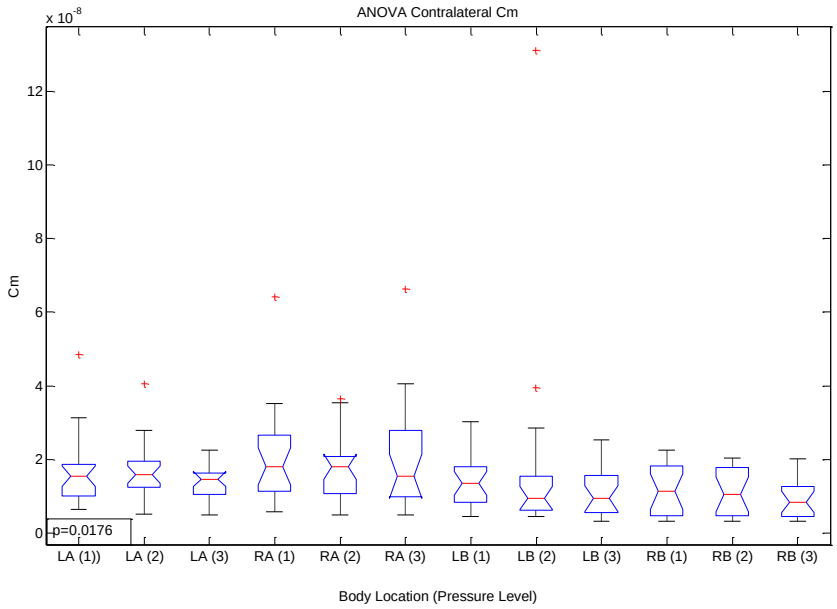

Figure 6-3 ANOVA1 for membrane capacitance of 11 healthy subjects' arm and bicep contralateral data

4. Tissue Maximum Phase Angle

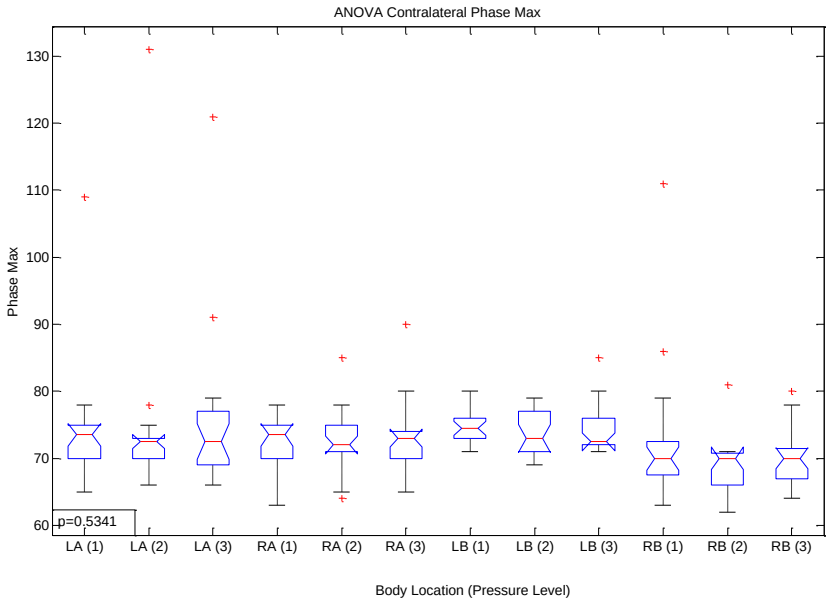

Figure 6-4 ANOVA1 for maximum phase angle of 11 healthy subjects' arm and bicep contralateral data

5. Tissue Frequency at Maximum Phase Angle

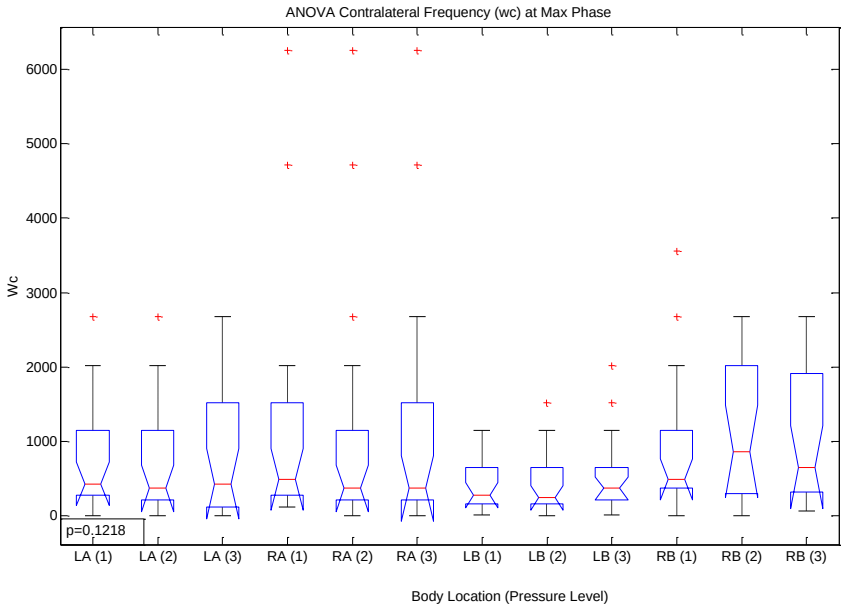

Figure 6-5 ANOVA1 for frequency at maximum phase angle of 11 healthy subjects' arm and bicep contralateral data

6. Tissue Phase Angle at 5KHz frequency

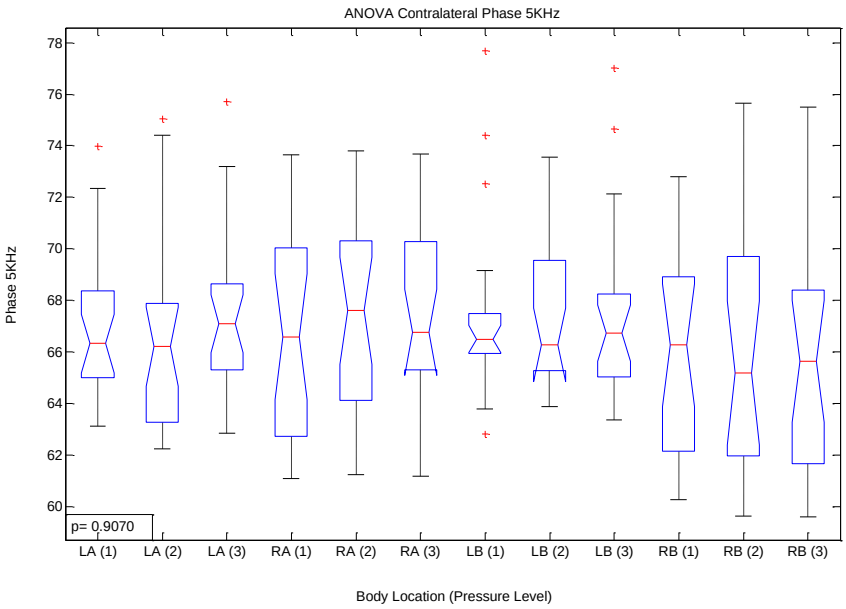

Figure 6-6 ANOVA1 for phase angle at 5 KHz frequency of 11 healthy subjects' arm and bicep contralateral data

6.1.2. Conclusion

According to the obtained p-values from ANOVA1 analysis of the data, Table 6.1, it was found that all the extracted parameters do not behave similarly. Parameter R_{ext} showed the maximum number of outliers and a low p-value of .0793. In comparison R_{int} showed less number of outliers but its p-value was significantly low. However, R_{int} provided some information regarding the tissue depth. C_m also showed a low p-value of .0176. On the other hand the parameters based upon phase showed better p-values. Phase at 5 KHz showing a p-value of .9070, concluding that this is the best parameter that can be used for further classification of healthy and malignant tissue. Phase based parameters also showed less variability with application of pressure, whereas R_{int}, R_{ext} and C_m followed a particular pattern with increase in pressure level.

Table 6.1 ANOVA Result Comparison

ANOVA1 p-Value Comparison for Different Healthy and Contralateral Healthy Tissue

Extracted Parameter	ANOVA1 p-value
R_{ext}	.0793
R_{int}	3.45e-20
C_m	.0176
Phase_Max	.53
Critical Frequency_Phase_Max	.1218
Phase_5KHz frequency	.9070

6.2. Tissue Classification: Multimodality (*In vivo* – Malignant Human Tissue)

The results from classification of healthy human tissue using parameter extraction and data analysis based upon ANOVA1 motivated me to extend the multimodality data collection over malignant tissue and observe the variation of electrical impedance with pressure or temperature. This study was carried over malignant skin tumors with the control as a contralateral healthy body tissue. This was collaborative research with the BC Cancer Agency. The research had to be carried over skin tumors as after repetitive meeting with oncologists it was suggested that due to the sensitivity involved in breast cancer patient population it will be best to test the device over skin

tumors first. After a constant effort of two years, I was able to collect data over five skin tumors. This study 'Electrical Impedance Analysis of Malignant and Benign Tissue: Effects of Temperature and Pressure' was done under the UBC BCCA Research Ethics Board under Dr. Paris Ann Ingledew as the Principal Investigator and REB Number H13-02887.

6.2.1. Tissue Classification: Multimodality (*In Vivo* – Malignant Human Tissue)

Study involving *in vivo* malignant tissue using a specific patient population was done to determine the variation in the multimodalities of malignant tissue and benign tissue. The aim of the research was to find the variation in the tissue model due to changes in tissue cellular structure as a result of malignancy. After consultation with oncologists at BC Cancer Agency I was advised to test the tool over skin tumors rather than breast tumors due to the complexities involved in recruiting breast tumor patients and associated ethical issues.

Skin cancer is the most common of all cancer types. Screening for skin cancer is usually made by visual inspection of the lesions. Due to its subjective nature, the clinical accuracy of this screening can range from good to poor depending on the experience of the clinician. It is desirable to replace this subjective process with a non-invasive, reliable, simple, and objective technique with high sensitivity and specificity.

One promising avenue of research for diagnosing skin cancer accurately, non-invasively, and potentially at an earlier stage is Electrical Impedance (EI) [225] [226]. Various studies have shown a statistically significant difference in electrical impedance between skin cancers [138][227][148][228] and several devices, such as the SciBase system [229], have been developed to diagnose skin cancer using multi-frequency EI.

Malignant Skin Tissue multimodality Study Procedure

Ethics approval for conducting the study named 'Electrical Impedance Analysis of Malignant and Benign Skin Tissue: Effects of Temperature and Pressure (Ethics

approval H13-02887) was taken from the UBC BCCA Research Ethics Board and from SFU ethics Board. The details of the ethics application are attached in the Appendix B.

6.3. CASE STUDY

CASE STUDY 1

Age	90
Sex	Female
Tumor Type	BCC (Basal Cell Carcinoma)
Tumor Position	Left side of nose along sidewall (small lesion<1cm)

Note: Post Radiation Therapy results available

CASE STUDY 2

Age	97
Sex	Female
Tumor Type	SCC (Squamous Cell Carcinoma)
Tumor Position	Left cheek centre (big lesion>2cm)

Note: Data not gathered over malignant tissue as malignant tissue has wounds that are bleeding, data gathered from a close by site.

Patient passed away, no post RT results

CASE STUDY 3

Age	81
Sex	Male
Tumor Type	SCC (Squamous Cell Carcinoma)
Tumor Position	Right Temple of head (big lesion>2cm)

Note: Had surgery so even had scar tissue.

CASE STUDY 4

Age	93
Sex	Female
Tumor Type	SCC (Squamous Cell Carcinoma)
Tumor Position	Left cheek (medium lesion size, around 2 cm)

Note: Very sensitive tumor, took only one frequency data.

CASE STUDY 5

Age	87
Sex	Female
Tumor Type	BCC (Basal Cell Carcinoma)
Tumor Position	Left cheek under the eye (small lesion size <2 cm)

CASE STUDY 6

Age	93
Sex	Female
Tumor Type	BCC (Basal Cell Carcinoma)
Tumor Position	Left mid neck (medium lesion size, around 2 cm)

6.3.1. Electrical Impedance Spectroscopy Results

The pressure sensors could not be used due to absence of palpable mass at the skin lesion site. Data presented is for two frequency ranges. Comparative data for all six subjects is presented for all six extracted parameters. Blue bar represents healthy tissue data and red bar represents malignant tissue data. Three trials for each subject are repeated. For few subjects only two trials could be taken as the patients comfort level was given more priority than data collection. For example for subject 4 data over malignant tissue could only be collected in frequency range 1 KHz to 1 MHz as lesion site was very sensitive to touch.

1. Frequency Range: 1Hz to 10 MHz

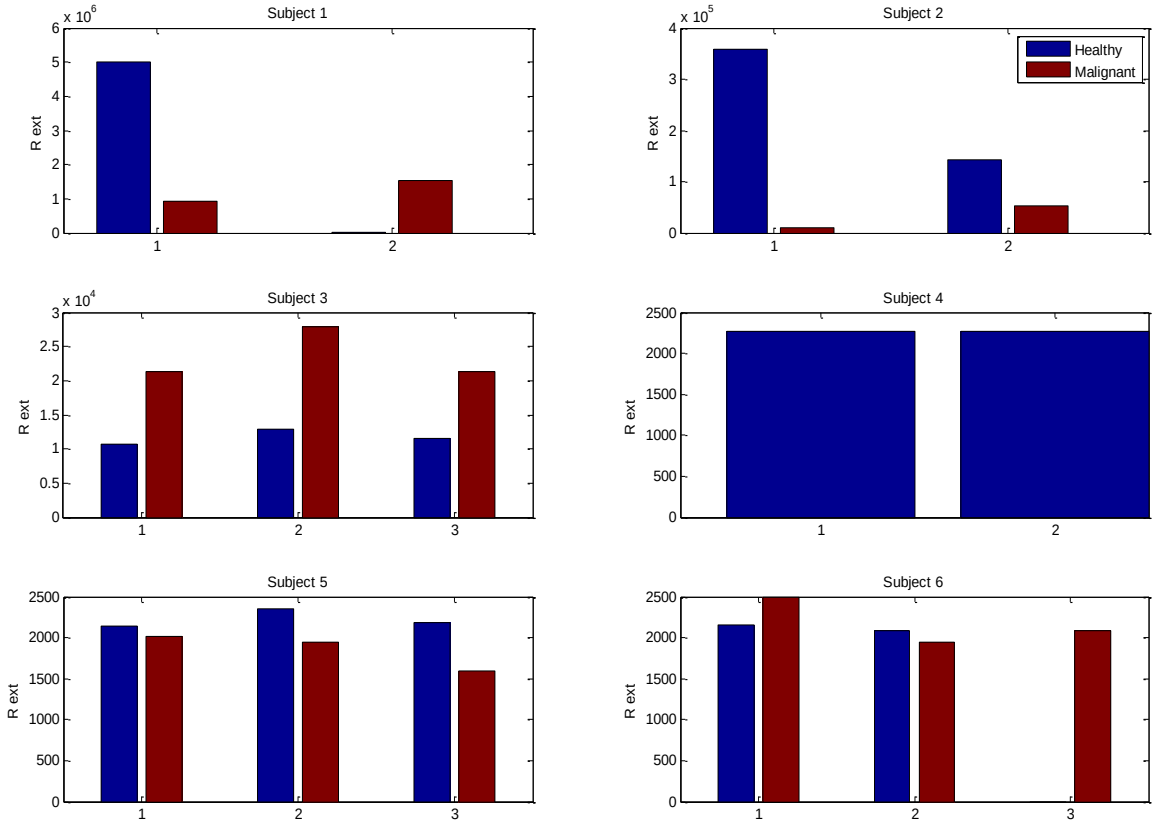

Figure 6-7 Comparative representation of malignant (red bar) and contralateral healthy tissue (blue bar) Extracellular Resistance parameter (ohm) for 6 subjects (Freq: 1Hz to 10 MHz). Three simultaneous trials were repeated for each measurement however for subject 1 and subject 2 simultaneous two trials were obtained and for subject 4 only two trials for contralateral healthy tissue were obtained. For subject 6 only two trials of malignant tissue were obtained. The Extracellular Resistance is decreasing in value for malignant tissue for 66.6% cases, contradicting literature [230]; this may be attributed to high skin resistance at low frequency.

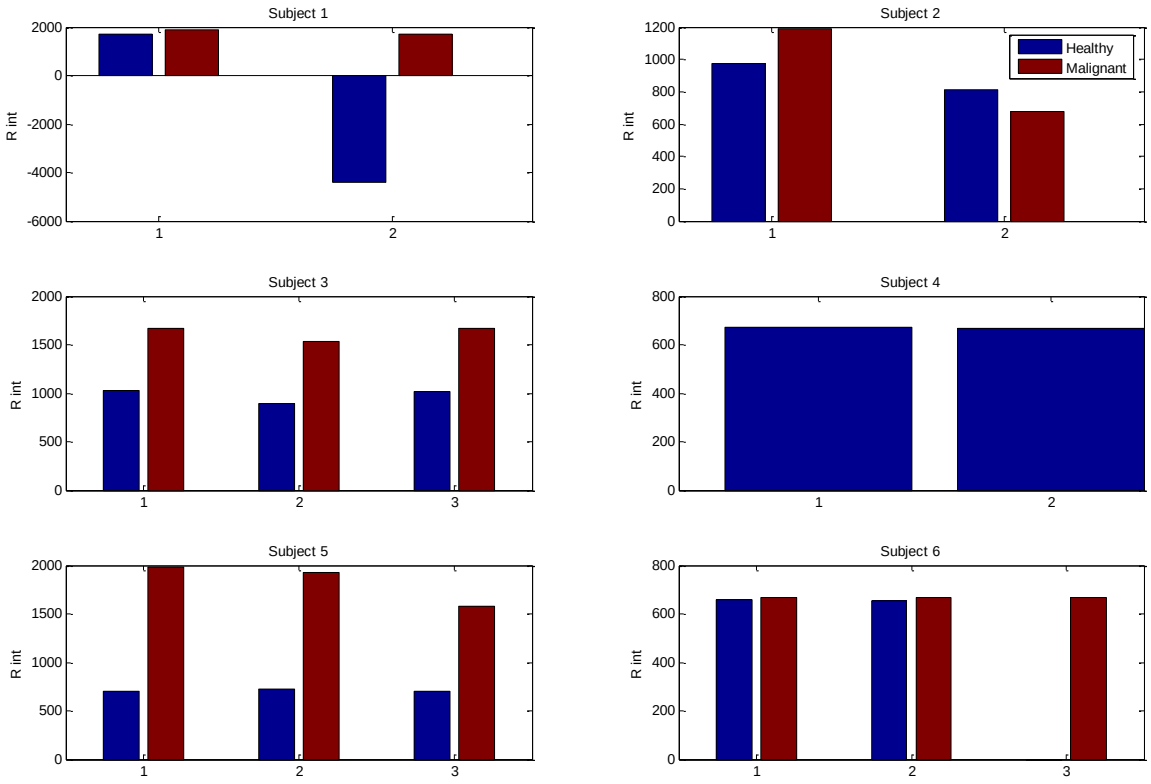

Figure 6-8 Comparative representation of malignant (red bar) and contralateral healthy tissue (blue bar) Intracellular Resistance parameter (Ohm) for 6 subjects (Freq: 1Hz to 10 MHz). Three simultaneous trials were repeated for each measurement however for subject 1 and subject 2 simultaneous two trials were obtained and for subject 4 only two trials for contralateral healthy tissue were obtained. For subject 6 only two trials of malignant tissue were obtained. The Intracellular Resistance is increasing in value for malignant tissue for 2 out of 6 cases, in line with literature [230]. Subject 1, 2 and 6 data is inconclusive and subject 4 data is insufficient for comparative analysis.

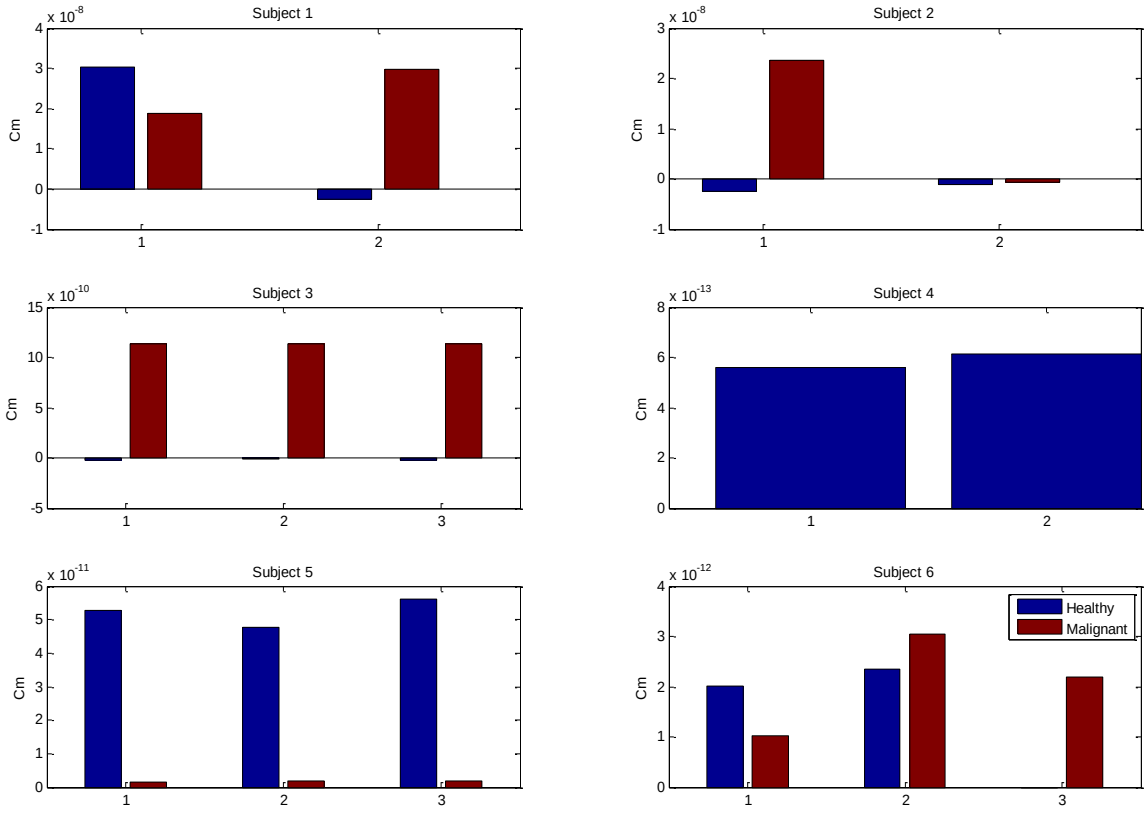

Figure 6-9 Comparative representation of malignant (red bar) and contralateral healthy tissue (blue bar) membrane capacitance parameter (Farad) for 6 subjects (Freq: 1Hz to 10 MHz). Three simultaneous trials were repeated for each measurement however for subject 1 and subject 2 simultaneous two trials were obtained and for subject 4 only two trials for contralateral healthy tissue were obtained. For subject 6 only two trials of malignant tissue were obtained. The membrane capacitance is increasing in value for malignant tissue for 1 out of 6 cases and is decreasing in value for 1 out of 6 cases. Subject 1, 2 and 6 data is inconclusive and subject 4 data is insufficient for comparative analysis.

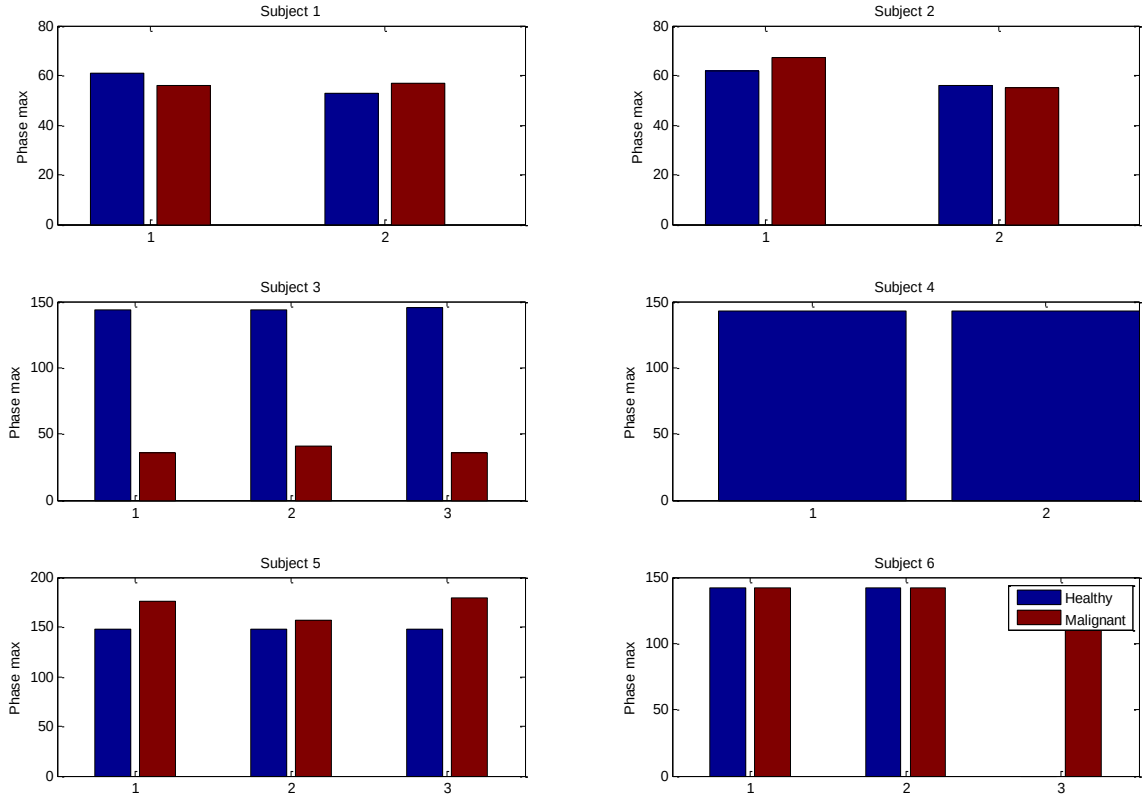

Figure 6-10 Comparative representation of malignant (red bar) and contralateral healthy tissue (blue bar) maximum phase parameter (degree) for 6 subjects (Freq: 1Hz to 10 MHz). Three simultaneous trials were repeated for each measurement however for subject 1 and subject 2 simultaneous two trials were obtained and for subject 4 only two trials for contralateral healthy tissue were obtained. For subject 6 only two trials of malignant tissue were obtained. The maximum phase is increasing in value for malignant tissue for 1 out of 6 cases, and decreasing in value for malignant for 1 out of 6 cases. Subject 1, 2 and 6 data is inconclusive and subject 4 data is insufficient for comparative analysis.

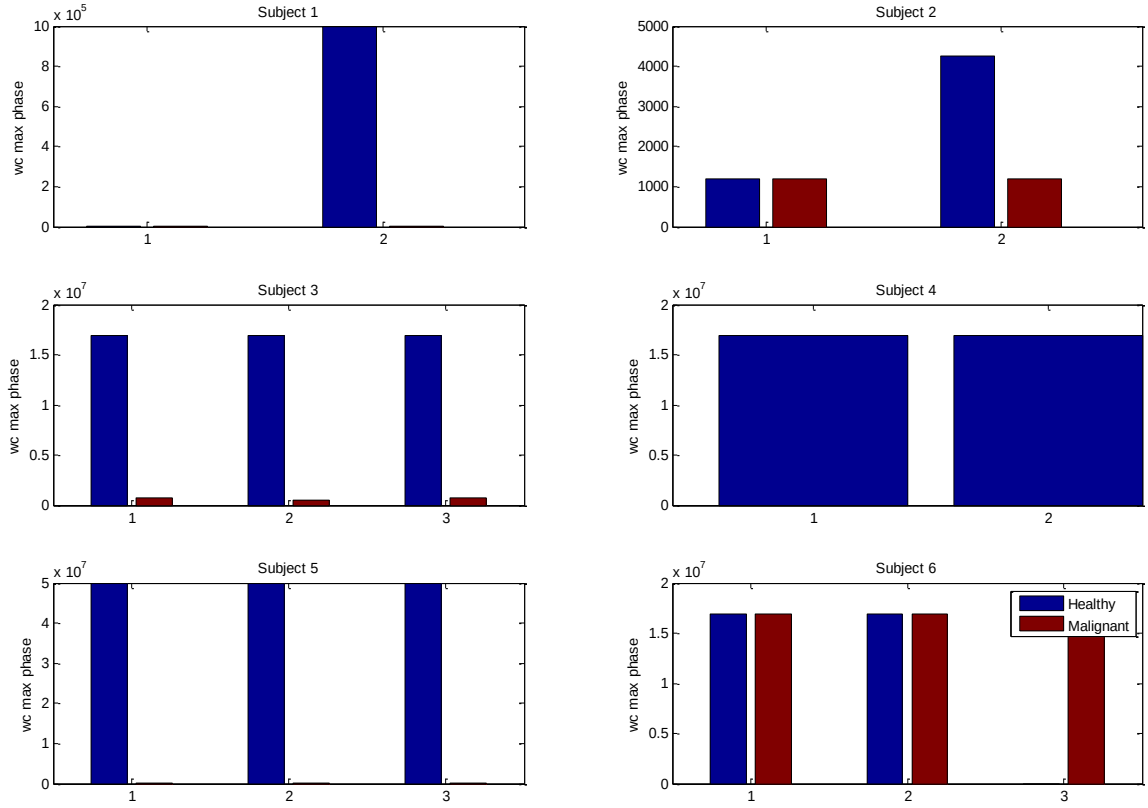

Figure 6-11 Comparative representation of malignant (red bar) and contralateral healthy tissue (blue bar) maximum phase frequency parameter (Hz) for 6 subjects (Freq: 1Hz to 10 MHz). Three simultaneous trials were repeated for each measurement however for subject 1 and subject 2 simultaneous two trials were obtained and for subject 4 only two trials for contralateral healthy tissue were obtained. For subject 6 only two trials of malignant tissue were obtained. The maximum phase frequency is decreasing in value for malignant tissue for 2 out of 6 cases. Subject 1, 2 and 6 data is inconclusive and subject 4 data is insufficient for comparative analysis.

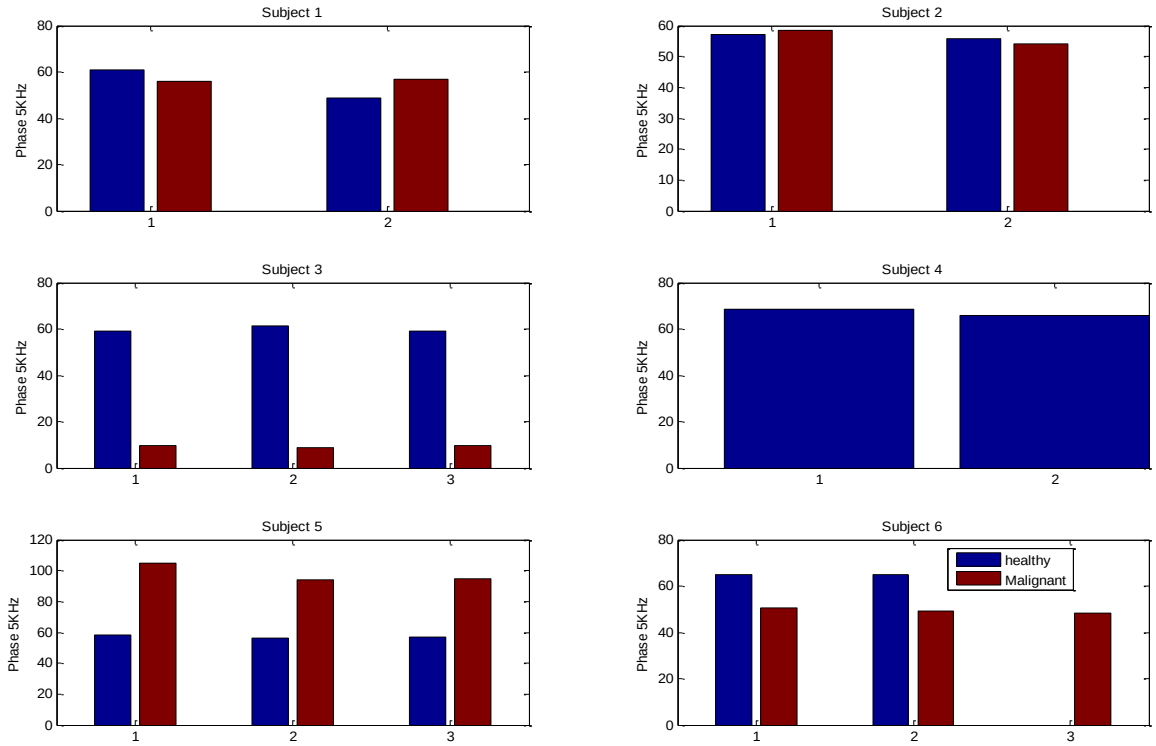

Figure 6-12 Comparative representation of malignant (red bar) and contralateral healthy tissue (blue bar) phase at 5 KHz parameter (degree) for 6 subjects (Freq: 1Hz to 10 MHz). Three simultaneous trials were repeated for each measurement however for subject 1 and subject 2 simultaneous two trials were obtained and for subject 4 only two trials for contralateral healthy tissue were obtained. For subject 6 only two trials of malignant tissue were obtained. The phase at 5 KHz frequency is decreasing in value for malignant tissue for 2 out of 6 cases. Subject 1 and 2 data is inconclusive and subject 4 data is insufficient for comparative analysis. However, it is observed that the parameter varies from 60 to 76 degree for all the healthy tissue data.

2. Frequency: 1KHz to 1 MHz

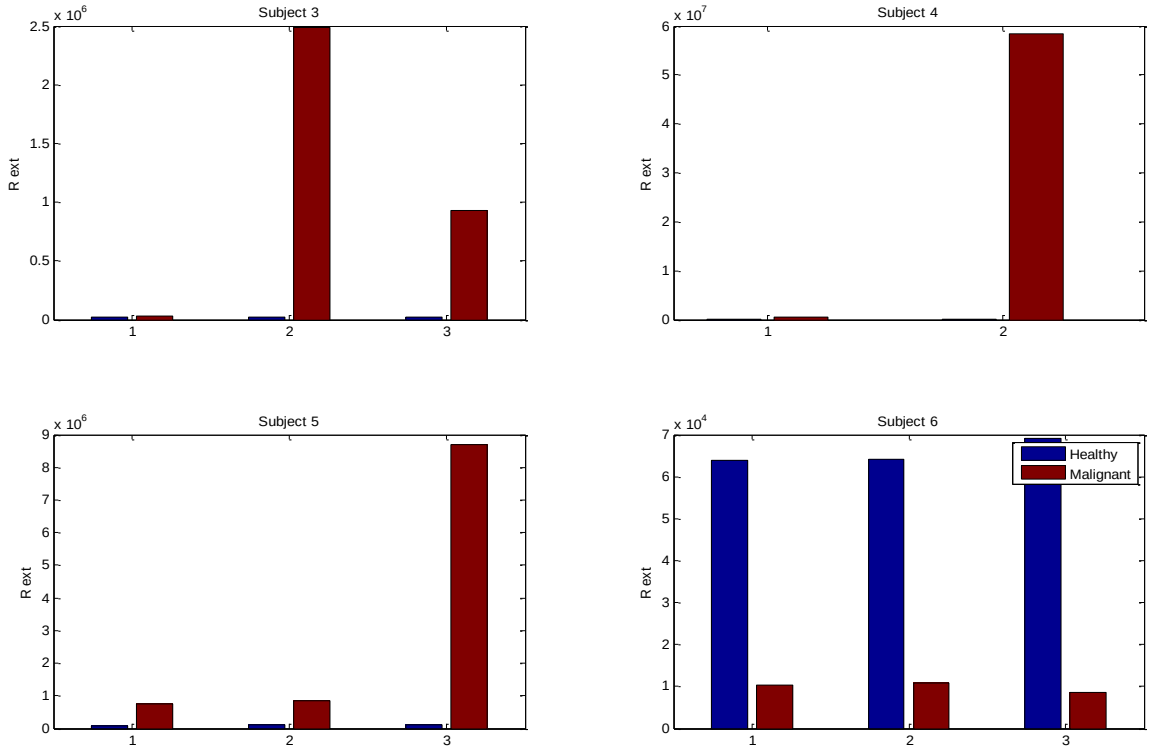

Figure 6-13 Comparative representation of malignant (red bar) and contralateral healthy tissue (blue bar) Extracellular Resistance parameter (Ohm) for 4 subjects (Freq: 1 KHz to 1MHz). Three simultaneous trials were repeated for each measurement however for subject 4 simultaneous two trials were obtained. The Extracellular Resistance is increasing in value for malignant tissue for 3 out of 4 cases, in line with literature.

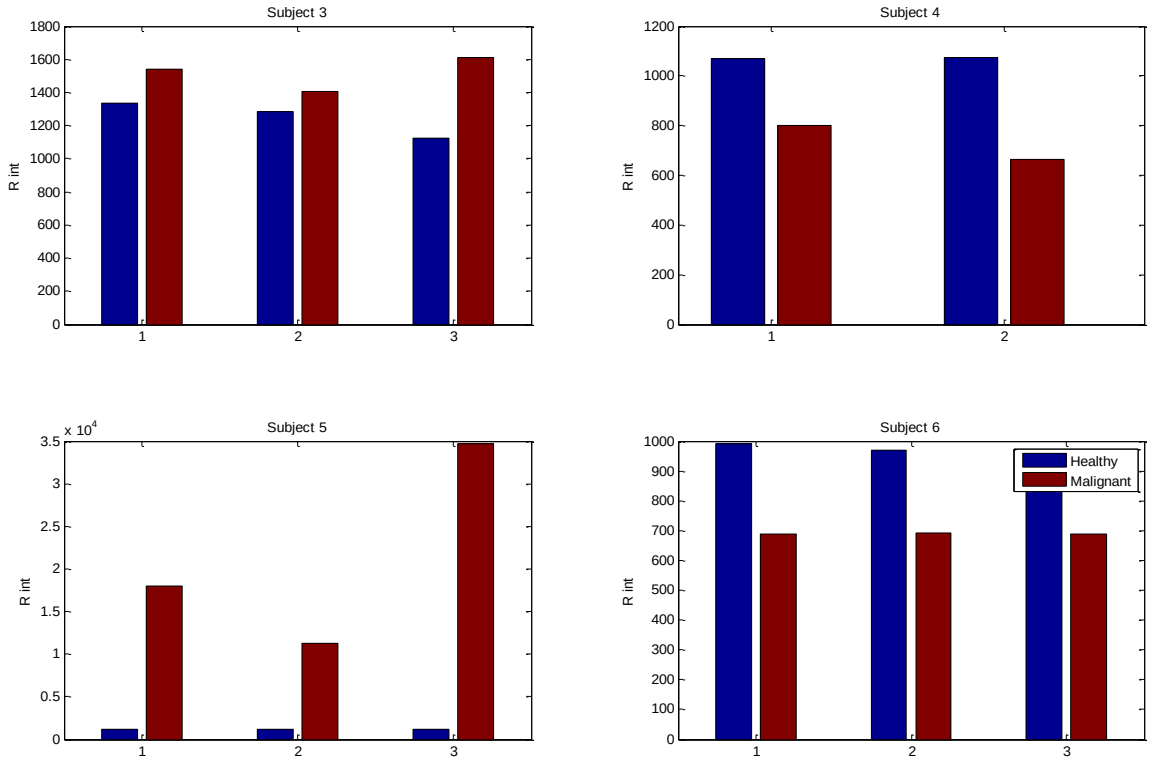

Figure 6-14 Comparative representation of malignant (red bar) and contralateral healthy tissue (blue bar) Intracellular Resistance parameter (Ohm) for 4 subjects (Freq: 1 KHz to 1MHz). Three simultaneous trials were repeated for each measurement however for subject 4 simultaneous two trials were obtained. The Intracellular Resistance is increasing in value for malignant tissue for 2 out of 4 cases, in line with literature [230].

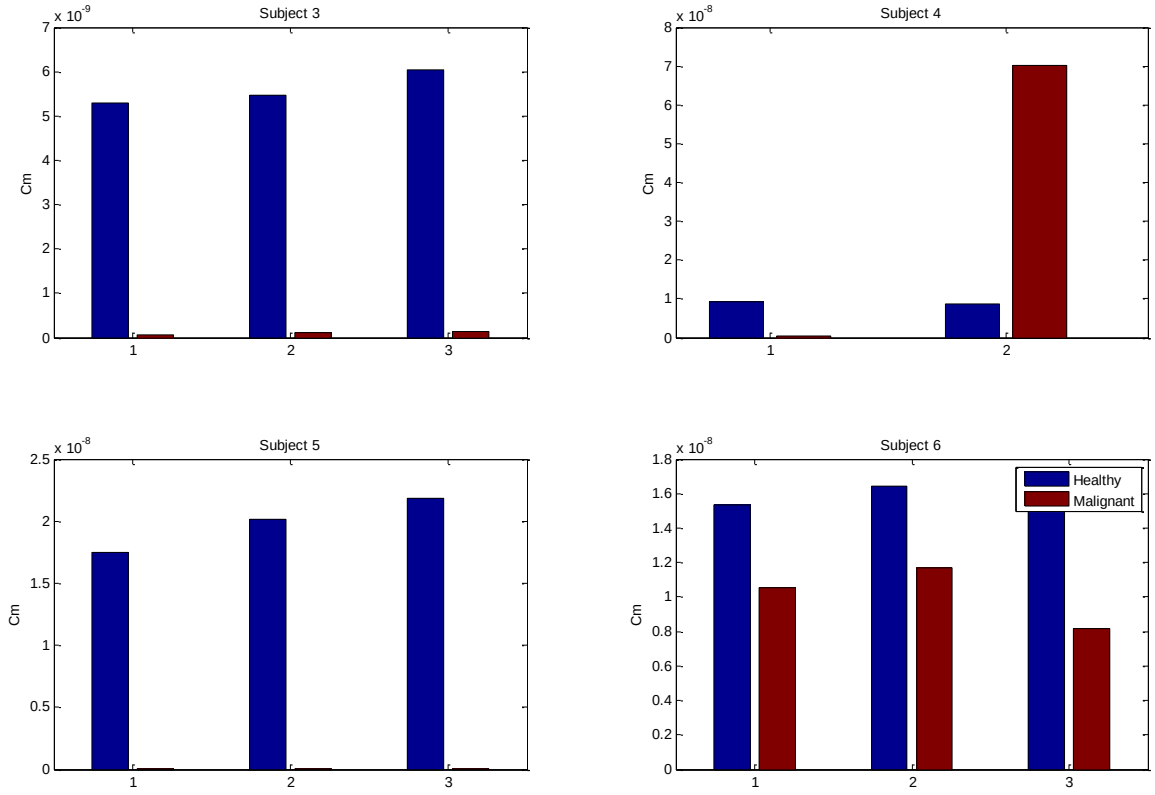

Figure 6-15 Comparative representation of malignant (red bar) and contralateral healthy tissue (blue bar) membrane capacitance parameter (Farad) for 4 subjects (Freq: 1 KHz to 1MHz). Three simultaneous trials were repeated for each measurement however for subject 4 simultaneous two trials were obtained. The membrane capacitance is decreasing in value for malignant tissue for 100%, 4 out of 4 cases, in line with literature [230].

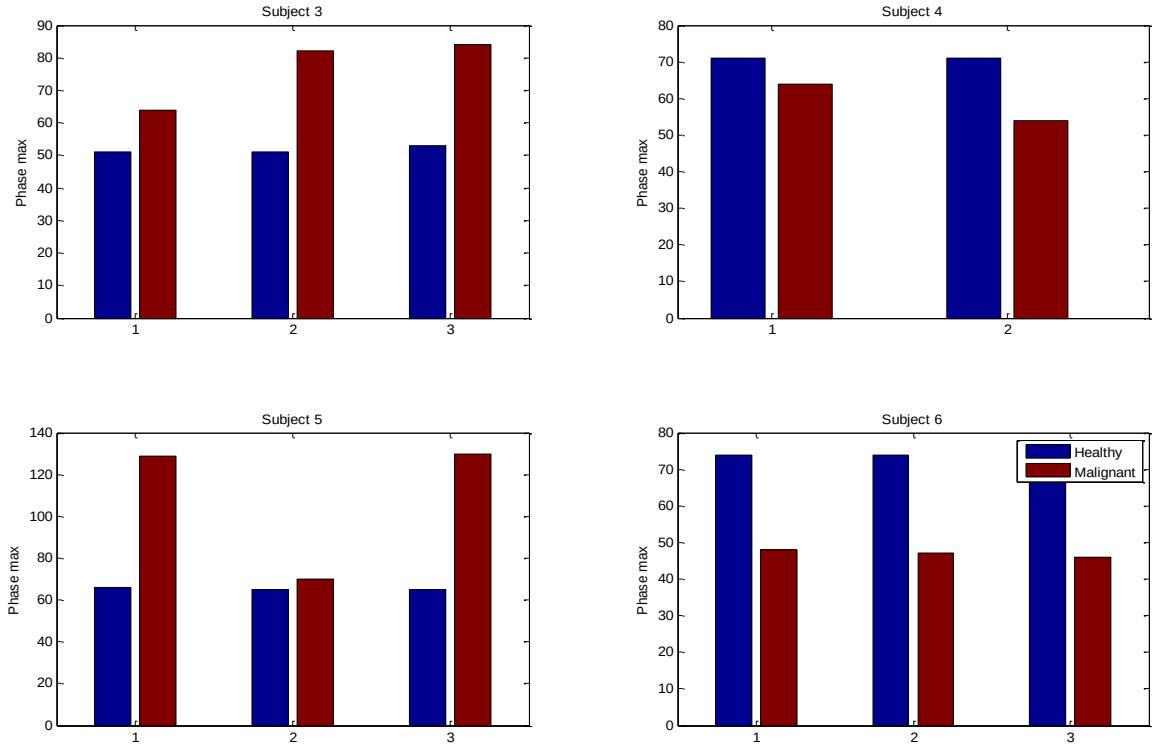

Figure 6-16 Comparative representation of malignant (red bar) and contralateral healthy tissue (blue bar) maximum phase parameter (degree) for 4 subjects (Freq: 1 KHz to 1MHz). Three simultaneous trials were repeated for each measurement however for subject 4 simultaneous two trials were obtained. The maximum phase parameter is decreasing in value for malignant tissue for 50%, 2 out of 4 cases, and increasing for 50% cases, therefore inconclusive.

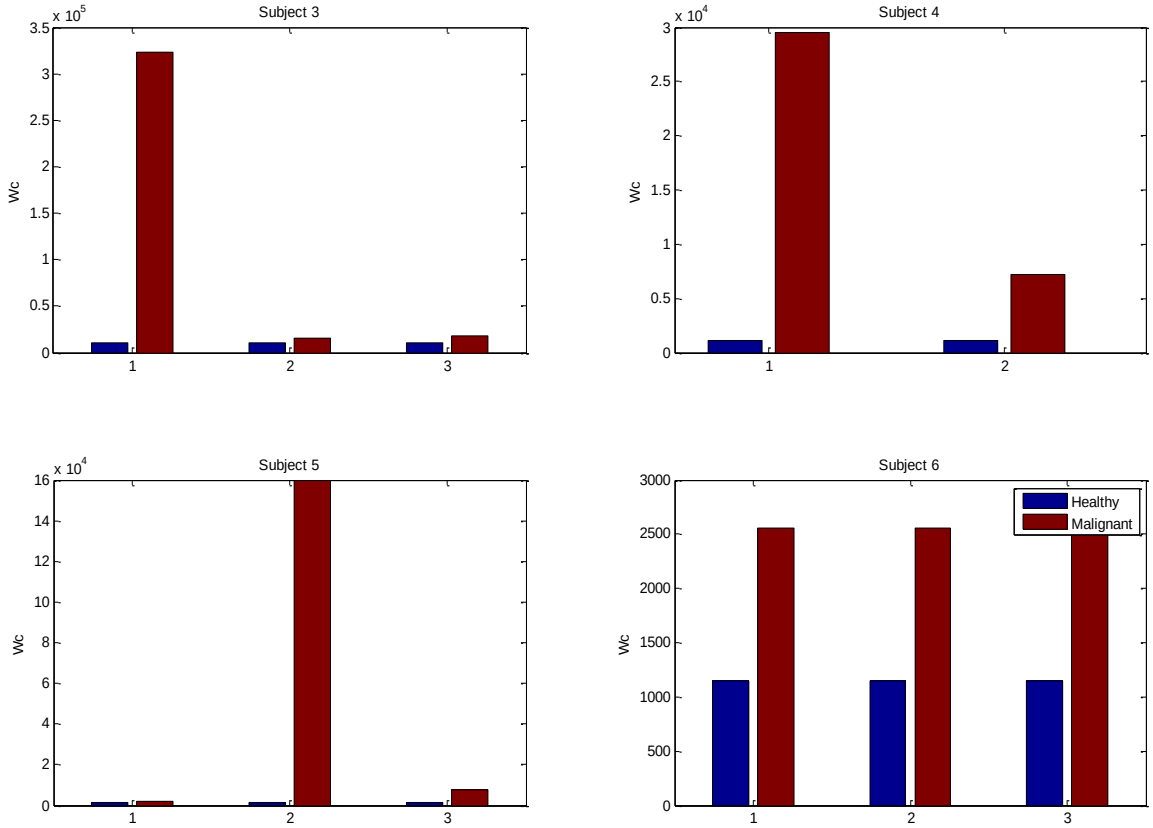

Figure 6-17 Comparative representation of malignant (red bar) and contralateral healthy tissue (blue bar) maximum phase frequency W_c parameter (Hz) for 4 subjects (Freq: 1 KHz to 1MHz). Three simultaneous trials were repeated for each measurement however for subject 4 simultaneous two trials were obtained. The maximum phase frequency parameter is increasing in value for malignant tissue for 100%, 4 out of 4 cases.

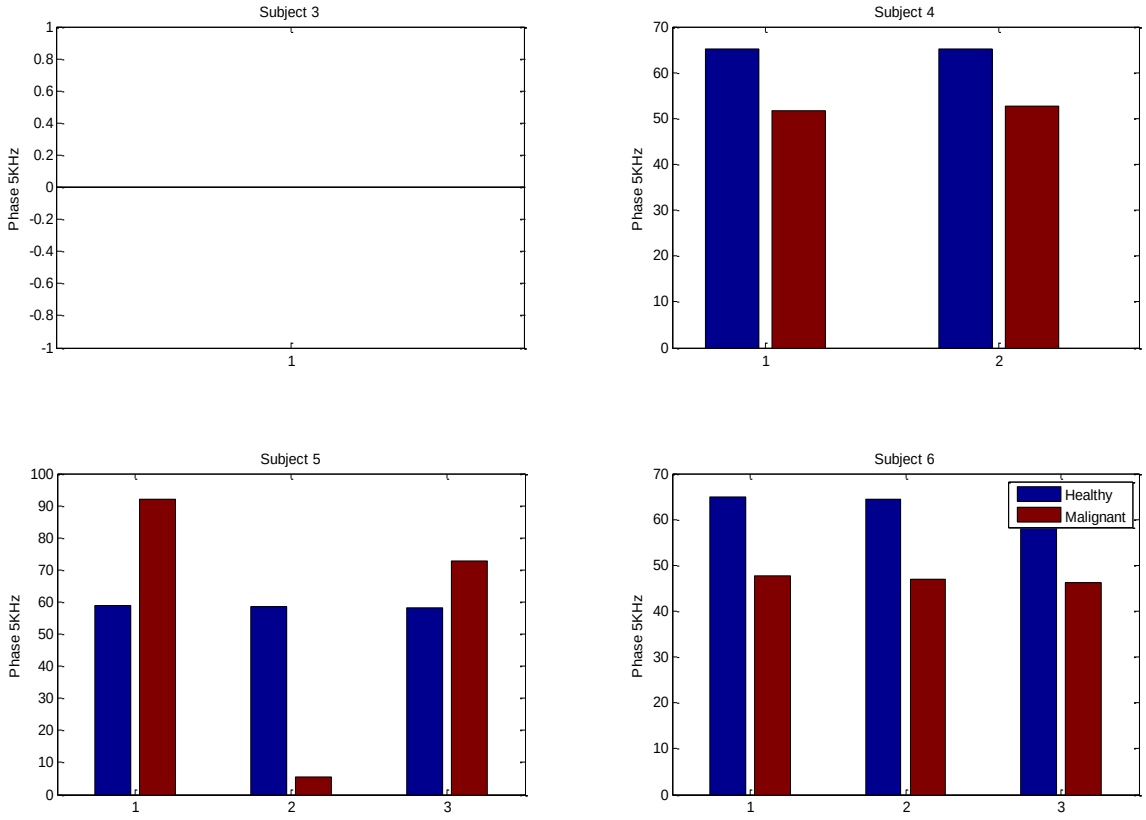

Figure 6-18 Malignant and contralateral healthy tissue phase at 5 KHz parameter for 4 subjects (Freq: 1 KHz to 1MHz). Comparative representation of malignant (red bar) and contralateral healthy tissue (blue bar) phase at 5 KHz parameter (degree) for 4 subjects (Freq: 1 KHz to 1MHz). Three simultaneous trials were repeated for each measurement however for subject 4 simultaneous two trials were obtained. For healthy tissue the parameter varies from 60-76 degrees, but for malignant tissue the parameter is always either above or below the 60-76 range. Subject three data was unavailable.

Discussion and Conclusion

For frequency range 1Hz to 10 MHz, extracellular resistance (R_{ext}) parameter shows a decrease in the value for malignant tissue (Figure 6.7), this is not in line with literature as R_{ext} for malignant tissue is much higher than normal tissue. This is because of the high skin resistance that dominates at lower frequencies than 1 KHz leading to false results. When results from frequency range 1 KHz to 1MHz are compared the R_{ext} for malignant tissue is much higher than contralateral healthy tissue in three out of four cases (Figure 6.13). Subject 3 showed reverse results due to the scar tissue that was

present after the surgery. The results with 75% sensitivity for observed Rext of malignant and healthy tissue are in line with literature [230].

Similarly, for parameter intracellular resistance (R_{int}) does not provide any concrete results for the 1 Hz to 10 MHz frequency range (Figure 6.8) but show an increase in value for malignant tissue, in line with literature [230], with sensitivity of 50% (Figure 6.14).

Membrane Capacitance for malignant tissue is lower compared to healthy tissue [230], this is inconclusive in the 1 Hz to 10 MHz frequency range (Figure 6.9) but observable in the 1 KHz to 1 MHz range with 100% sensitivity (Figure 6.15).

Maximum Phase parameter at lower frequencies (less than 1 KHz) does not give much information about the tissue therefore phase parameter comparison must be used only at higher frequencies [54]. Similar results are observed as lower frequency results (Figure 6.10) are in conclusive but 1 KHz to 1 MHz range does show the phase max with a sensitivity of 50% that is in line with literature [54] (Figure 6.16).

Parameter ω_c, frequency at maximum phase in the present study has not been a very useful parameter to differentiate malignant and healthy tissue in both frequency ranges as observed in Figure 6.11 and Figure 6.17.

Parameter $Phase_{5KHz}$ has been a very interesting parameter to analyze. Referring back to the results from healthy contralateral arm bicep tissue data (Figure 6.6) this parameter showed the maximum p-value of .9070 for ANOVA1 analysis, Table 5.1. Therefore this parameter showed least variation in healthy tissue. Increasing pressure also did not affect this parameter, it almost remained same. The parameter varied from around 60 to 76 degrees for all the healthy tissue data. When observed in the malignant skin study, this parameter again varied in the same range 60 to 76 degrees for almost all the healthy tissue data for five out of six subjects in the 1 Hz to 10 MHz range and three out of three in the I KHz to 1 MHz range (Figure 5.12 and Figure 5.18). Whereas; malignant tissue was either higher than 70 degrees or lower than 55 degrees with 50% sensitivity (Figure 6.12) and 100% sensitivity (Figure 6.18) in the two frequency ranges respectively.

Conclusively, R_{ext}, R_{int} and C_m are showing results as per the literature [230] with C_m showing 100% sensitivity in the 1KHz to 1MHz range, therefore the frequency to be considered in future should be 1KHz to 1MHz. Special attention needs to be paid to parameter $Phase_{5Khz}$ as it can be a very useful parameter for automated decision making looking at its p-value of .9070 and consistency in malignant skin lesion data.

Data from subject 1 and subject 2 was not very useful for analysis as the number of samples available for the 1 KHz to 1 MHz range was low. Subject 4 and Subject 6 showed data contradictory to literature [230], affecting the overall results.

Though promising results but more data needs to be collected and further decision making algorithms need to be developed based upon the discussed parameters and observations.

6.3.2. Thermal Analysis Results

EIS analysis of the malignant tissue showed that EIS data from few subjects was not useful for differentiating malignant and healthy tissue, these included subjects 1, 4 and 6. Thermal data collected from these subjects was analysed as depicted in Figure 6.19.

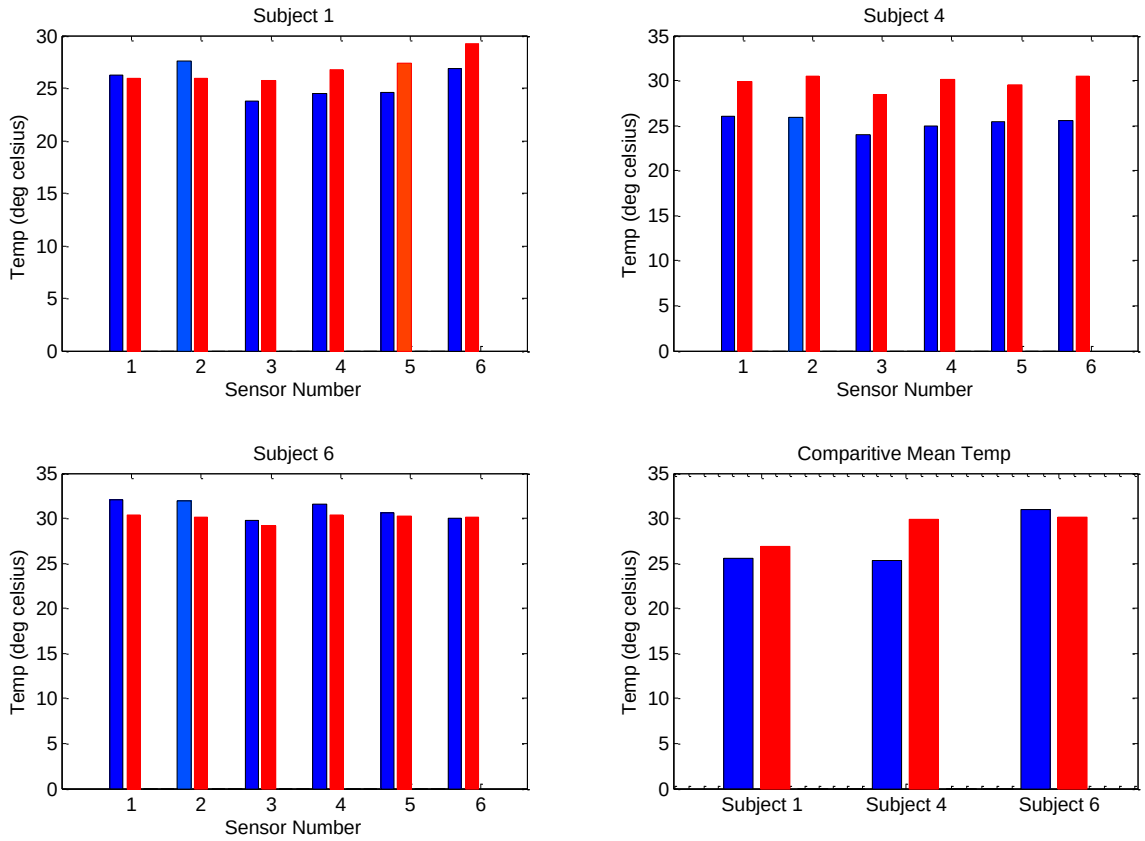

Figure 6-19 Comparative representation of malignant and collateral healthy tissue Extracellular Resistance Parameter for 6 subjects

Each subject thermal data was collected from six LWIR sensors as depicted in each subplot. In each pair of bars, left hand side bar shows healthy tissue thermal index and right side bar shows malignant tissue thermal index. Comparative Mean Temperature plot shows the mean temperature of healthy and malignant tissue of all the six sensors for the three subjects, left hand side bar showing the mean healthy tissue thermal index and right side bar showing the mean malignant tissue thermal index for each pair of bars.

Discussion and Conclusion

As observed in the comparative mean plot the thermal index of malignant tissue is higher (1-3ºC) than the thermal index of healthy tissue. However, subject 6 shows contradictory results. Thermal index is able to correctly classify with 66.6% sensitivity

malignant and healthy tissue that were not correctly classified through Electrical Impedance Spectroscopy.

6.3.3. Conclusion

Conclusively, malignant and healthy tissue can be correctly classified with a sensitivity of 75% using the multimodality approach of electrical impedance spectroscopy in frequency range from 1 KHz to 1 MHz with tissue thermal analysis. However, more data needs to be collected and further decision making algorithms need to be developed based upon the discussed parameters and observations. Even with the proposed multimodality of thermal and EIS few malignancies will remain undetected. Addition of Diffuse Optical Tomography (DOT) may be able to overcome the present deficiency.

Chapter 7.

Conclusion, Discussion and Future Work

7.1. Conclusion

Based upon the results the following conclusions are made:

- Developed hardware and software of a multimodality tool integrating EIS modality, thermal index measurement modality and tissue relative stiffness measurement modality
- Wearable force sensors' with fuzzy inference system algorithms is capable of identifying anomaly in breast phantoms with diameter more than .8cm to a depth of 6cm.
- EIS system hardware with support vector machine algorithms and data binning and data pruning technique has improved the sensitivity from 76.23% to 76.76% and specificity from 74.15% to 89.23% for classifying data obtained from healthy breast tissue.
- In phantom based study the LWIR sensor with fuzzy based algorithms is capable of detecting an anomaly that is around 2^{o}Celsius higher in temperature than the surrounding phantom material
- Malignant and Healthy tissue can be correctly classified with a sensitivity of 75% using the multimodality approach of electrical impedance spectroscopy in frequency range from 1 KHz to 1 MHz with tissue thermal analysis

7.2. Discussion and Future Work

The developed multimodality probe is capable of providing tissue electrical impedance, thermal index and relative stiffness measurement simultaneously using the developed integrated hardware and software with off shelf sensors. The probe design has been successfully used over malignant skin lesions. Few areas where the probe design requires improvement are firstly the size of the probe. The Ag/AgCl electrodes used in this design are from GRASS® instruments. These were used as they conform to

the requirements of CSA for 'protected' patient leads having no exposed metal contacts. Use of GRASS® electrodes makes the probe very safe but leads to considerably large size of the probe. The size of the probe needs to be decreased to increase its usability over small skin lesions (<2cm). To accomplish this more research needs to be focused on effect of different sizes of electrode on measured tissue electrical impedance.

The LWIR sensors Melexis MLX90615 proved to provide real time surface thermal data with good repeatability and accuracy. It was able to detect malignant tissue with 1ºC higher temperature than healthy tissue. However, these were off shelf sensors and sensor industry is growing considerably providing improved and more accurate sensors. Melexis itself is providing array based sensors that would be capable of providing better improved surface thermal data. An improvement of the design will be to consider the MLX90620 array sensor from Melexis.

The glove design is a very useful concept to be applied in clinical practice. The initial results using the fat/tumor elastic property phantoms are promising but due to the inherent size of the sensory unit, it was possible only to detect tumor mimicking phantom around $2x2x2cm^3$ at a depth of 2cm, Similarly the surface area of the force sensors is $349mm^2$, it is anticipated that smaller size custom force sensors will increase the sensitivity and specificity of the system. The developed latex based prototype glove is a good start but extensive work is required to be done to take this from a prototype stage to a commercially available commodity. The PPS finger wearable force sensors used in the glove design provide relative stiffness measurement from three fingers. The resolution of the system needs to be improved to make the glove design successful. This can be achieved using the Tactarray sensors design from PPS that has an array of 32 x32 and will lead to a much higher resolution. The *in vivo* indentation results showed the palm, forearm and biceps showed hyperelastic behaviour.

Decision based algorithms were tested over a commercially available phantom system. Training as well as testing data was acquired using the breast phantom from CIRS Model 013. The decision making algorithm were based upon Fuzzy Inference System (FIS). The results from the above tests conclude that the FIS algorithms cannot detect lumps of diameter less than 0.8 cm. The code was able to detect lumps having

diameter more than 0.8 cm up to a depth of 6 cm. Therefore, addition of FIS to the developed relative stiffness measurement hardware increased the capability of the overall system to find three times deeper (up to 6 cm deep) and half the size smaller (up to .8cm diameter) anomalies with stiffness comparable to tumors.

Market available tactile sensing systems[52] show the capability of detecting as small as 5 mm lesions under the skin surface, but as no information regarding the depth is available therefore a direct comparison is not possible.

The limitation of the anomaly stiffness measurement test up and analysis includes the assumption made in this study that breast muscle consists of homogeneous stiffness tissue. Human breast is composed of a number of tissue types (refer section 1.1.1) and in reality is a non-homogeneous mass. This limitation can be overcome only when the system is tested over in vivo human breast. Ethics application is under review in front of the FHREB to move forward with this study.

Another limitation is the use of the commercial phantom Model 013 obtained from CIRS. The application of this phantom is in biopsy training. Though the phantom is made from a proprietary gel with a physical consistency similar to human tissue, surrounded by an elastic skin-like membrane but is not specifically made for CBE training therefore the relative stiffness of the anomalies with respect to surrounding tissue is not available.

The electrical impedance spectroscopy set up when used with ANFIS based algorithms can distinguish the fat phantom from the muscle phantom, but the system was incapable of differentiating the muscle embedded in fat phantom group due to the close association of this group data to the fat phantom data. This can be attributed to the availability of small set of training data along with the low resolution of the system. Further, this classification was based upon only the real part of impedance as gelatine based phantoms does not show complex impedance characteristics as shown by biological tissue. Therefore, these results were insufficient and *in vivo* complex impedance data definitely needed to be collected for tissue classification.

SVM based classification techniques, used over data collected from healthy *in vivo* human tissue was successful in classifying breast tissue data. Data binning and

data pruning improved the sensitivity of the SVM from 76.76% to 89.23% but the specificity decreased from 76.23% to 74.15% implying that the SVM with data binning and data pruning is better at classifying positive results but more error prone at classifying negative results. Further improvement in classification is possible and required through feature extraction in *in vivo* data collected over malignant and contralateral healthy tissue, using both conventional and non-conventional parameters.

As in a glove module the tissue electrical impedance will be varied by the amount of applied pressure, study involving *in vitro* animal tissue was performed to understand the relationship between the amount of applied pressure and the associated variability in tissue electrical impedance. In this context parameter extraction from the Cole-Cole plots was done and was found that the extracellular resistance increases by 42% when 3 (lb) force was applied to the tissue and an increase of 70% was observed at the membrane capacitance, and a 28% decrease was observed in the intracellular resistance.

The limitations in validating the capability of the system to measure tissue electrical impedance were firstly the low resolution of the system, more work needs to be done to increase the number of electrodes and decrease the distance between the electrodes. Systems in direct competition to this technology, like ACT4[182], support up to 60 electrodes in two 5X6 radiolucent arrays. In other EIS systems the electrode area are as small as 1X1 mm^2 and a space of 2.5mm between adjacent electrodes. The proposed system has a much lower resolution with finger module composed of 4 Ag/AgCl electrodes, 4mm in radius, 1cm apart, in a square configuration. This limitation exists because this is a first generation prototype and the electrodes have been manually placed over the glove. Use of commercially available techniques (sputtering techniques) will be useful to further improve the resolution of the system as the impedance spectroscope is capable of multiplexing 32 signals. Electrical Impedance Tomography (EIT) can only be looked into once the required resolution of the system is obtained.

For thermal analysis of tissue, results using phantoms have been quite promising but it has been realized that there is further challenge to apply this system to biological tissue. The sensitivity of the sensor is high enough to detect the thermal variation due to

surface veins in the arm and this makes the future work challenging as the overall sensitivity of the system needs to be programmed such that surface veins in the breast tissue are not detected as anomaly. The FIS seems to be a valuable tool in overcoming this challenge, but its success depends upon large amount of training data. Ethics approval to obtain the required training data on breast cancer patients is under review.

Overall, the system shows good potential, but does lack high spatial resolution, resulting in low quality images. To be considered as equivalent to thermography; further work in image processing and sensor integration is required.

Result for contralateral healthy tissue as control show that phase at 5 KHz with a p-value of .9070, is the best parameter that can be used for further classification of healthy and malignant tissue. Phase based parameters also showed less variability with application of pressure, whereas R_{int}, R_{ext} and C_m followed a particular pattern of increase or decrease with increase in pressure level.

Analysis of malignant skin tumors with contralateral healthy tissue as control show that in frequency range 1 KHz to 1Mhz parameter R_{ext} is higher in malignant tissue compared to control, R_{int} is higher in malignant tissue compared to control and C_m is lower in malignant compared to control all being in line with literature [230]. R_{ext} shows sensitivity of 75% , R_{int} shows sensitivity of 50% and C_m shows sensitivity of 100%. Special attention needs to be paid to parameter $Phase_{5Khz}$ as it can be a very useful parameter for automated decision making looking at its p-value of .9070 and consistency in malignant skin lesion data. Though promising results but more data needs to be collected and further decision making algorithms need to be developed based upon the discussed parameters and observations.

The thermal index of malignant tissue is higher (1-3ºC) than the thermal index of healthy tissue. Thermal index is able to correctly classify malignant and healthy tissue with a sensitivity of 66.6% that were not correctly classified through Electrical Impedance Spectroscopy.

Conclusively, malignant and healthy tissue can be correctly classified with a sensitivity of 75% using the multimodality approach of electrical impedance

spectroscopy in frequency range from 1 KHz to 1 MHz with tissue thermal analysis. However, more data needs to be collected and further decision making algorithms need to be developed based upon the discussed parameters and observations. Even with the proposed multimodality of thermal and EIS few malignancies will remain undetected. Addition of Diffuse Optical Tomography (DOT) may be able to overcome the present gap.

Though the presented software is capable of depicting real time multimodality data but with envisioned hardware improvement the software will have to be modified as well. Presently available GUI is not capable of providing real time decision based upon tissue electrical impedance as multi-frequency approach is being used. Advanced algorithms need to be developed to provide real time decision based upon tissue EIS.

Future direction of the research includes improving spatial resolution, increasing the number of EIS electrodes, advancing the EIS system to EIT system and integrating DOT as well. Work in this direction has been undertaken with a publication on combining EIT with CT and DOT, with details as follows:

- Grewal,P.K., Shokoufi,M., Liu,J., Krishnan,K., and Kohli, K.S., 2014, “Electrical Characterization of Bolus material, as Phantom for use in Electrical Impedance and Computed Tomography fusion Imaging”, Journal of Electrical Bioimpedance, vol.5, pp. 34-39.
- Shokoufi, M., Grewal, P., and Golnaraghi, F., 2014, “Breast cancer Diagnosis using combined diffuse optical tomography and electrical impedance spectroscopy”, CMBEC37, May21-23, Vancouver, BC, Canada.

Another future application foreseen as in new probes that replace surgeons sense of touch [231], a multimodality approach with stress and EIS sensors is envisioned to be quite beneficial to surgeons in this context.

7.3. Accomplishments

So far the outcomes from the research have been presented in various posters, conferences and journals as listed below:

1. Grewal, P., De Vaz, D., and Golnaraghi, F., 2010, “Quantifying Radiation Induced Skin Reaction using Skin Parameters Quantification Sensor Probe and 3-D Stereo Imaging Technique for Minimization of Position Uncertainty”, Proceedings of 33rd Conference of the Canadian Medical and Biological Engineering Society, June 15-18, Vancouver, BC, Canada.
2. Grewal, P., Mansour, H., Arzanpour, S., and Golnaraghi, F., 2010, “A comparative study to measure audible release (Crepitus) from Human Joints”, Proceedings of ASME International Mechanical Engineering Congress and Expositions IMECE2010, Nov 12- 18, Vancouver, BC, Canada.
3. Grewal, P. K., Viswanath, K.S., and Golnaraghi, F., 4-6July 2013, “Minimization of position uncertainty using 3-D stereo imaging technique for the real-time positioning of a handheld breast tissue anomaly detection probe”, Computing, Communications and Networking Technologies (ICCCNT), 2013, Fourth International Conference on, 4-6July,1-6, Tiruchengode, India.
4. Golnaraghi, F., Grewal, P.K., Abdi, B., Shoukoufi, M, M., Moqadam, S., Zaeimdar, S., 2013, “Breast Cancer Early Detection”, Innovation Boulevard, 14 November, Surrey.
5. Grewal,P.K., Shokoufi,M., Liu,J., Krishnan,K., and Kohli, K.S., 2014, “Electrical Characterization of Bolus material, as Phantom for use in Electrical Impedance and Computed Tomography fusion Imaging”, Journal of Electrical Bioimpedance, vol.5, pp. 34-39.
6. Grewal,P.K., Golnaraghi, F., 2014, “ Pilot Study: Electrical Impedance based Tissue Classification using SVM Classifier” , IET Science, Measurement and Technology (Accepted)
7. Shokoufi, M., Grewal, P., and Golnaraghi, F., 2014, “Breast cancer Diagnosis using combined diffuse optical tomography and electrical impedance spectroscopy”, CMBEC37, May21-23, Vancouver, BC, Canada.
8. Moqadam, S., Grewal, P., and Golnaraghi, F., 2014, “Effect of Compression over electrical admittance of chicken breast and rat breast”, CMBEC37, May21-23, Vancouver, BC, Canada.

References

[1] P. H. A. of C. Canadian Cancer Society, Statistics Canada, “Canadian Cancer Statistics 2013,” 2013.

[2] J. Ferlay, H. Shin, F. Bray, D. Forman, C. Mathers, and D. Parkin, “‘Estimates of worldwide burden of cancer in 2008: GLOBOCAN 2008,,’” *Int J Cancer*, 2010.

[3] “Canadian Breast Cancer Foundation.”

[4] R. L. A. . K. C. . E. B. . H. B. . Miller B.A, “SEER cancer statistis reveiw 1973 - 1996,” *Tech. Rep. Natl. Cancer Intitute, Bethesda*, 1999.

[5] A. M. R. Agur, A. F. Dalley, and W. Kluwer, *Atlas of Anatomy*, 12th ed. 2009.

[6] D. C. Pamplona and C. D. A. Alvim, “Breast reconstruction with expanders and implants: a numerical analysis,” *Artif. Organs*, vol. 8, pp. 353–356, 2004.

[7] J. . Grassley, “Breast reduction surgery, What every women needs to know,” *Lifelines*, vol. 6, pp. 244–249, 2002.

[8] L. ; Tabar and P. Dean, “A new era in the diagnosis and treatment of breast cancer,” *J. Breast*, vol. 16, pp. S2–S4, 2010.

[9] L. Tabar, C. Fagerberg, A. Gad, L. Baldetorp, and E. Al, “Reduction in mortality from breast cancer after mass screening with mammography: Randomised trial from the Breast Cancer Screening Working Group of the Swedish Nation Board of Health and Welfare,” *Lancet*, vol. 325, pp. 829–832.

[10] B.Hellquist, S. Duffy, S.Abdsaleh, L. Bjorneld, L. P. Bordas, B. Tabar, S. Vitak, Zackrisson, L. Nystrom, and H. Jonsson, “Effectiveness of population-based service screening with mammography for women 40 to 49 years: Evaluation of the Swedish mammography Screening in Young Women (SCRY) cohort,” *Cancer*, vol. 117, no. 4, pp. 714–722, 2011.

[11] S. . Fletcher, W. Black, R. Harris, B. . Rimer, and S. Shapiro, “Report of the International Workshop on Screening for Breast Cance,” *J. Natl. Cancer Inst.*, vol. 85, pp. 1644 – 1656, 1993.

[12] M. Brown, F. Houn, E. Sickles, and L. Kessler, “Screening mammography in community practice,” *AJR, Am. J. Roentgenol*, vol. 165, pp. 1373 – 1377, 1995.

[13] P. Huynh, A. Jarolimek, and S.Daye, “The false-negative mammogram,” *Radiographics*, vol. 18, pp. 1137–1154, 1998.

[14] A. Howell, “The emerging breast cancer epidemic : early diagnosis and treatment Early detection,” vol. 12, no. Suppl 4, pp. 11–13, 2010.

[15] T. Rastogi, A. Hildesheim, and R. Sinha, “Oppurtunities for cancer epidemiology in developing countries,” *Nat Rev Cancer*, vol. 4, pp. 909– 917, 2004.

[16] M. Kalager, M. Zelen, F. Langmark, and H. Adami, “Effect of screening mammography on breast – cancer mortality in Norway,” *New Engl. J. Med.*, vol. 363, no. 13, pp. 1203–1210.

[17] A. B. de Gonzalez and S. Darby, “Risk of cancer from diagnostic X-rays: Estimates for the U.K. and 14 other countries,” *Lancet*, vol. 363, pp. 345–351.

[18] C. Ronckers, C. Erdmann, and C. Land, “Radiation and breast cancer: A review of current evidence,” *Breast Cancer Res.*, vol. 7, no. 1, pp. 21–32.

[19] W. a Berg, L.Guitierrez, M. NessAiver, W. Carter, M. Bhargavan, R. Lewis, and O. Loffe, “Diagnostic Accuracy of Mammography, Clinical Examination, US, MR Imaging in Preoperative Assessment of Breast Cancer,” *Breast Imaging*, vol. 233, no. 3, 2004.

[20] P. Porter, A. Bastawissi, M. Mandelson, M. Lin, N. Khalid, E. Watney, L. Cousens, D. White, S. Taplin, and E. White, “Breast Tumor Characteristics as Predictors of Mammographic Detection: Comparison of Interval and Screen Detected Cancers,” *J. Natl. Cancer Inst.*, vol. 91, no. 23, 1999.

[21] J. . Elmore and E. Al, “Ten-year risk of false- positive screening mammograms and clinical breast examinations,” *N Engl J Med.*, vol. 338, pp. 1089–1096, 1998.

[22] W. Goodson, “Clinical Breast Examination,” *West J Med.*, vol. 164, no. 4, pp. 355–358, 1996.

[23] “American Cancer Society (ACS). ACS guidelines for the early detection of cancer. American Cancer Society.”

[24] A. C. Society, “American Cancer Society recommendations for early breast cancer detection in women without breast.” [Online]. Available: http://www.cancer.org/Cancer/BreastCancer/MoreInformation/BreastCancerEarlyDetection/breast-cancer-early-detection-acs-recs.]. .

[25] C. . Baines, “Physical examination of the breasts in screening for breast cancer,” *J. Gerontol*, vol. 47, pp. 63–67, 1992.

[26] C. Ahern and Y. Shen, “Cost-effectiveness analysis of mammography and clinical breast examination strategies,” *Cancer Epidemiol Biomarkers*, vol. 18, no. 3, pp. 718–725, 2009.

[27] S. McDonald, D. Saslow, and M. H. Alciati, “Performance and reporting of Clinical Breast Examiantion: a review of the Literature,” *CA cancer J Clin*, vol. 54, pp. 345–361, 2004.

[28] S. W. Fletcher, M. S. O’Malley, and L. a Bunce, “Physicians’ abilities to detect lumps in silicone breast models.,” *JAMA*, vol. 253, no. 15, pp. 2224–8, Apr. 1985.

[29] J. Michaelson, S. Satija, R. Moore, G. Weber, E. Halpern, A. Garland, D. Kopans, and K. Highes, “Estimates of the sizes at which Breast Cancers Become Detectable on Mammographic and Clinical Grounds,” *J. Women’s Imaging*, vol. 5, no. 1, pp. 3–10, 2003.

[30] K. Flobbe, “The role of ultrasonography as an adjunct to mammography in the detetction of breast cancer, a systematic review,” *Eur J Cancer*, vol. 38, no. 8, pp. 1044–50, 2002.

[31] C. A. for D. and T. in Health, “InquiryService, Health Technology. Ultrasound for Breast Cancer Screening: Clinical Effectiveness.,” 2008.

[32] W. Berg, L.Guitierrez, M. NessAiver, W. Carter, M. Bhargavan, R. Lewis, and O. Ioffe, “Diagnostic accuracy of mammography, clinical examination, U.S., and MR imaging in preoperative assessment of breast cancer,” *Radiology*, vol. 233, pp. 830–849.

[33] D. Ikeda, D. Baker, and B. Daniel, “Magnetic resonance imaging of breast cancer: Clinical indications and breast MRI reporting system,” *J. Magnet. Reson. Imag*, vol. 12, pp. 975–983, 2000.

[34] S. Orel and M. Schnall, “MR imaging of the breast for the detection, diagnosis, and staging of breast cancer,” *Radiology*, vol. 220, no. 1, pp. 13–30, 2001.

[35] K. Kerlikowske, D. Grady, J. Barclay, E. Sickles, and V. Ernster, “Effect of age, breast density, and family history on the sensitivity of first screening mammography,” *J Am Med Assoc*, vol. 276, pp. 33–38, 1996.

[36] A. M. Hassan, S. Member, M. El-shenawee, and S. Member, “Review of Electromagnetic Techniques for Breast Cancer Detection,” *IEEE Rev. Biomed. Eng.*, vol. 4, pp. 103–118, 2011.

[37] R. Siegel, E. Ward, O.Brawley, and A. Jemal, “Cancer Statistics, 2011: The impact of eliminating socioeconomic and racial disparities on pre-mature cancer deaths,” *CA Cancer J. Clin’*, vol. 61, no. 4, pp. 212–236, 2011.

[38] R. Siegel, D. Naishadham, and A. Jemal, “Cancer Statistics , 2013,” *A Cancer J. Clin.*, vol. 63, no. 1, pp. 11–30, 2013.

[39] H. Igene, “Global health inequalities and breast cancer: an impending public health problem for developing countries,” *Breast J*, vol. 14, pp. 428–434, 2008.

[40] D. Berry, K. Cronin, S. Plevritis, D. Fryback, L. Clarke, M. Zelen, J. Mandelblatt, A. Yakovlev, J. Habbema, and E. Feuer, “Effect of screening and adjuvant therapy on mortality from breast cancer,” *N Engl J Med*, vol. 353, pp. 1784–1792, 2005.

[41] R. Mead, “The Design of Experiments,” *Cambridge Cambridge Univ. Press*, 1988.

[42] B. Weigelt and J. S. Reis-Filho, “Histological and molecular types of breast cancer:is there a unifying taxonomy?,” *Nat. Rev. Clin. Oncol.*, vol. 6, pp. 718–730, 2009.

[43] G. Arpino, V. Bardou, G. . Clark, and R. . . Elledge, “Infiltrating lobular carcinoma of the breast: tumor characteristics and clinical outcome,” *Breast Cancer Res.*, vol. 6, pp. R149–R156, 2004.

[44] K. N. Krecke and J. J. Gisvold, “Invasive Lobular carcinoma of the breast: mammographic findings and extent of disease at diagnosis in 184 patients,” *Am. J. Roentgenol.*, vol. 161, pp. 957–960, 1993.

[45] K. . Mathis, T. . Hoskin, J. . Boughey, B. . Crownhart, K. R. Brandt, C. M. Vachon, C. . Grant, and A. . Degnim, “Palpable presentation of breast cancer persists in the era of screening mammography.,” *J Am Coll Surg.*, vol. 210, no. 3, pp. 314–8, 2010.

[46] “Physicians Insurers Association of America.” .

[47] J. . Bobo, N. . Lee, and S. F. Thanmes, “Findings from 752,081 clinical breast examinations reported to a national screening program from 1995 through 1998,” *J Natl Cancer Inst*, vol. 92, pp. 971–976, 2000.

[48] N. Oestreicher, “Predictors of sensitivity of clinical breast examination (CBE),” *Breast Cancer Res Treat*, vol. 76, pp. 73–81, 2002.

[49] T. Kolb, J. Lichy, and J. Newhouse, “Comparison of the performance of screening mammography, physical examination, and breast US and evaluation of factors that influence them; an analysis of 27,825 patient evaluations.”

[50] M. B. Barton and R. Harris, “Does This Patient Have Breast Cancer ? The Screening Clinical Breast Examination : Should It Be Done ? How ?,” 1999.

[51] H. Campbell and E. Al., “Improving physicians’ and nurses' clinical breast examination: a randomized controlled trial.,” *Am J Prev Med*, vol. 7, pp. 1 –8.

[52] P. P. Systems., “SureTouch.” [Online]. Available: Aug 2011. http://www.pressureprofile.com/case-study-mti.php.

[53] D. Li, P. M. Meaney, T. D. Tosteson, S. Jiang, T. E. Kerner, T. O. McBride, B. W. Pogue, A. Hartov, and K. D. Paulsen, “Comparisons of three alternative breast modalities in a common phantom imaging experiment,” *Med. Phys.*, vol. 30, no. 8, p. 2194, 2003.

[54] A. Stojadinovic, A. Nissan, Z. Gallimidi, S. Lenington, and W. Logan, “Electrical Impedance Scanning for the early detection of Breast Cancer in young Women:Preliminary Results of a Multicenter Prospective Clinical Trial,” *J. Clin. Oncol.*, vol. 23, no. 12, pp. 2703–2715, 2005.

[55] R. . Davies, “Diagnosis of Breast Cancer using Ductal Epethelial Impedance Spectroscopy,” in *IFMBE, 13th International Conference on Electrical Bio-impedance & 8th Conference on Electrical Impedance Tomography*, 2007, pp. 633–635.

[56] D. a Kennedy, T. Lee, and D. Seely, “A comparative review of thermography as a breast cancer screening technique.,” *Integr. Cancer Ther.*, vol. 8, no. 1, pp. 9–16, Mar. 2009.

[57] C. Song, V. Appleyard, K. Murray, T. Frank, W. Sibbett, A. Cuschieri, and A. Thompson, “Thermographic assessment of tumor growth in mouse xenografts.,” *Int. J. cancer*, vol. 121, no. 5, pp. 1055–8, Sep. 2007.

[58] X. Tang, H. Ding, Y. Yuan, and Q. Wang, “Morphological measurement of localized temperature increase amplitudes in breast infrared thermograms and its clinical application,” *Biomed. Signal Process. Control*, vol. 3, no. 4, pp. 312–318, Oct. 2008.

[59] N. M. Sudharsan, E. Y. K. Ng, and S. L. Teh, “Surface Temperature Distribution of a Breast with and without tumour,” *Comput. Methods Biomech. Biomed. Engin.*, vol. 2, no. 3, pp. 187–199, 1999.

[60] Y. Ohashi and I. Uchida, “Applying Dynamic Thermography in the Diagnosis of Breast Cancer Techniques for Improving Sensitivity of Breast Thermography,” *IEEE Eng. Med. Biol.*, vol. 19, no. June, pp. 42–51, 2000.

[61] “U.S. Food and Drug Administration,” 2011. .

[62] J. R. Keyserlingk, P. D. Ahlgren, E. Yu, and N. Belliveau, “Infrared Imaging of the Breast:Initial Reappraisal Using High-Resolution Digital Technology in 100 Succesive Cases of Stage I and II Breast Cancer,” *Breast J.*, vol. 4, no. 4, pp. 245–51, 1998.

[63] N. Arora, D. Martins, D. Ruggerio, E. Tousimis, A. J. Swistel, M. P. Osborne, and R. M. Simmons, “Effectiveness of a noninvasive digital infrared thermal imaging system in the detection of breast cancer,” *Am. J. Surg.*, vol. 196, no. 4, pp. 523–6, Oct. 2008.

[64] Y. A. Tkachenko, J. P. Potekhina, M. V. Golovanova, R. A. Plokhov, I. E. Davydov, and D. A. Golovachev, “Smart Thermometer Technology for Detection and Monitoring of More than 100 Diseases at Home,” *Mod. Instrum.*, vol. 3, pp. 1–7, 2014.

[65] “Zurich Instruments.” [Online]. Available: http://www.zhinst.com/products/hf2is.

[66] “Zurich Instruments Amplifiers.” [Online]. Available: http://www.zhinst.com/products/hf2preamps/hf2ta.

[67] “Melexis.” [Online]. Available: http://www.melexis.com/Infrared-Thermometer-Sensors/Infrared-Thermometer-Sensors/Digital-plug--play-infrared-thermometer-in-an-ultra-small-TO-can-685.aspx.

[68] J. S.-M. Francisco, C.-C. Sergio, and V.-M. Carlos, “Novel approach to assess the emissivity of the human skin,” *J. Biomed. Opt.*, vol. 14, 2009.

[69] D. J. Watmough and R. Oliver, “Emissivity of Human Skin in the Waveband between 2μ and 6μ,” *Nature*, vol. 219, no. 5154, pp. 622–624, 1968.

[70] “Honeywell FS03.” [Online]. Available: http://sensing.honeywell.com/index.cfm?ci_id=154286&la_id=1&Ne=3025&sid=132D09EF1C8B&ci_id=154325&N=3475&la_id=1.

[71] C. Marchal, M. Nadi, A. . Tosser, C. Roussey, and M. . Gaulard, “Dielectric properties of gelatine phantoms used for simulations of biological tissues between 10 and 50 MHz,” *Int J Hyperth.*, vol. 5, no. 6, pp. 725–32, 1989.

[72] M. P. Robinson, M. J. Richardson, J. L. Green, and a W. Preece, “New materials for dielectric simulation of tissues.,” *Phys. Med. Biol.*, vol. 36, no. 12, pp. 1565–71, Dec. 1991.

[73] M. A. Stuchly and S. . Stuchly, “Dielectric properties of biological substances-tabulated,” *J.Microwave Power*, vol. 15, pp. 19–26, 1980.

[74] S. Jenkins, R. N. Clarke, M. Horrocks, and A. . Preece, “Dielectric measurements on human tissue between 100 Mhz and 3 GHz,” in *EAT Microwave Group*, 1989.

[75] I. Rosenthal, “Uber die specifiche Warme thierische Grewebe Archiv.,” *Anat. Physiol.*, pp. 215–7, 1878.

[76] M. Rubner, “Der Kalorimetrie Handbuch der Physiologischen Methodik ed r Tigerstedt (Leipzig: Hirsel),” vol. 3, pp. 168–72, 1911.

[77] F. C. Henriques and A. Moritz, “Studies of thermal injury. The conduction of heat to and throught he skin and the temperatures attained therein,” *Am J. Pathol.*, vol. 23, pp. 531–49, 1947.

[78] “Pressure Profile Systems-FingerTPS.” [Online]. Available: http://www.pressureprofile.com/case-study-touch.php.

[79] A. . Fischer, “Pressure algometry over normal muscles. standard values, validity and reproducibility of pressure threshold,” *Pain*, pp. 115–26.

[80] W. . Hayes, L. . Keer, G. Hermann, and L. . Mockros, “A mathematical analysis for indentation test of articular cartilage,” *J. Biomech.*, vol. 5, pp. 541–551, 1972.

[81] A. M. Galea, “Mapping tactile imaging information: Parameter estimation and deformable registration,” Harvard University,Cambridge, MA, USA, 2004, 2004.

[82] M. Hosseini, “Detection of tumours using a computational tactile sensing approach †,” no. October, pp. 333–340, 2006.

[83] P. Dario, M. Bergamasco, and A. Sabatini, “Sensing body structures by an advanced robot system,” *Proc. IEEE ICRA*, vol. 3, pp. 1758–63, 1988.

[84] E. Frei, B. Sollish, and S. Yerushalmi, “No Title,” U.S. Patent # 4,250,894, 1981.

[85] C. R. Gentle, “Mammobarography: a possible method of mass breast screening,” *J . Biomed. Eng.*, vol. 10.

[86] K. Koganezawa, A. Takanishi, and S. eds Sugano, *Development of Waseda Robot: The study of Biomechanisms and Kato Laboratory*, 3rd ed. Waseda University, 1991.

[87] A. . Mahmoud, O. . Mukdadi, B. Teng, and S. . Mustafa, “No Title,” in *Biomedical Engineering (MECBME), 2011 1st Middle East Conference*.

[88] F. Imania, “Tissue classification using depth-dependent ultrasound time series analysis: In vitro animal study,” in *Proc. of SPIE*, 2011.

[89] F. L. Greenebaum, M. Feleppa, E. J. Elbaum, and D. J. Coleman, “Theoretical framework for spectrum analysis in ultrasonic tissue characterization,” *J. Acoust. Soc. Am.*, vol. 73, pp. 1366–1373, 1983.

[90] P. David, M. Collet, and J.-M. Cote, “Experimental implementation of acoustic impedance control by a 2D network of distributed smart cells,” *Smart Mater. Struct.*, vol. 19, no. 3, p. 035028, Mar. 2010.

[91] V. Jalkanen, “Hand-held resonance sensor for tissue stiffness measurements- a theoretical and experimental analysis,” *Meas. Sci. Technol.*, vol. 21, 2010.

[92] S. Moromugi, “A sensor to measure hardness of tissue,” in *Sensors,5th IEEE Conference*, 2006, pp. 388–391.

[93] A. M. . Fath El Bab, “New compensation technique for the soft tisuue stiffness measurement using two sensor probes configuration,” in *Procedia Engineering 5*, 2010, pp. 1304–1307.

[94] A. . Darling, P. K. Yalavarthy, M. . Doyley, and H. Dehghani, “Interstitial fluid pressure in soft tissue as a result of an externally applied contact pressure,” *Phys. Med. Biol.*, vol. 52, pp. 4121–4136, 2007.

[95] H. Mohsen, S. Najarian, S. Motaghinasab, and J. Dargahi, “Detection of Tumors using a computational tactile sensing approach,” *Int. J. Med. Robot. Comput. Assist. Surg.*, vol. 2, pp. 333–340, 2006.

[96] A. Sarvazyan, A. Skovoroda, S. Emelianov, J. Fowlkes, J. Pipe, R. Adler, R. Buxton, and P. Carson, “Biophysical Bases of Elasticity Imaging,” *Acoust. Imaging*, vol. 21, p. 1995.

[97] A. Sarvazyan, A. Skovoroda, and Y. Pyt’ev, “Mechanical Introscopy-A New Modality of Medical Imaging for Detection of Breast and Prostate Cancer,” in *Eighth IEEE Symposium on Computer Based Medical Systems*.

[98] Y. Zhang, Y. Mukaibo, and T. Maeno, “A Multi-Purpose Tactile Sensor Inspired by Human Finger for Texture and Tissue Stiffness Detection,” *2006 IEEE Int. Conf. Robot. Biomimetics*, pp. 159–164, 2006.

[99] P. S. Wellman and R. D. Howe, “Extracting Features from Tactile Maps,” pp. 1133–1142, 1999.

[100] A. M. Galea and R. D. Howe, “Mammography Registered Tactile Imaging,” pp. 183–193, 2003.

[101] N. Rao, J. Dargahi, M. Kahrizi, and S. Prasad, “Design and fabrication of a microtactile sensor,” in *Canadian Conference on Electrical and Computer Engineering: Towards a Caring and Human Technology*, 2003.

[102] J. Dargahi and S. Najarian, “Human tactile perception as a standard for artificial tactile sensing,” *A Rev. Int J Med Robot Comput Assist Surg*, vol. 1, no. 13, pp. 23–35, 2004.

[103] J. Dargahi and S. Najarian, “Advances in tactile sensors design/manufacturing and its impact on robotics application.,” *A Rev. Indus Robot*, vol. 32, no. 3, pp. 268–281, 2005.

[104] H. Rininsland, “Basics of robotics and manipulators in endoscopic surgery,” *Endosc. Surg Allied Technol*, vol. 1, pp. 154–159, 1993.

[105] P. S. Wellman, R. D. Howe, E. Dalton, and K. A. Kern, “Breast Tissue Stiffness in Compression is Correlated to Histological Diagnosis,” pp. 1–15.

[106] G. Weber, “Using tactile images to differentiate breast cancer types,” Harvard University, Cambridge, MA, USA.

[107] Y. Fung, “Mechanical Properties of Living Tissues,” in *Biomechanics*, 2nd ed., Springer Verlag, 1993.

[108] “Mechanics of the normal woman’s breast,” *Technol. Heal. Care*, vol. 15, pp. 259–271, 2007.

[109] J. J. . Hagan and A. Samani, “Measurement of the hyperelastic properties of 44 pathological ex vivo breast tissue samples,” *Phys. Med. Biol.*, vol. 54, no. 8, p. 2557, 2009.

[110] A. Skovoroda, A. Klishko, D. Gusakyan, Y. Mayevskii, V. Yermilova, G. Oranskaya, and A. Sarvazyan, “Quantitative Analysis of the Mechanical Characteristics of Pathological Changed Soft Biological Tissues,” *Biophysics (Oxf).*, vol. 40, no. 6, pp. 1359–1364, 1995.

[111] P. Wellman and R. Howe, “The mechanical properties of breast tissue in compression,” Harvard BioRobotics Laboratory, Cambridge, MA, USA, 1999.

[112] “CIRS phantom MODEL 013.” [Online]. Available: http://www.cirsinc.com/products/all/44/stereotactic-needle-biopsy-training-phantom/.

[113] S. Zaeimdar, “Mechanical Characterization of Breast Tissue Constituents for Cancer Assessment,” Simon Fraser University, 2014.

[114] T. a Hope and S. E. Iles, “Technology review: the use of electrical impedance scanning in the detection of breast cancer.,” *Breast Cancer Res.*, vol. 6, no. 2, pp. 69–74, Jan. 2004.

[115] P. Mohr, U. Birgersson, C. Berking, C. Henderson, U. Trefzer, L. Kemeny, C. Sunderkötter, T. Dirschka, R. Motley, M. Frohm-Nilsson, U. Reinhold, C. Loquai, R. Braun, F. Nyberg, and J. Paoli, “Electrical impedance spectroscopy as a potential adjunct diagnostic tool for cutaneous melanoma.,” *Skin Res. Technol.*, vol. 19, no. 2, pp. 75–83, May 2013.

[116] H. Fricke and S. Morse, “The electric capacity of tumors in the breast,” *J Cancer Res*, vol. 16, pp. 340–376, 1926.

[117] A. Surowiec, S. Stuchly, R. Barr, and A. Swarup, “Dielectric properties of breast caricinoma and the surrounding tissues,” *IEEE Trans Biomed Eng*, vol. 35, pp. 257–263, 1988.

[118] J. Jossinet, “My IOPscience The impedivity of freshly excised human breast tissue,” vol. 61, 1998.

[119] B. Singh, C. . Smith, and R. Hughes, “In Vivo dielectric spectrometer,” *Med. Biol. Eng .& Comput.*, vol. Vol. 17, pp. 045–060, 1979.

[120] J. Jossinet, “Variability of impedivity in normal and pathological breast tissue.,” *Med. Biol. Eng. Comput.*, vol. 34, pp. 346–350, 1996.

[121] J. Jossinet, “The Impeditivity in normal and pathological breast tissue,” *Physiol. Meas.*, vol. 19, pp. 61–75, 1998.

[122] T. Morimoto, “Measurement of the Electrical Bio-Impedance of Breast Tumors.,” *Eur. Surg. res.*, vol. 22, pp. 86–92, 1990.

[123] T. Morimoto, “Study of the Electrical Bioimpedance of tumors,” *J. Investig. Surg*, vol. 6, pp. 25–104, 1993.

[124] N. Mitsuyama, T. Morimoto, Y. Kinouchi, T. Iritani, T. Sumi, S. Kimura, and Y. Monden, “In Vivo measurements of electrical bio-impedance of breast tumors,” *Nippon Geka Gakkai Zasshi*, vol. 89, pp. 251–255, 1988.

[125] B. Scholz and R. Anderson, “On Electrical Impedance Scanning –,” pp. 35–44, 2000.

[126] M. Assenheimer, O. Laver-moskovitz, D. Malonek, D. Manor, U. Nahaliel, R. Nitzan, and A. Saad, “The T-SCAN TM technology : electrical impedance as a,” vol. 1, 2001.

[127] Y. A. Glichman, O. Filo, U. Nachaliel, S. Lnington, S. Amin-Spector, and R. Ginor, “Novel EIS postprocessing algorithm for breast cancer diagnosis,” *IEEE Trans. Med. Imaging*, vol. 21, pp. 710–12, 2002.

[128] J. K. Seo, O. Kwon, H. Ammari, and E. . Woo, “A mathematical model for breast cancer lesion estimation: electrical impedance technique using TS2000 commercial system,” *IEEE Trans. Biomed.Eng.*, vol. 51, pp. 1898–906, 2004.

[129] T. Diebold, V. Jacobi, B. Scholz, C. Hensel, C. Solbach, M. Kaufmann, F. Vianna, J. Balzer, J. Peters, and T. Vogl, “Value of electrical Impedance Scanning (EIS) in the evaluation of BI-RADSTM III/IV/V- lesions,” *Technol. Cancer Res. Treat.*, vol. 4, pp. 1–5, 2005.

[130] “Transcan T-Scan 2000 Gets Panel Nod As Mammography Adjunct.,” *Gray Sheet*, vol. 24, no. 34, pp. 5–6, 1998.

[131] C. K. Latgé and M. N. Souza, “Report Documentation Page,” pp. 1–4.

[132] “An adaptive current tomography for breast cancer detection,” Rennsselaer polytechnic Institute,Troy, NY, USA, 2003.

[133] N. Liu, G. J. Saulnier, J. C. Newell, D. Isaacson, and T. . Kao, “ACT4: A high precision, multi frequency electrical impedance tomography,” in *Proc. 6th Conf. On Biomedical Appl. Electrical Impedance Tomography*.

[134] B. . Brown and D. . Barber, “Applied potential tomography- A new in vivo medical imaging technique,” in *In Porceedings of Hospital Physicists’ Association, Annual Conference,*, 1982.

[135] R. . Kohn and M. Vogelius, “Determining the conductivity by boundary measurement,” *Commun.Pure Appl. Math.*, vol. 37, p. 289, 1984.

[136] R. . Kohn and M. Vogelius, “Identification of an unknown conductivity by means of the boundary,” in *SIAM-AMS Proc. 14:113*, 1984.

[137] J. Sylvester and G. Uhlmann, “A uniqueness theorem for an inverse boundary value problem in electrical prospection,” *Commmun Pure Appl. Math*, vol. 39, no. 91, 1986.

[138] K. . Foster and H. Schwan, “Dielectric Properties of Tissues and Biological Materials: A Critical Review’,” *Crit. Rev. Biomed. Eng.*, vol. 17, no. 1, pp. 25–104, 1989.

[139] M. . Stuchly and S. S. Stuchly, “Electrical Properties of Biological Substances,” in *Biological Effects and Medical Applications of Electromagnetic Energy*, O. P. Gandhi, Ed. .

[140] J. . Morucci, “Bioelectrical Impedance Techniques in Medicine,” *Crit. Rev. Biomed. Eng.*, vol. 24, p. 275, 1996.

[141] M. Analoui, D. Joseph, Bronzino, Rp. Donald, N. Huber, W. Wang, and D. . Barber, *Medical Imaging, Principles and Practices,*. CRC Press, 2012.

[142] H. Fricke, “The electrical capacity of suspensions with special reference to blood,” *J. Gen. Physiol.*, vol. 9, pp. 137–152, 1925.

[143] J. Jossinet, “Variability of impedivity in normal and pathological breast tissue.,” *Med. Biol. Eng. Comput.*, vol. 34, pp. 346–350, 1996.

[144] T. Morimoto, “Measurement of the Electrical Bio-Impedance of Breast Tumors.,” *Eur. Surg. res.*, vol. 22, pp. 86–92, 1990.

[145] J. Heinitz and O. Minet, “Dielectric properties of female breast tumors,” in *Proc 9th Int. Conf. On Electrical Bioimpedance*, 1995, pp. 356–9.

[146] A. Surowiec, S. Stuchly, R. Barr, and A. Swarup, “Dielectric properties of breast caricinoma and the surrounding tissues,” *IEEE Trans Biomed Eng*, vol. 35, pp. 257–263, 1988.

[147] *Atlas of Diseases of the Breast*. 1979, pp. 95–103.

[148] T. Morimoto and E. Al, “Study of the Electrical Bioimpedance of tumors,” *J. Investig. Surg.,*, vol. 6, pp. 25–104, 1993.

[149] A. M. Campbell and D. V Land, “Dielectric properties of female breast tissue measured in vitro at 3.2 Ghz,” *Phys. Med. Biol.*, vol. 37, pp. 193–210, 1992.

[150] R. Pethig, “Dielectric properties of biological materials: biophysical and medical applications,” in *IEEE Trans. Elect. Insul.*, 1984, pp. 453–74.

[151] J. Heinitz and O. Minet, “Dielectric properties of female breast tumors,” in *Proc 9th Int. Conf. On Electrical Bioimpedance*, 1995, pp. 356–9.

[152] K. . Cole and R. . Cole, “Dispersion and absorption in dielectrics,” *J. Chem. Phys.*, vol. 9, pp. 341–351, 1941.

[153] E. . McAdams and J. Jossinet, “Tissue impedance: A historical overview,” *Physiol. Meas.*, vol. 16, pp. A1–A13, 1995.

[154] H. Fricke and S. Morse, “The electric capacity of tumors in the breast,” *J Cancer Res*, vol. 16, pp. 340–376, 1926.

[155] H. . Schwan, “Electrical properties of tissue and cell suspensions,” *Adv. Biol. Med. Phys.*, vol. 5, pp. 147–207, 1957.

[156] K. . Cole, “Membranes, Ions and Impulses: A Chapter of Classical Biophysics,” Berkley, CA: University of California Press, 1968, pp. 6–102.

[157] D. A. McRae and M. A. Esrick, “Deconvolved electrical impedance spectra track distinct cell morphology changes.,” *IEEE trans. BME*, vol. 43, pp. 607–618, 1996.

[158] J. R. Macdonald, “Impedance Spectroscopy,” *Ann.Biomed. Eng.*, vol. 20, pp. 289–305, 1992.

[159] C. Aligne, N. Chauveau, B. Riguard, and J. . Morucci, “Normal and tumoral tissue modelling from in vivo spectrometric measurements of electrical bioimpedance,” *ITBM Themat.*, no. 16, pp. 689–693, 1995.

[160] J. Jossinet and M. Schmitt, “A review of Parameters for the Bioelectrical characterization of Breast tissue,” *Inser. U281*, vol. 69424 Lyon.

[161] J. E. da Silva, J. P. de Sá, and J. Jossinet, “Classification of breast tissue by electrical impedance spectroscopy.,” *Med. Biol. Eng. Comput.*, vol. 38, no. 1, pp. 26–30, Jan. 2000.

[162] Swain, “The decision tree classifier: design and potential,” *IEEE Trans. Geosci. Electron.*, vol. GE-15, pp. 142–147, 1977.

[163] R. Liu, X. Dong, F. Fu, F. You, X. Shi, Z. Ji, and K. Wang, “Multi-frequency parameter mapping of electrical impedance scanning using two kinds of circuit model.,” *Physiol. Meas.*, vol. 28, no. 7, pp. S85–100, Jul. 2007.

[164] B. S. Kim, D. Isaacson, H. Xia, T.-J. Kao, J. C. Newell, and G. J. Saulnier, “A method for analyzing electrical impedance spectroscopy data from breast cancer patients.,” *Physiol. Meas.*, vol. 28, no. 7, pp. S237–46, Jul. 2007.

[165] J. Jossinet, “The Impeditivity in normal and pathological breast tissue,” *Physiol. Meas.*, vol. 19, pp. 61–75, 1998.

[166] D. McGivney, D. Calvetti, and E. Somersalo, “Quantitative imaging with electrical impedance spectroscopy’,” *Phys Med Biol.*, vol. 57, no. 22, pp. 7289–7302, 2012.

[167] V. . Vapnik, *The nature of statistical learning theory’*. .

[168] M. A. Shini, S. Laufer, and B. Rubinsky, “SVM for prostate cancer using electrical impedance measurements,” *Physiol. Meas.*, vol. 32, no. 9, p. 1373, 2011.

[169] S. Laufer and B. Rubinsky, “Tissue Characterization with an Electrical Spectroscopy SVM Classifier’,” *Biomed. Eng.IEEE Trans.,*, vol. 56, no. 2, pp. 525–528, 2009.

[170] D. Gur, B. Zheng, D. Lederman, S. Dhurjaty, J. Sumkin, and M. Zuley, “A support vector machine designed to identify breasts at high risk using multi-probe generated REIS signals: a preliminary assessment,” *Proc. SPIE*, vol. 7627, p. 76271B–76271B–10, 2010.

[171] M. . Daliri, “Combining extreme learning machines using support vector machines for breast tissue classification’,” *Comput. Methods Biomech. Biomed. Eng.*, vol. 2013.

[172] “Vermed.” [Online]. Available: http://www.vermed.com/diagnostic-ekg.

[173] “Breast Cancer Research.” [Online]. Available: http://breast-cancer-research.com/.

[174] H. P. Schwan, “Electrical properties of tissue and cell suspensions,” *Adv. Biol. Med. Phys.*, vol. 5, pp. 147–207, 1957.

[175] R. J. Halter, T. Zhou, P. M. Meaney, A. Hartov, R. J. Barth, K. Rosenkranz, and W. Wells, “The correlation of in vivo and ex vivo tissue dielectric properties to validate electromagnetic breast imaging:initial clinical experience,” *Physiol. Meas.*, vol. 30, pp. S121–S136, 2009.

[176] C. Polk and E. Postow, “CRC Handbook of Biological Effects of Electromagnetic Fields,” *Boca Rat.*, pp. 27–96, 1986.

[177] J. Dheeba and S. S. Tamil, “Classification of malignant and Benign Microcalcification Using SVM classifier,” in *Proc. Of ICETECT*, pp. 686–690.

[178] C. C. Chang and C. J. Lin, “LIBSVM: a library for support vector machines,” *ACM Trans Intell Syst Technol.*, pp. 2:27.1–27.27, 2011.

[179] C. Hsu, C. Chang, and C. Lin, “A Practical Guide to Support Vector Classification’,” *Natl. Taiwan Univ.*, 2010.

[180] F. Melgani and L. Bruzzone, “Classification of Hyperspectral remote sensing images with support vector machines’,” *IEEE Trans. Geosci. Remote Sens.*, vol. 42, no. 8, pp. 1778–1790, 2004.

[181] P. Clarkson and P. J. Moreno, “On the use of support vector machines for phonetic classification,” *Proc. IEEE Int. Conf. Acoust. Speech, Signal Process.*, vol. 42, no. 8, pp. 1778–1790, 2004.

[182] N. Liu, G. J. Saulnier, J. C. Newell, D. Isaacson, and T. . Kao, “ACT4: A high precision, multi frequency electrical impedance tomography,” in *Proc. 6th Conf. On Biomedical Appl. Electrical Impedance Tomography*.

[183] G. Stuttgen, U. Flesch, H. Witt, and H. Wendt, “Thermographic analysis of skin test reaction using AGA thermovision,” *Arch. Dermatol. Res.*, vol. 268, no. 2, pp. 113–128, 1980.

[184] iact-org, “Thermography Guidelines, Standards and protocols, International Academy of Clinical Thermology,” [Online]. Available: http://www.iact-org.org/professionals/thermog-guidelines.html.

[185] M. Gautherie and C. Gros, “Breast thermography and cancer risk prediction,” *Cancer*, vol. 45, no. 1, pp. 51–60, 1980.

[186] J. R. Keyserlingk, P. D. Ahlgren, E. Yu, N. Belliveau, and M. Yassa, “Functional infrared imaging of the breast.,” *IEEE Eng. Med. Biol. Mag.*, vol. 19, no. 3, pp. 30–41, 2000.

[187] N. Arora, D. Martins, and D. Ruggerio, “Effectiveness of a noninvasive digital infrared thermal imaging system in the detection of breast cancer.,” *Am J Surg*, vol. 196, no. 4, pp. 523–526, 2008.

[188] R. Lawson, “Implications of surface temperature in the diagnosis of breast cancer,” *Canad Med Assoc J*, vol. 75, pp. 309–310, 1956.

[189] W. K. Lloyd and R. Handley, “Infra-red thermometry in the diagnosis of breast disease.,” *Lancet*, vol. 2, pp. 1378–1381, 1961.

[190] R. Handley, “The temperature of breast tumors as a possible guide to prognosis.,” *Acta Unio Int Contra Cancrum*, vol. 18, p. 822, 1962.

[191] J. H. Isard, C. J. Sweitzer, and G. R. Edelstien, “Breast thermography. A prognostic indicator for breast cancer survival,” *Cancer*, vol. 62, pp. 484–488, 1988.

[192] J. Head, F. Wang, and R. Elliott, “Breast thermography is a non invasive prognostic procedure that predicts tumor growth rate in breast cancer patients,” *Ann NY Acad Sci*, vol. 30, no. 698, pp. 153–158, 1993.

[193] R. Lawson and M. Chughtai, “Breast cancer and body temperatures,” *Can Med Assoc J*, vol. 88, no. 2, pp. 68–70, 1963.

[194] C. Jones, “Thermography of the female breast.,” in *Diagnosis of Breast Disease.*, C. Parsons, Ed. Baltimore: University Park Press, 1983, pp. 214–234.

[195] J. Haberman, “The present status of mammary thermography,” *Ca-A Cancer J. Clin.*, vol. 18, pp. 314–321, 1968.

[196] H. Isard, W. Becker, and R. Shilo, “Breast thermography after four years and 10,000 studies,” *Am J Roentgenol*, vol. 115, pp. 811–821, 1972.

[197] G. Dodd, “Thermography in breast cancer diagnosis.,” in *Abstracts for the Seventh National Cancer Conf Proc.*, 1972, p. Sept. 27–29.

[198] H. Isard, “Other imaging techniques,” *Cancer*, vol. 53, pp. 658–664, 1984.

[199] J. S. Penn, *Retinal and Choroidal Angiogenesis*. Springer., 2008, p. 119.

[200] M. Moskowitz, J. Milbrath, and P. Gartside, “Lack of efficacy of thermography as a screening tool for minimal and Stage 1 breast cancer,” *N Engl J Med*, vol. 295, pp. 249–252, 1976.

[201] B. Threatt, J. M. Norbeck, N. S. Ullman, R. Kummer, and Roselle.P.F., “Thermography and breast cancer: An analysis of a blind reading,” *Ann NY Acad Sci*, vol. 335, pp. 501–519, 1980.

[202] “Report of the working group to review the national cancer institute breast cancer detection demonstration projects,” *J Natl Cancer Inst*, vol. 62, pp. 641–709, 1979.

[203] L. Mariel, D. Sarrazin, and A. Daban, “The value of mammary thermography, A report on 655 cases,” *Sem. Hop.*, vol. 57, pp. 699–701, 1981.

[204] I. Nyirjesy and F. Billingsley, “Detection of breast carcinoma in a gynecologic practice,” *Obs. Gynecol*, vol. 64, pp. 747–751, 1984.

[205] G. Bothmann and F. Kubli, “Plate thermography in the assessment of changes in the female breast, Clinical and thermographic results,” *Fortschr Med*, vol. 102, pp. 390–393, 1984.

[206] H. Useki, “Evaluation of the thermographic diagnosis of breast disease: relation of thermographic findings and pathologic findings of cancer growth,” *Nippon Gan Chiryo Gakkai Shi*, vol. 23, pp. 2687–2695, 1988.

[207] S. C. Fok, E. Y. K. Ng, and K. Tai, “Early Detection and Visualization of Breast Tumor with Thermogram and Neural Network,” *J. Mech. Med. Biol.*, vol. 2, no. 2, p. 185, 2002.

[208] E. Y-K Ng and N. Sudharshan, “Computer simulation in conjunction with medical thermography as an adjunct tool for early detection of breast cancer,” *BMC Cancer*, vol. 4, no. 17, 2004.

[209] M. Mital and R. M. Pidaparti, “Breast Tumor Simulation and parameters estimation Using Evolutionary Algorithms,” *Model. Simul. Eng.*, vol. 2008.

[210] T. Tan, C. Quek, G. Ng, and E. Ng, “A novel cognitive interpretation of breast cancer thermography with complementary learning fuzzy neural memory structure,” *Expert Syst. Appl.*, vol. 33, no. 3, pp. 652–666, Oct. 2007.

[211] G. Schaefer, M. Závišek, and T. Nakashima, “Thermography based breast cancer analysis using statistical features and fuzzy classification,” *Pattern Recognit.*, vol. 42, no. 6, pp. 1133–1137, Jun. 2009.

[212] L. Jiang, W. Zhan, and M. H Loew, “Modelling static and dynamic thermography of the human breast under elastic deformation,” *Phys. Med. Biol.*, vol. 56, pp. 187–202, 2011.

[213] M. Gautherie, “New protocol for the evaluation of breast thermograms,” *Thermol. Methods*, pp. 227–235, 1985.

[214] M. Anbar, “Hyperthermia of the cancerous breast: Analysis of mechanism,” *Cancer Lett*, vol. 84, pp. 23–29, 1994.

[215] M. Anbar, “Breast Cancer In:Quantitative Dynamic Telethermometry in Medical Diagnosis and Management,” *Ann Arbor*, pp. 84–94, 1994.

[216] O. Yasuhiko and U. Isao, “Applying Dynamic Thermography in the Diagnosis of Breast Cancer,” *IEEE Eng. Med. Biol.*, vol. 19, no. 3, pp. 42–51, 2000.

[217] N. M. Sudharsan and E. Y. Ng, “Parametric optimization for tumour identification: bioheat equation using ANOVA and the Taguchi method.,” *Proc. Inst. Mech. Eng. H.*, vol. 214, no. 5, pp. 505–12, Jan. 2000.

[218] E. Y. K Ng and N. M. Sudharsan, “An improved three-dimensional direct numerical modelling and thermal analysis of a female breast with tumour,” *Proc. Inst. Mech. Eng. Part H J. Eng. Med.*, vol. 215, no. 1, pp. 25–37, Jan. 2001.

[219] “Fluke Temperature Sensor.” [Online]. Available: http://www.fluke179.com/, http://www.fluke179.com/p1362/fluke_80bk-a.php.

[220] J. S. R. Jang, C. T. Sun, and E. Mizutani, *Neuro-Fuzzy and Soft Computing: A Computational Approach to learning and Machine Intelligence*. 1997.

[221] “MLX90620” [Online]. Available: http://www.melexis.com/Assets/Datasheet-IR-thermometer-16X4-sensor-array-MLX90620-6099.aspx.

[222] H. F. Bowmann, “Heat Transfer and thermal dosimetry,” *J. Microw. Power*, vol. 16, pp. 121–33, 1981.

[223] “FLIR.” [Online]. Available: http://www.flir.com/.

[224] “FLIR SC600.” [Online]. Available: http://www.flir.com/thermography/americas/us/content/?id=31095.

[225] D. . Beetner, “Differentiation among basal cell carcinoma, benign lesions, and normal skin using electrical impedance,” *IEEE Trans Biomed Eng*, vol. 50, pp. 1020–1025, 2003.

[226] Y. . Glickman, “Electrical impedance scanning: a new approach to skin cancer diagnosis,” *Ski. Res Technol*, vol. 9, no. 3, pp. 262–268, 2003.

[227] S. Ollmar1 and L. Emtestam, “Electrical impedance applied to non-invasive detection of irritation in skin,” *Dermatology*, vol. 27, no. 1, pp. 37–42, 2006.

[228] A. Malich, T. Fritsch, C. Mauch, T. Boehm, M. Freesmeyer, M. Fleck, R. Anderson, and K. W.A, “Electrical impedance scanning: a new technique in the diagnosis of lymph nodes in which malignancy is suspected on ultrasound,” *Br J Radiol*, vol. 74, pp. 42–47, 2001.

[229] “SciBase.” [Online]. Available: http://www.scibase.se/en/.

[230] T. Morimoto and E. Al, “Study of the Electrical Bioimpedance of tumors,” *J. Investig. Surg.,*, vol. 6, pp. 25–104, 1993.

[231] E. Waltz, “New probes replace surgeons’ sense of touch,” *IEEE Spectr.*, no. Feb, pp. 16–18, 2014.

Appendix A.

Probe Prototypes

Probe to assess unhealthy tissue

The project began with the development of a biosensor probe for medical diagnostic application. Temperature changes of inflamed tissues can indicate the presence of diseases tissue and if that tissue is improving or getting worse. The goal in the project was to combine four known sensors into a singular biosensor probe to obtain simultaneous differentials in skin measurements for soft tissue assessment. Differential skin data comparison alerts users indicating if there is an inflamed tissue. Once remedied, the measurements go back to a normal readout. The whole project consisted of two parts:

- Electronic and software designing and testing
- Mechanical Designing of Probe

Conclusion

Circuits were developed and tested to a Labview® display. Taking forward a compression device was designed and prototyped in Dec. 2008, to give objective readouts during pressure applications and the body's reaction to pressure. The probe was capable of measuring the galvanic skin resistance (GSR) and tissue temperature variation. Four different GSR sensors had been incorporated in the same probe to make the comparative analysis. The GSR sensor also had features to analyze pit edema as the sensor probe had been designed to show pit edema effect. The probe was also capable of measuring temperature at five different points, two around the centre GSR sensor and three at the boundaries to give a comparative study between the point of pain and tissue around it. A solution had been provided for the measurement of crepitus (sound related to tissue health condition). The study recommended to use contact microphone instead of condenser microphone as the contact microphone reduces background noise enormously as was verified through experiments.

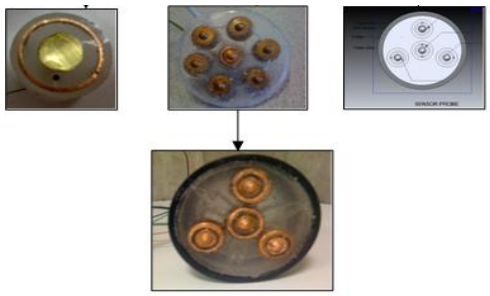

Unhealthy Tissue Detection Probe Development Cycle

BC Cancer Agency: Probe for Quantifying Radiation induced skin side effects and Position Tracking

To develop ergonomically efficient enclosure, using compact electronic module designing techniques and the computer-aided-design software SolidWorks®, sensors along with electronic circuitry were architectured into an enclosure. The prototype was developed using rapid prototyping techniques and a 3-D printer. A CAD rendering along with the prototype of the assembled probe is shown.

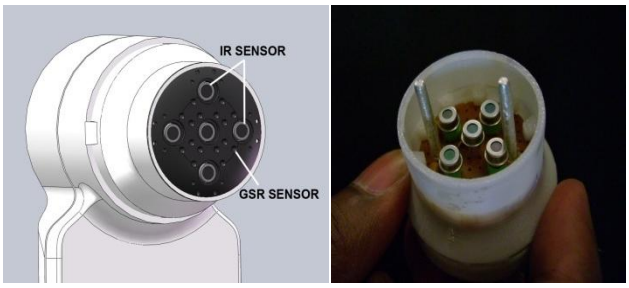

Probe Sensor Head (CAD rendering, Prototype)

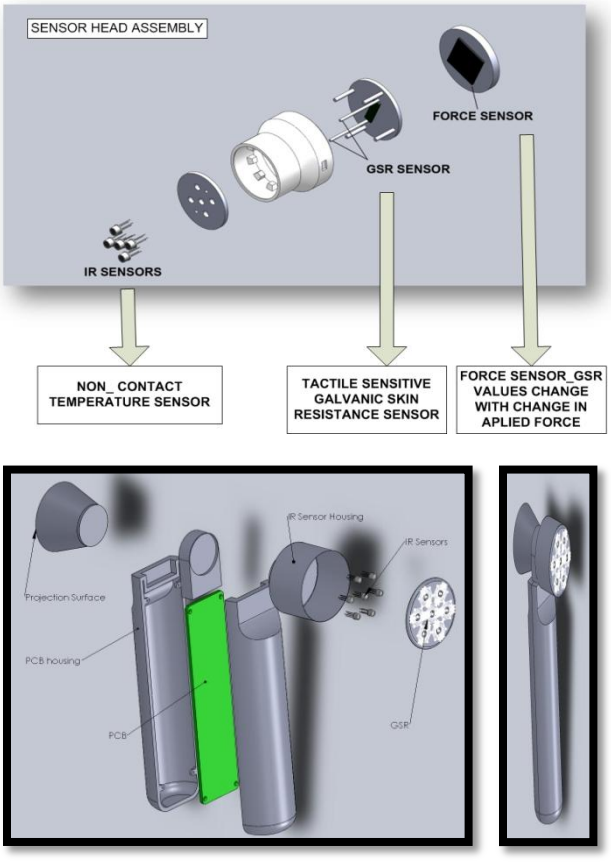

Probe Sensor Head Assembly

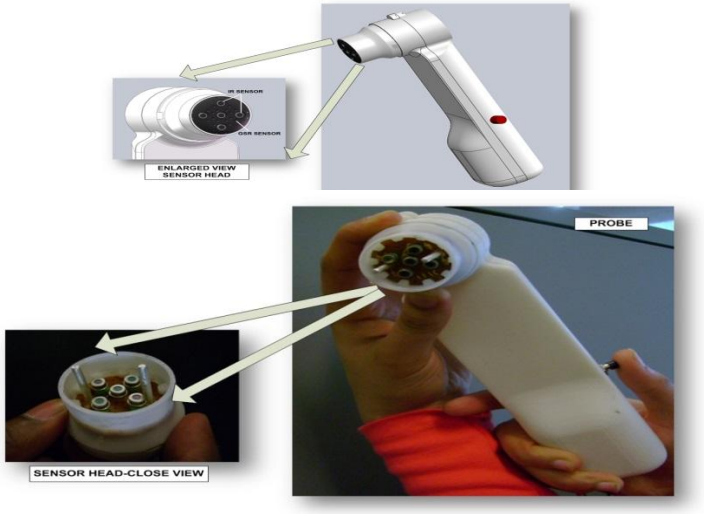

Final Probe: (CAD rendering, Prototype)

Conclusion

A sensor probe that can quantify the adverse skin reaction due to radiation exposure was developed. The probe has been tested on a healthy human hand. Images of the GUI are shown below. The red thermometers show the five IR sensor temperatures. It can be seen that one of the IR sensors is not showing any output, as during fabrication of sensor head, one of the IR sensors got damaged. This provides a good comparative index. The Blue waveform shows the GSR sensor reading and time history. To the right of the GSR waveform, the pressure sensor indicator is shown. The first image shows a screenshot of the GUI when the probe is idle. The second image shows the probes response to making contact with the skin. The GSR and the pressure sensors response is made clear by comparing these two images. Note that all sensors are being activated simultaneously when the probe contacts the patient's skin.

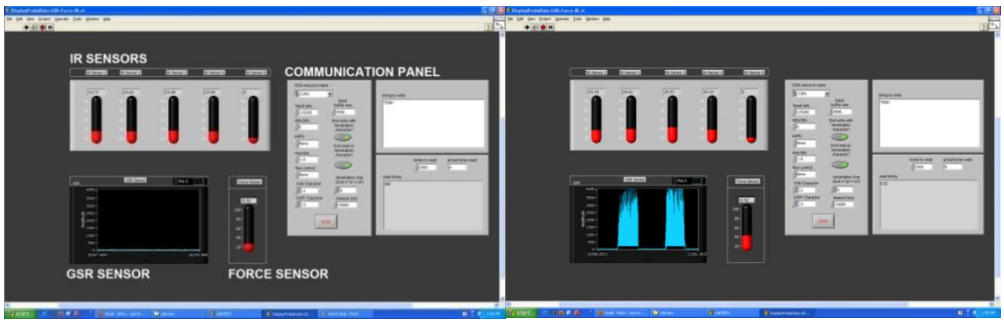

Labview® based Graphical User interface

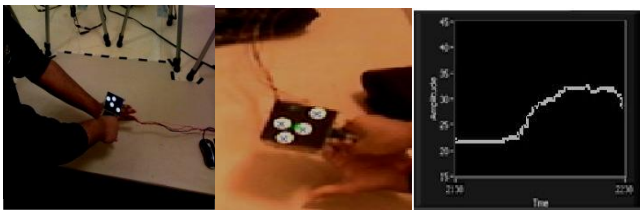

Initial probe prototype being tracked and the temperature (^{o}C) of the hand measured with respect to time in real time

The next step was to gather experimental data through clinical trials and test the results against different levels and severities of damaged skin.

Position Tracking System

The vision system is used to track the position of the probe in real-time. The system consists of two binocular cameras (GIOTTOS MODEL No: AST-36CS) with a resolution of 756*480. Hence in real-time, an actual map of the sensor data with respect to the position is obtained. The position determination obtained is as close as 2.5 mm. Few surface reconstruction algorithms were also developed to mimic the structure of the

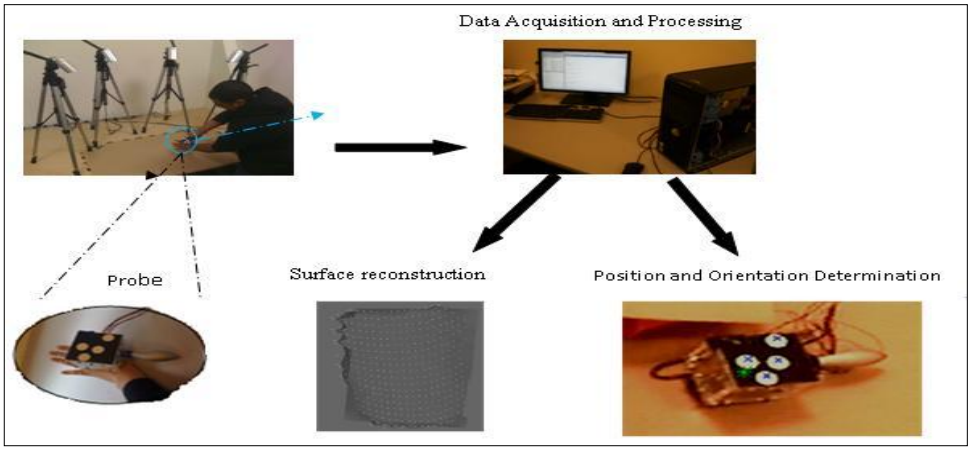

imaged object. The development of this project has been detailed below.

3-D Stereo Imaging technique to determine position and orientation along with surface reconstruction

With the help of the tissue surface information and the probe position one can determine the variation of parameters like temperature and galvanic skin resistance with respect to space and distance from the object (human phantom) surface giving a minimization in position uncertainty.

Conclusion

In this research, a binocular vision system to track a hand held probe has been developed that is very cost effective and can be incorporated by installing two to four

digital cameras in the patient examination room. Information about the relative position of diagnostic hand held device and the object (human phantom) can be found using this method with a position determination error of as low as 2.5mm; using very low resolution cameras. This error can be reduced further by using better resolution cameras though it will add to the overall cost of the system. A non-invasive hand held probe for quantifying skin temperature has been used to show the change in temperature along with the relative position information.

Appendix B.

Study Protocols

Study Number. #2011s0523

The tissue data collection will be done using the hardware created at MSE Dept, Surrey. The hardware consists of integration of three types of sensors:

1). Infrared temperature Sensors: The infrared sensor is Melexis MLX90615. It is an Infra Red thermometer for non contact temperature measurements. Both the IR sensitive thermopile detector chip and the signal conditioning ASIC are integrated in the same miniature TO-46 can.
With its small size it is especially suited for medical applications like ear thermometers or other applications where "small things make a big difference". The thermometer is factory calibrated with a digital SMBus output giving full access to the measured temperature in the complete temperature range(s) with a resolution of 0.02°C. These infrared sensors are non-contact, and are able to detect surface temperature to 0.5 °C of accuracy. The temperature range it can detect is -40 to 115 °C.

These sensors are used for Comfort Sensing, Fever measurement and Diagnosis Systems; therefore they are totally safe to be used on human body. The sensor is based upon infrared radiation; Infrared (IR) radiation is simply one of the many types of 'light' that comprise the electromagnetic (EM) spectrum. Infrared light is characterized by wavelengths that are longer than visible light (4000-7000 Angstroms, or 0.4 0.7 micrometers; also denoted as microns). We are immersed in infrared radiation every day. It is nothing more than heat. This sensor just measures the infra red radiations emitted from the human tissue. No external source of radiation is involved in the study making it completely safe for humans.

2). Pressure and Displacement Sensors: The FingerTPS™ (Finger Tactile Pressure Sensing) is used to measure the applied pressure; the system utilizes highly sensitive capacitive-based pressure sensors to reliably quantify forces applied by the human hand. The amount of applied pressure will be less than 10 N and the subject would be subjected to pressure depending on his tolerance power. Never pressure values above subjects comfort zone will be used.

The displacement measurement is being done with a string potentiometer by Celesco, the SP1.It is a compact, economical and durable device that utilizes a flexible cable, a spring-loaded spool, and a potentiometer to detect and measure linear position. The displacement measured with this will be in the maximum 5 mm always within the elastic limits of human tissue. Displacement measurements that make the subject uncomfortable will never be applied. Therefore the sensor and the measurement do not consist of any parts that may pose danger to human tissue health.

3). Electrical Impedance scanning: EIS is a new modality being used to characterise tissue and currently is being evaluated in multiple clinical studies worldwide. It uses an excitation source current, or voltage injected by electrodes. The amplitude of the signal is controlled such that the safe current/ voltage limits are never exceeded as per the

AAMI. American national standard: safe current limits for electromedical apparatus guidelines. The electrodes to be used are Ag/AgCl and the low current signals at low frequencies will be developed using Lock-in-Amplifier by Zurich Instruments. The measurements are in vivo and pose no danger to the health of human tissue. TransScan TS2000 is the commercially available electrical impedance scanner. It uses the Electrical Impedance Scanning technology, for safety regulations it limits the voltage to 2.5V and current to 5mA. Same norms will be followed in the proposed research. The TS2000 has been granted FDA approval to be used as an adjunctive technology, therefore is safe to be used on human tissue.

All the above mentioned sensors have been integrated into a finger cap glove module. This module will be used to capture the human tissue properties data. No risk or danger is involved to the human tissue during this study as all the used sensors and hardware are completely safe and utmost care will be taken not to exceed the safety limits. No sensor emits any radiations therefore are completely safe.

To recruit the subjects' volunteer offer will be proposed to the Faculty, Students or Staff of Engineering Simon Fraser University. The subjects will be 18 yrs or above male/female candidates. This would be done through advertising on information boards or through email. 10 to 20 subjects will be recruited for this study. The subjects will be given $20 for the ½ hour of data collection.

The protocol for the study will consists of 3 trials each on the subject's palm, arm bicep muscle and stomach. The tests would take about half an hour for all the trials. A conducting gel may be used on subject skin to overcome skin resistance. This will be the same gel as used in ultrasound scanning and is totally safe for to be used on human skin. If the subject feels uncomfortable or shows discomfort, he will have the option to refuse to participate any time.

Data capturing will consist of two parts: firstly holding the sensors on to human tissue and secondly running the software to capture and save the data. Therefore, a research assistant 'Parvind Grewal' and a co op student will be working in collaboration to collect the data. The system is a human controlled system thus forces and displacement applied to the subject can be carefully controlled and stopped at any time. If the subject feels uncomfortable or shows discomfort, he will have the option to refuse to participate any time. The age, body temperature and gender of the subject will also be recorded for comparison purpose.

The raw data will be stored till December 2016. The data will be anonymized and it will all be stored on a password protected computer in a locked lab. There will be no identifying information kept from individuals in the study to ensure confidentiality of the participants. No one will have access to the lab except authorised personnel's. The machines have secure passwords (only known to those involved in the study) and the computers are stored in a locked and secured lab. Data collection and storage will be in the same location, therefore eliminating any risk of data loss in transportation. Therefore the data will be fully protected. The data representation will be such that it is anonymized and none of the participant's identity will be disclosed.

Study Number. REB Number H13-02887

Methodology

Patient population

The patient population to be studied is any patient with a basal or squamous cell skin cancer being treated with radiation therapy at the BCCA - Fraser Valley Centre.

Inclusion criteria:

The subjects will be:

- Patients with basal or squamous cell skin cancer (confirmed by biopsy or dermatologic consult).
- Patients above 18 years of age
- Patients able to speak and communicate in English
- Patients able to provide consent

Exclusion criteria:

Patients will be excluded:

- If they have an implanted electrical device e.g. pace-maker
- If they have skin lesions that are easily friable or painful (as determined by clinical exam by the primary investigator).

Eligible patients will be identified and approached by their oncologist during the patient's initial oncology consult at the BCCA-FVC. The oncologist will present the study and consent form and invite the potential subject to participate. If the potential subject is interested and requires further information, the potential subject will meet with the research assistant who will provide additional information about the study, go over the consent form, and answer any questions. The potential subject will have until their first day of radiation treatment to decide whether or not to participate. If the subject decides to participate, formal consent will be obtained. The first EI measurements will be done just prior to treatment on their first treatment day.

Twenty patients will be recruited and consented for EI analysis.

Measurement systems: overview

- EI measurements will be made using an Impedance Spectroscope HF2IS from Zurich Instruments, along with Grass Safelead electrodes.
- The temperature will be measured using non contact infrared sensor by Melexis MLX90615.
- The pressure will be measured using Finger TPS™ (Finger Tactile Pressure Sensing) sensors.

All three sensor systems have been integrated into a single multi-modality finger wearable device.

Study procedures

For each subject, height, weight, age, gender, and details of their skin cancer (date of diagnosis, pathological diagnosis, treatment to date for the skin cancer) of each subject will be recorded.

For each subject, two sets of measurements will be taken: 1) just prior to the start of radiation treatment; 2) at the six-week follow-up appointment after radiation treatment has been completed.

For each set of measurements:

- The subject will be asked to relax for 5 minutes in a temperature controlled room to stabilize their body temperature.
- The subject will be asked to be in the treatment position.
- The skin to which the electrodes will be attached will be cleaned with alcohol prep pads.
- The EI electrodes with conductive gel will be placed over the lesion, covering the lesion.
- A constant low level pressure will be applied and maintained using the feedback from the pressure sensors.
- A mild current (less than 1 volt) will be applied across the EI electrodes, at 50 different frequencies from 1.0 KHz to 1 MHz. The frequency sweep will not take more than 2 minutes.
- Two trials will be taken at one pressure level.
- A second pressure level will be applied and the EI measurements repeated
- The temperature sensor will be placed over the tissue to record tissue temperature
- The measurements will be repeated on collateral healthy skin tissue from the subject to serve as a baseline control.

Measurements should take approximately 30 minutes.

Data analysis

EI spectrums will be compared for malignant and healthy skin tissue before treatment, and after radiation treatment. We will examine the effects of pressure and temperature variations on the EI analysis.

Study Number. #2014s0134

Same procedure as followed in study REB Number H13-02887

Appendix C.

Phantom based experiments: Stiffness measurement

Proposed Set Up 1

As discussed malignant tissue is much stiffer than normal fat tissue of the breast,[Wellman PS, Howe RD. The mechanical properties of breast tissue in compression. Technical Report No. 99003. Harvard BioRobotics Laboratory, Cambridge, MA, USA, 1999.] and it is assumed to be nearly incompressible , elastic and isotropic. Same assumptions have been made during this study. In order to classify tissue based upon tissue stiffness two different methodologies of tissue stiffness measurement were studied, these included use of force sensor with displacement sensor and use of multi force sensors as used in tactile mapping.

Soft elastic materials, like human tissue, tend to absorb and distribute input forces in various directions that cause decrement in returning force. For the same reason, any amount of force applied to a soft object will result in a larger magnitude of displacement than that applied to a hard object. The first study focuses on comparison between the multi force sensor and; force sensor with displacement sensor measurement methodology for tissue stiffness measurement. Figure 20 illustrates the set up and the resulting effect between two materials, soft and hard, when a force is applied over soft, elastic, isotropic, incompressible material.

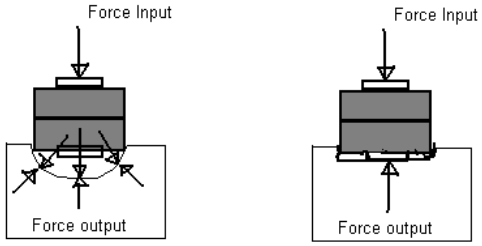

Effect of Applied Force

The methodology of using multiple force sensor is to place two force sensors, one facing the operator while the other facing the object. This arrangement allows the user to measure the returned force, as well as measure the applied input force. When applying a downward force to a soft object, a large distortion is produced. This causes the force to be distributed towards non-vertical directions and results in a lower return force than when the same experiment is performed on a hard object. Although it is difficult to verify how the forces are dispersed within different materials, the difference between applied and returned force is enough to help classify different types of tissue. In order to accurately identify the difference in stiffness between two materials, the relationship between applied and return pressures at location of interest is carefully studied. By maintaining the force level of one of the force sensors, considered as apply force, the ratio and difference between itself and the other response force can successfully identify

the stiffness of object. The first sensor used to measure material stiffness was FS03 from Honeywell.

Honeywell Pressure Transducer

Honeywell's FS03 series force transducer [70],is a compensated, amplified, piezoresistive sensor with force range of 0 lb to 3.0 lb. It is temperature compensated, calibrated, zero noise and usually used for medical applications. As the force sensor outputs analog voltage it had to be fed through an ADC (analog to digital converter) for digitizing the results, followed by calibration using weights. The calibration equation is shown in equation 27; F_{real} is the force after calibration.

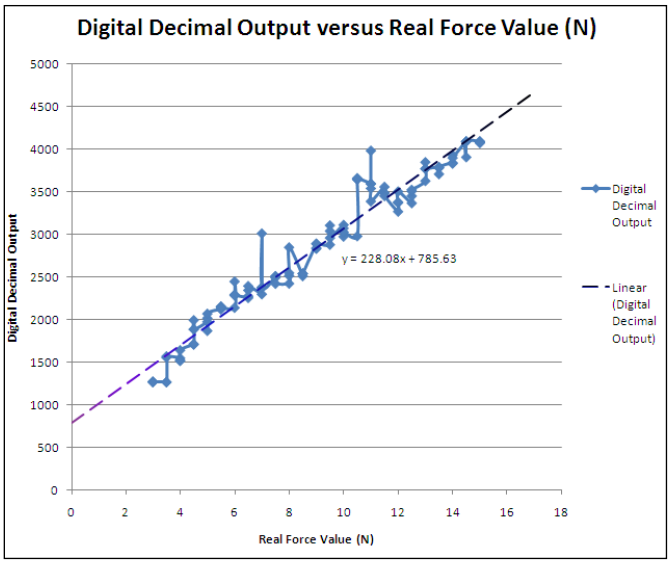

FS03 Calibration Graph

After calibration, the force equation is as follows:

$$F_{real} = \frac{\text{Digital Reading} - 785.63}{228.08}$$

The multi force method consists of two force sensors, one facing the physician, and one facing the object. As discussed in the above section, an amount of force applied to a soft object will result in larger magnitude of displacement than that applied to a harder object. Since the FS03 only detects components of the force orthogonal to the sensor, this should result in a lower F_{out} to F_{in} ratio. This result can thus be used to classify soft and hard objects.

This method's advantage is that we do not have to keep track of displacement, and its disadvantage is that we need two force sensors.

The second method is based upon displacement measurement along with the force measurement. In order to keep track of depth and to apply a constant force, a force sensor is attached to a precision vice as shown below.

The vice system used to control depth and force

Each complete screw rotation is equal to 1 mm increase in depth, which can be used in conjunction with the force reading to draw conclusion on the object's hardness. The differential equation describing our system can be shown as

$$mx + cx + kx = F_o u(t)$$

Where x is the depth from the surface of the object, m is the mass of the object, c is the damping constant, F_o is the magnitude of the applied force, and k is the spring constant. The step input u(t) takes t = 0 is the start time for application of force.

At steady state (i.e. t >> 0), there is no acceleration or velocity, hence

$$m * 0 + c * 0 + kx = F_o$$

Therefore $$k = \frac{F_0}{x_o}$$

Which can be used to classify the object at steady-state.

Simulated Material

One of the most important parts of proof of concept is the credibility of our simulated material (also called Phantoms). The phantom for these experiments is made of 90%

water and 10% Knox gelatine [2], this mixture called “ballistic gelatine” has roughly the density of human tissue. In order to introduce anomaly to the mixture, a ½ W, 100-Ω resistor is inserted into the gelatine. The resistor will serve as “hard” object which can be felt by palpation.

Test Bed Software

MATLAB software is designed to obtain data from the microcontroller UART. The program produces a mapping force, and location into one graph. Force data is mapped to the height (Z-axis), location is mapped to X and Y axes. As the force setup can probe only one location at a time, only one of the “nodes” contains true reading from the force sensor, and the rest hold simulated values.

Using the first force method, the height of the graph follows equation 30, which is force reading from the sensor divided by displacement, which is controlled to be constant. Using the second method, the height of the graph is the ratio between the two force sensors, which, is

$$\frac{F_{out}}{F_{in}}$$

Results

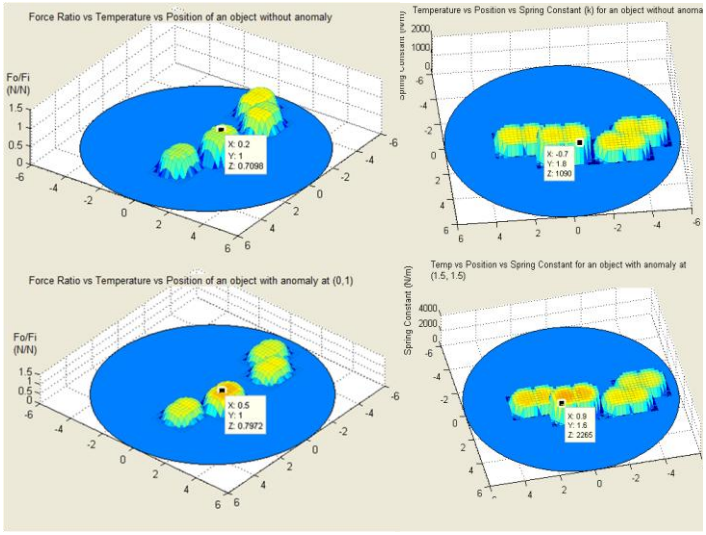

A). Force and displacement sensor methodology. Z axis represents the force constant, Top graph is phantom without anomaly and bottom is with anomaly

B). Force sensor ratio methodology. Z axis represents the force constant, Top graph is phantom without anomaly and bottom is with anomaly

Matlab GUI representing Force Data

There is a noticeable difference between soft object (0.7 N/N) and hard object (0.8 N/N), using the force ratio methodology as seen in Figure 23(A). This difference is easily repeatable. This method is not subject to human error as it only requires readings from

sensors to make conclusions about hardness. However, this methodology is more space-consuming and more costly as it requires two sensors per each location.

Using the force displacement measurement methodology, as seen in figure 23 (b), the hard object can be detected via a substantial difference between soft object (1090 N/m) and hard object (2265 N/m). This method, however, is subject to some amount of uncertainty because our method of keeping track of displacement – by using screws – is subject to human error, especially when dealing with displacements in the millimetre scale. Instead a digitized displacement reading can be used, to make this method more reliable. Nevertheless, the difference between the readings from the soft and hard object is by far repeatable.

Tissue stiffness measurement using force sensor and string potentiometer

To improve the displacement measurement a string potentiometer was used instead of the vice. The displacement sensor (string potentiometer) is first clamped on an adjustable arm and connected to the force sensor at the bottom of the cable to create a steady pivot point. Measurements are taken with precision in millimetres as the changes in displacement are often small when testing on gelatine phantoms.

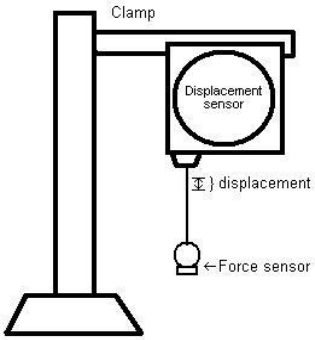

Displacement and force sensor setup

Proposed Set up 2

Two force sensors are considered in this set up, Honeywell pressure transducer FS03 [70] and Pressure Profile System (PPS) Finger TPS sensor [78]. These sensors have been selected after thorough market review to meet the requirements of being small enough to be finger wearable and capable of measuring human applied force during physical examination. As per specifications, Honeywell's pressure transducer is a much more sensitive device in terms of precision and sensitivity. However, the communication ability and its physical shape are not as ideal for tissue classification as a wearable device. Pressure Profile System's sensor on the other hand, gives a much faster steady data transmission that gradually reduces the overall system delay as discussed later and is a finger wearable sensor.

FS03 and Pressure Profile Finger TPS system

Pressure Profile System's Finger Tactile Pressure Systems (Finger TPS)

This wearable tactile pressure sensor reliably quantifies forces applied by the human hand. This capacitive and sensitive device has a surface area of 349 mm2 and detects up to 10 lbs. Since the system is hard coded in C language, its software takes care of the calibration between analog and digital values using a calibration unit. As the research only focuses on single point measurement, only the finger sensors are used.

Celesco Cable Extension Transducer

This cable extension transducer, model SP2-25 [28], provides a full stroke range of 25 inches that allows the user to accurately measure the displacement over a wide length. This sensor has also been calibrated like the Honeywell's transducer and the calculated calibration equation is shown below. D is the displacement.

$$\mathrm{D} = \frac{\text{Digital Reading} - 580}{228.08}$$

In terms of communication with the sensors, implementation is programmed in C environment using Texas Instrument microcontroller MSP430F169. For data analysis, MATLAB® program has been used for further analysis because of its flexibility in data representation.

Tissue Equivalent Materials

As various materials were considered throughout this experiment, many of them are used to define what a soft and hard object is. For example, an extreme contrast can be found between a sponge and plastic bead. Since the final goal of the study is to differentiate and identify very small change in tissue stiffness, this extreme case cannot be used as conclusion. Therefore a list of gelatine based phantoms with specified concentrations is made to represent smaller intervals in stiffness differences. Before any of the experiments in determining the change in stiffness is performed, a static reference must be created for the comparison. Therefore a durometer is applied to obtain a unit less measurement which indicates the ratio of displacements on all of the test materials including desk, sponges and different gelatine concentration phantoms to represent different hardness. These readings can provide initial impressions for the stiffness of listed objects.

Varying the gelatine concentration by mixing it with distilled water was used to create phantoms. Percentage of gelatine in water by weight can represent human tissue such as muscle and fatty tissue, as well as abnormal fibroglandular and cancerous tissues [28]. In this study, the experiment has emphasized more on the fatty and cancerous tissues which are simulated at 10.77% and 20.75% of gelatine respectively. These gelatine based phantoms are constructed by heating the mixture up to about 80°C to allow the gelatine powder to fully dissolve. The samples are then poured into beakers, 10cm in diameter. The experiments were performed as soon as the samples are cooled

to about 4°C. The dimensions and durometer readings for all the samples and materials are noted in table 3.

It is important to note that the orange sponge has no durometer reading because the material is too soft to be measured. As for the last two materials, composition 1 and 2, listed in table 3 are made of 40% distilled water, 48% ethanediol (as anti-freezer), 10% gelatine and 2% of salt. This high permittivity mixture is originally used to simulate muscle tissue [29] and its good durability allows the experiment to be performed repeatedly. Although both compositions are created with same concentration of all ingredients, composition 2 had been kept in the freezer for longer period which resulted in a much higher durometer reading.

Material	Height (mm)	Durometer reading (unit less)	Material Reference
Desk	-	100	A
10% gelatin	28	6	B
10.7% gelatin	30	10	C
15% gelatin	25	20	D
20% gelatin	25	26	E
27.5% gelatin	29	30	F
Sponge (Yellow)	65	14	G
Sponge (Orange)	25	-	H
Sponge (black)	6.5	43	I
Comp 1	40	22	J
Comp 2	40	39	K

Durometer readings

Experimental Set Up

Four set ups have been arranged to find out the best capability to identify change in phantom stiffness, as the outcome can get affected due to the difference between sensors' specifications. Throughout all the set ups, at least one force sensor is kept at a constant value at throughout the experiment to be considered as input force. By studying the outcome including returned force and displacement, many set up can successfully identify stiffness differences. Although double force sensors is a more straightforward set up since it requires no reference point, the results often are unstable due to multiple factors including error range overlapping and surrounding deformation. In contrast, combination of force sensor and displacement sensor indeed represented a much better resolution in determining the difference between stiffness. The only constraint for this particular set up is the reference point, e.g. the adjustable arm to stabilize the sensor.

Before any of the experiments in determining the change in stiffness is performed, a static reference must be created for the comparison. Therefore a durometer is applied to obtain a unit less measurement which indicates the ratio of displacements on all of the test materials including desk, sponges and phantoms to represent different hardness. These readings can give us a good idea how soft or hard an object is.

Honeywell's FS03 & Honeywell's FS03 (Set Up 1)

Using two of Honeywell's pressure transducers was originally thought to be the best set up because these transducers provide very precise measurement in vertical direction. This particular specification would help to minimize all the other surrounding effects. However, its bulky physical shape causes problems when the sensor is pressed down

into soft materials. The edges of the sensor, where the actual sensing pad is not present, tend to apply much more force and saturate the sensing pad output. Force values captured in this section are unreliable and the results are often unstable. Therefore it is concluded that this set up cannot provide accurate information to identify the difference in stiffness and its data is neglected.

Finger TPS & Finger TPS (Set Up 2)

This particular set up gives the best flexibility since the sensors come in finger wearable shape. Having the sensing pad sewed on the finger shape cloth overcomes the issues that were encountered in the previous setup. The rate of data transmission is also excellent as it has its separate software which basically removed all the delay when analyzed with MATLAB®. Although the data acquisition has been improved, one issue that came up was the alignment of the two sensors. Since Finger TPS sensor consisting of capacitive type sensors, does not have a rigid component that holds the pad like Honeywell's pressure transducer, they tend to move around over the finger pad throughout the experiment. The other major disadvantage is that the sensing pads are made too thin and the distance between two sensors is too small when they are placed together bringing in crosstalk issues. This causes the measurements of one sensor often affecting the other due to the overlap of error ranges.

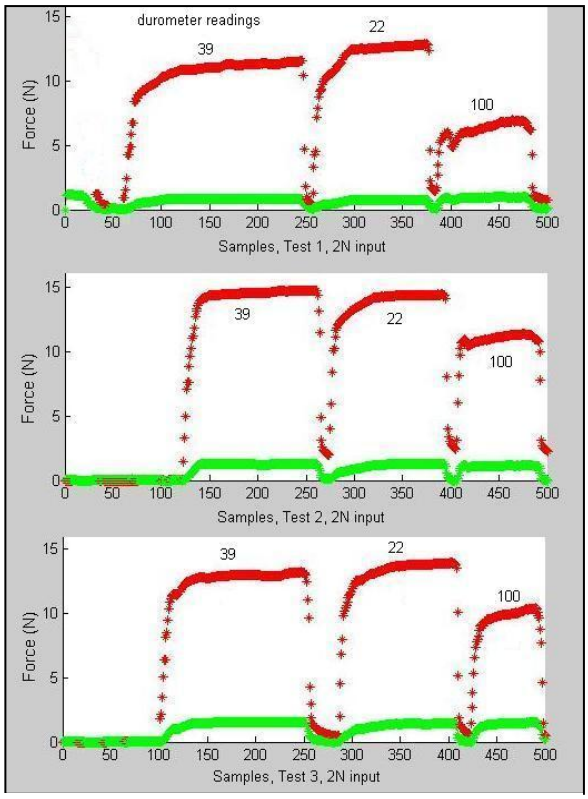

Comparison of returned forces on different materials

However, this issue can be resolved by placing a rigid sheet between the sensors. In this section of the experiments, 2N and 3N forces are applied against three kinds of materials including desk (A, durometer reading 100), composition 1 (J, durometer reading 22), and composition 2 (K, durometer reading 39). According to durometer readings, material J (durometer reading 22) is softer than K (durometer reading 39) which is softer than A(durometer reading 100), which implies that different levels of returned forces should be expected. Figure 27, clearly indicates three levels of returned force where the green lines are the input forces and kept at 2N in order to keep consistency throughout the experiment. Red lines are the observed output force. Although a difference between material J and K is observable, the magnitude is still not as significant as that of J and A. Test number 2 is an example showing the fuzzy range for two materials with similar stiffness. The returned force for material K is actually greater than J in this case due to many other factors such calibration of the force sensor.

These sensors need precise calibration else the results are quite unstable. Therefore, this set up is only useful when proper calibration of the sensors has been done, secondly the sensors also show crosstalk problem as no rigid surface separates the sensing pad of the sensors.

Finger TPS & Honeywell's FS03 (Set Up 3)

With two different type of force sensors (Honeywell FS03 and PPS Finger TPs System), this set up had overcome many previous set up problems; example crosstalk and conformal shape. Phantoms with different concentration of gelatine were used to perform the experiments. Shown in figure 6 is a phantom, composition 1 (J), with durometer reading of 22 tested against desk (A), durometer reading of 100. Again, the green line represents the input force and the red line shows the returned force. Their average differences between input and return forces are 2.3N, and 2.09N.

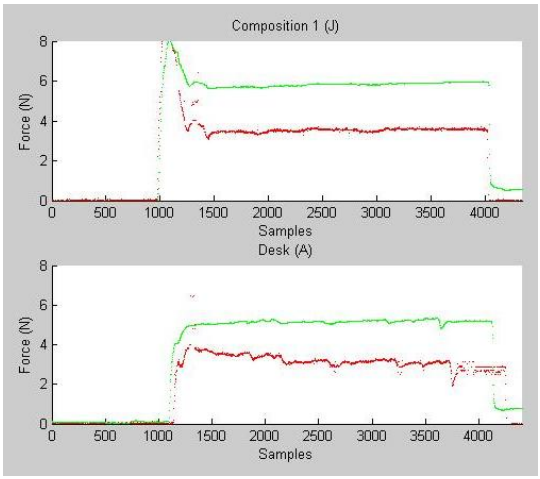

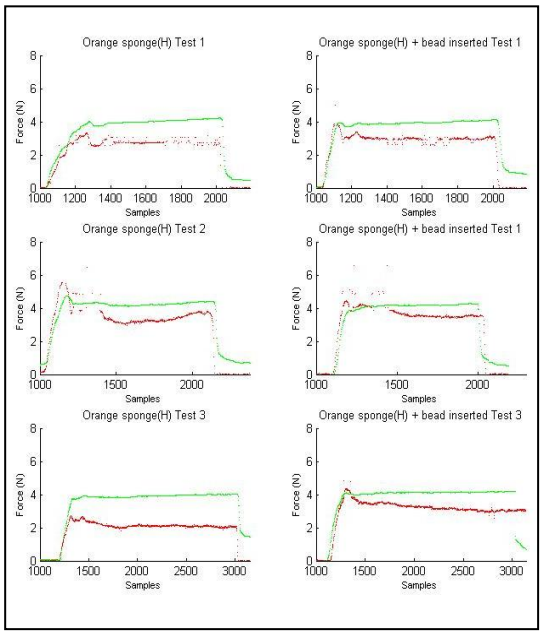

Comparison of returned forces on Orange Sponge (H), and a bead inserted

Although the outcome is reasonable, the results needed verification by inserting high stiffness material in low stiffness material. Shown in figure 29 are three tests performed on the orange sponge with a rigid bead inserted inside. The left column is the reference for normal orange sponge while the right column represents embedded object. The force differences are calculated and provided in table 2.

Force difference for orange sponge without bead and with bead

	Orange Sponge (H) force difference	Orange Sponge (H) + bead force difference
Test 1	1.28N	1.04N
Test 2	0.94N	0.68N
Test 3	1.82N	0.95N

The output input force difference in each test was at least 0.3N. This number is quite significant compared to the other previous set up, but, the difference in stiffness between orange sponge and rigid bead is severe. None the less, the combination of two different force sensors fairly reduces issues of crosstalk and conformal shape. Its data transmission delay is acceptable and the physical size is adequate for the designed experiments.

Finger TPS &Celesco Cable Extension Transducer (Set Up 4)

Honeywell FS03sensor was not considered in this set up because of its non conformal shape. Since input force was the only force measured, only PPS finger sensor was used. Replacing one force sensor by a displacement sensor gives much better comparable data in order to determine the difference in stiffness. Figure 30 shows the experimental set up.

Experimental Set Up

With constant input force being applied on a material, the stiffness of the target is calculated with the change in displacement that eventually leads to differentiating materials based upon stiffness. During the experiment, force sensor is brought down to the surface level of the phantom. Then 5N of input force is applied against the test samples. With reference to stationary arm, reliable displacement measurements were measured and applied to Equation 27.

Figure 30 shows the result for 10% (B), 15% (D), and 20% (E) of gelatine based phantoms. The average displacements for three different phantoms are measured to be 7.42mm, 4.73mm, and 3.66mm from top to bottom. These values show significant differences which allow the system to further identify changes in stiffness. Two more phantoms with 10.77% and 20.75% were constructed to stimulate different types of tissues. As a result, 10.54mm and 5.81mm were obtained for average displacements. Figure 30 illustrates the change in length for both materials.

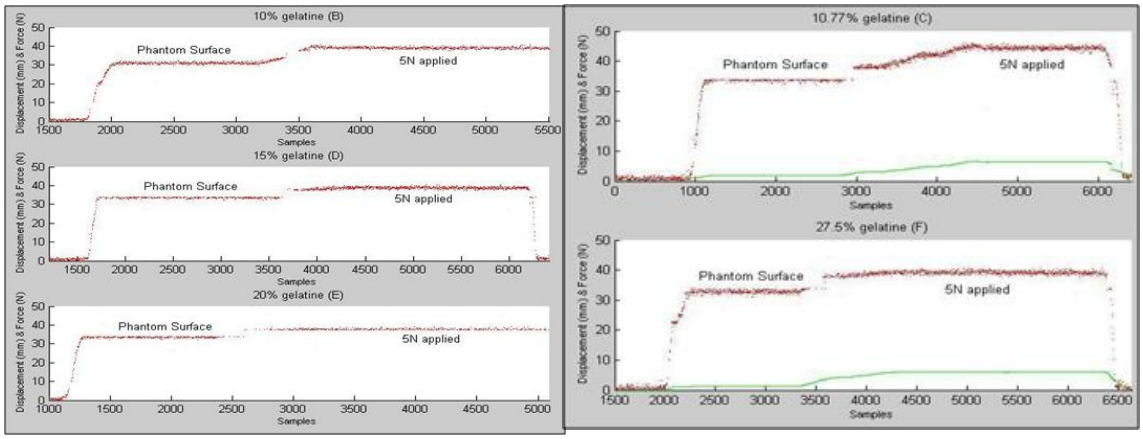

Comparison of change in length on 10% (B), 15% (D), 20% (E), 10.77% (C) and 27.5% (F) gelatine phantoms

Phantom based experiments: Electrical Impedance measurement

The developed hardware/ software and the set up could not be used for *In Vivo* data collection directly without prior verification of set up. Small amount of the muscle material (2cm x 2cm x1cm) was inserted into the fat material; this simulates quite closely the electrical properties of breast tissue with anomaly. Data was collected using the developed hardware/software and phantoms. Algorithms based upon ANFIS (Adaptive Neural Fuzzy Inference System) were developed to intelligently distinguish between the muscle and fat phantom using the collected Electrical Impedance Frequency Sweep Data.

The first results were only for measurement of conductivity without considering the complex impedances. The input voltage amplitude was kept 125mV. Two phantom samples were created, one without any anomaly (Control) and the other with anomaly at a fixed position (Specimen). Four rectangular ditches the same size of electrodes was carved into the phantom material in order to insert the electrodes at the positions shown in the figure. In order to get more authentic results, a cube of 2cm x 2cm x 1cm of higher conductivity material was inserted as an anomaly at a depth of 1cm at the position (0-3.0) into the less conductive phantom mimicking the breast fat.

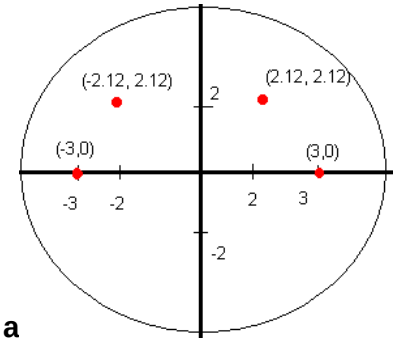

a

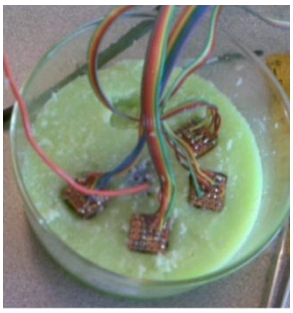

b

a) Positions of EIS sensors b) Carving holes in the specimen to keep track of position and area of contact in EIS measurement

The EIS data can be separated into two parts: conductivity with the unit Siemens per meter (S m^{-1}) and permittivity. The conductivity and permittivity are found as follows:

$$\sigma(\omega) = \frac{L}{A \cdot real\ \ Z\ j\omega}$$

$$\varepsilon(\omega) = \frac{L}{A \cdot \omega \cdot imag[Z\ j\omega\ ]}$$

L is the distance from the ground plane and A is the area of contact.

EIS Data Presentation

EIS data is further presented in 2-D using MATLAB®, mapping conductivity (color) to position (X and Y axes). A set of four electrodes were fixed at a position as shown by each sphere. 16 electrodes are depicted by four spheres. The color of the sphere is an indicator of the average conductivity value. Various readings were taken at different frequencies shown as set1 and set2. Set1 depicts conductivity values as : a, b at 1 kHz; c, d at 10 kHz; e, f at 50 kHz and set2 shows conductivities as a, b at 100 kHz; c, d at 250 kHz; e, f at 500 kHz; g, h at 1 MHz and i at 10 MHz. Right side of each set depicts the control results and left side depict the specimen with anomaly results. It was concluded that frequencies above10 kHz should be used for classification. This test set up verified that the developed hardware as well as software can be used for reliable EIS measurement. The frequency range was limited within the range of 30 Khz to 30 MHz considering the measurement requirement and hardware capability.

Raw data of conductivity and permittivity at each position. Note that the anomaly is at (-3, 0)

Frequency (kHz)	X position (cm)	Y Position (cm)	Conductivity σ (S/m)	Absolute Permittivity ε (F/m)
1	1.5	1.5	0.87633	0.0081061
1	-3	0	1.1897	0.0010767
10	1.5	1.5	1.0846	0.00011886
10	3	0	0.93303	9.98E-05
10	-1.5	1.5	1.1177	9.81E-05
10	-3	0	1.9654	7.55E-05
100	1.5	1.5	0.90256	1.74E-05
100	3	0	1.0999	2.42E-05
100	-1.5	1.5	1.3745	3.45E-05
100	-3	0	3.4669	6.79E-05
250	1.5	1.5	1.3482	3.50E-06
250	3	0	1.2037	2.70E-06
250	-1.5	1.5	1.4519	4.14E-06
250	-3	0	3.4784	1.77E-05
500	1.5	1.5	1.5534	1.11E-06
500	3	0	1.453	9.02E-07
500	-1.5	1.5	1.6269	1.24E-06
500	-3	0	3.2979	5.84E-06
1000	1.5	1.5	1.5511	5.50E-07
1000	3	0	1.4449	4.53E-07
1000	-1.5	1.5	1.616	6.29E-07
1000	-3	0	3.2427	3.07E-06

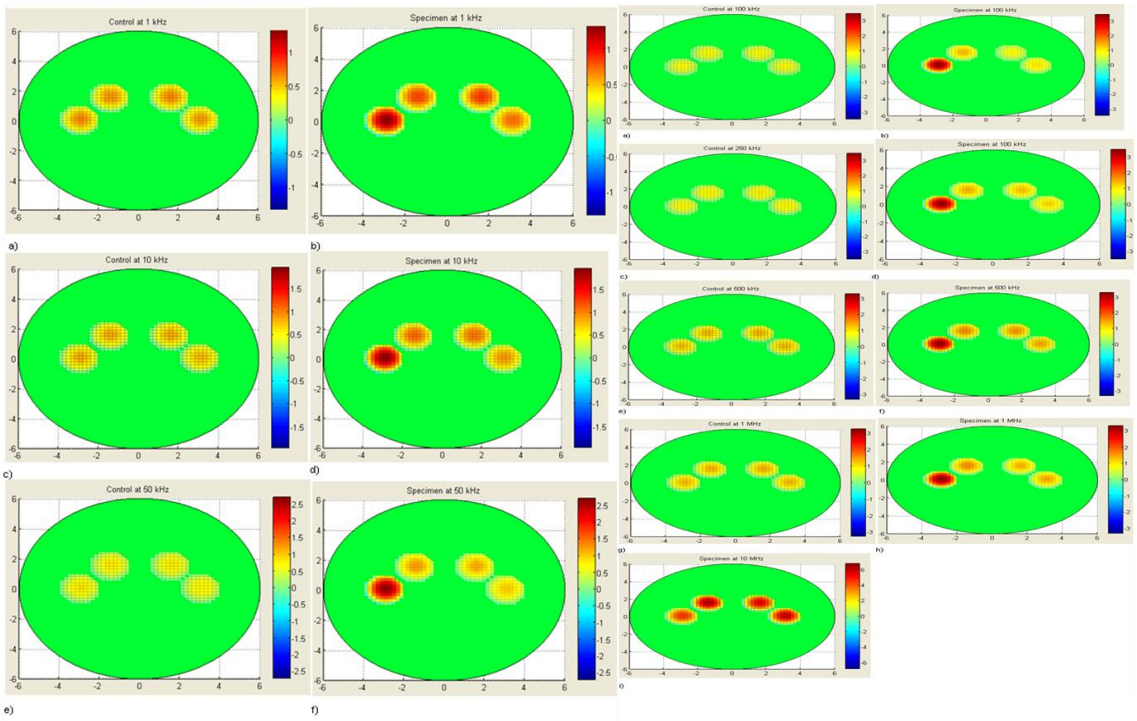

Conductivity (S/m) of material at fixed locations at: Right Control Specimen Pair: a), b) 1 kHz, c), d) 10 kHz, e), f) 50 kHz. Left Control Specimen Pair: a), b) 100 kHz, c), d) 250 kHz, e), f) 500 kHz, g), h) 1 MHz and i) 10 MHz

A further step forward was to change the single frequency sweep module to multi frequency sweeps and study complex impedances rather than considering only the conductance values. Thereafter required software was implemented and multiple frequency sweep methodology was used on the two types of phantoms. It was required to verify the effect of applied force on the phantoms therefore, reading were taken using different level of applied force. Four trials for each set up was taken using LOW force level and HIGH force level. Figure15 shows the mutifrequency Resistance/ Capacitance plots against Frequency from 1 KHz to 1 MHz for 49 sample points. Application of force does affect the impedance readings therefore the amount of applied force has been kept constant and same while measuring the electrical impedance. The third phantom *Superflab* acquired from BC Cancer Agency that is usually used in radiation calculation experiments was also tested. As this phantom was not homogeneous in composition therefore was not further used for the study.

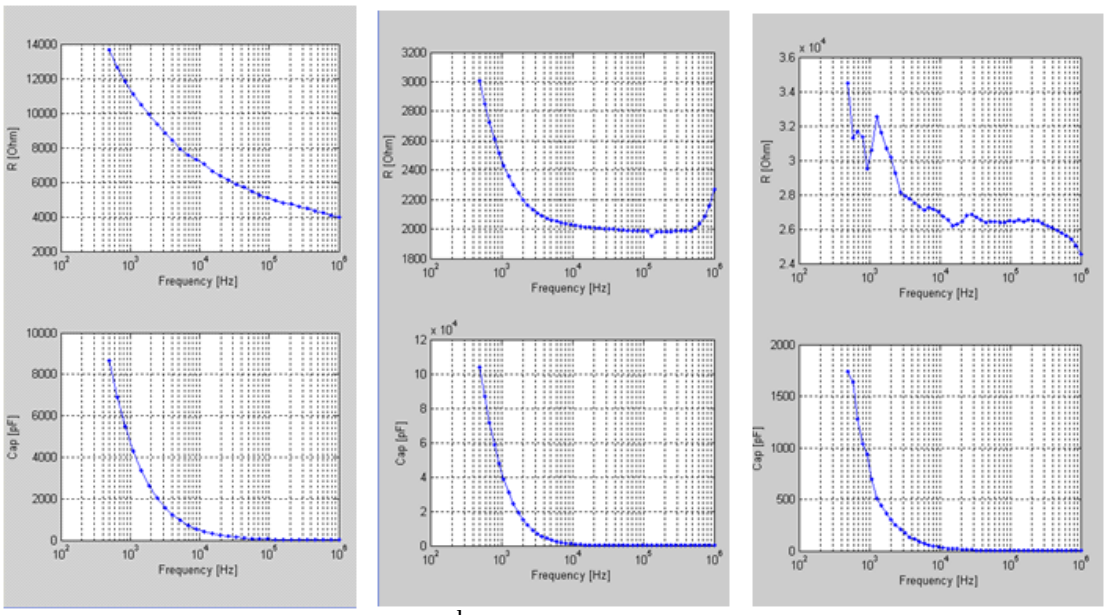

a b c

Resistance versus Capacitance plots for a). Fat Phantom b). Muscle Phantom c). Superflab Phantom

Figure shows the plots for complex impedance for each electrode, real part of impedance in the Y axis versus the imaginary part of impedance in the X axis. Single electrode was used for the initial data collection. Four data sets were collected at four different locations in each phantom to test the homogeneity of the phantoms and the repeatability of the hardware and software. The data was collected over three phantoms fat equivalent phantom, muscle equivalent phantom and muscle embedded in fat phantom depicting anomaly in homogeneous tissue. The data collected is quite repeatable and reliable except few glitches that can be attributed to the electrode contact loss. This data was further used to develop a decision making algorithm that categorised the data into fat or muscle phantom group. The decision making algorithms were built by training the system using Adaptive Neuro Fuzzy Inference System (ANFIS). The number of membership functions used was 5, the membership function type was ‘gbellmf’ and the number of epochs were 20.

Appendix D.

Support Vector Machine: Classification results

(Note: ✓ implies correct classification and ✗ implies an incorrect classification)

(SUBJECT 3) Tissues	Trial 1	Trial 2	Trial 3	Trial 4	Trail 5
Arms	✗	✗	✗	✗	✗
Biceps	✓	✓	✓	✓	✓
Lower Inner Quadrant of Breast	✓	✓	✓	✓	✓
Lower Outer Quadrant of Breast	✓	✗	✗	✗	✗
Outer Upper Quadrant of Breast	✗	✗	✗	✗	✗
Upper Inner Quadrant of Breast	✓	✓	✓	✓	✓
Nail	✓	✓	✓	✓	✓
Palm	✓	✓	✓	✓	✓
Wrist Bone	✓	✓	✓	✓	✓
(SUBJECT 4)	**Trial 1**	**Trial 2**	**Trial 3**	**Trial 4**	**Trail 5**
Arms	✗	✗	✗	✗	✗
Biceps	✓	✗	✗	✗	✗
Lower Inner Quadrant of Breast	✓	✓	✓	✓	✓
Lower Outer Quadrant of Breast	✓	✓	✓	✓	✓
Outer Upper Quadrant of Breast	✗	✗	✗	✗	✗
Upper Inner Quadrant of Breast	✓	✓	✓	✓	✓
Nail	✓	✓	✓	✓	✓
Palm	✓	✓	✓	✓	✓
Wrist Bone	✓	✓	✓	✓	✓
(SUBJECT 5)	**Trial 1**	**Trial 2**	**Trial 3**	**Trial 4**	**Trail 5**
Arms	✗	✗	✗	✗	✗
Biceps	✓	✓	✓	✓	✓
Lower Inner Quadrant of Breast	✓	✓	✓	✓	✓
Lower Outer Quadrant of Breast	✓	✓	✓	✗	✗
Outer Upper Quadrant of Breast	✓	✓	✗	✗	✗
Upper Inner Quadrant of Breast	✗	✗	✗	✗	✗
Nail	✓	✓	✓	✓	✓

Palm	✓	✓	✓	✓	✓
Wrist Bone	✓	✓	✓	✓	✓
(SUBJECT 6)	**Trial 1**	**Trial 2**	**Trial 3**	**Trial 4**	**Trail 5**
Arms	✓	✓	✓	✓	✓
Biceps	✗	✗	✗	✗	✗
Lower Inner Quadrant of Breast	✓	✓	✓	✓	✓
Lower Outer Quadrant of Breast	✓	✓	✓	✓	✓
Outer Upper Quadrant of Breast	✓	✓	✓	✓	✓
Upper Inner Quadrant of Breast	✓	✓	✓	✓	✓
Nail	✓	✓	✓	✓	✓
Palm	✓	✓	✓	✓	✓
Wrist Bone	✓	✓	✓	✓	✓
(SUBJECT 7)	**Trial 1**	**Trial 2**	**Trial 3**	**Trial 4**	**Trail 5**
Arms	✗	✗	✗	✗	✗
Biceps	✗	✗	✗	✗	✗
Lower Inner Quadrant of Breast	✓	✓	✓	✓	✓
Lower Outer Quadrant of Breast	✓	✓	✓	✓	✓
Outer Upper Quadrant of Breast	✓	✓	✓	✓	✓
Upper Inner Quadrant of Breast	✓	✓	✓	✓	✓
Nail	✓	✓	✓	✓	✓
Palm	✓	✓	✓	✓	✓
Wrist Bone	✓	✓	✓	✓	✓
(SUBJECT 8)	**Trial 1**	**Trial 2**	**Trial 3**	**Trial 4**	**Trail 5**
Arms	✗	✗	✗	✗	✗
Biceps	✗	✗	✗	✗	✗
Lower Inner Quadrant of Breast	✓	✓	✓	✓	✓
Lower Outer Quadrant of Breast	✗	✗	✗	✗	✗
Outer Upper Quadrant of Breast	✓	✗	✗	✗	✗
Upper Inner Quadrant of Breast	✓	✓	✓	✓	✓
Nail	✓	✓	✓	✓	✓
Palm	✓	✓	✓	✓	✓
Wrist Bone	✓	✓	✓	✓	✓

(SUBJECT 9)	Trial 1	Trial 2	Trial 3	Trial 4	Trail 5
Arms	✖	✖	✖	✖	✖
Biceps	✖	✖	✖	✖	✖
Lower Inner Quadrant of Breast	✓	✓	✓	✓	✓
Lower Outer Quadrant of Breast	✓	✓	✓	✓	✓
Outer Upper Quadrant of Breast	✓	✓	✓	✓	✓
Upper Inner Quadrant of Breast	✓	✓	✓	✓	✓
Nail	✓	✓	✓	✓	✓
Palm	✓	✓	✓	✓	✓
Wrist Bone	✓	✓	✓	✓	✓
(SUBJECT 10)	Trial 1	Trial 2	Trial 3	Trial 4	Trail 5
Arms	✖	✖	✖	✖	✖
Biceps	✓	✖	✖	✖	✖
Lower Inner Quadrant of Breast	✖	✖	✖	✖	✖
Lower Outer Quadrant of Breast	✖	✖	✖	✖	✖
Outer Upper Quadrant of Breast	✖	✖	✖	✖	✖
Upper Inner Quadrant of Breast	✖	✖	✖	✖	✖
Nail	✓	✓	✓	✓	✓
Palm	✓	✓	✓	✓	✓
Wrist Bone	✓	✓	✓	✓	✓
(SUBJECT 11)	Trial 1	Trial 2	Trial 3	Trial 4	Trail 5
Arms	✖	✖	✖	✖	✖
Biceps	✖	✖	✖	✖	✖
Lower Inner Quadrant of Breast	✓	✓	✓	✓	✓
Lower Outer Quadrant of Breast	✓	✓	✓	✓	✓
Outer Upper Quadrant of Breast	✓	✓	✓	✓	✓
Upper Inner Quadrant of Breast	✓	✓	✓	✓	✓
Nail	✓	✓	✓	✓	✓
Palm	✓	✓	✓	✓	✓
Wrist Bone	✓	✓	✓	✓	✓
(SUBJECT 12)	Trial 1	Trial 2	Trial 3	Trial 4	Trail 5
Arms	✖	✖	✖	✖	✖

Biceps	✗	✗	✗	✗	✗
Lower Inner Quadrant of Breast	✓	✓	✓	✓	✓
Lower Outer Quadrant of Breast	✓	✓	✓	✓	✓
Outer Upper Quadrant of Breast	✗	✗	✗	✗	✗
Upper Inner Quadrant of Breast	✓	✓	✓	✗	✗
Nail	✓	✓	✓	✓	✓
Palm	✓	✓	✓	✓	✓
Wrist Bone	✓	✓	✓	✓	✓
(SUBJECT 13)	**Trial 1**	**Trial 2**	**Trial 3**	**Trial 4**	**Trail 5**
Arms	✓	✓	✓	✓	✓
Biceps	✓	✓	✓	✓	✓
Lower Inner Quadrant of Breast	✓	✓	✓	✓	✓
Lower Outer Quadrant of Breast	✓	✓	✓	✓	✓
Outer Upper Quadrant of Breast	✓	✓	✓	✓	✓
Upper Inner Quadrant of Breast	✓	✓	✓	✓	✓
Nail	✓	✓	✓	✓	✓
Palm	✓	✓	✓	✓	✓
Wrist Bone	✓	✓	✓	✓	✓
(SUBJECT 14)	**Trial 1**	**Trial 2**	**Trial 3**	**Trial 4**	**Trail 5**
Arms	✓	✓	✓	✓	✓
Biceps	✓	✓	✓	✓	✓
Lower Inner Quadrant of Breast	✓	✓	✓	✓	✓
Lower Outer Quadrant of Breast	✓	✓	✓	✓	✓
Outer Upper Quadrant of Breast	✓	✓	✓	✓	✓
Upper Inner Quadrant of Breast	✓	✓	✓	✓	✓
Nail	✓	✓	✓	✓	✓
Palm	✓	✓	✓	✓	✓
Wrist Bone	✓	✓	✓	✓	✓
(SUBJECT 15)	**Trial 1**	**Trial 2**	**Trial 3**	**Trial 4**	**Trail 5**
Arms	✓	✓	✓	✓	✓
Biceps	✗	✗	✗	✗	✗
Lower Inner Quadrant of Breast	✓	✗	✗	✗	✗

Lower Outer Quadrant of Breast	✓	✓	✓	✓	✓
Outer Upper Quadrant of Breast	✓	✓	✓	✓	✓
Upper Inner Quadrant of Breast	✓	✓	✓	✓	✓
Nail	✓	✓	✓	✓	✓
Palm	✓	✓	✓	✓	✓
Wrist Bone	✓	✓	✓	✓	✓
(SUBJECT 16)	**Trial 1**	**Trial 2**	**Trial 3**	**Trial 4**	**Trail 5**
Arms	✓	✓	✓	✓	✓
Biceps	✓	✓	✓	✓	✓
Lower Inner Quadrant of Breast	✓	✓	✓	✓	✓
Lower Outer Quadrant of Breast	✓	✓	✓	✓	✓
Outer Upper Quadrant of Breast	✓	✓	✓	✓	✓
Upper Inner Quadrant of Breast	✓	✓	✓	✓	✓
Nail	✓	✓	✓	✓	✓
Palm	✓	✓	✓	✓	✓
Wrist Bone	✓	✓	✓	✓	✓
(SUBJECT 17)	**Trial 1**	**Trial 2**	**Trial 3**	**Trial 4**	**Trail 5**
Arms	✓	✓	✗	✗	✗
Biceps	✓	✓	✓	✓	✓
Lower Inner Quadrant of Breast	✓	✓	✓	✓	✓
Lower Outer Quadrant of Breast	✗	✗	✗	✗	✗
Outer Upper Quadrant of Breast	✓	✓	✓	✓	✓
Upper Inner Quadrant of Breast	✓	✓	✓	✓	✓
Nail	✓	✓	✓	✓	✓
Palm	✓	✓	✓	✓	✓
Wrist Bone	✓	✓	✓	✓	✓
(SUBJECT 18)	**Trial 1**	**Trial 2**	**Trial 3**	**Trial 4**	**Trail 5**
Arms	✓	✓	✓	✓	✓
Biceps	✗	✗	✗	✗	✗
Lower Inner Quadrant of Breast	✗	✗	✗	✗	✗
Lower Outer Quadrant of Breast	✗	✗	✗	✗	✗
Outer Upper Quadrant of Breast	✓	✓	✓	✓	✓

Upper Inner Quadrant of Breast	✓	✓	✓	✓	✓
Nail	✓	✓	✓	✓	✓
Palm	✓	✓	✓	✓	✓
Wrist Bone	✓	✓	✓	✓	✓